Laterally Loaded Deep Foundations

Analysis and Performance

Langer/Mosley/Thompson
editors

ASTM STP 835

LATERALLY LOADED DEEP FOUNDATIONS: ANALYSIS AND PERFORMANCE

A symposium sponsored by
ASTM Committee D-18 on
Soil and Rock
Kansas City, MO, 22 June 1983

ASTM SPECIAL TECHNICAL PUBLICATION 835
J. A. Langer, Gannett Fleming Geotechnical Engineers, Inc., E. T. Mosley, Raamot Associates, and C. D. Thompson, Traw Group Limited, editors

ASTM Publication Code Number (PCN)
04-835000-38

1916 Race Street, Philadelphia, Pa. 19103

Library of Congress Cataloging in Publication Data

Laterally loaded deep foundations.

(ASTM special technical publication; 835)
"ASTM publication code number (PCN) 04-835000-38."
Includes bibliographical references and index.
1. Foundations—Congresses. 2. Piling (Civil engineering)
—Congresses. I. Langer, J. A. (James A.)
II. Mosley, E. T. III. Thompson, C. (Christopher)
IV. ASTM Committee D-18 on Soil and Rock. V. Series.
TA775.L37 1984 624.1'54 83-72942
ISBN 0-8031-0207-0

Library of Congress Catalog Card Number: 83-72942

Printed in Baltimore, Md.
Sept. 1984

Frank Fuller

Dedication

It is with deep appreciation to Frank Fuller for his work as chairman of ASTM Subcommittee D18.11 on Deep Foundations that this publication is dedicated. Among the accomplishments during his term as chairman of the subcommittee from 1973 through 1983 were two substantial revisions to ASTM Testing Piles Under Static Axial Compressive Loads (D 1143); two new standards, ASTM Testing Individual Piles Under Static Axial Tensile Load (D 3689) and ASTM Testing Piles Under Lateral Loads (D 3966); initiation of the development of standards for testing soil and rock anchors, dynamic testing of piles, and calibration of test jacks and load cells; and two symposia, Behavior of Deep Foundations, ASTM STP 670, *June 1978, and* Laterally Loaded Deep Foundations: Analysis and Performance, ASTM STP 835, *June 1983.*

Frank Fuller recently retired from Raymond International Builders, Inc., as vice-president and manager of Technical Sales after having held various positions there since his graduation from Renssalaer Polytechnic Institute in 1949. During his career, he has shared unselfishly his expertise on many pile foundation organizational committees for the American Society of Civil Engineers,

American Concrete Institute, Prestressed Concrete Institute, and Transportation Research Board as well as ASTM. In addition he has participated in the development of building code requirements for pile foundations, served as editor and principal writer of "Foundation Facts," contributed piling information to numerous textbooks, publications, symposia and recently authored Engineering of Pile Installations. *For Frank's dedication to the advancement and dissemination of pile foundation knowledge, the engineering community expresses its sincere appreciation and best wishes.*

Foreword

The symposium Design and Performance of Laterally Loaded Piles and Pile Groups was presented at Kansas City, MO, 22 June 1983. The symposium was sponsored by ASTM Committee D-18 on Soil and Rock. J. A. Langer, Gannett Fleming Geotechnical Engineers, Inc. E. T. Mosley, Raamot Associate, and C. D. Thompson, Traw Group Limited presided as chairmen of the symposium and editors of the publication.

Related ASTM Publications

Testing of Peats and Organic Soils, STP 820 (1983), 04-820000-38

Geotechnical Properties, Behavior, and Performance of Calcareous Soils, STP 777 (1982), 04-777000-38

Behavior of Deep Foundations, STP 670 (1979), 04-670000-38

Dispersive Clays, Related Piping, and Erosion in Geotechnical Projects, STP 623 (1977), 04-623000-38

Performance Monitoring for Geotechnical Construction, STP 584 (1975), 04-584000-38

A Note of Appreciation to Reviewers

The quality of the papers that appear in this publication reflects not only the obvious efforts of the authors but also the unheralded, though essential, work of the reviewers. On behalf of ASTM we acknowledge with appreciation their dedication to high professional standards and their sacrifice of time and effort.

ASTM Committee on Publications

ASTM Editorial Staff

Janet R. Schroeder
Kathleen A. Greene
Rosemary Horstman
Helen M. Hoersch
Helen P. Mahy
Allan S. Kleinberg
Susan L. Gebremedhin

Contents

Erratum for STP 835

On the Title page and in the Foreward, Editor C. D. Thompson's affiliation is incorrect. The correct company name is Trow Ltd.

Introduction

With the introduction of ASTM Testing Piles Under Lateral Loads (D 3966) in 1981, ASTM Subcommittee D18.11 on Deep Foundations began formulation of a symposium to be held in June 1983. The purpose of the symposium was to provide a forum for the presentation of recent advances in the analysis, design, and performance of laterally loaded piles and pile groups. Specifically, the symposium committee sought papers addressing analysis and design methods, computer solutions, effects of pile spacing and soil disturbance during pile installation, cyclic and dynamic loading, determination of appropriate soil and rock parameters by laboratory and field testing and by the use of references, effects of rate and duration of load application, instrumentation, concurrent vertical loading, and case histories of performance.

Of the 27 papers initially offered for consideration 11 papers were accepted and presented at the symposium. Those papers presented and included in this volume were by: R. Pyke and M. Bikae; K. Habibagahi and J. Langer; R. Sogge; L. Reese and S. Wright; S. Gleser; J. Briaud et al; W. Cox et al, K. Bhushan and S. Askari; D. Gle and R. Woods; L. Johnson et al; and M. Oakland and J. L. Chameau. The other papers contained herein were accepted but submitted too late for presentation.

The symposium sessions were chaired by members of the organizing committee. The morning session, chaired by Ernest Mosley, addressed design and analysis; the afternoon session, chaired by Christopher Thompson, addressed case histories; and the concluding panel discussion, moderated by the symposium chairman, included all of the symposium speakers as panelists.

In 1953, ASTM sponsored a symposium on laterally loaded piles. That symposium was a milestone as one of the earliest opportunities for discussion of the limited testing and analysis procedures available at that time. Significant advances have been made in the intervening 30 years in the procedures for analysis and testing and in the unique applications of laterally loaded piles. This volume contains some of the latest analysis and testing techniques and applications of piles subject to lateral loading. Several papers are the result of recent technology including heliostat foundations subject to cyclic loading and very small tolerable deflections, offshore drilled shafts subject to large cyclic loads, microcomputer analysis, and the use of the pressuremeter. One paper summarizes and expands much of the previous work concerning the appropriate horizontal subgrade modulus for granular soils. Other papers present special testing procedures and applications including dynamic and group testing and

use of piles for slope stabilization. Still others present new methods of analysis. Although many questions remain unanswered, this volume is a valuable tool for the engineers and researchers who seek current knowledge on the design, analysis, and performance of laterally loaded piles and pile groups.

James A. Langer
Gannett Fleming Geotechnical Engineers, Inc., Harrisburg, PA. 17105, symposium chairman and coeditor

Robert Pyke[1] *and Mohsen Beikae*[1]

A New Solution for the Resistance of Single Piles to Lateral Loading

REFERENCE: Pyke, R. and Beikae, M., **"A New Solution for the Resistance of Single Piles to Lateral Loading,"** *Laterally Loaded Deep Foundations: Analysis and Performance, ASTM STP 835*, J. A. Langer, E. T. Mosley, and C. D. Thompson, Eds., American Society for Testing and Materials, 1984, pp. 3-20.

ABSTRACT: A new analytical solution for the resistance of a horizontal slice through a pile to lateral loading is presented. The solution assumes that a pile is surrounded by an infinite elastic medium, but it allows for the tendency of this medium to separate from the back of the pile. Procedures for determining Young's modulus for various soils are given and comparisons of the overall results are made with previously published results.

KEY WORDS: piles, lateral loads, elasticity, soil properties, evaluation, Young's modulus

There are three general approaches that are available for the analysis of single piles subjected to lateral loads.

1. The Winkler or subgrade reaction approach in which the pile is considered to be supported by an array of uncoupled springs. These springs can be taken to be linear elastic, but more correctly they are taken to be nonlinear, and the shapes of the load-deformation relationships are described by *p-y* curves. Finite-element or finite-difference techniques can then be used to determine the response of the pile and spring system to applied loads.
2. An approach in which the soil surrounding the pile is modelled as a homogeneous elastic continuum, as described, for example, by Poulos [*1*].
3. Approaches in which the pile and the soil continuum surrounding it are modelled numerically using either finite-element or finite-difference techniques and, desirably, using nonlinear representations of soil stress-strain relationships is described, for example, by Faruque and Desai [*2*].

[1]Principal and research associate, Telegraph Avenue Geotechnical Associates, Berkeley, Calif. 94705.

Each of these approaches has deficiencies but, on balance, it appears that the first approach, that is, the approach in which the soil is discretized as an array of uncoupled springs, represents a versatile and practical approach for routine analyses. Thus, there is a continuing need to define the linear or nonlinear springs used in this kind of analysis. However, many of the procedures used in the past to define these springs have assumed, at least for the initial stage of loading, that the laterally loaded pile meets the same resistance to deformation as a strip load on a semi-infinite mass of soil, as illustrated in Fig. 1*a*. Such procedures neglect the existence of the soil on the back side of the pile, and, intuitively, it would seem that this assumption must lead to an underestimate of the soil stiffness. On the other hand, if it is assumed that soil adheres to the pile around its full circumference, as shown in Fig. 1*b*, the stiffness might be overestimated. A more correct mechanism, which shows soil fully surrounding the pile but only adhering to it along part of the circum-

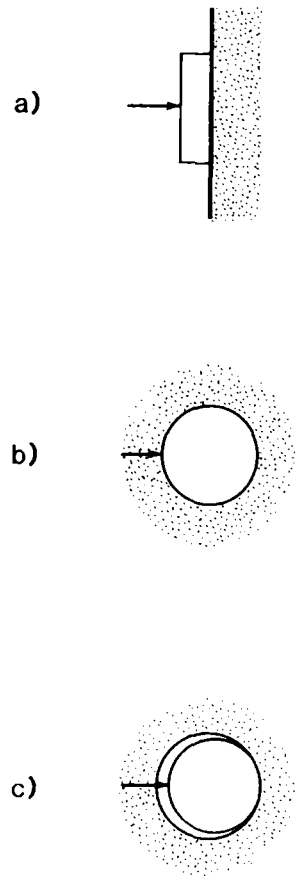

FIG. 1—*Assumptions regarding mechanism of resistance to lateral loading.*

ference, is shown in Fig. 1*c*. A solution for the contact stresses and the stiffness of a spring, which represents the resistance to loading provided by the soil assuming the mechanism (Fig. 1*c*), is presented in this paper. The solution does require assumption of a linearly elastic soil, however, it is possible to adjust the soil modulus to account for its strain dependence and for cyclic and rate-of-loading effects using procedures similar to those suggested by Poulos [*3*] for extending the elastic continuum approach to more general loadings. The solution also assumes that the elastic medium is infinite in extent and thus neglects the presence of the ground surface. To some extent the fact that the elastic modulus decreases with confining pressure accounts for the presence of the free surface, but a correction should also be applied for the difference in deformation conditions near the surface.

Previous Solutions

In the Winkler approach to studying the lateral resistance of piles, the soil pressure p is related to the lateral deflection y through the modulus of subgrade reaction k_h

$$p = k_h y \tag{1}$$

The modulus of subgrade reaction has units of force/length.[2] If k_h is multiplied by the length and diameter of a given pile segment, the equivalent spring stiffness is obtained. If k_h is assumed to increase linearly with depth z normalized in terms of the pile width or diameter D, we may write

$$k_h = n_h (z/D) \tag{2}$$

where n_h is called the coefficient of subgrade reaction.[2]

Terzaghi [*5*] discussed various methods for obtaining k_h and suggested typical values for n_h in sands. Assuming that displacements beyond a distance of three diameters have practically no influence on bending moments in the pile and using elastic theory, Terzaghi suggested more generally that

$$k_h = 0.74E_s/D \tag{3}$$

where E_s is the Young's modulus of the soil. Unless otherwise stated, all reference to E_s is this paper should be taken to mean the secant modulus for the load level of interest. For working load levels the secant modulus is commonly determined at 50% of the maximum load.

Vesic [*6*] studied the bending of an infinite beam on an elastic foundation,

[2]The terminology used in this paper is that of Poulos and Davis [*4*]; others have called k_h the coefficient of subgrade reaction and n_h the constant of subgrade reaction.

and by comparing Winkler and elastic continuum solutions obtained an expression for the modulus of subgrade reaction in terms of the relative stiffness of the pile and the soil. By substituting values appropriate for the undrained loading of piles in clay in Vesic's expression, Broms [7] found that

$$k = (0.48 \text{ to } 0.90E_s)/D \tag{4}$$

where the smaller coefficient is for a steel H-pile in soft clay, and the larger coefficient is for a timber pile in stiff clay.

Poulos [1] has also compared the Winkler and elastic continuum approaches. By equating the displacement obtained by modelling a stiff fixed-head pile as an embedded beam using the elastic continuum approach and the displacement obtained by modelling the pile as a beam on an elastic half space using the Winkler approach, Poulos found that the modulus of subgrade reaction could be expressed as

$$k_h = 0.82E_s/D \tag{5}$$

Using this value Poulos then found that the lateral displacements of more flexible piles computed by the Winkler approach could be as much as 2.5 times those obtained by the elastic continuum approach. These results would suggest that the modulus obtained for a beam bearing on a half space should perhaps be doubled in order to account for the half space on the back side of an embedded beam, that is, a laterally loaded pile.

The fact that k_h decreases with increasing load level or deflection appears to have first been taken into account by McClelland and Focht [8] who suggested using an empirical relationship between the shape of the stress-strain curve obtained from consolidated-undrained triaxial tests and the load-deflection, or a p-y curve for a pile in the field. Subsequent studies at the University of Texas led to the publication of more elaborate procedures for constructing p-y curves. These procedures are based in part on a simple theory and soil properties, but they rely more heavily on empirical data from a very limited number of lateral pile load tests.

Matlock [9] describes a procedure for constructing p-y curves for soft clays in which the initial portion of the curve for static loading is described by an equation that gives an infinite modulus of subgrade reaction, however, Matlock uses a formula for an embedded strip footing quoted by Skempton [10] to determine the deflection at 50% of the ultimate capacity, and the equivalent modulus of subgrade reaction is given by

$$k = 1.8E_s/D \tag{6}$$

Reese and Cox [11] describe a procedure for constructing p-y curves for stiff clays with brittle stress-strain relationships. This procedure defines an

initial curve for static loading similar to Matlock's, but the curve is cut off at small load levels by a straight line, which corresponds to a modulus of subgrade reaction determined as a function of a coefficient of subgrade reaction, as in Eq 2. Reese and Cox recommend values for the coefficient of subgrade reaction for static loadings as a function of the undrained shear strength, but these values cannot be directly related to the Young's modulus of the soil, as was the case for soft clay.

Reese et al [*12*] describe a procedure for constructing *p-y* curves for saturated sands in which the initial portion is a straight line given by a modulus of subgrade reaction, which is again determined as a function of a coefficient of subgrade reaction. Appropriate values of this modulus are suggested for loose, medium, and dense sands. The values given are 2½ to 4 times stiffer than those suggested by Terzaghi, perhaps because Terzaghi's values were intended to apply more at working loads whereas the Reese et al values are for initial loading.

The procedures for constructing *p-y* curves that were recommended in these three University of Texas studies continue to be used widely, particularly in offshore construction, even though significant advances have been made in understanding and evaluating soil properties since the procedures were first developed, and while the procedures are largely based on a very limited number of pile load tests, little effort seems to have been made to incorporate the results of additional pile load tests into the procedures. Stevens and Audibert [*13*], however, have compared the results of seven sets of lateral-pile load tests in soft to medium stiff clays with predictions based on the Matlock procedure for soft clays. They concluded that, in general, the observed deflections were less than those predicted but that the maximum bending moments were underestimated. Stevens and Audibert attribute these findings to both underestimating the ultimate lateral capacity and overestimating the values of the deflection at 50% of the ultimate capacity and suggest that this deflection increases only with the square root of the diameter, rather than the diameter. Sullivan et al [*14*] have also reviewed the procedures used to construct *p-y* curves for clays and proposed a unified procedure to cover both soft and stiff clays that includes an updated tabulation of the coefficient of subgrade reaction for initial loading in terms of the undrained shear strength.

Scott [*15*] has checked the Reese et al procedure for constructing *p-y* curves for sands against the results of centrifuge tests on model piles and found reasonably good agreement between the predicted and observed results for static loading. However, Scott concluded that the Reese et al procedure seems unduly complicated and suggested that a simple bilinear curve would serve just as well. The first segment of this curve has a slope equivalent to using a modulus of subgrade reaction given by

$$k_h = E_s/D \tag{7}$$

where the secant Young's modulus is determined for a strain of about 1%. This choice was based on the results of an analysis of the lateral deformation of a rigid cylinder in a finite elastic medium by J. P. Bardet and a comparison of Winkler and clastic continuum solutions [*16*]. It should be noted that Bardet's solution to the problem of a rigid cylinder displaced laterally in an elastic medium and a similar solution by Baguelin et al [*17*] are very sensitive to the distance to the outer boundary of the elastic medium, and Scott's suggested value for the modulus of subgrade reaction corresponds to a distance to the outer boundary of 50-pile radii in Bardet's solution. This distance is greater than most conventional guesses as to the radius of influence of axially or laterally loaded piles, and it therefore seems desirable to attempt a solution of the problem of a rigid cylinder displaced laterally in an elastic medium, which is not sensitive to the distance to the outer boundary. Such a solution is presented in the following section. Nonetheless, Scott's overall approach represents a step in a positive direction, since it attempts to improve both the modelling of the mechanism of deformation and the connection between the resistance to deformation and real soil properties, while maintaining simplicity in application.

Finally, mention should be made of the plane strain finite-element analyses conducted by Yegian and Wright [*18*] and Thompson [*19*] in order to obtain both *p-y* curves and displacements. While still a little complex for routine use, such analyses may well find increasing use in the future.

The New Solution

In the approach that is described herein, the problem of a laterally loaded pile is idealized as that of an infinitely long rigid cylinder moving laterally in an infinite elastic medium or, alternately, the plane strain problem of a rigid disk moving laterally in an infinite linear elastic medium. The assumption of plane strain is equivalent to Winkler's hypothesis that each support spring acts independently of the others. The assumption of a linear clastic material is clearly not correct for soils exccpt for very small strains, however, an equivalent linear modulus can be selected as a function of load level and other factors in order to apply the elastic solution more generally, albeit, with some approximation. The third key assumption that is made in the solution is that the elastic medium is in contact with the disk only over a limited zone in which there is an increase in the normal pressure as a result of lateral movement of the disk. Around the remainder of the circumference the elastic medium is, in effect, separated from the disk as shown in Fig. 1*c*.

In reality separation at the back of the pile will not occur, except perhaps at shallow depths in cohesive soils, because elements of soil adjacent to the pile are already loaded and compressed by the weight of the overburden and possibly also by stresses induced by installation of the pile. Thus the soil on the back side of the pile will tend to follow the pile as the pile moves laterally, but

the contact pressures will fall from at-rest to active values. Because soil takes little or no tension, the pile cannot pull the soil after it, and therefore it is reasonable to assume separation at the back of the pile when calculating the increase in pressure on the front of the pile to lateral loading. The pressure distributions on a pile cross section before lateral loading and with the positive and negative increments resulting from lateral loading are shown schematically in Fig. 2.

The solution procedure uses a technique resulting from Muskhelishvili [*20*], which involves transformation of the original problem described in cartesian coordinates to a complex coordinate system and then uses Cauchy's integral to transform the inner boundary condition to the complex domain in which the outer boundary of the elastic medium is at infinity. The Muskhelishvili potential functions may then be formulated in terms of the assumed boundary conditions. From these potential functions, which are the equivalent of the Airy stress function in the real domain, the stresses throughout the elastic medium can be obtained. While it turns out that the integrodifferential equations that govern the distributions of the normal and shear stress on the inner boundary, that is, on the face of the pile, cannot be solved exactly, a very good approximation to the correct solution can be obtained by trigono-

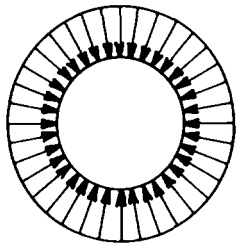

a) Prior to loading

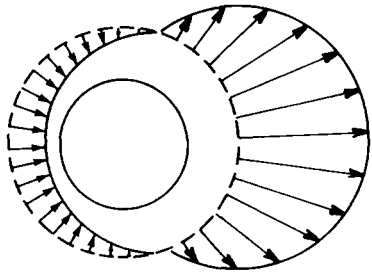

b) After lateral loading

FIG. 2—*Pressure distributions around pile.*

metric expansion of the unknown functions and use of the Galerkin technique. However, since evaluation of the solution is time consuming if the distribution of shear stress is sought as well as the distribution of normal stress, the preliminary solution that is presented in this paper assumes that there are no shear stresses on the inner boundary. This is equivalent to assuming that the pile is perfectly smooth. Full details of the solution procedure are given by Beikae [*21*]. The distributions obtained for the normal stresses on the inner boundary for three different values of Poisson's ratio ν are shown in Fig. 3.

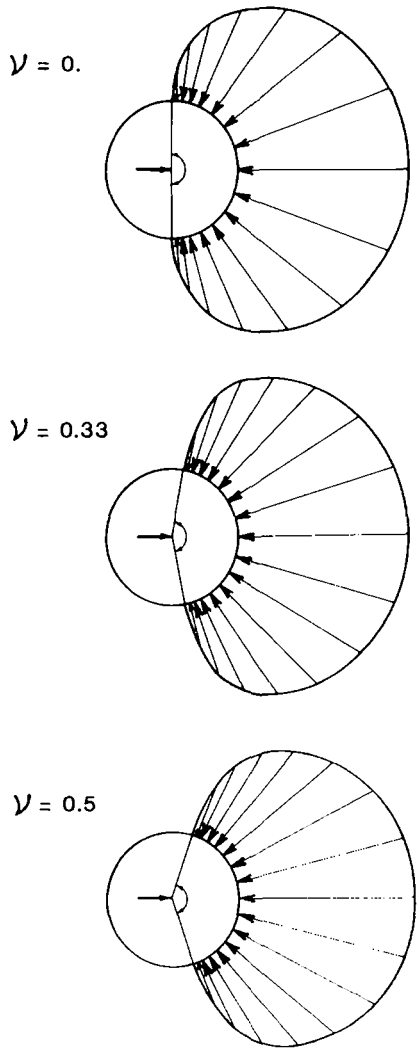

FIG. 3—*Distributions of normal stress on face of pile caused by lateral loading.*

The displacements throughout the elastic medium can also be obtained from the Muskhelishvili potential functions, but they are unbounded at infinity and are only valid on the inner boundary. This is all that is required for present purposes, however, and it is possible to obtain an expression for the ratio of the average stress on the pile cross section to the displacement of the inner boundary, that is, the modulus of subgrade reaction, which is a function of the Young's modulus and the distributions of the normal stress on the pile face. Using the three distributions of the normal stress that have been obtained previously, the modulus of subgrade reaction is found to be equal to 2.3, 2.0, and 1.8 times E/D for Poisson's ratio equal to zero, 0.33 and 0.5, respectively. For practical purposes we might take

$$k_h = 2E_s/D \tag{8}$$

It should be noted that this solution has neglected the distribution of shear stress around the inner boundary, which is equivalent to assuming a smooth pile, and it has also neglected the decrease in pressure on the back of the pile. Nonetheless, a value in the order of $2E/D$ does not seem unreasonable as it is about twice the value obtained by considering a strip footing acting on the surface of a half space. Note that the value of the modulus of subgrade reaction at working loads implied by Matlock [*9*], who considered the pile to be similar to an embedded footing, is closer to the suggested value than most other solutions. Moreover, the value of $2E/D$ corresponds to a distance to the outer boundary in Bardet's solution of the problem of a laterally loaded cylinder or disk of 10- to 20-pile radii, and this is more consistent with popular conceptions of the radius of influence of laterally loaded piles than the 50-pile radii, which corresponds to the value of E/D. Thus it would seem to be reasonable to use a modulus of subgrade reaction in the order of $2E/D$ for Winkler analyses of laterally loaded piles, recognizing that corrections may still have to be made for the relative length and stiffness of the pile as well as for the effect of the free surface.

Evaluation of Young's Modulus

Use of the new solution, or any of the previous formulations that employ elastic theory, requires that the Young's modulus can be determined with reasonable accuracy, and even for initial loading this is no easy task. In this section of the paper the various factors affecting the Young's modulus on initial loading up to working load levels are discussed and typical values for the initial tangent modulus are presented.

In general these methods can be used to determine Young's modulus: (1) field tests, (2) laboratory tests on laboratory tests obtained from relatively undisturbed samples, and (3) back calculation from pile load tests. Each of these methods has advantages and disadvantages, but full discussion of these

is beyond the scope of this paper. However, in choosing the method or methods to be used on a particular project the responsible engineer should be aware of the factors that can affect the Young's modulus. In addition to the load level and cyclic loading effects, the horizontal Young's modulus in the field may be affected by the preexisting in-situ stresses, material anisotropy, changes in stress caused by installing the pile, the drainage conditions for the loading in question, more pure rate of loading effects, and the previous history of loading. In addition to the drainage conditions and the rate of loading, the Young's modulus measured in laboratory tests may also be a function of the degree of sample disturbance, the extent to which the effects of sample disturbance are minimized by the stress path followed in reconsolidating test specimens and the time of consolidation, the type of test, and the loading stress path.

Several of these factors deserve special comment. Anisotropy of both stiffness and strength has been observed in many soils particularly for undrained loadings, but it is usually ignored in practice. For normally consolidated soils the stiffness in the horizontal direction will normally be less than that in the vertical direction, but the reverse may be true for overconsolidated soils. Thus, it would appear to be desirable to measure Young's modulus in the horizontal direction for application to the study of lateral loading of piles. This might be accomplished in the field by use of a self-boring pressuremeter or in the laboratory by increasing the lateral stress in the triaxial test, rather than the axial stress.

The effect of the drainage conditions on soil properties is also often ignored in foundation engineering as applied to piles. Commonly it is assumed that clays are always loaded undrained, even under long-term static loadings, and sands are always loaded drained, even under rapid loadings such as those resulting from ocean waves or earthquakes. However, for any soil the drainage conditions during loading are a function of the rate of loading, the pile diameter, and the permeability and compressibility of the soil. At large load levels the stiffness and strength of soil can vary by factors of up to three depending on whether the loading is drained or undrained, but this difference is smaller at low load levels. Ignoring anisotropy, the undrained Young's modulus E_u and the drained Young's modulus E' are related [*4*] by the expression

$$E_u = 3E'/2(1+\nu') \tag{9}$$

Typically the drained Poisson's ratio ν' at very low strains is equal to about 0.15. Thus, the initial tangent moduli would be related as follows

$$E_u = 1.3E' \tag{10}$$

Usually the difference between drained and undrained loading conditions will be more significant than pure rate of loading effects on soils, but for more

plastic clays the stiffness may be increased by up to about 100% over normal values for times to failure in the order of 1 s [*22*]. This effect appears to diminish with increasing overconsolidation ratio.

In more critical design situations the responsible engineer should specify and supervise appropriate field or laboratory tests, or both, to determine the values of Young's modulus required for use in design, but for less critical designs and for feasibility studies or preliminary design it may be adequate to rely on data available from the literature. Such data should always be used with caution, however, as published data may not be applicable to the design procedure being used, or the data may simply be in error.

Several of the more reliable published correlations between the undrained Young's modulus and undrained shear strength are shown in Table 1. The correlations provided by Poulos and Davis are back figured from lateral pile load tests using elastic continuum theory. Poulos and Davis note that it is not clear whether their values apply to drained or undrained loadings, but they suggest that the values are probably applicable to undrained loading. Poulos and Davis also point that their initial tangent values are about half of those normally associated with surface foundations and that this may reflect the influence of anisotropy and pile-soil separation. The values given by Sullivan are for overconsolidated North Sea clays, push sampling, and unconsolidated-undrained triaxial tests. The corresponding values of E_u/S_u obtained from driven samples were about 100, indicating the possible magnitude of sample disturbance effects.

One of the difficulties with most earlier correlations of the kind shown in Table 1 is that the undrained shear strength varies markedly both with sample disturbance and the type of test that is conducted. However, in the last decade improved sampling and laboratory testing procedures have been implemented on at least some projects, and preliminary relationships for the initial tangent for Young's modulus based on some of this recent data are presented in Figs. 4 through 7.

Figure 4 shows the ratio of the undrained initial tangent modulus obtained from static tests and the modulus at small strains in dynamic tests to undrained shear strength as a function of the plasticity index of normally consolidated clays, as given by Koutsoftas and Fischer [*24*], Andersen et al [*25*], and Foott and Ladd [*26*]. The authors have extrapolated the Andersen et al and the Foott and Ladd published data to a load level of zero in order to obtain

TABLE 1—*Typical values of* E_u/S_u.

Study	Initial Tangent Modulus	Secant Modulus at Working Loads
Skempton [*10*]	...	50 to 200
Poulos and Davis [*4*]	250 to 400	15 to 95
Sullivan [*23*]	...	100 to 250

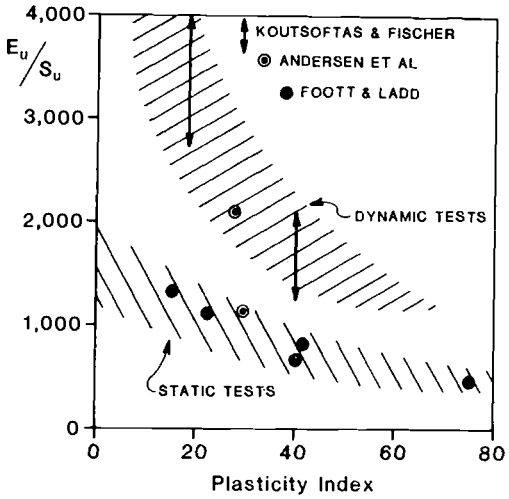

FIG. 4—*Variation of normalized undrained initial tangent modulus with plasticity index for normal consolidated clays.*

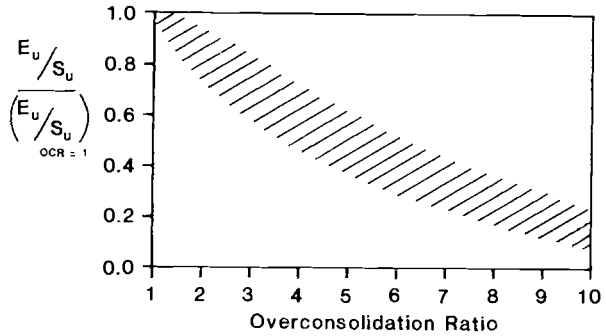

FIG. 5—*Decrease in normalized undrained initial tangent modulus with overconsolidation ratio.*

estimates of the initial tangent modulus. The three studies cited involved use of simple shear, triaxial, and resonant column data, but in each case specimens were reconsolidated so as to ensure normal consolidation. Published values of shear modulus were multiplied by a factor of three to obtain Young's modulus. Each set of data is reasonably consistent, but it may be seen that the moduli obtained from the dynamic tests are about three times higher than those from the static tests as a result of pre-straining and rate of loading effects that increase the modulus measured in the dynamic tests. The decrease in the secant modulus with increasing load level shown in these studies appears to be reasonably linear so that, for instance, the secant modulus at a

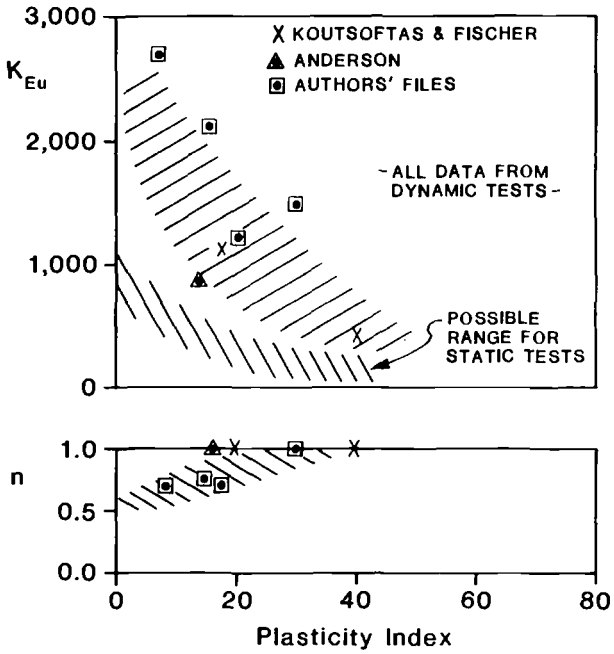

FIG. 6—*Variation of Young's modulus parameters with plasticity index for normally consolidated clays.*

load level of 50% is half the initial tangent modulus. All three studies also show that the ratio E_u/S_u decreases with increasing overconsolidation ratio. That is, with increasing overconsolidation ratio the modulus does not increase as much as the undrained strength. The rate of decrease of the ratio E_u/S_u is indicated in Fig. 5. It may be seen by comparing the values of E_u/S_u listed in Table 1 and those shown in Figs. 4 and 5 that the values in Table 1 are reasonably consistent with newer data from static tests on more plastic or more heavily overconsolidated clays, but that E_u/S_u can be rather greater for less plastic, normally consolidated clays.

While it has been usual to normalize the modulus of clays in terms of the undrained shear strength, it may in fact be preferable to express the modulus in terms of the vertical consolidation stress σ'_{vc} or the mean consolidation stress σ'_{mc}. Not only does this eliminate the problem of S_u varying widely with the type of test, but it also allows presentation of data for sands and clays using the same format, and thus intermediate soils can be included without difficulty. A convenient form for common presentation of data is

$$E = K_E p_a \, (\sigma'_{mc}/p_a)^n \tag{11}$$

where K_E and n are dimensionless parameters, and p_a is atmospheric pres-

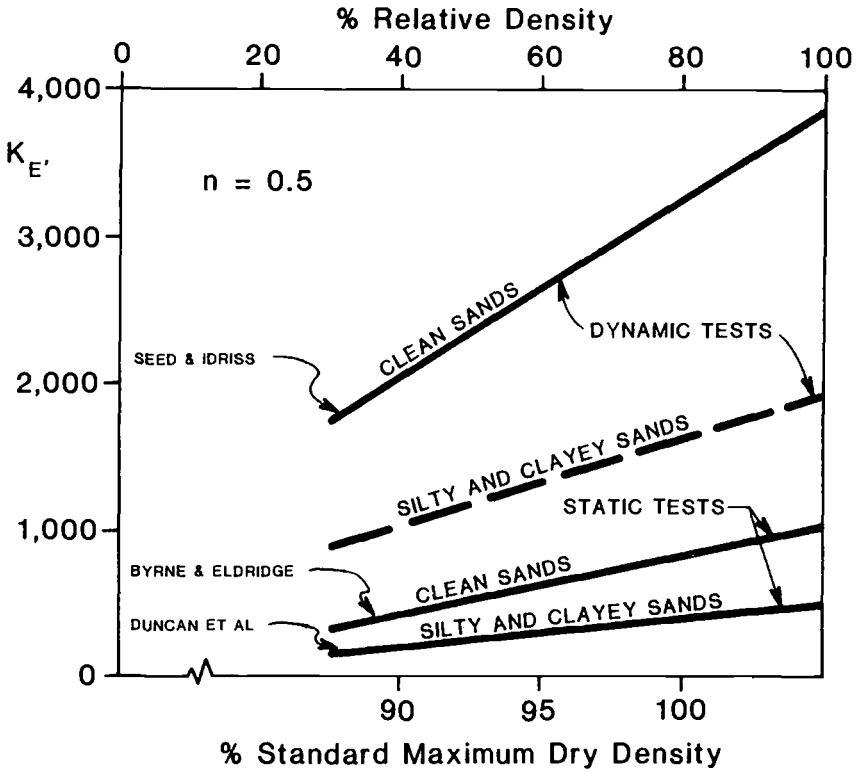

FIG. 7—*Variation of Young's modulus parameter with density for granular soils.*

sure. This form is commonly used to express the initial tangent modulus for static loadings using σ_{3c} as the measure of confining stress [*27,28*].

Only limited data exist from which K_{Eu} and n for normally consolidated clays can be readily obtained, but values for these parameters obtained from data presented by Koutsoftas and Fischer [*24*] and Anderson [*29*] and from the authors' files are shown in Fig. 6 as a function of the plasticity index. The data shown are for dynamic tests and the equivalent values of K_{Eu} from static tests may be some three times smaller.

For granular soils the parameter n is normally found to be close to 0.5. Typical values of the parameter K_E, are shown in Fig. 7 and approximate values of K_{Eu} can be obtained by use of Eq 11. The values of K_E, for clean sand from dynamic tests have been obtained by multiplying the shear moduli given by Seed and Idriss [*30*] by a factor of 2.3. As noted previously by Byrne and Eldridge [*28*], these values are four to five times higher than the values obtained from static tests. This may be due in part to the values of initial tangent Young's modulus in static tests being read off at strain levels where the modulus has already decreased by a factor of two or more from its true

maximum value. However, the effect of the prestraining induced by the resonant column test, from which most of the dynamic test data have been obtained, appears to be more significant for sands than it is for clays since the difference between static and dynamic values for K_E is greater while pure rate of loading effects in sands are expected to be small. The line for silty and clayey sands and dynamic tests in Fig. 7 has been obtained simply by increasing the values from static tests by the same amount as for clean, sands but the result is consistent with data in the authors' files, which show the maximum shear moduli for silty and clayey sands to be somewhat less than those for clean sands.

Field values for the initial tangent modulus for static loading probably falls in between the bands of data shown in Figs. 4, 6, and 7 for static and dynamic tests. Using such values as a starting point the engineer can then reduce them to account for load level and for anisotropy if this is thought to be important. For rapid loadings that may have been preceded by low-level cyclic loadings, such as occur offshore, more weight should be placed on the dynamic values.

Comparison of Different Solutions

Several of the available solutions for the modulus of subgrade reaction are compared in Tables 2 and 3 using in each case the procedure for choosing E_s or the values of n_h recommended by the original authors. The comparisons are made for the case of a 1-m-diameter pile at a depth of 5 m and with the water table at the surface. It is assumed that clays are loaded undrained, and sands are loaded drained. For clays the values of S_u that correspond to each of the overconsolidation ratios (OCRs) shown in the table were taken to be 12, 24, and 60 kPa.

In comparing the various values shown in Tables 2 and 3, it may be seen that the values derived in this study are of the same order as those provided by Sullivan et al [*14*] for clays and Reese et al [*12*] for sands. The values derived

TABLE 2—*Modulus of subgrade reaction for clays, in NM/m³, for different solutions.*

	Initial Loading			Working Loads		
	Overconsolidation Ratio					
Study	1	2	8	1	2	8
Broms [7]	...	...	...	0.8	1.7	4.2
Matlock [9]	...	...	...	2.2	4.3	10.8
Sullivan et al [14]	20	70	280	...	...	...
This study						
plastic clay	24	40	54	12	20	27
silty clay	72	118	164	36	56	81

TABLE 3—*Modulus of subgrade reaction for sands, in MN/m³, for different solutions.*

Study	Initial Loading			Working Loads		
	Loose	Medium	Dense	Loose	Medium	Dense
Terzaghi [5]	...	...	...	6	22	54
Reese et al [12]	27	81	170	...	...	...
This study						
clean sand	85	103	165	43	52	83
silty sand	42	52	84	21	26	42

in this study for the softer clays are, however, rather greater than those given by Matlock [9]. This is consistent with the findings of Stevens and Audibert [13] that were cited previously, but the new solution, as with previous elastic solutions, does not show the dependence on diameter that was observed by Stevens and Audibert. A possible explanation of this is that for larger piles the rate of excess pore-pressure dissipation is slower, and therefore the loading is more undrained compared to the loading of smaller diameter piles, and the Young's modulus of the soil is therefore greater. Alternatively, if there is drainage, the increase in the average effective confining pressure acting on the soil in front of the pile will be relatively greater for larger diameter piles, and the Young's modulus will be correspondingly greater. In either case, the effect observed by Stevens and Audibert would be a soil property effect rather than a strictly geometric effect.

Conclusions

The expression for the modulus of subgrade reaction that has been developed herein is believed to more correctly represent the mechanics of the development of resistance to the lateral loading of a pile than previous solutions. If used in conjunction with appropriate values of the Young's modulus, it should provide reasonable guidance on the resistance to lateral loading on initial loading and for working loads. The engineer should, however, be aware of the limitations of the assumptions made in developing the new solution and of the possible need to account for the relative length and flexibility of the pile as well as for the effect of the free surface.

References

[1] Poulos, H. G., "Behavior of Laterally Loaded Piles: I—Single Piles," *Proceedings of the American Society of Civil Engineers*, Vol. 97, No. SM5, May 1971, pp. 711–731.

[2] Faruque, M. O. and Desai, C. S., "3-D Material and Geometric Nonlinear Analysis of Piles," *Proceedings of the 2nd International Conference on Numerical Methods in Offshore Piling*, University of Texas, Austin, Tex., April 1982.

[3] Poulos, H. G., "Single Pile Response to Cyclic Lateral Load," *Proceedings of the American Society of Civil Engineers*, Vol. 108, No. GT3, March 1982, pp. 355-376.
[4] Poulos, H. G. and Davis, E. H., *Pile Foundation Analysis and Design*, Wiley, New York, 1980.
[5] Terzaghi, K., "Evaluation of Coefficients of Subgrade Reaction," *Geotechnique*, Vol. 5, No. 4, Dec. 1955, pp. 297-326.
[6] Vesic, A. S., "Bending of Beam Resting on Isotropic Elastic Solid," *Proceedings of the American Society of Civil Engineers*, Vol. 87, No. EM2, March 1961, pp. 35-53.
[7] Broms, B. B., "Lateral Resistance of Piles in Cohesive Soils," *Proceedings of the American Society of Civil Engineers*, Vol. 90, No. SM2, March 1964, pp. 27-63.
[8] McClelland, B. and Focht, J. A., "Soil Modulus of Laterally Loaded Piles," *Transactions of the American Society of Civil Engineers*, Vol. 123, 1958, pp. 1049-1063.
[9] Matlock, H., "Correlations for the Design of Laterally Loaded Piles in Soft Clay," Paper No. 1204, Offshore Technology Conference, Dallas, TX, 1970.
[10] Skempton, A. W., "The Bearing Capacity of Clays," *Proceedings of the Building Research Congress*, Division 1, Part 3, London, 1981, pp. 180-189.
[11] Reese, L. C. and Cox, W. R., "Field Testing and Analysis of Laterally Loaded Piles in Stiff Clay," Paper No. 2312, Offshore Technology Conference, Houston, 1975.
[12] Reese, L. C., Cox, W. R., and Koop, F. D., "Analysis of Laterally Loaded Piles in Sand," Paper No. 2080, Offshore Technology Conference, Dallas, TX, 1974.
[13] Stevens, J. B. and Audibert, J. M. E., "Re-examination of *p-y* Curve Formulations," Paper No. 3402, Offshore Technology Conference, Dallas, TX, 1979.
[14] Sullivan, W. R., Reese, L. C., and Fenske, C. W., "Unified Methods for Analysis of Laterally Loaded Piles in Clay," *Numerical Methods in Offshore Piling*, Institute of Civil Engineers, London, 1980.
[15] Scott, R. F., "Analysis of Centrifuge Pile Tests," Report of American Petroleum Institute, Dallas, Tex., June 1980.
[16] Scott, R. F., *Foundation Analysis*, Prentice-Hall, Inc., Englewood Cliffs, N. J., 1981.
[17] Baguelin, F., Frank, R., and Said, Y. H., "Theoretical Study of Lateral Reaction Mechanism of Piles," *Geotechnique*, Vol. 27, No. 3, Sept. 1977, pp. 405-434.
[18] Yegian, M. and Wright, S. G., "Lateral Soil Resistance-Displacement Relationships for Pile Foundations in Soft Clay," Paper No. 1893, Offshore Technology Conference, Dallas, TX, 1973.
[19] Thompson, G. R., "Application of the Infinite Element Method to the Development of *p-y* Curves for Saturated Clays," M. S. thesis, University of Texas, Austin, 1977.
[20] Muskhelishvili, N. I., *Some Basic Problems of the Mathematical Theory of Elasticity*, translated by J. R. M. Radok, Erven P. Noordhoff, N. V., Groningen, the Netherlands, 1963.
[21] Beikae, M., "A New Solution for the Stresses and Displacements Caused by Lateral Loading of a Pile," Technical Note TAGA 82-02, Telegraph Avenue Geotechnical Associates, Berkeley, Calif., Nov., 1982.
[22] Lacasse, S. and Andersen, K. H., "Effect of Load Duration on Undrained Behaviour of Clay and Sand; Summary," Internal Report No. 40007-4, Norwegian Geotechnical Institute, Oslo, Norway, 1979.
[23] Sullivan, R. A., "North Sea Foundation Investigation Techniques," *Marine Geotechnique*, Vol. 4, No. 1, 1980, pp. 1-30.
[24] Koutsoftas, D. C. and Fischer, J. A., "Dynamic Properties of Two Marine Clays," *Proceedings of the American Society of Civil Engineers*, Vol. 106, No. GT6, June 1980, pp. 645-657.
[25] Andersen, K. H., Pool, J. H., Brown, S. F, and Rosenbrand, W. F., "Cyclic and Static Laboratory Tests on Drammer Clay," *Proceedings of the American Society of Civil Engineers*, Vol. 106, No. GT5, May 1980, pp. 499-529.
[26] Foott, R. and Ladd, C. C., "Undrained Settlement of Plastic and Organic Clays," *Proceedings of the American Society of Civil Engineers*, Vol. 107, No. GT8, Aug. 1981, pp. 1079-1094.
[27] Duncan, J. M., Byrne, P., Wong, K. S., and Mabry, P., "Strength, Stress-Strain and Bulk Modulus Parameters for Finite Element Analyses of Stresses and Movements in Soil Masses," Report No. UCB/GT/80-01, University of California, Berkeley, Aug. 1980.

[*28*] Byrne, P. M. and Eldridge, T. L., "A Three Parameter Dilatant Elastic Stress-Strain Model for Sand," Proceedings of the International Symposium on Numerical Models in Geomechanics, Balkema, Rotterdam, Sept. 1982, pp. 73-80.

[*29*] Anderson, D. G., "Dynamic Modulus of Cohesive Soils," Report No. UMEF-74RZ, University of Michigan, Ann Arbor, June 1974.

[*30*] Seed, H. B. and Idriss I. M., "Soil Moduli and Damping Factors for Dynamic Response Analyses," Report No. EERC 70-10, University of California, Berkeley, Dec. 1970.

Karim Habibagahi[1] *and James A. Langer*[1]

Horizontal Subgrade Modulus of Granular Soils

REFERENCE: Habibagahi, K. and Langer, J. A., **"Horizontal Subgrade Modulus of Granular Soils,"** *Laterally Loaded Deep Foundations: Analysis and Performance, ASTM STP 835*, J. A. Langer, E. T. Mosley, and C. D. Thompson, Eds., American Society for Testing and Materials, 1984, pp. 21-34.

ABSTRACT: Although the horizontal subgrade modulus plays a significant role in problems dealing with lateral-load carrying capacity of piles, a rather wide range of values is available in literature depending upon the equation, chart, or table used to obtain the modulus. This task is further complicated on account of lack of uniformity of definitions used. The accuracy of simple, let alone elaborate, methods of analysis for lateral-pile capacity is often controlled by the accuracy of the modulus value used in the computations. For many engineering computations, the engineer must strike a balance between a simple and an accurate enough procedure to obtain the modulus. One of the simplest ways of computing the modulus is by means of empirical and semiempirical relationships. In this paper, the available empirical and semiempirical relations for estimating the horizontal subgrade modulus of granular soils are reviewed, and then a simple relationship for computing the horizontal subgrade modulus of such soils is presented. The values of the modulus from the proposed relationship are compared with those given by others.

KEY WORDS: lateral loads, piles, piers, caissons, subgrade modulus, granular soils

With urban growth and congested building sites, the use of vertical piles to carry large lateral loads has become more common as the presence of adjacent structures precludes application of batter piles on sites that otherwise would have been suitable for such piles. In problems dealing with lateral resistance of soil against buried structures, such as piles and conduits, one needs to have a knowledge of the horizontal subgrade modulus. There are several empirical and semiempirical relationships as well as charts and tables available for estimating the horizontal subgrade modulus. In addition, a variety of field and laboratory techniques have been used to determine the hori-

[1]Chief soils engineer and senior geotechnical engineer, respectively, Gannett Fleming Geotechnical Engineers, Inc., Harrisburg, PA 17105.

zontal subgrade modulus, among which are standard penetration test [*1-4*],[2] pressuremeter test [*5*], plate load test [*1,6*], consolidation test [*7*], unconfined compression test [*8-10*], and triaxial compression test [*11*].

Even though the value assigned to the horizontal subgrade modulus plays a significant role in the computations of soil resistance of laterally loaded piles, a rather wide range of values is available in literature depending upon the equation, chart, or table used to obtain the modulus. The accuracy of elaborate methods of analysis for lateral-load carrying capacity is often controlled by the accuracy of the modulus value used in the computations. In selecting a procedure to obtain the modulus for lateral-pile capacity computations, the engineer must strike a balance between accuracy and simplicity. One of the simplist methods of computing the modulus is by means of empirical and semiempirical relationships, which relate the modulus to other known or easily obtainable soil properties.

This paper reviews such relationships for granular soils and presents a simple and yet a reasonably conservative relationship to obtain the horizontal subgrade modulus of granular soils.

Definitions and Units

Terms frequently used in literature dealing with the horizontal subgrade modulus are the lateral subgrade modulus, the horizontal subgrade modulus, the lateral modulus of subgrade reaction, the coefficient and the constant of horizontal subgrade reaction, the coefficient of variation of lateral subgrade reaction, and the soil spring constant. The units associated with these terms range from force per unit of length to force per unit of length cubed. The lateral subgrade modulus, the horizontal subgrade modulus, the lateral modulus of subgrade reaction, and the soil spring constant all refer to the horizontal soil modulus and are interchangeable. The horizontal subgrade modulus is used herein for its simplicity. The coefficient of variation of lateral subgrade reaction and the constant of horizontal subgrade reaction are the same. The relationship of the horizontal subgrade modulus with the coefficient and the constant of horizontal subgrade reaction as well as its relationship with the horizontal subgrade reaction becomes clear with the definition of the horizontal subgrade modulus.

The horizontal subgrade modulus K_h is defined as the ratio of the horizontal subgrade reaction at any point and the displacement produced by the application of the reaction at that point, that is

$$K_h = F/y \tag{1}$$

[2] Bhushan, K. and Askari, S., "Design of Solar Plant Heliostat Foundation," in this publication, pp. 140-156.

where F is the applied horizontal force or reaction, and y is the resulting displacement. The unit of K_h is therefore force per unit of length. In problems dealing with piles, it is convenient to use force per unit of length Q instead of total force F. The force per unit of length Q is related to side pressure p on the pile according to

$$Q = pB$$

where B is the pile width or diameter. The horizontal subgrade modulus thus becomes

$$K_h = Q/y = pB/y \tag{2}$$

and has units of force per length squared. This relationship is often presented in the following form

$$K_h = k_h B \tag{3}$$

in which

$$k_h = p/y \tag{4}$$

is the coefficient of horizontal subgrade reaction and has units of force per length cubed. The coefficient of horizontal subgrade reaction, commonly used in the soil mechanics literature, is related to the horizontal subgrade modulus by means of Eq 3. The constant of horizontal subgrade reaction is defined below.

Existing Relationships and Charts

The coefficient of horizontal subgrade reaction can be obtained by means of various empirical and semiempirical relationships. Assuming that the coefficients of horizontal subgrade is a function of depth Z and unit weight γ, Terzaghi [*1*] showed that

$$k_h = n_h(Z/B) \tag{5}$$

where n_h is the constant of horizontal subgrade reaction and is given by

$$n_h = 2A\gamma/1.35$$

where A is a constant. Typical values of n_h for sands are given in Table 1.

From combining Eqs 2, 4, and 5 it is observed that

$$Q = n_h Z y \tag{6}$$

TABLE 1—*Values of the constant of horizontal subgrade reaction* n_h, *kcf* [1].

Parameters	Relative Density of Sand		
	Loose	Medium	Dense
Blows/ft, N	4 to 10	10 to 30	30 to 50
ϕ, degrees	30	34	39
Dry or moist sand n_h	14	42	112
Submerged sand n_h	8	28	68

Note: to convert kcf to kN/m^3, multiply by 157.09.

In other words the lateral force per unit of length needed to displace the soil in the direction of the applied force by a unit of length (for example, 1.0 cm) is equal to n_h times the depth under consideration. As can be seen, the lateral force is a direct function of depth. Recent experiments and field data, however, indicate that the vertical bearing capacity in granular soils increases with depth only up to a given depth depending on the locations of water table and the relative density of the soil. Beyond this depth, there is little increase in bearing capacity. The limiting depth is 10B to 40B. It is possible that the lateral resistance may also follow the same general trend and not continue to increase with depth indefinitely as indicated by Eq 6. Further examination of Eq 6 reveals that for a given lateral force per unit of length, displacement is independent of the width of the loaded area. Alternately, if k_h is known at a given depth, the lateral force per unit of length can be obtainable from Eqs 5 and 6 as

$$Q = k_h B y$$

Zurabov and Bugayeva [*12*] give the range of the coefficient of horizontal subgrade reaction k_h to be used for various soil types. Their recommendations for granular soils are presented in Table 2. These values are considerably greater than those recommended by Terzaghi for depths of practical interest.

Work by Bowles [*13*] suggests using the following relationship

$$k = \bar{A} + \bar{B}Z^n \tag{7}$$

to predict distribution of the coefficient of horizontal or vertical subgrade reaction k with depth Z. In this equation, $\bar{A}$, $\bar{B}$, and n are constants. Values to be assigned to $\bar{A}$, $\bar{B}$, and n are not known at this time, but they can be determined for each particular site by working backward from the results of lateral-pile load tests.

TABLE 2—*Range of values of the coefficient of horizontal subgrade reaction* k_h [12].

Soil Type	k_h, kcf[a]
Silty fine sand	520 to 600
Medium sand	520 to 780
Dense sand and clay	2600 to 3460

[a]Note: to convert kcf to kN/m^3, multiply by 157.09.

For vertical coefficient of subgrade reaction k_v, Bowles [*13*] computes k_v from the ultimate bearing capacity (q_{ult}) of a continuous footing as

$$k_v = q_{ult}/y$$

For ultimate displacement of $y = 25.4$ mm (1 in.)

$$k_v = 12q_{ult} = 12CN_c + 12qN_q + 6\gamma BN\gamma \text{ (kcf)}$$

where

C = cohesion, ksf,
q = surcharge = γZ, ksf,
γ = unit weight, kcf, and
N_c and N_q = vertical bearing capacity factors with respect to cohesion and surcharge, respectively.

For granular soils, $C = 0$ and

$$k_v = 6\gamma BN\gamma + 12\gamma ZN_q \text{ (kcf)} \tag{8}$$

From a comparison of Eqs 7 and 8

$$\bar{A} = 6\gamma BN\gamma,\ \bar{B} = 12\gamma N_q, \text{ and } n = 1$$

Using above $\bar{A}$, $\bar{B}$, and n values, k_v can be obtained for a deflection of 25.4 mm (1 in.). Based on Francis [*14*] recommendations, k_h can be obtained by multiplying k_v by two to take account of side shear, thus

$$k_h = 12\gamma BN\gamma + 24\gamma ZN_q \text{ (kcf)} \tag{9}$$

The values of k_h obtained by means of Eq 9 are then checked against those given in Table 3 for possible gross errors. The recommended values for k_h of fine sand and medium sand in Table 3 are close to those of Zurabov and Bu-

TABLE 3—*Range of values of the coefficient of horizontal subgrade reaction* k_h *for sand and gravel* [13].

Soil Type	k_h, kcf[a]
Fine sand	500 to 1200
Medium sand	700 to 1800
Medium dense coarse sand	1000 to 2000
Dense sandy gravel	1400 to 2500

[a]Note: to convert kcf to kN/m^3, multiply by 157.09.

gayeva [*12*]. Research by Bowles [*13*] indicates that k_h is influenced by the pile shape as well. He recommends using Eq 9 for square piles but multiplying $\bar{A}$ and $\bar{B}$ by correction factors for round piles. It is noted that Eq 9 incorporates ultimate bearing capacity factors that correspond to the limiting state of a lateral bearing capacity failure. Such a condition is generally satisfied near the ground line at large lateral displacements of the pile, which in this case is assumed equal to 25.4 mm (1 in.).

Soletanche [*15*] based on experience from past projects prepared a plot of k_h as a function of shear strength parameters of soils. The k_h values for granular soils obtained from this plot are summarized in Table 4. These values are quite lower that those given by others in Tables 2 and 3.

Johnson and Kavanagh [*2*] obtained values of the constant of horizontal subgrade reaction n_h for granular soils above the water table using the bearing capacity criterion and assuming the horizontal and vertical soils moduli at shallow depths to be equal. These values are summarized in Table 5. The n_h

TABLE 4—*Values of the coefficient of horizontal subgrade reaction* k_h *for granular soils according to Soletanche* [15].

Angle of Internal Friction	k_h, kcf[a]
10	50
20	87
30	168
40	374

[a]Note: to convert kcf to kN/m^3, multiply by 157.09.

TABLE 5—*Values of the constant of the horizontal subgrade reaction* n_h, *kcf* [2].

Blows/ft N	8	10	15	20	30
n_h, kcf[a]	17	26	47	62	92

[a]Note: to convert kcf to kN/m^3, multiply by 157.09.

values are greater than those of Terzaghi (Table 1) except for loose sand where they are about equal.

For granular soils the Navy Design Manual [*16*] uses the following relationship to obtain the coefficient of horizontal subgrade reaction

$$k_h = fZ/B \tag{10}$$

where

f = coefficient of variation of lateral subgrade reaction,
Z = depth, and
B = width or diameter of loaded area.

From a comparison of Eqs 5 and 10, it is observed that the coefficient of variation of lateral subgrade reaction is the same as the constant of horizontal subgrade reaction. Typical values of f are presented in Table 6. These values are very close to Terzaghi values except at high relative densities where they are lower.

According to Menard [*5*] and test results on instrumented piles by Baguelin and Jazequel [*17*], the coefficient of horizontal subgrade reaction can be obtained from

$$k_h = 3.3E_m/B = 25\,P_\ell/B \tag{11}$$

where

k_h = coefficient of horizontal subgrade reaction, kN/m^3,
E_m = pressuremeter modulus, kPa,
P_ℓ = limit pressure, kPa, and
B = pile diameter, m.

Another method to estimate k_h from pressuremeter data is to use the following equation given by Poulos [*18*]

$$k_h = 0.8E_m/B \tag{12}$$

TABLE 6—*Values of the constant of horizontal subgrade reaction* n_h, kcf [15].[a]

	Relative Density of Sand			
Parameter	Loose	Medium	Dense	Very Dense
Blows/ft N	4 to 10	10 to 30	30 to 50	50+
ϕ, degrees	30	34	39	42
$n_h = f$	12	44	80	108

[a]Note: to convert kcf to kN/m^3, multiply by 157.09.

As can be seen, Eq 11 yields k_h values about four times those of Eq 12. Schmertmann [*19*] recommends using Eq 11 for flexible piles and Eq 12 for rigid piles.

Bowles [*13*] reviews several equations that can be used to estimate k_h from values of stress-strain modulus E_s. For practical range of interest he obtains

$$k_h = 0.8 \text{ to } 1.3E_s/B$$

Various laboratory and field tests to obtain E_s are summarized by Bowles [*13*].

Reese et al [*20*] performed field load tests on instrumented piles in saturated sand and obtained n_h values, which were 2.5 to 3.9 times greater than those recommended by Terzaghi for static and cyclic loadings, respectively. Their recommended n_h values for submerged sand are shown in Table 7.

Audibert et al [*21*], based upon results of an extensive laboratory testing program and an in-situ test, presented the following relationship for buried pipes in air-dried sand

$$k_h = 1/(A + By) \tag{13}$$

where

$A = 0.145y_u/\gamma ZN_q$,
$B = 0.855/\gamma ZN_q$,
y_u = ultimate displacement, and
N_q = bearing capacity factor given by charts.

Sogge [*22*] proposes the following simple relationship to obtain a range of k_h values for shallow piles

$$k_h = (2 \text{ to } 30)Z/B(\text{kcf})$$

in which B is pile width, and Z is depth.

Robinson [*4*] shows that k_h is practically independent of the pile width and, based upon the results of field load tests on timber piles in cohesionless soils, presents the relationship between the constant of the horizontal subgrade re-

TABLE 7—*Recommended values of the constant of the horizontal subgrade reaction* n_h, *kcf, for submerged sand* [20].[a]

Parameter	Relative Density		
	Loose	Medium	Dense
Recommended n_h, kcf	35	104	216

[a]Note: to convert kcf to kN/m^3, multiply by 157.09.

action n_h and the standard penetration resistance. In computing n_h, the displacements were measured at the ground surface. The computed n_h was then plotted against the average blow count of the upper 3.05 m (10 ft). Robinson's results indicate that the horizontal subgrade modulus is not only a function of the relative density of the sand but also a function of the magnitude of the applied horizontal load and, therefore, the displacement. Typical values of n_h obtained from Robinson's plot are shown in Table 8. For comparison, Terzaghi's range of n_h for the same blow counts is 1257 to 2199 KN/m^3 (8 to 14 kcf) (Table 1). Robinson's values are 2 to 14 times greater than those given by Terzaghi.

Based on a series of field load tests, Alizadeh and Davisson [*23*] obtained curves of n_h versus pile deflection. They showed that n_h is a function of pile deflection particularly for deflections less than 0.5 in. At greater deflections, however, n_h approached a constant value. They reported n_h values that are many times greater than those of Terzaghi.

Bhushan and Askari[2] reported a series of seven field load tests on piers 0.61 to 1.22 m (2 to 4 ft) in diameter in sand. Lateral loads of up to 880 KN (200 kips) were applied, and measurements of groundline deflection versus load were made. Based on the results of the load tests, the following relationship between n_h and the deflection was obtained

$$\log n_h = 0.82 + \log N - 0.62 \log (y/B)$$

where

N = blows per foot and
y/B = ratio of pile deflection to pile width in percent.

Ever since Terzaghi presented his typical values of the constant of the horizontal subgrade reaction (Table 1), there has been a growing trend to adopt higher modulus values as more load test data have become available. Based on available data, it is observed that Terzaghi's values present conditions approaching large lateral displacements. For lateral displacements of less than 12.7 mm (0.5 in.), Terzaghi values appear to be quite conservative.

TABLE 8—*Values of the constant of the horizontal subgrade reaction* n_h, *kcf* [4].[a]

	N, blows/ft			
Load, kip	2	4	6	8
6	26	69	130	259
10	14	43	95	173
12	10	29	69	147

[a]Note: to convert kcf to kN/m^3, multiply by 157.09; to convert kip to kN multiply by 4.448.

The range of values of the coefficient of horizontal subgrade reaction recommended by various authors are summarized in Fig. 1 for $\phi = 30°$. In preparing this plot Eq 5 was used when necessary to obtain k_h. Terzaghi values are for dry or moist sand; Alizadeh and Davisson values and the Bhushan and Askari line are for pile deflections of 12.7 mm (0.5 in.); Robinson values are for the lateral loads shown. Reese et al values correspond to the initial tangent modulus, and Sogge values are for shallow piles. Bowles equation is based on a pile deflection of 25.4 mm (1.0 in.). At a typical pile depth of $Z/B = 10$, it is seen that k_h can vary from a minimum of about 25.1 MN/m^3 (160 kcf) to a maximum of 377 MN/m^3 (2400 kcf), or a variation of 15 folds.

Proposed Relationship

The coefficient of horizontal subgrade reaction is influenced by many factors among which are the pile deflection, the effective overburden pressure, the relative density of soil, groundwater condition, nature of applied load (static or dynamic), and the properties and shape of the pile section. Load test data by Alizadeh and Davisson [*23*], Robinson [*4*], and Bhushan and Askari[2] have shown the importance of deflection, groundwater condition and the overburden pressure on the computed modulus value of granular soils. In particular they demonstrate that the constant of horizontal subgrade reaction is not a constant but decreases with increasing pile deflection. In Fig. 1, the

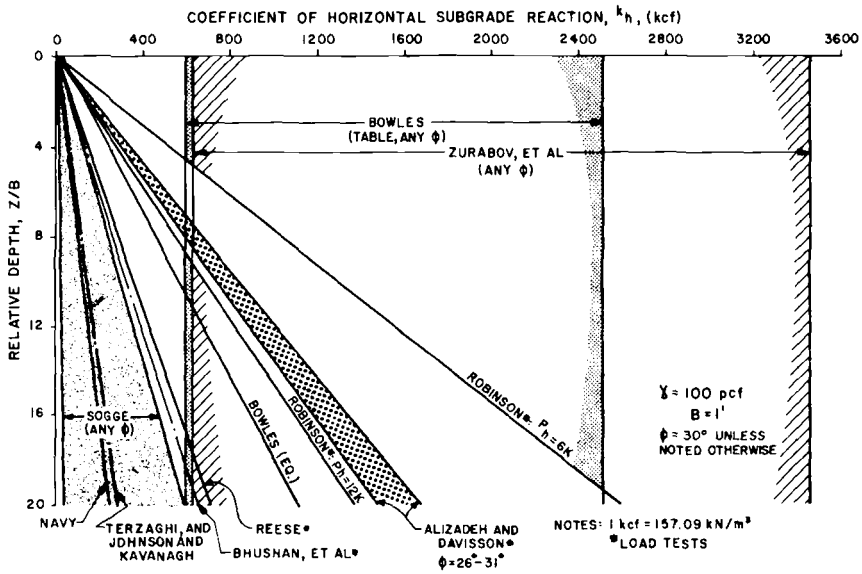

FIG. 1—*Comparison of* k_h *values from different sources.*

k_h values recommended by Terzaghi, Johnson and Kavanagh, and Sogge are satisfactory at high deflections, but they are quite conservative when used for small deflections. The coefficient of horizontal subgrade reaction k_h increases with depth and decreases with deflection. Equation 5 can be used to obtain k_h at a given depth by selecting the proper n_h value corresponding to the deflection at that depth. In a similar manner, if deflections over a pile segment can reasonably be assumed constant, Eq 5 can be used to obtain k_h for that segment.

Based on the bearing capacity concept as suggested by work of Bowles [*13*], and Audibert et al [*21*], a simple relationship to predict k_h as a function of deflection and effective overburden stress $\bar{\sigma}$ for a moist or dry granular soil is proposed as follows

$$k_h = \bar{\sigma} N_q / y \tag{14}$$

in which N_q is a lateral bearing capacity factor dependent on deflection. For laterally loaded piles, it is suggested to obtain N_q from the following relationship

$$N_q = (A + \sqrt{Z/B}) \tag{15}$$

in which A is a constant for any given deflection and angle of internal friction, and B is pile width. Using available load test data, the following values for A are recommended. For $\phi = 30°$, $A = 5$, 9, 12, and 15 for $y = 2.54$, 6.35, 12.7, and 25.4 mm (0.1, 0.25, 0.5, and 1.0 in.), respectively. N_q approaches ultimate N_q at high deflections.

From Eqs 14 and 15, the following equation for the coefficient of horizontal subgrade reactions is obtained

$$k_h = \bar{\sigma} / y (A + \sqrt{Z/B}) \tag{16}$$

A plot of variations of k_h with depth is shown in Fig. 2 for $y = 2.54$, 6.35, 12.7, and 25.4 mm (0.1, 0.25, 0.5, and 1.0 in.). For $y = 2.54$ mm (0.1 in.); the k_h values are several times greater than corresponding ones for $y = 25.4$ mm (1.0 in.). It is also noted that the k_h values for $y = 12.7$ mm (0.5 in.) are not close to the average of those for $y = 2.54$ and 25.4 mm (0.1 and 1.0 in.) but are closer to those for $y = 25.4$ mm (1.0 in.). In other words, a slight increase in deflection results in a rather large drop in the modulus. Since pile deflection decreases with depth, it is reasonable to divide the pile into segments and assign k_h values corresponding to large deflections for the upper portions, k_h values corresponding to low deflections for the lower pile segments, and k_h values in between these limits for the mid segments.

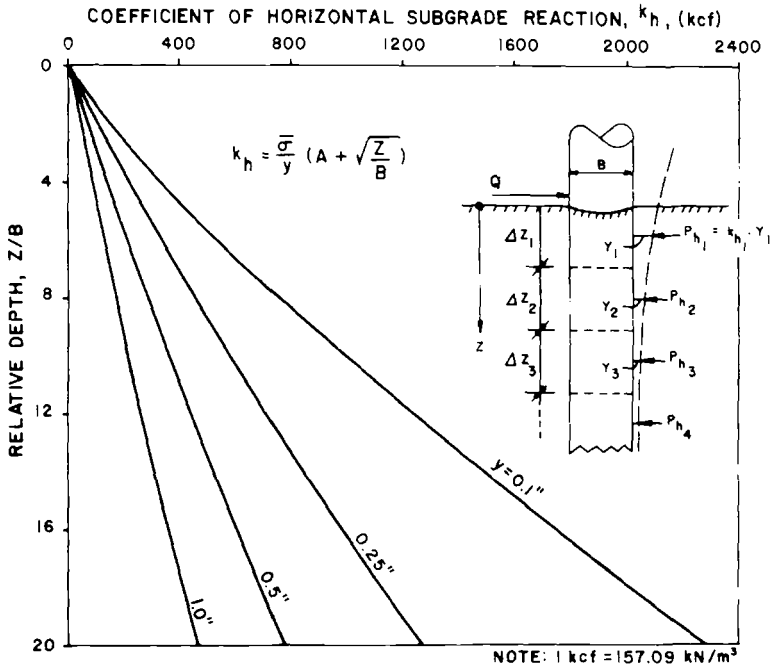

FIG. 2—*Proposed chart for estimating* k_h.

The coefficients of horizontal subgrade reaction obtained by means of Eq 16 are within the range of and, in general, lower than those reported by available load test data [*4,20,23*].[2] From a comparison of Figs. 1 and 2, it is seen that Eq 16 yields k_h values approaching Terzaghi's recommendations when deflections are in excess of 25.4 mm (1.0 in.).

Summary and Conclusions

The available empirical and semiempirical relationships as well as tables and charts for predicting the coefficient of horizontal subgrade reaction are reviewed. It is shown that a wide range of values of horizontal subgrade modulus can be obtained depending on the table, chart, or relationship used. From the available field load test data, it is observed that among the many factors that influence the coefficient of horizontal subgrade reaction, the magnitude of pile deflection, the effective overburden pressure and the relative density of the soil play a significant role. A simple relationship, Eq 16, is presented for predicting k_h of dry to moist granular soils based on these parameters. Predicted values from this equation for $\phi = 30°$ are within the range of available field data. Much more field load test data are needed for

a better understanding of the factors affecting the horizontal subgrade modulus and for refining and expanding the proposed relationship to other ϕ values.

Acknowledgments

The writers wish to thank Messrs. L. C. Reese and K. Bhushan for providing us with their data on laterally loaded piles, Mr. Joseph E. Bowles for his review of the manuscript and making many helpful suggestions, and Gannett Fleming Geotechnical Engineers, Inc., for their encouragement and support.

References

[1] Terzaghi, K., "Evaluation of Coefficients of Subgrade Reaction," *Geotechnique*, Vol. 5, No. 4, Dec. 1955, pp. 297-326.

[2] Johnson, M. S. and Kavanagh, C. T., *The Design of Foundations for Buildings*, McGraw Hill, New York, 1968.

[3] Kubo, K., "A New Method for the Estimation of Lateral Resistance of Piles," Report of the Port and Harbour Technical Research Institute, Vol. 2, No. 3, Tokyo, Japan, 1964.

[4] Robinson, K. E., "Horizontal Subgrade Reaction Estimated From Lateral Loading Tests on Timber Piles," *Behavior of Deep Foundations, STP 670*, American Society of Testing and Materials, Philadelphia, 1979, pp. 520-536.

[5] Menard, L., "Comportement d'une Foundation Profonde soumise a' des Efforts de Renversement," *Sols-Soils*, No. 3, Dec. 1962, pp. 9-23.

[6] Palmer, L. A., "Field Loading Tests for the Evaluation of the Wheel-Load Capacity of Airport Pavements," *Symposium on Load Tests of Bearing Capacity of Soils, STP 79*, American Society for Testing and Materials, Philadelphia, 1947, pp. 9-40.

[7] Yong, R. Y. N., "A Study of Settlement Characteristics of Model Footings on Silt," First Pan-American Conference on Soil Mechanics and Foundation Engineering, Mexico City, Mexico, 1960, pp. 492-513.

[8] Broms, B. B., "Lateral Resistance of Piles in Cohesive Soils," *Proceedings of the American Society of Civil Engineers*, Vol. 90, No. SM2, March 1964, pp. 27-63.

[9] Skempton, A. W., "The Bearing Capacity of Clays," Building Research Congress, Institute of Civil Engineers, London, Division I: 180, 1951.

[10] Davisson, M. T., "Lateral Load Capacity of Piles," National Academy of Sciences, Highway Research Record, No. 333, Washington, D.C., 1970, pp. 104-112.

[11] Vesic, A. B., "Beams on Elastic Subgrade and Winkler's Hypothesis," *5th International Conference on Soil Mechanics and Foundry Engineering*, Paris, 1961.

[12] Zurabov, G. G. and Bugayeva, D. E., *Vysokie Svaynue Rostverki Mostov*, Moscow, 1949.

[13] Bowles, J. E., *Foundation Analysis and Design*, McGraw Hill, New York, 1982.

[14] Francis, A. J., "Analysis of Pile Groups with Flexural Resistance", *Proceedings of the American Society of Civil Engineers*, Vol. 90, No. SM-3, May 1964.

[15] Soletanche Design Criteria, Permanent Ground Anchors, Final Report No. FHWA/RD-81/150, U.S. Department of Transportation, Federal Highway Administration, Sept. 1982, pp. 18-22.

[16] Navy Design Manual, *Foundations and Earth Structures*, Design Manual 7.2, Department of the Navy, Naval Facilities Engineering Command, May 1982.

[17] Baguelin, F. and Jazequel, J., "Etude Experimentale du Comportement de Picux Sollicite's Horizontalement," Laboratoire Central des Ponts et Chaussees Bulletin de Liaison des Laboratoires des Routiers Ponts et chaussees, No. 62, Laboratoire, Paris, France, Nov.-Dec., 1972.

[18] Polous, H. G., "Behavior of Laterally Loaded Piles: I. Single Piles," *Proceedings of the American Society of Civil Engineers*, Vol. 97, SM5, May 1971, pp. 711-731.

[19] Schmertmann, J. H., *Guidelines for Cone Penetration Test Performance and Design*, Federal Highway Administration, U.S. Dept. of Transportation, Washington, D.C., 1978.

[20] Reese, L. C. Cox, W. R., and Koop, F. D., "Analysis of Laterally Loaded Piles in Sand," *6th Annual Offshore Technology Conference*, Houston, Tex., 1974.

[21] Audibert, J. M. E. and Nyman, K. J., "Soil Restraint Against Horizontal Motion of Pipes," *American Society of Civil Engineers, Proceedings of the Geotechnical Engineering Division*, Vol. 103, No. GT 10, Oct. 1977, pp. 1119-1142.

[22] Sogge, R. L., "Laterally Loaded Pile Design," *Proceedings of the American Society of Civil Engineers*, Vol. 107, No. GT 9, Sept. 1981, pp. 1179-1199.

[23] Alizadeh, M. and Davisson, M. T., "Lateral Load Tests on Piles—Arkansas River Project," *Proceedings of the American Society of Civil Engineers*, Vol. 96, No. SMS, Sept. 1970, pp. 1583-1604.

Robert L. Sogge[1]

Microcomputer Analysis of Laterally Loaded Piles

REFERENCE: Sogge, R. L., **"Microcomputer Analysis of Laterally Loaded Piles,"** *Laterally Loaded Deep Foundations: Analysis and Performance, ASTM STP 835*, J. A. Langer, E. T. Mosley, and C. D. Thompson, Eds., American Society for Testing and Materials, 1984, pp. 35-48.

ABSTRACT: The finite-element formulation is applied to the vertical beam-on-elastic foundation idealization of a laterally loaded pile system. This representation is such that any standard structural analysis program having beam members can be used. An example problem consisting of a laterally loaded pile in a nonhomogeneous soil is analyzed in detail. The simulation is conducted on a CP/M 64K random access memory (RAM) microcomputer. The soil strength properties are defined in terms of a net coefficient of subgrade reaction and represented by bar members. The input data file and the computer output are presented. The numerical analysis clearly demonstrates the influence of soil and structural stiffness on pile behavior and the ease of obtaining a solution, by use of a computer, when nonhomogeneous soil conditions exist.

KEY WORDS: computers, computer analysis, design method, laterally loaded piles, soil structure interaction, soil stresses, coefficient of subgrade reaction

Theories for analyzing the behavior of piles subject to lateral loads and moments with various top-end restraints have been available for some time. Because of the complexity of solving the problem, approximate methods have been used by engineers to predict pile behavior. With the recent development of small computers having the power of the large mainframe computers used 15 years ago, laterally loaded pile models and their numerical complexities can be handled easily using a structural computer program on a desktop microcomputer.

The advantages of modeling a soil continuum by discrete springs or discrete continuous elements are great when compared to solutions by differential equation [*1*] and elastic continuum [*2,3*] formulations. These latter solutions suffer from difficulties when the soil modulus varies with depth.

[1]Principal engineer, Desert Earth Engineering, 524 N. 6th Ave., Tucson, Ariz. 85705.

The theories used to predict laterally loaded pile performance can be grouped into two types, those that use a soil strength defined by a coefficient of subgrade reaction and those that use an elastic modulus. The latter approach requires extensive modeling of the entire soil region. The former soil strength characterization requires a more convenient discrete modeling of the soil with springs. This approach is identical to the Hetenyi [*4*] beam-on-elastic foundation model, which uses the Winkler assumption of independent springs. Such modeling, complete with strength variation with depth, can easily be developed. Solutions obtained with this model are identical to those obtained using the closed form solution of the governing differential equation.

A discrete model will be used in this presentation. Springs (bar members) will be used to represent the soil and beam members to represent the pile.

Soil Strength

For this model, the soil strength must be characterized by a relation between soil pressure and displacement. A coefficient of subgrade reaction k provides such a representation. The soil strength curves shown in Fig. 1 represent pressure-displacement relations for various soils. The pressure p value represented in Fig. 1 is a net resistance value or the combination of active on one side and passive on the other. A secant relation is used to linearize the relation. This secant k value should represent pressure values less than one-half their ultimate values.

Ranges of values for the maximum value of the coefficient of subgrade reaction k_{max} are presented in Table 1. These values are similar to those presented by Terzaghi [*5*]. Various soil strength distributions can be portrayed using a parameter n defining the rate of variation of k with depth below the ground surface y. The soil strength at any depth y is then

$$k = k_{max}(y/L)^n$$

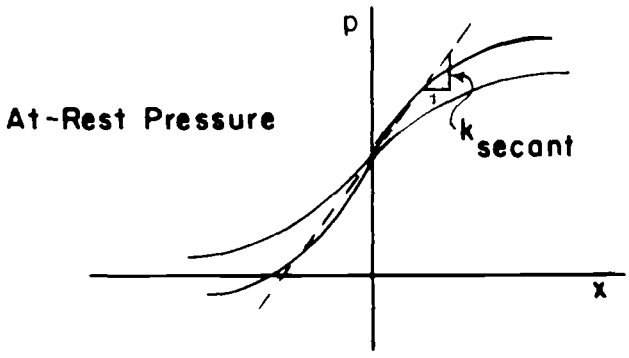

FIG. 1—*Soil pressure-displacement strength relation.*

TABLE 1—*Typical* k_{max} *values.*[a]

Sands, kcf		Clays, kcf
Dry or moist	5 to 40 L/B	50 to 110 $q_u/1.5B$
Submerged	3 to 25 L/B	...

[a]Note: L = distance below ground to bottom of sand layer or pile, whichever is smaller, ft, B = pile width, ft, and q_u = unconfined compressive strength, ksf.

where L equals the length of the pile. Distributions are shown in Fig. 2 for various n values. It is most important to describe the soil strength accurately in the upper third of the pile since k values below this depth have little influence on pile behavior.

Bowles [6] describes the soil strength as

$$k = A + By^n$$

where A, B, and n are constants. Such a characterization can be used where appropriate.

Model

The example problem to be analyzed consists of the pile and nonhomogeneous soil layers shown in Fig. 3. The finite-element model representation of this system is presented in Fig. 4. A model similar to this idealization has been used by Bowles [6] and Desai and Kuppusamy [7].

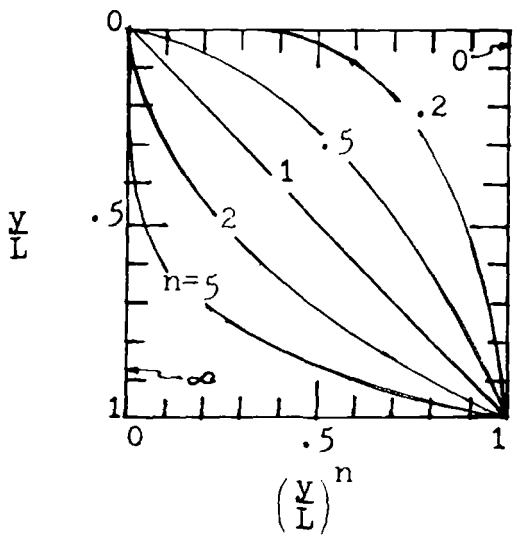

FIG. 2—*Soil strength variation with depth versus* n.

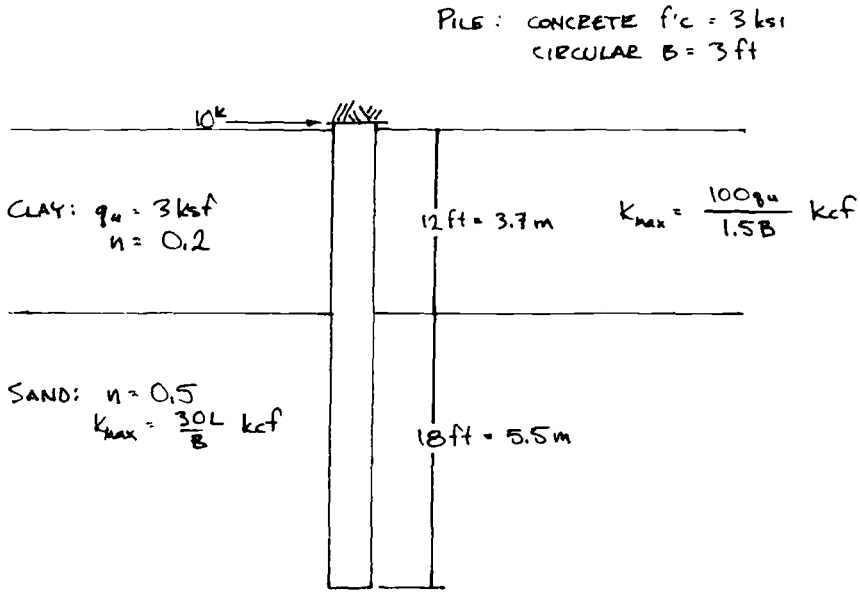

FIG. 3—*System configuration.*

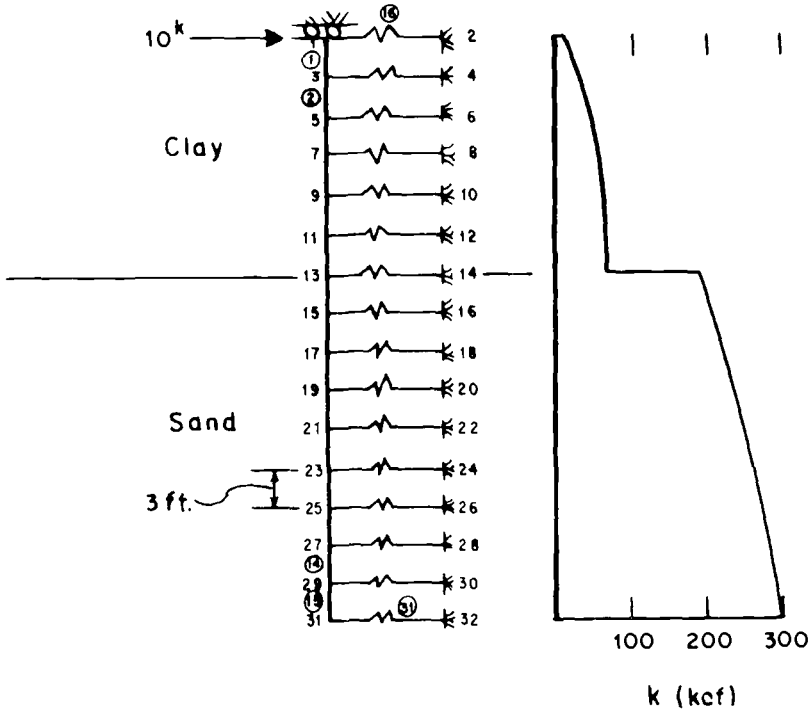

FIG. 4—*Finite-element model.*

Springs need only to be placed on one side of the pile since a net resistance value, passive minus active type, of resistance is used. The output soil pressure value is the pressure additional to the at-rest pressure.

The bar member representation of the soil is developed as follows.

For a bar member

$$P = A\sigma$$
$$\sigma = E\epsilon$$
$$\epsilon = (1/L)x$$

where $P, A, \sigma, E, \epsilon, L$ and x are the member load, area, stress, elastic modulus, strain, length and displacement, respectively.

Combining the above relation yields.

$$P = (AE/L)x$$

But, for soil

$$P = Akx$$

Therefore, let

$$A \text{ of bar} = \text{contributory soil area}$$
$$L \text{ of bar} = \text{unity}$$
$$E \text{ of bar} = k \text{ of soil}$$

To make a bar member out of a beam member, set its moment of inertia equal to zero and support its rotational degree of freedom at the support. In lieu of this approach a beam element with a very small moment of inertia could be used.

In this model the gross moment of inertia of the pile section is used. This value assumes that the section is uncracked, a reasonable assumption in the elastic range at loads less than one-half ultimate values. Both the beam and the bar properties in this model can be readily altered to simulate step-tapered piles and soil properties for layered systems. In representing layered systems only those layers within 0.3 times the pile length from the ground surface greatly affect system response. Top-end restraint conditions can be imposed. The support conditions at the bottom tip are not important.

Computer Program

The analysis outlined can be carried out by any structural analysis program containing beam elements. Because of the small size of the structural system and the resulting small memory storage requirements for the stiffness array, this analysis can readily be conducted using a microcomputer. The analysis program for this could be the same as used on large mainframe computers.

```
Program  PLNFRAM  by R. L. SOGGE  -  Desert Earth Engineering
INPUT DRIVE, INPUT FILENAME = B, PFILLP5
PLNFRAM - Laterally Loaded Pile - Example Problem
NO OF  JTS   MEMBERS     MATLS SUPTD JTS LODED JTS  FEF MBRS
      32        31         17        17         1         0
JOINT          X-COORDINATE  Y-COORDINATE
 1               0              0
 2               1              0
 3               0             -2
 4               1             -2
 5               0             -4
 6               1             -4
 7               0             -6
 8               1             -6
 9               0             -8
 10              1             -8
 11              0            -10
 12              1            -10
 13              0            -12
 14              1            -12
 15              0            -14
 16              1            -14
 17              0            -16
 18              1            -16
 19              0            -18
 20              1            -18
 21              0            -20
 22              1            -20
 23              0            -22
 24              1            -22
 25              0            -24
 26              1            -24
 27              0            -26
 28              1            -26
 29              0            -28
 30              1            -28
 31              0            -30
 32              1            -30
MEMBER         P-JOINT       Q-JOINT       MATL TYPE
 1               1             3             1
 2               3             5             1
 3               5             7             1
 4               7             9             1
 5               9             11            1
 6               11            13            1
 7               13            15            1
 8               15            17            1
 9               17            19            1
 10              19            21            1
```

(cont'd)

```
 11              21            23            1
 12              23            25            1
 13              25            27            1
 14              27            29            1
 15              29            31            1
 16              1             2             2
 17              3             4             3
 18              5             6             4
 19              7             8             5
 20              9             10            6
 21              11            12            7
 22              13            14            8
 23              15            16            9
 24              17            18            10
 25              19            20            11
 26              21            22            12
 27              23            24            13
 28              25            26            14
 29              27            28            15
 30              29            30            16
 31              31            32            17
MATL TYPE      ELASTIC MOD   AREA          MOM INRTA
 1              450000        7.07          3.98
 2              12            1             0
 3              47            2             0
 4              54            2             0
 5              58            2             0
 6              61            2             0
 7              64            2             0
 8              129           2             0
 9              205           2             0
 10             219           2             0
 11             232           2             0
 12             245           2             0
 13             257           2             0
 14             268           2             0
 15             279           2             0
 16             290           2             0
 17             300           1             0
SUPPORT DIRECTIONS (INDICATED BY 1)
JOINT          HORZ          VERT          ROTATION
 1              0             1             1
 2              1             1             1
 4              1             1             1
 6              1             1             1
 8              1             1             1
 10             1             1             1
 12             1             1             1
 14             1             1             1
```

FIG. 5—*Computer input listing.*

The program used is a straightforward beam-element program. It is 344 lines in length as written in Microsoft's version of the BASIC language. Input data are stored as a sequential data file on a floppy disk. The file is created by using a word processing program. The data are then called off of the disk by the program during execution. This approach is more efficient than inputting the data interactively. The approach simulates the data deck or tape file input used with mainframes. If a change or correction in data is desired, it is not necessary to recreate the entire data file.

```
 16          1           1           1
 18          1           1           1
 20          1           1           1
 22          1           1           1
 24          1           1           1
 26          1           1           1
 28          1           1           1
 30          1           1           1
 32          1           1           1
JOINT       HORZ LOAD    VERT LOAD    MOMENT
 1           10           0           0
MEMBER                  FIXED-END  FORCES
  NO.   MOMENT-P    MOMENT-Q     SHEAR-P     SHEAR-Q     AXIAL-P     AXIAL-Q
          THERE ARE NO MEMBER FIXED-END FORCES APPLIED
```

Continuation of Fig. 5.

The pattern for the data input is identical to that shown on the input listing of Fig. 5. The units used for input into this program are kips and feet. Metric conversion factors for the units used are given in Table 2. This listing is created by the program that reads the data off of the sequential data file and immediately writes it out.

The program took 5 min and 15 s to set up the 96 simultaneous equations and 1 min and 30 s to solve them. Figure 6 presents the computer output. A graphical plot of the output is presented in Fig. 7*a* through *c*.

Design Approach

1. Select a design configuration, both length and section, to be analyzed.
2. Choose soil properties and variation of k with depth.
3. Develop k values with depth.
4. Create input data file.
5. Run computer program.
6. Check to see that chosen section can handle moment imposed in section, deflections are tolerable, and soil pressure is reasonable. Typically, the maximum soil pressure should be less than 2 q_u for clays and 1.3 times the Rankine active pressure for sands. This limit on soil pressure occurs since a linear value of k is used in the model.

TABLE 2—*Conversion factors.*

Inch-Pound Units	Metric
1 ft	0.305 m
1 ft^2	0.093 m^2
1 ft^3	0.028 m^3
1 kip	4.45 KN
1 ksf	47.9 KN/m^2
1 ksi	6900 KN/m^2
1 kcf	159 KN/m^3

Soil-Structure Interaction

The soil-structure interaction inherent in these systems can be investigated by varying the ratio of the soil stiffness to the structural stiffness. It is this ratio that governs the moment and deflection of the pile and the soil pressure. The soil stiffness is proportional to

$$\sqrt[4]{Bk_{\max}}$$

The structural stiffness is proportional to

$$\sqrt[4]{4EI/L^4}$$

Their ratio denoted as the soil-structure stiffness ratio is

$$S = \sqrt[4]{(Bk_{\max}L^4)/(4EI)}$$

NO. OF EQNS = 96 BANDWIDTH = 9 JOINT SEP = 2

JOINT	HORZ DISP	VERT DISP	ROTATION
1	.0077573	0	3.02322E-13
2	7.16059E-11	0	0
3	7.64375E-03	0	1.09866E-04
4	7.56329E-11	0	0
5	7.33205E-03	0	1.98408E-04
6	7.26479E-11	0	0
7	6.86321E-03	0	2.67314E-04
8	6.80455E-11	0	0
9	6.27471E-03	0	3.18359E-04
10	6.22369E-11	0	0
11	5.60052E-03	0	3.53287E-04
12	5.5571E-11	0	0
13	.0048712	0	3.73756E-04
14	4.85239E-11	0	0
15	4.11367E-03	0	3.81965E-04
16	4.10366E-11	0	0
17	3.34932E-03	0	3.81203E-04
18	3.34169E-11	0	0
19	2.59249E-03	0	3.74988E-04
20	2.58692E-11	0	0
21	1.85101E-03	0	3.66304E-04
22	1.84724E-11	0	0
23	1.12735E-03	0	3.57506E-04
24	1.12516E-11	0	0
25	4.19955E-04	0	3.50255E-04
26	4.19173E-12	0	0
27	-2.75298E-04	0	3.45448E-04
28	-2.74805E-12	0	0
29	-9.63519E-04	0	3.43166E-04
30	-9.61861E-12	0	0
31	-1.64912E-03	0	3.42614E-04
32	-1.64364E-11	0	0

(cont'd)

JOINT	HORZ REACTION	VERT REACTION	MOMENT
1	-1.02901E-03	0	-108.291
2	-.0930876	0	0
4	-.718512	0	0
6	-.791862	0	0
8	-.796132	0	0
10	-.765514	0	0
12	-.716866	0	0
14	-1.25677	0	0
16	-1.6866	0	0
18	-1.467	0	0
20	-1.20292	0	0
22	-.906995	0	0
24	-.579458	0	0
26	-.225096	0	0
28	.153616	0	0
30	.558841	0	0
32	.494734	0	0

FIG. 6—*Computer output listing.*

OUTPUT DRIVE:OUTPUT FILENAME = B:PFO

MEMBER	MOMENTS		SHEARS		AXIAL FORCES		AXL STRS
NO.	P-END	Q-END	P-END	Q-END	P-END	Q-END	
1	-1.08E+02	8.85E+01	9.91E+00	-9.91E+00	0.00E+00	0.00E+00	0.00E+00
2	-8.85E+01	7.01E+01	9.19E+00	-9.19E+00	0.00E+00	0.00E+00	0.00E+00
3	-7.01E+01	5.33E+01	8.40E+00	-8.40E+00	0.00E+00	0.00E+00	0.00E+00
4	-5.33E+01	3.81E+01	7.60E+00	-7.60E+00	0.00E+00	0.00E+00	0.00E+00
5	-3.81E+01	2.44E+01	6.83E+00	-6.83E+00	0.00E+00	0.00E+00	0.00E+00
6	-2.44E+01	1.22E+01	6.12E+00	-6.12E+00	0.00E+00	0.00E+00	0.00E+00
7	-1.22E+01	2.49E+00	4.86E+00	-4.86E+00	0.00E+00	0.00E+00	0.00E+00
8	-2.49E+00	-3.86E+00	3.17E+00	-3.17E+00	0.00E+00	0.00E+00	0.00E+00
9	3.86E+00	-7.27E+00	1.71E+00	-1.71E+00	0.00E+00	0.00E+00	0.00E+00
10	7.27E+00	-8.28E+00	5.05E-01	-5.05E-01	0.00E+00	0.00E+00	0.00E+00
11	8.28E+00	-7.48E+00	-4.03E-01	4.03E-01	0.00E+00	0.00E+00	0.00E+00
12	7.48E+00	-5.51E+00	-9.82E-01	9.82E-01	0.00E+00	0.00E+00	0.00E+00
13	5.51E+00	-3.10E+00	-1.21E+00	1.21E+00	0.00E+00	0.00E+00	0.00E+00
14	3.10E+00	-9.90E-01	-1.05E+00	1.05E+00	0.00E+00	0.00E+00	0.00E+00
15	9.90E-01	2.44E-04	-4.95E-01	4.95E-01	0.00E+00	0.00E+00	0.00E+00
16	0.00E+00	0.00E+00	0.00E+00	0.00E+00	-9.31E-02	-9.31E-02	-9.31E-02
17	0.00E+00	0.00E+00	0.00E+00	0.00E+00	-7.19E-01	-7.19E-01	-3.59E-01
18	0.00E+00	0.00E+00	0.00E+00	0.00E+00	-7.92E-01	-7.92E-01	-3.96E-01
19	0.00E+00	0.00E+00	0.00E+00	0.00E+00	-7.96E-01	-7.96E-01	-3.98E-01
20	0.00E+00	0.00E+00	0.00E+00	0.00E+00	-7.66E-01	-7.66E-01	-3.83E-01
21	0.00E+00	0.00E+00	0.00E+00	0.00E+00	-7.17E-01	-7.17E-01	-3.58E-01
22	0.00E+00	0.00E+00	0.00E+00	0.00E+00	-1.26E+00	-1.26E+00	-6.28E-01
23	0.00E+00	0.00E+00	0.00E+00	0.00E+00	-1.69E+00	-1.69E+00	-8.43E-01
24	0.00E+00	0.00E+00	0.00E+00	0.00E+00	-1.47E+00	-1.47E+00	-7.34E-01
25	0.00E+00	0.00E+00	0.00E+00	0.00E+00	-1.20E+00	-1.20E+00	-6.01E-01
26	0.00E+00	0.00E+00	0.00E+00	0.00E+00	-9.07E-01	-9.07E-01	-4.53E-01
27	0.00E+00	0.00E+00	0.00E+00	0.00E+00	-5.79E-01	-5.79E-01	-2.90E-01
28	0.00E+00	0.00E+00	0.00E+00	0.00E+00	-2.25E-01	-2.25E-01	-1.13E-01
29	0.00E+00	0.00E+00	0.00E+00	0.00E+00	1.54E-01	1.54E-01	7.68E-02
30	0.00E+00	0.00E+00	0.00E+00	0.00E+00	5.59E-01	5.59E-01	2.79E-01
31	0.00E+00	0.00E+00	0.00E+00	0.00E+00	4.95E-01	4.95E-01	4.95E-01

FIG. 6—*Computer output listing—continued.*

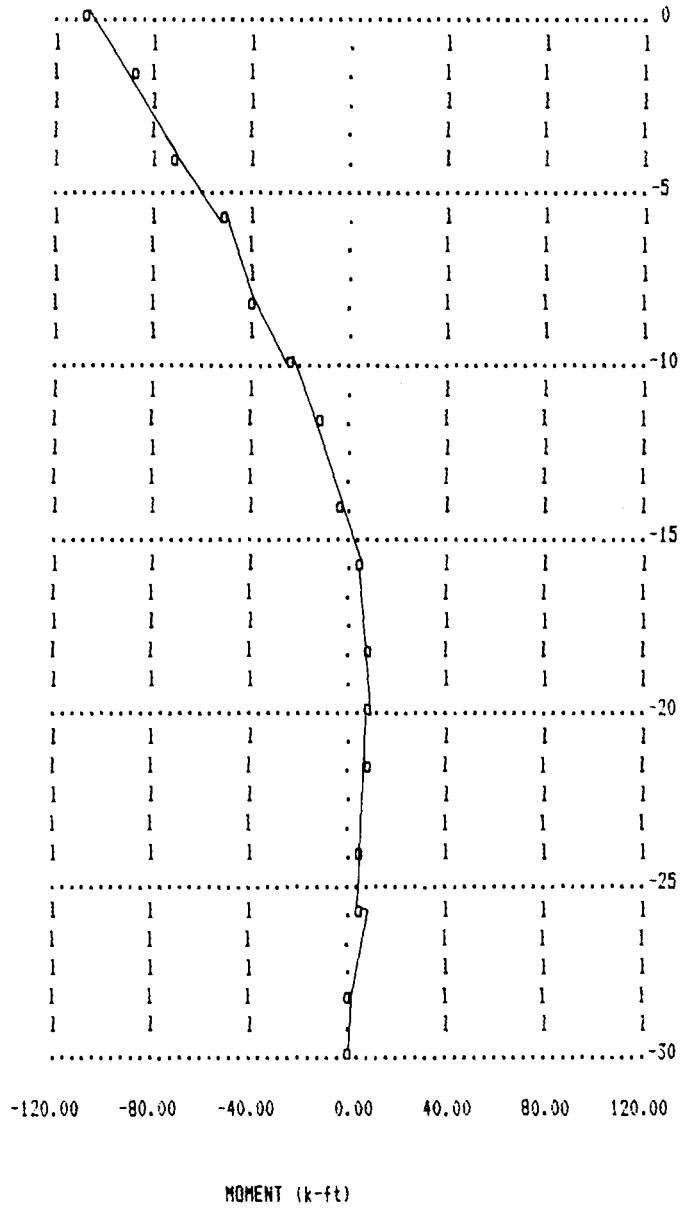

FIG. *7a—Computer output plot—moment.*

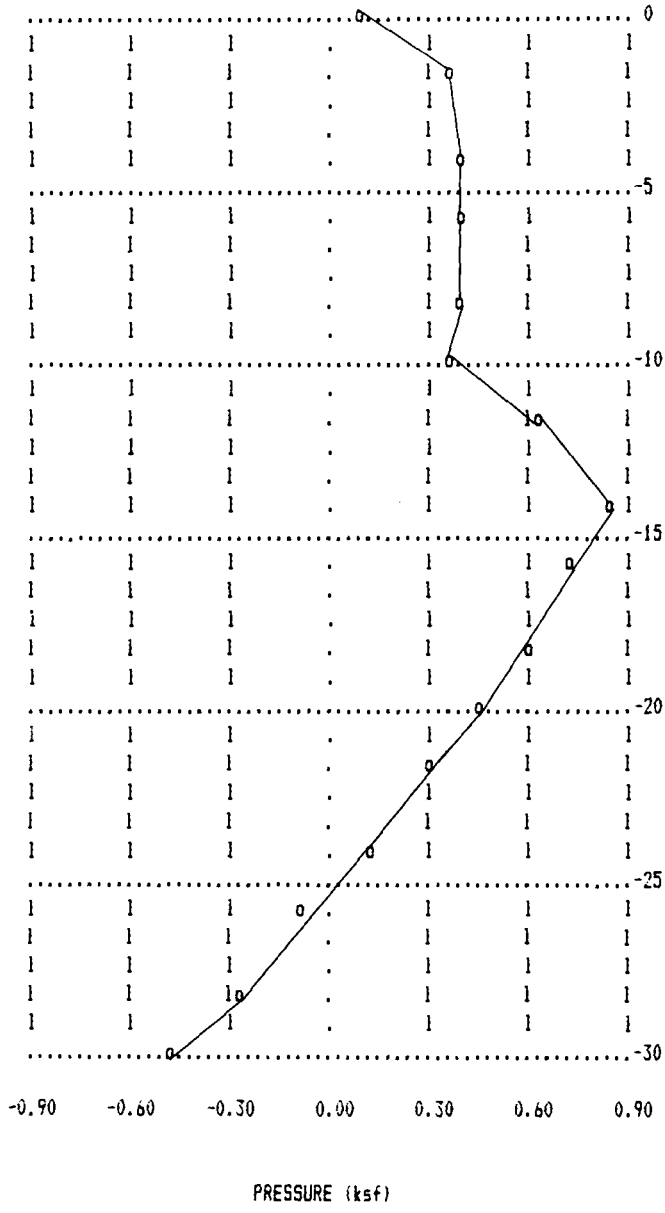

FIG. 7*b*—*Computer output plot—pressure.*

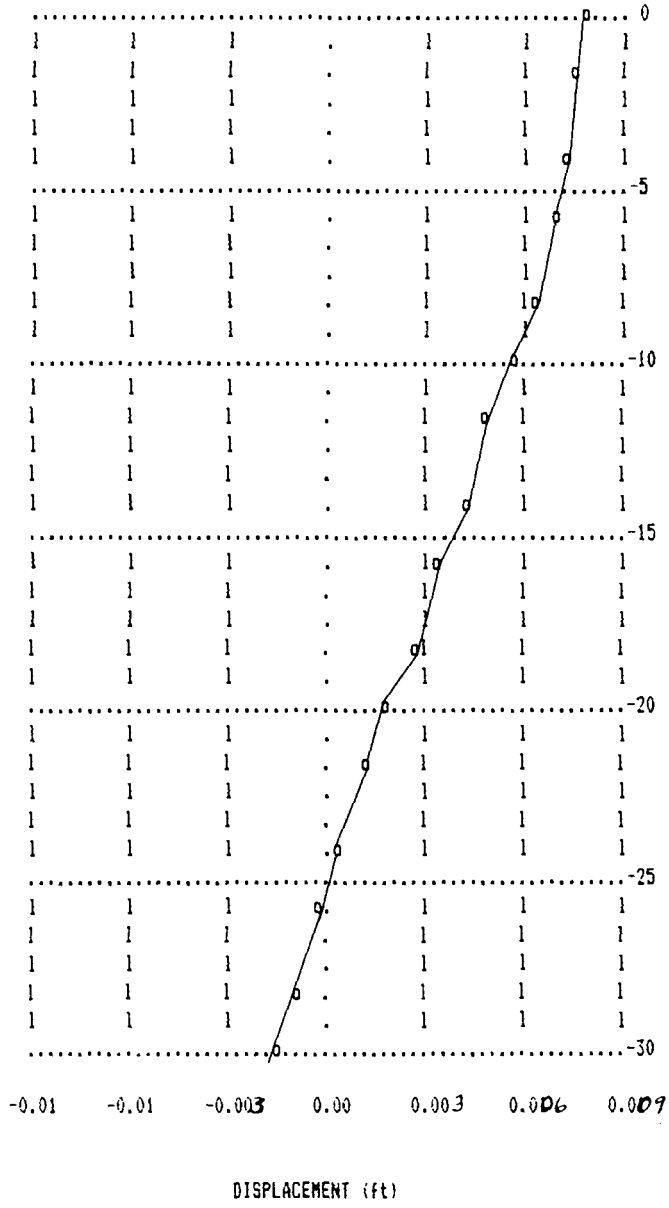

FIG. 7c—*Computer output plot—displacement.*

A plot showing how variations in this ratio affect the pile moment for a homogeneous soil-pile system subjected to a lateral load of Q on a free-end pile is presented in Fig. 8 [8].

Analysis of Entire System

Normally, the approach in the past has been to model the soil and structure as separate entities. The soil supporting the structure was modeled by a beam-on-elastic foundation supporting a laterally loaded pile or caisson. Loads anticipated from the structure were applied to the shaft. This analysis was done sometimes by the soil engineer and sometimes by the structural engineer. It provided the structural engineer the nebulous point of fixity from which he could make the highly indeterminate support reaction a fixed point support at a known location. This fixity point is often taken as the point of maximum moment.

To just fix such a point is not entirely correct since such a point will have some lateral translation as well as rotation. Truly, an interactive solution would be required to match the set of displacements on the soil and structure model for an equal but opposite applied force state. For such an approach, the most convenient spot for separating the two models is at the ground line.

A unified, more direct, and easier approach, rather than the disjointed approach presently employed, is to incorporate the soil model into the structure model. Such procedures are being used where the soil and the structural engineer work together in developing the model of the soil-structure system that is to be analyzed. Computer capabilities can easily handle the added degrees of

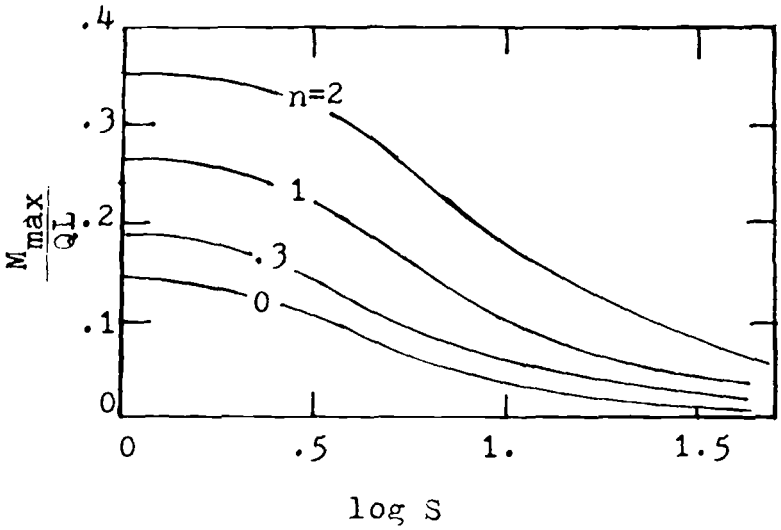

FIG. 8—*Soil-structure interaction.*

freedom imposed by the combined system model, and it is not necessary to take the "pseudo" substructure approach used in the past.

Different Soil Situations

Another laterally loaded pile situation arises where a cantilevered or anchored soldier pile system supports wood lagging. An uneven initial soil pressure would exist on each side of the pile. For such a system, it is necessary to use more complex models. Such models must be able to model the nonlinear $p - x$ soil properties since the movements of these systems reach active and passive failure states. Thus an incremental or an iterative solution as proposed by Haliburton [9] is necessary. It is also beneficial to model the construction sequence.

Disadvantages of Model

A disadvantage of the type of analysis presented herein as that it does not directly relate vertical loading to lateral soil pressures. Therefore, any vertical arching arising from horizontal pile movement is not apparent. Also, a dredge or backfill construction sequence cannot be modeled because of this limitation.

References

[1] Matlock, H. and Reese, L. C., "Generalized Solutions for Laterally Loaded Piles," *Journal of the Soil Mechanics and Foundations Division, Proceedings of the American Society for Civil Engineers*, Vol. 86, No. SM5, Oct. 1969, pp. 63-91.

[2] Spillers, W. R. and Stoll, R. D., "Lateral Response of Piles," *Journal of the Soil Mechanics and Foundations Division, Proceedings of the American Society for Civil Engineers*, Vol. 90, No. SM6, Nov. 1964, pp. 1-9.

[3] Poulos, H. G., "Behavior of Laterally Loaded Piles: I-Single Piles," *Journal of the Soil Mechanics and Foundations Division, Proceedings of the American Society for Civil Engineers*, Vol. 97, No. SM5, May 1971, pp. 711-731.

[4] Hetenyi, M., *Beams on Elastic Foundation*, University of Michigan Press, Ann Arbor, Mich., 1946, 255 pp.

[5] Terzaghi, K., "Evaluation of Coefficients of Subgrade Reaction," *Geotechnique*, London, England, Vol. 5, No. 4, Dec. 1955, pp. 297-326.

[6] Bowles, J. E., *Analytical and Computer Methods in Foundation Engineering*, McGraw-Hill Book Co., Inc., New York, 1974, p. 519.

[7] Desai, C. S. and Kuppusamy, T., "Procedure for a Soil-Structure Interaction Problem: Analysis and Evaluation," *Computing in Civil Engineering, Proceedings of the American Society for Civil Engineers*, Atlanta, Ga., June 1978, pp. 200-218.

[8] Sogge, R. L., "Laterally Loaded Pile Design," *Journal of the Geotechnical Engineering Division, Proceedings of the American Society for Civil Engineers*, Vol. 107, No. GT9, Sept. 1981, pp. 1179-1199.

[9] Haliburton, T. A., "Numerical Analysis of Flexible Retaining Structures," *Journal of the Soil Mechanics and Foundations Division, Proceedings of the American Society for Civil Engineers*, Vol. 94, No. SM6, Nov. 1968, pp. 1233-1251.

A. P. S. Selvadurai[1]

On the Torsional Stiffness of Rigid Piers Embedded in Isotropic Elastic Soils

REFERENCE: Selvadurai, A. P. S., **"On the Torsional Stiffness of Rigid Piers Embedded in Isotropic Elastic Soils,"** *Laterally Loaded Deep Foundations: Analysis and Performance, ASTM STP 835*, J. A. Langer, E. T. Mosley, and C. D. Thompson, Eds., American Society for Testing and Materials, 1984, pp. 49-55.

ABSTRACT: This paper develops an approximate expression for the torsional stiffness of a rigid cylindrical pier embedded in an isotropic elastic soil mass. The approximate solution is derived by considering the torsion of a hemispheroidal rigid inclusion embedded in bonded contact with an elastic medium. The expression for the torsional stiffness of the pier is expressed as a function of its length to diameter aspect ratio.

KEY WORDS: torsion, lateral forces, piles, embedded piers, embedded piles, torsional stiffness, isolated piles, torsional loading, elastic stiffness of piers

Relatively rigid pier-type foundations are used quite extensively as supports for structures that are subjected to lateral loads induced by wind or earthquakes [*1-3*]. In particular, isolated rigid piers form the most economical foundation system for supporting sensitive devices such as solar cell arrays. Owing to the large widths associated with these arrays the pier-type foundations are subjected to significant torsional effects. Other applications of the embedded rigid pier-type structures include foundations for pole-type transmission towers. Estimates for the torsional stiffnesses of these embedded pier-type rigid foundations are required in the static and dynamic analysis of the soil-pier interaction problem. This paper presents a method for estimating the static torsional elastic stiffness of rigid cylindrical piers embedded in an isotropic elastic soil medium (Fig. 1). The estimate is obtained by representing the embedded cylindrical pier as an inclusion that consists of an axisymmetric

[1]Professor and chairman of civil engineering, Carleton University, Ottawa, Ontario, Canada K1S 5B6.

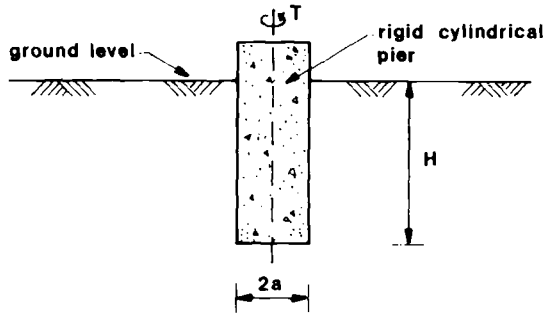

FIG. 1—*Geometry of the embedded rigid cylindrical pier.*

shape with a continuous surface. The problem is formulated within the context of a classical elasticity problem referred to a spheroidal coordinate system. The estimate for the torsional elastic stiffness of the cylindrical pier is provided as a set of bounds that can be determined from an exact analytical solution. From the numerical results presented in the paper it is possible to compute the elastic stiffness for the embedded cylindrical pier from a knowledge of its radius to length aspect ratio.

The modelling of the problem of torsional loading of the rigid pier discussed in this paper has similarities to the problem of the slow rotation of a spheroidal object in a viscous fluid [*4*]. Similar results have been derived by Apsel and Luco [*5*] and Selvadurai [*6*] in connection with the estimation of the dynamic and static torsional response, respectively, of foundations embedded either partially or fully in elastic soil media. The presentation of the theoretical development adopts the more direct formulation given in Ref *6*.

Analysis

To develop the elastic torsional stiffness for the embedded cylindrical foundation we consider the auxiliary problem of a hemispheroidal prolate rigid inclusion that is embedded in bonded contact with an elastic half space (Fig. 2). (A hemispheroidal inclusion is the solid of revolution obtained by rotating the half ellipse bounded by $z = 0$ and $\alpha = \alpha_0$ about the z axis.)

We consider a system of prolate spheroidal coordinates (α, β, γ) defined by the transformation

$$[x; y; z] = c_p[\sinh\alpha \sin\beta \cos\gamma; \sinh\alpha \sin\beta \sin\gamma; \cosh\alpha \cos\beta] \tag{1}$$

where c_p is a positive constant. The torsion of the hemispheroidal inclusion induces a state of rotationally symmetric deformation, which is characterized by the displacement field

$$u_\alpha = 0; \qquad u_\beta = 0; \qquad u_\gamma = u_\gamma(\alpha, \beta) \tag{2}$$

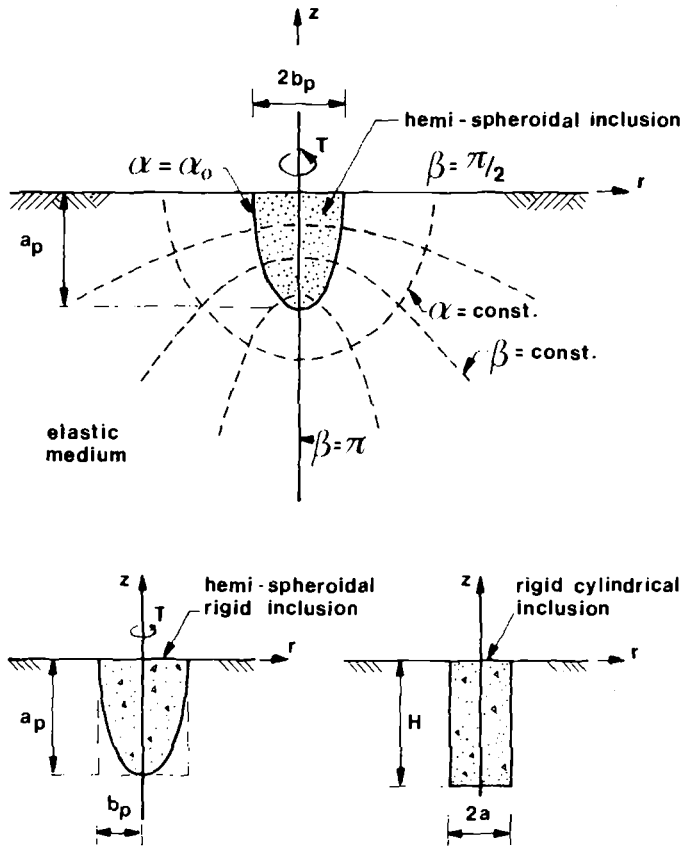

FIG. 2—*Geometry of the embedded hemispheroidal rigid inclusion.*

For this deformation, the nonzero components of the Cauchy stress tensor $\underline{\sigma}$ referred to the (α, β, γ) coordinate system are given by

$$\underline{\sigma} = \begin{bmatrix} 0 & \sigma_{\alpha\gamma} & 0 \\ \sigma_{\alpha\gamma} & 0 & \sigma_{\beta\gamma} \\ 0 & \sigma_{\beta\gamma} & 0 \end{bmatrix} \tag{3}$$

The corresponding linear elastic stress-strain relations are given by

$$[\sigma_{\alpha\gamma}; \sigma_{\beta\gamma}] = (Gh/h_3)[(\partial/\partial\alpha)(h_3 u_\gamma); \quad (\partial/\partial\beta)(h_3 u_\gamma)] \tag{4}$$

where

$$h = [c_p^2(\sinh^2\alpha + \sin^2\beta)]^{-1/2}; \qquad h_3 = [c_p \sinh\alpha \sin\beta]^{-1} \tag{5}$$

It can be shown [6] that a displacement function $\Omega(\alpha, \beta)$ can be introduced such that

$$u_\gamma = h_3 \Omega \tag{6}$$

and the equation of equilibrium yields the following differential equation for $\Omega(\alpha, \beta)$

$$[(\partial^2\Omega/\partial\alpha^2) + (\partial^2\Omega/\partial\beta^2) - \coth\alpha\,(\partial\Omega/\partial\alpha) - \cot\beta\,(\partial\Omega/\partial\beta)] = 0 \tag{7}$$

We now apply these results to develop an expression for the torsional stiffness of the prolate hemispheroidal inclusion that is embedded in bonded contact with the elastic medium. The boundary of the inclusion is denoted by $\alpha = \alpha_0$. To reproduce action of torsion of the embedded inclusion, we subject the inclusion to a torque T that causes a rigid body rotation ω about the axis of symmetry $\beta = 0$. The displacement boundary condition at the interface is

$$u_\gamma(\alpha_0, \beta) = \omega c_p \sinh\alpha_0 \sin\beta \tag{8}$$

Furthermore, since the elastic medium is of infinite extent, the displacements and stresses induced in the elastic medium should reduce to zero as $\alpha \to \infty$ and be single valued in $\alpha \in (\alpha_0, \infty)$, $\beta \in (\pi/2, \pi)$. It can be shown that the relevant solution for $\Omega(\alpha, \beta)$ takes the form

$$\Omega(\alpha, \beta) = (\omega c_p^2/\Phi_0) \sinh^2\alpha \sin^2\beta\, \Phi(\alpha) \tag{9}$$

where

$$\Phi(\alpha) = [(1/2)\,\ell n\,\xi - \coth\alpha\,\mathrm{csch}\,\alpha]; \xi = (\cosh\alpha + 1)/(\cosh\alpha - 1) \tag{10}$$

and $\Phi_0 = \Phi(\alpha_0)$. Expressions for the stresses and displacements in the elastic medium can be obtained by making use of Eq 9 and Eqs 4 and 6. In this paper we are primarily interested in developing a result for the torsional stiffness for the embedded inclusion. To this end, we evaluate the torque induced at the inclusion elastic medium interface. The resultant torque is given by

$$T = \int_0^{2\pi} \int_{\pi/2}^{\pi} [\sigma_{\alpha\gamma} c_p (\sinh\alpha \sin\beta / h\, h_3)]_{\alpha = \alpha_0} d\beta d\gamma \tag{11}$$

where the integrand is evaluated at $\alpha = \alpha_0$. Evaluating Eq 11 we obtain

$$T = \frac{16\pi G b_p^3\, \omega (1 - \lambda^2)^{3/2}}{3\lambda \left\{ 2(1 - \lambda^2)^{1/2} - \lambda^2\, \ell n \left[\dfrac{1 + (1 - \lambda^2)^{1/2}}{1 - (1 - \lambda^2)^{1/2}} \right] \right\}} \tag{12}$$

where b_p is the equatorial radius of the prolate spheroidal inclusion, and $\lambda (= b_p/a_p)$ is the aspect ratio.

Torsional Stiffness of the Rigid Cylindrical Pier

In order to develop an estimate for the torsional stiffness of the embedded rigid cylindrical pier we make use of Eq 12. The problem that remains is that of assigning a suitable value for λ and b_p in terms of the aspect ratio a/H and the radius a. To derive a value for λ in terms of a/H, it is possible to adopt three approaches.

Case I—It may be assumed that $\lambda = a/H$, indicating that the spheroidal region is contained within the boundary of the cylindrical surface of radius a and length H.

Case II—It may be assumed that $\lambda = a/H$ and that the volume of the hemispheroidal region is identical to the volume of the rigid cylindrical pier.

Case III— It may be assumed that $\lambda = a/H$ and that the surface area of the hemispheroidal region is identical to the surface area of the rigid cylindrical pier in contact with the elastic medium.

Considering the above cases it can be shown that the torsional elastic stiffness for the embedded rigid pier of embedded length H and radius a can be expressed in the form

$$(3T/16G\omega a^3) = T^* = C(\lambda)F(\lambda) \tag{13}$$

where

$$F(\lambda) = \frac{\pi(1-\lambda^2)^{3/2}}{\lambda\left\{2(1-\lambda^2)^{1/2} - \lambda^2 \ell n\left[\dfrac{1+(1-\lambda^2)^{1/2}}{1-(1-\lambda^2)^{1/2}}\right]\right\}} \tag{14}$$

where

$$\lambda = a/H \tag{15}$$

and $C(\lambda)$ is a function that depends on the three cases discussed previously. For example, for

$$\text{Case I:} \quad C(\lambda) = 1 \tag{16a}$$

$$\text{Case II:} \quad C(\lambda) = 3/2 \tag{16b}$$

$$\text{Case III:} \quad C(\lambda) = \left\{\frac{2(1-\lambda^2)^{1/2}}{[\lambda(1-\lambda^2)^{1/2} + \sin^{-1}\sqrt{1-\lambda^2}}\right\}^{3/2} \tag{16c}$$

Since in Case I the dimension b_p of the spheroidal region is set equal to a and since the aspect ratio $b_p/a_p = a/H$, it can be deduced that the torsional stiffness given by the results from Eqs 13 and 16a corresponds to the lower bound.

Case II represents an estimate in which the bulk volume of the rigid pier embedded in the elastic medium is related to the volume of the hemispheroidal region. This estimate would in general yield the upper bound of the elastic stiffness of the rigid pier. The estimate based on the concept of equal surface area, namely, Case III, is expected to yield an intermediate for the torsional stiffness of the rigid cylindrical pier.

Numerical Results and Conclusions

The estimates for the nondimensional elastic stiffness T^* for the rigid cylindrical pier as derived from the three cases discussed have been numerically evaluated for various values of H/a (Fig. 3). From these results it is evident

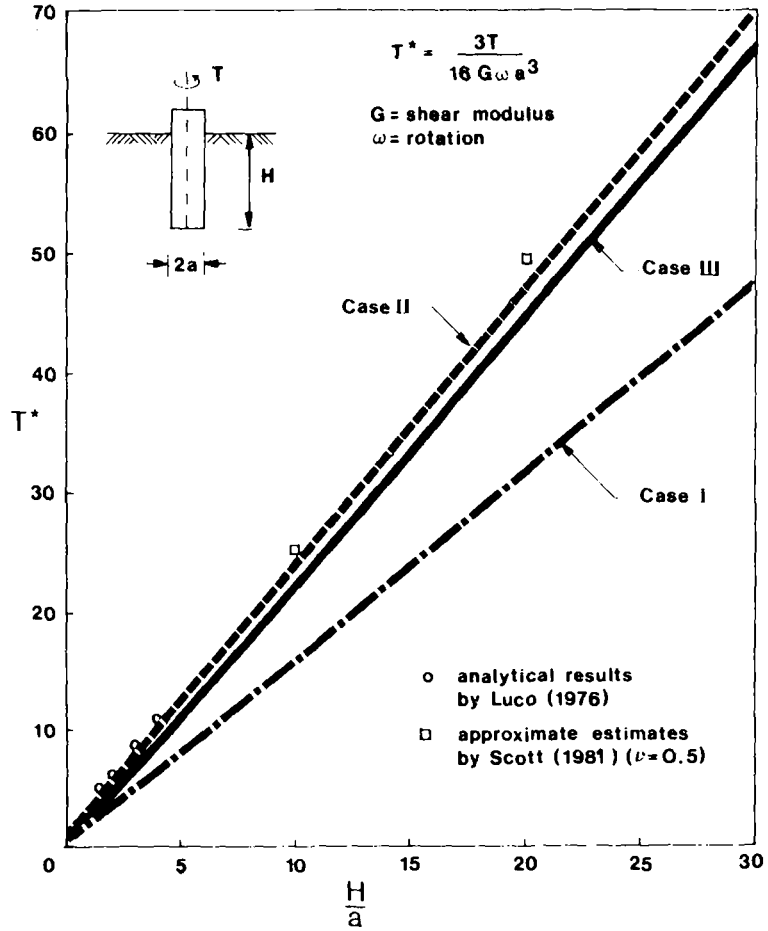

FIG. 3—*Variation of elastic torsional stiffness for a rigid circular pier with aspect ratio* H/a.

that the elastic stiffness is significantly influenced by the geometric aspect ratio H/a and that the results based on the hemispheroidal inclusion idealization yield results that may be used as suitable approximations in preliminary engineering calculations and estimates. An alternative to this approximate procedure is to use an exact mathematical formulation of the problem to derive the elastic stiffness for the embedded rigid pier. An example of such an analysis is given by Luco [7]. The mathematical analysis that is involved in the exact formulation is complicated and does not yield results that differ greatly from the present set of approximations. For purposes of comparison the results given by Luco [7] for $H/a = 1.5$, 2.0, 3.0, and 4.0 are also presented in Fig. 3. Other approximate procedures of the treatment of the embedded rigid pier problem use approximations in the representation of the stress state in the vicinity of the rigid pier. Details of these treatments together with accounts of finite-element studies of the static elastic stiffness of an embedded rigid cylindrical pier are discussed by Scott [8], Randolph [9], and Poulos and Davis [3].

References

[1] Stoll, U. W., "Torque Shear Test of Cylindrical Friction Piles," *Civil Engineering. American Society of Civil Engineers*, Vol. 42, No. 4, April 1972, pp. 63-65.

[2] Poulos, H. G., "Torsional Response of Piles," *Journal of the Geotechnical Engineering Division, Proceedings of the American Society of Civil Engineers*, Vol. 101, No. GT10, Oct. 1975, pp. 1019-1035.

[3] Poulos, H. G. and Davis, E. H., *Pile Foundation Analysis and Design*, John Wiley, New York, 1980, p. 237.

[4] Happel, J. and Brenner, H., *Low Reynolds Number Hydrodynamics*, Prentice-Hall, Englewood Cliffs, NJ, 1965, p. 351-353.

[5] Apsel, R. J. and Luco, J. E., "Torsional Response of Rigid Embedded Foundation," *Journal of the Engineering Mechanics Division, Proceedings of the American Society of Civil Engineers*, Vol. 102, No. EM6, Dec. 1976, pp. 957-970.

[6] Selvadurai, A. P. S., "On the Estimation of the Deformability Characteristics of an Isotropic Elastic Soil Medium by Means of a Vane Test," *International Journal for Numerical and Analytical Methods in Geomechanics*, Vol. 3, July-Sept. 1979, pp. 231-243.

[7] Luco, J. E., "Torsion of a Rigid Cylinder Embedded in an Elastic Halfspace," *Journal of Applied Mechanics*, Vol. 43, Sept. 1976, pp. 1-5.

[8] Scott, R. F., *Foundation Analysis*, Prentice-Hall, Englewood Cliffs, NJ, 1981, p. 298.

[9] Randolph, M. F., "Piles Subjected to Torsion," *Journal of the Geotechnical Engineering Division, Proceedings of the American Society of Civil Engineers*, Vol. 107, No. GT8, Aug. 1981, pp. 1095-1111.

Lymon C. Reese,[1] *Stephen G. Wright,*[1] *and Ravi P. Aurora*[2]

Analysis of a Pile Group Under Lateral Loading

REFERENCE: Reese, L. C., Wright, S. G., and Aurora, R. P., **"Analysis of a Pile Group Under Lateral Loading,"** *Laterally Loaded Deep Foundations: Analysis and Performance, ASTM STP 835*, J. A. Langer, E. T. Mosley, and C. D. Thompson, Eds., American Socicty for Testing and Materials, 1984, pp. 56–71.

ABSTRACT: One of the current approaches to the design of pile-supported structures in deep water is to place a cluster of piles along each of the four main legs of the platform. The piles in such a group would be in a circular pattern and spaced sufficiently close that significant interaction among piles in the soil would be expected.

The analysis of such a typical pile group in stiff clay is presented. Three approaches were used for performing the analyses: the Poulos-Focht-Koch approach, a modification of that approach, and the treatment of the pile group as an imaginary large diameter pile. With each of these methods, analyses were performed to investigate the effect of the variation of significant soil parameters through a range indicated by a study of the results from a field and laboratory investigation of soil properties. In each of the analytical approaches the methods of analysis of piles under lateral loading that makes use of curves showing soil resistance as a function of pile-deflection (p-y curves) were used.

The results of the analyses indicate the importance of the various parameters that are employed in the solution and should provide guidance in the acquisition of data on soil properties.

KEY WORDS: lateral loading, load tests, pile groups, p-y curves, single piles, soils, soil modulus

The analysis of the behavior of a closely spaced pile group under lateral loading is based on the concept that there is an interaction among piles in the group. The influence of one pile on the other piles in the group can be evaluated numerically by use of the equations of elasticity.

The single-pile behavior can be analyzed by the solution of a fourth-order, nonlinear differential equation in which the soil response is represented by a family of p-y curves. The p-y curves are dependent on pile geometry, soil

[1]The Nasser I. A. Rashid chair and associate professor of civil engineering, respectively, University of Texas, Austin, Tex. 78712.

[2]Marathon Oil United Kingdom, London, England.

properties, and depth below ground surface; degradation from cyclic loading is reflected. Several articles in the technical literature deal with the methods of determining p-y curves [*1-9*].

Focht and Koch [*10*] proposed a method of analysis that combines the use of elasticity to get influence coefficients [*11,12*] and the p-y analysis to obtain single pile behavior. The Focht-Koch method will be the principal method used in this paper.

Another approach is to assume that the pile group will behave as an imaginary large-diameter pile with the pile diameter taken as the diameter of the entire group and the stiffness of the imaginary pile taken as the sum of the stiffness of the individual piles.

The paper presents a study of the design of a nine-pile group at an offshore site. The study indicates the effects of varying certain parameters and should provide some guidance for those doing similar studies.

Summary of the Poulos-Focht-Koch Method

The following equation was developed by Poulos [*11,12*] to obtain the deflection and load on each of the piles in a group, assuming the soil to act elastically

$$\rho_k = \bar{\rho}_F \left(\sum_{\substack{j=1 \\ j \neq k}}^{m} H_j \alpha_{\rho Fkj} + H_k \right) \tag{1}$$

where

ρ_k = deflection of the k-*th* pile,
$\bar{\rho}_F$ = the unit reference displacement of a single pile under a unit horizontal load, computed by using the elastic theory,
H_j = lateral load on pile j,
$\alpha_{\rho Fkj}$ = the coefficient to get the influence of pile j on pile k,
H_k = the lateral load on pile k, and
m = number of piles in group.

If the total load on the group is H_G, then

$$H_G = \sum_{j=1}^{m} H_j \tag{2}$$

If the foundation is fabricated such that each of the piles is caused to deflect an equal amount, the deflection ρ_k is equal to the deflection of the group y_G. If there are m piles in the group $m + 1$ equations can be formulated using Eqs 1 and 2 and solved for the group deflection and the load H on each pile in the group.

In order to write the equations it is necessary to have the influence coeffi-

cients. Poulos has supplied a family of curves for the α-values with the curves based on a Poisson's ratio of 0.5. The curves must be entered with values of L/d, s/d, β, and K_R where L is pile length, d is pile diameter, s is center to center spacing, β is the angle between the line through the two piles in question and the line giving the direction of the loading, and K_R is defined by the following equation

$$K_R = (E_p I_p)/(E_s L^4) \tag{3}$$

where

E_p = modulus of elasticity of pile material,
I_p = moment of inertia of pile, and
E_s = soil modulus.

The Poulos curves [*12*] are used in this phase of the analyses.

Focht and Koch [*10*] have proposed modifications of the Poulos method. They suggested a revision of Eq 1 as follows

$$\rho_k = \bar{\rho}_F \left(\sum_{\substack{j=1 \\ j \neq k}}^{m} H_j \alpha_{\rho F k j} + R H_k \right) \tag{4}$$

where R is the relative stiffness factor.

The relative stiffness factor is the ratio of the mud-line deflection of a single pile computed by the p-y curve approach y_t to the deflection ρ computed by the Poulos method. In both instances, the lateral load on the single pile is the total lateral load on the pile group divided by the number of piles. Equation 5 is the Poulos equation for the deflection of a single pile with fixed head.

$$\rho = I_{\rho F}(H/E_s L) \tag{5}$$

The value of the influence coefficient $I_{\rho F}$ may be obtained from curves provided by Poulos [*11*], which assumes a Poisson's ratio of 0.5. The curves are entered with values of K_R and L/d.

It is important in using the Poulos equations to obtain a value of the soil modulus E_s that is as accurate as possible. It is generally agreed that the best method for determining E_s is to perform a field loading test. However, such tests frequently are not practical. In the absence of such tests some correlations of E_s with the undrained shear strength can be used as a rough guide, but stress-strain curves from triaxial tests can yield better values. Focht and Koch state that E_s should be selected from available stress-strain test results using a low stress level in the soil. They suggest that the value should be at least as great as the secant modulus corresponding to a stress equal to 50% of the strength and probably as great as the initial tangent modulus indicated by most laboratory tests.

Using Eqs 2 and 4, simultaneous equations are formulated and solved for the group deflection y_G and the lateral load on each pile in the group. The pile with the greatest load is selected for analysis by using modified p-y curves. The p-values are modified by employing a multiplication factor to reflect the "shadowing" effect of closely spaced piles. The y-values are modified by multiplying all of the deflections in the p-y curves by a Y factor of 2, 3, 4, and so on. The deflection of the single pile is computed with the modified p-y curves, and the Y factor is found that gives agreement between the single-pile deflection so computed and the deflection of the pile group. With this appropriate Y factor, the pile behavior can be computed with the modified p-y curves, completing the solution.

Comparison of Results

There are few experiments on groups of piles under lateral loading, Jamiolkowski [*13*] reports on the testing of a three-pile group. The piles were 45 m (148 ft) long, 500 mm (19.7 in.) in diameter, and were driven through a 10 m (32.8 ft) thick layer of loose to medium dense slightly silty sand, through 30 m (98.4 ft) of normally consolidated clay, and into dense sand. A load of 45 metric tons was applied through a rigid cap in a plane that passed through the axes of the piles. The piles were instrumented with inclinometer tubes, and a sensitive instrument was used to obtain the slope of the piles as a function of depth.

Jamiolkowski presented the results from analyses and experiment shown in Table 1.

Jamiolkowski concluded that the methods of computation were inadequate to predict the behavior of a pile group. He thought the main weakness in the methods was the inability to account for the effects of pile driving on soil properties, especially if displacement piles are driven.

The writers analyzed some experiments performed by Matlock et al [*14*]. Matlock and his associates tested a single pile, a five-pile group, and a ten-

TABLE 1—*Results from analyses and experiment by Jamiolkowski* [13].

Parameters	Ground-Line Displacements, cm	Distribution of Horizontal Load, tons-metric		
		Pile A	Pile B	Pile C[a]
Load test	0.8	14.4	17.5	13.1
Poulos method	0.8 to 1.17[b]	17.3	10.5	17.3
Poulos-Focht-Koch method	1.0 to 1.38[b]	16.7	11.7	16.7

[a]Pile C is closest to the applied load.

[b]The range in the computed values is a result of the selection of a range of values for the soil stiffness.

pile group. The piles were 168 mm (6.625 in.) in diameter and penetrated soft clay to a depth of 11.6 m (38 ft). The results from the test of the single pile were analyzed and values of soil response were obtained for use in the analyses of the ten-pile group.

The ten-pile group was subject to short-term static loads and to cyclic loads. The group sustained a load of approximately 169 kN (38 kips). The analyses were performed for a load of 153 kN (34.5 kips) by using the Poulos-Focht-Koch method with the results shown in Table 2. Two assumptions were made for the modulus of elasticity of the soil, that it was equal to 40 and 200 times the undrained shear strength.

The examples analyzed in Table 2 indicate that the Poulous-Focht-Koch method will yield values for the deflection of a pile group that are in the proper range if values of the modulus of elasticity E_s of the soil can be estimated properly. The estimation of E_s will be discussed in the following sections of this paper.

Soil Profile

The soil at the site consists predominantly of clay with undrained shear strength at the mud line ranging from very stiff to extremely stiff and with strength decreasing with depth. The bouyant unit weight is also higher at the mud line and decreased somewhat with depth.

The quantity ϵ_{50} is defined as the strain at a stress of one-half of the failure stress where the failure stress is defined as $(\sigma_1 - \sigma_3)_f$. The value of ϵ_{50} is needed in performing analyses of a single pile in clay. There is obviously in most natural soils a range in the value of ϵ_{50} as obtained from the results. Skempton [*15*] states that the value of ϵ_{50} for clays should range from 0.005 to 0.02. Recent evidence shows that values of ϵ_{50} of higher than 0.02 can be found.

The criteria that are used for predicting the soil response (p-y curves) for clay are dependent on the nature of the clay. The clay at the site is relatively homogeneous and without a highly developed secondary structure. These facts were considered in selecting the criteria used in the analyses.

In the analyses that were done, the soil properties were varied through a range that was thought to encompass the properties at the site. The justifica-

TABLE 2—*Analyses of an experiment by Matlock* [14] *using the Poulos-Focht-Koch method.*

Parameters	Deflection (Nine in. Above Ground line), in.
Load test	2.36
Analysis ($E_s = 40\, s_u$)	4.54
Analysis ($E_s = 200\, s_u$)	1.88

tion for this approach is that the techniques that must be used in obtaining soil specimens inevitably yield properties that are different (usually lower) than those obtained by the techniques that are available for onshore studies.[3] Furthermore, the procedures for analysis, as has been noted and as will be noted later, continue to be checked against experimental results as those results become available and improvements are being made.

Group Geometry and Loadings

There are nine piles in a group with the radius to the centers of the piles being 7 m (23 ft). The piles were spaced on approximately equal distances from center to center except as the spacing was adjusted because of the presence of braces. The piles had a wall thickness of 57.2 mm (2.25 in.). The length for lateral analysis was selected as 76 m (250 ft.). The diameter is 2134 mm (84 in.).

The axial load used in the analyses of the group was approximately 356 MN (80 000 kips), and the lateral load was approximately 40 MN (9000 kips). The pile heads were assumed to be fixed against rotation.

Analysis of Single Piles under Lateral Loading

The analysis of a single pile under lateral loading is made by use of a well-established procedure, employing a computer program that has been in general use [*16*]. The program models the lateral and axial loading, the pile-head restraint, and the soil response. The principal decisions to be made in the use of the method are the selection of the most appropriate soil-response criteria (procedures for developing p-y curves) and the determination of the soil parameters to be used.

Soil Response Criteria

The strength of the stiff clay at the mud line is relatively high, indicating the possible use of the criteria for p-y curves proposed by Reese et al [*5*] for stiff clay below the water surface. However, the relatively large values of ϵ_{50} suggest that the clay will behave more like a soft to medium clay [*3*] rather than as a stiff brittle clay.

The recommendations for p-y curves for submerged stiff clay, subjected to cyclic loading, allow for severe degradation of soil resistance when the pile deflections reach the "plastic" range of the soil. The degradation occurs mainly because of erosion as water is "pumped" out of gaps that form around the pile. Another cause of degradation is the remolding of the surrounding clay. While soft to medium clay also degrades under cyclic loading, the degrada-

[3] Young, A. C., Quiros, G. W., and Ehlers, C. J., "Effects of Offshore Sampling and Testing on Soil Shear Strength," Texas Section, American Society of Civil Engineers, 1981, unpublished.

tion is not as severe as in the case of stiff clay. Therefore, the selection of the soil criteria to be used in the analyses was closely examined as discussed next.

Preliminary Analysis

In order to gain some insight into the problem, some preliminary analyses were made for a pile with 57.2 mm (2.25 in.) wall thickness and with a lateral load of 4.448 MN (1000 kips). Both stiff clay criteria [*5*] and soft clay criteria [*3*] were used. The values of ϵ_{50} were varied from 0.01 to 0.03, and the three strength profiles were employed. The results of the analyses are shown in Table 4.

As may be seen by examining the Table 4, the maximum deflection that was computed was less than 50.8 mm (2 in.), an amount equal to about 2% of the pile diameter. At this deflection the degradation resulting from cyclic loading is negligible according to all of the recommendations for *p-y* curves.

The maximum combined stress shown in Table 3 is the result from the analyses that is most important in determining design. However, an examination shows that the stress versus deflection yields almost a straight line. Therefore, in the single-pile analyses that follow, emphasis will be given to the computation of deflection. The single-pile deflections, of course, are needed in doing the Poulos-Focht-Koch analyses.

Analyses of Pile Groups Under Lateral Loading

Influence Coefficients for Group Action

As indicated previously, Poulos [*12*] has published curves from which the α-values needed for the solution of Eq 4 can be obtained. The curves that were selected for use in this case were for a Poisson's ratio of the soil of 0.5 and for the case where the pile has a fixed head. In order to enter the curves, one must have the pile geometry, the modulus of elasticity of the pile material (2.07×10^8 kPa [3×10^7 psi]), and the modulus of the soil E_s (see Eq 3). The values of α are not greatly sensitive to relatively minor changes in K_R, defined in Eq 3; therefore, the values of α were obtained by selecting E_s as equal to 40 times the undrained shear strength, a value suggested by Poulos

TABLE 3—*Pile stresses with assumed value of* R *one.*[a]

Soil Strength	y_t, in.	y_G, in.	Maximum Combined Stress, kip/in.^{2}
Average	1.59	5.52	55.4
Upper-bound	0.86	2.98	45.2
Lower-bound	2.11	7.32	62.0

[a] 1 in. = 25.4 mm; 1 kip/in.^{2} = 6.895 MN/m^2.

NOTE—all piles have an 84-in. outer diameter and 2.25-in. wall thickness.

TABLE 4—*Results of preliminary single-pile computations.*[a]

Strength Profile	ϵ_{50}	Maximum Lateral Deflection, in.	Maximum Combined Stress, kip/in.^{2}	Maximum Bending Moment $\times 10^{-5}$, in.−k
		p-y CURVE CRITERIA FOR STIFF CLAY		
Lower-bound	0.02	1.27	33.2	2.2
Upper-bound	0.02	0.56	29.5	1.8
Average	0.02	0.75	30.6	1.9
Average	0.01	0.47	28.9	1.7
Average	0.03	0.99	31.9	2.1
		p-y CURVE CRITERIA FOR SOFT CLAY		
Lower-bound	0.02	1.74	35.7	2.5
Upper-bound	0.02	0.60	30.0	1.8
Average	0.02	0.93	32.1	2.1
Average	0.01	0.64	30.2	1.8
Average	0.03	1.15	33.4	2.2

[a] 1 in.−k = 113 m-N; 1 kip/in.^{2} = 6.895 MN/m^2.

NOTE: all piles have an 84-in. outer diameter and 2.25 in. wall thickness; axial load = 10 000^k/ pile; and lateral load = 1 000^k/pile.

[*11*]. In comparison with values of E_s suggested by others, this is a relatively conservative estimate of E_s. However, as shown later the values of $\bar{\rho}_F$ the unit "elastic" deflection (see Eq 5), has a strong influence on the solution and is given careful attention.

Sensitivity of Computation of Deflection of Group to Value of R

With appropriate values of α, the set of simultaneous equations (Eq 4) can be solved to investigate the sensitivity of the solution to the value selected for the relative stiffness factor R.

As mentioned earlier, because the piles will all deflect laterally equal distances, the deflection ρ_k in Eq 4 is equal to the deflection y_G of the pile group. For convenience, the left-hand side of Eq 4 was rewritten as $\rho_K/\bar{\rho}_F$ or $y_G/\bar{\rho}_F$. Because the left-hand term was obtained when Eq 4 was solved by matrix techniques, the values of y_G/y_t could be computed. The results of the computations are shown in Fig. 1.

As may be seen by examining Fig. 1, the multiplier to obtain y_G from y_t was sensitive to the value selected for R. Thus, as much care as possible should be exercised in computing the value of R. It should be noted that y_G approached y_t as R becomes larger.

There is, of course, a range of values for y_t as shown in the previous section. The value of ρ is computed by Eq 5. An examination of Eq 5 shows that the soil modulus E_s has a strong influence on the value of ρ. Computations of ρ were made for the average shear for the group, using values of E_s that cover

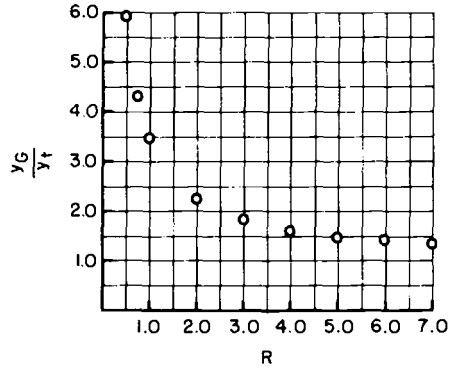

FIG. 1—*Effect of* R *on deflection of a nine-pile group.*

a range that might be expected. The results are shown in Fig. 2. As may be seen, the value of ρ is sensitive to the value of E_s that may be selected.

The above discussion shows that the computed deflection of the pile group is sensitive to the value of R that is used.

Results of Computations for R *of One*

There is a reason for selecting a value of unity for R, at least for the initial analyses. The computations in the previous section have shown that the computed deflection using p-y curves are small when compared to the pile diameter and that they plot on the initial branches of the p-y curves. Thus, it

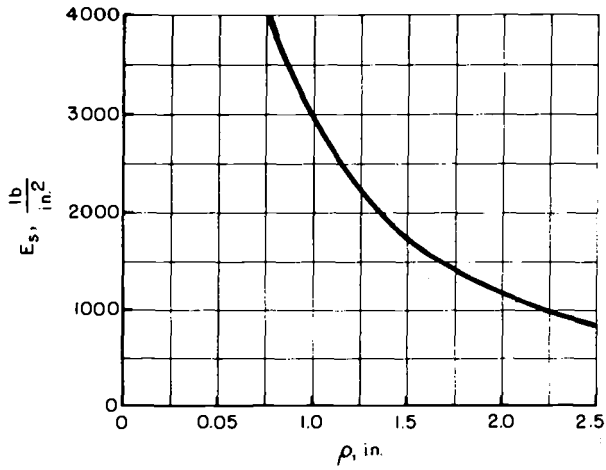

FIG. 2—*Effect of the value of* E_s *on* ρ.

can be considered that the soil is in the "elastic" range for the p-y analyses and that identical values of y_t and ρ would be computed. Furthermore, it is not reasonable that values of R less than unity would occur; therefore, R should have values of one or larger. An examination of Fig. 1 shows that the value of y_G will get smaller as larger values of R are used; thus, the use of a value of R of unity will either yield correct results or results that are conservative.

The results of the solution of Eq 4 are

- Average shear = 4.448 MN (1000 kips).
- Maximum shear = 4.834 MN (1087 kips).
- $y_G/y_t = 3.47$.

With the multiplier of 3.47 and the lateral load of 4.834 MN (1087 kips), the computer solution was used for the single pile to find the bending moment and the maximum combined stress.

The p-y curves are modified by multiplying the y-values by constants, 2, 3, 4, 5, and so on. The p-values are also multiplied by a constant to account for the "shadowing" effect. Computations were made for the ultimate resistance of a single pile and for an imaginary pile that encircled the nine-pile group. The patterns of these ultimate resistances were different because the depth of the wedge-type behavior in the vicinity of the ground surface is dependent on diameter. Therefore, it was necessary to compare the ultimate resistances at several depths to obtain a value for the "shadowing" effect. Before making the comparisons, the ultimate resistances for the pile group were divided by the number of piles in the group.

The values from the several comparisons range from about 0.75 to 0.6, and it was decided to select a value of two-thirds for the p-multiplier. The results of the computations, assuming a value of R equals one, are shown in Table 3. As may be seen, the combined stresses are relatively high for this conservative solution, particularly where a conservative assumption was made for the values of the soil shear strength.

Analyses of Data to Determine Upper-Bound Values of R

An upper-bound value of 25 000 kPa (3626 psi) based on general information at the site, was selected for recomputation of the elastic deflection ρ. Using this value for E_s and the Poulos equations, the deflections for the single pile was 21.84 mm (0.86 in.).

A second approach was used. The unified clay criteria [*7*] and the soft clay criteria [*3*] were employed, and curves were computed (Fig. 3). It was assumed that the elastic behavior of the piles could be obtained from an analysis of the early portion of the curves. A lateral load of 890 kN (200 kips) was selected, the soft clay criteria were employed (the unified clay criteria gives results that are similar), and a value of ρ of 7.72 mm (0.304 in.) was computed. It was decided to use this value for the elastic deflection of the single pile.

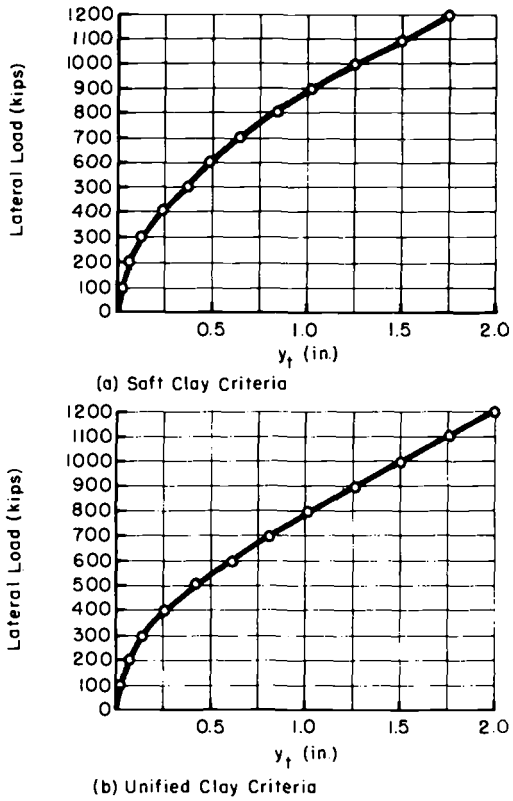

FIG. 3—*Plot of deflection versus lateral load for a single pile.*

In the computations that follow, the soft-clay criteria [*3*] were used because Fig. 3 shows that the results of the single-pile analyses differ only slightly between the soft-clay and the unified-clay methods. Further, it is thought that the use of the soft-clay criteria leads to a somewhat better prediction of the actual behavior of the piles at the site.

Using the value of ρ of 7.72 mm (0.304 in.) values of R were obtained (Table 5).

Results of Computations Using Upper-Bound Values of R

The results of the solutions of Eq 4 are shown in Table 6. The form of the results is the same as for the computations with R equal to unity; therefore, Table 6 indicates only the pile with the most critical loading.

The multiplier in the right-hand column was used, the p-y curves were modified as was done previously, and the behavior of the heaviest loaded pile was computed. The results are presented in Table 7. As may be seen, the

TABLE 5—*Values of* R.

Soil	*R*-Value
Avg	4.01
Upper-bound	3.19
Lower-bound	6.01

TABLE 6—*Results of computations for upper-bound values of* R.[a]

Average Shear, kips	Soil	Maximum Shear, kips	y_G/y_t
1012	average	1035.9	1.313
1012	upper-bound	1028.2	1.409
1012	lower-bound	1041.6	1.774

[a]1 kip = 4.448 kN.
NOTE—all piles have an 84-in. outer diameter and 2.25-in. wall thickness.

TABLE 7—*Pile stresses using upper-bound values of* R.[a]

Soil Strength	y_t, in.	y_G, in.	Maximum Combined Stress, kips/in.^{2}
Average	1.22	1.97	41.9
Upper-bound	0.97	1.72	40.1
Lower-bound	1.83	2.58	45.3

[a]1 in. = 25.4 mm; 1 kip/in.^{2} = 6.895 MN/m^2.
NOTE—all piles have an 84-in. outer diameter and 2.25-in. wall thickness.

combined stresses are considerably lower than for the case where values of unity were used for *R*.

Results of Computations Assuming the Group to Behave as an Imaginary Large-Diameter Pile

Computations were made using the soil criteria for a single pile. The diameter of the imaginary pile was assumed to be 16.1 m (52.9 ft), and the moment of inertia of the group was assumed to be nine times that for a single pile. The Matlock [*3*] criteria were used in the analyses.

The results of the analyses are shown in Table 8. The results compare reasonably well with those for the assumption of an *R* of one.

TABLE 8—*Results of computations assuming an imaginary large-diameter pile.*[a]

Soil Strength	ϵ_{50}	y_G, in.	Maximum Combined Stress, kip/in.^{2}
Average	0.012	3.41	47.3
	0.025	4.03	50.2
Upper-bound	0.012	2.86	44.6
	0.025	3.47	47.6
Lower-bound	0.012	4.15	50.8
	0.025	4.82	53.5

[a] 1 in. = 25.4 mm; 1 kip/in.^{2} = 6.895 MN/m^2.

NOTE—all piles have an 84-in. outer diameter and 2.25-in. wall thickness.

Mindlin p-y *Analysis*

Two additional analyses were performed using an alternate analysis procedure to provide an independent check on the reasonableness of the other solutions presented herein. The procedure involves analyzing each pile in the group by conventional *p-y* analysis procedures, except that each pile is considered to be subjected to an additional "free-field" soil displacement. The free-field displacements are computed as elastic displacements produced by distributed reactions along the length of all other piles in the group, excluding the particular pile being considered. The displacements are computed using the Mindlin solutions with an approximation for moduli varying with depth. The *p-y* procedures for analyzing the piles in a soil displacement field are identical to the procedures used for analyses of piles in a soil mass where mud-slide movements occur.

The analyses were performed using average soil properties and Matlock's *p-y* criteria for soft clays. Two sets of elastic soil moduli were used to compute field displacements of the soil. The first set of values was obtained by multiplying the shear strength by 100, that is, $E_s = 100s_u$, which is near the upper range of values suggested by Poulous [*11*], but may be conservative with respect to the recommendation of Focht and Koch [*10*]. The second set of moduli was constant with depth. A value of 19 000 kPa (2750 psi) was selected for E_s.

The analysis with the variable elastic modulus ($E_s = 100s_u$) produced a lateral pile-group displacement of 121 mm (4.77 in.) at the pile head; while the analysis with a constant modulus (E_s = 19 000 kPa [2750 psi]) produced a lateral pile group displacement of 85 mm (3.36 in.) at the pile head. The corresponding maximum combined stresses in the pile resulting from axial plus lateral loads were 276 and 280 MN/m^2 (40 053 and 40 647 psi), respectively.

Bending Moment Curves

Curves similar to those presented in Fig. 4 may be useful in considering the design of the piles. The curves show that the bending moments decrease rapidly with depth. The combined stresses are large only for a few pile diameters below the top of the pile. Because the computed bending moments are affected only to a minor degree by moderate changes in bending stiffness of the pile, the curves in Fig. 4 can be used to determine any additional wall thickness that is required over the upper portion of the pile to reduce the combined stress to the desired level.

Another factor of importance is that a slight rotation at the pile head (the analyses assumed the pile head to be perfectly fixed against rotation) will cause a significant reduction in the magnitude of the negative bending moment at the pile head. There will, of course, be some increase in lateral deflection and some increase in the maximum positive bending moment.

Conclusions

1. The results from the computations described herein indicate that the *R*-factor used in the Focht-Koch analysis has an important effect on the computed behavior of a pile group. Careful attention, therefore, should be given

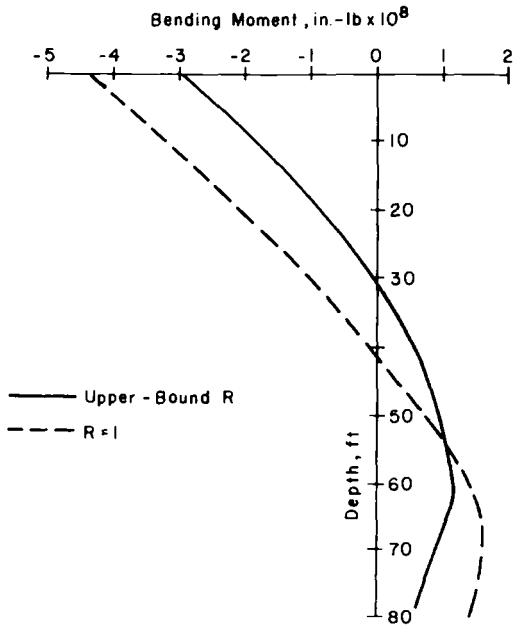

FIG. 4—*Bending moment curves from the Poulos-Focht-Koch analyses.*

to the selection of the soil modulus that is used in the Poulos analysis of a single pile.

2. The parametric studies outlined in this paper are useful in gaining an understanding of the probable behavior of the pile foundations for the proposed structure. In view of the character of natural deposits and of the lack of precision in the currently available methods of investigating such deposits, the use of upper-bound and lower-bound values of soil parameters in making analyses of pile groups is a desirable procedure. The parametic studies should also include a consideration of various methods of analyses as indicated herein.

3. The rapid decrease in bending moments below the mud line leads to the possibility of increasing the bending resistance of piles with a small percentage increase in quantity of steel. However, a critical factor of placing the pile to the computed penetration simultaneously arises.

4. Studies of the expected behavior of a pile group under lateral load leads to the obvious fact that more experimental data are needed to allow the improvement of analytical procedures. In this regard, a quote from Terzaghi [*17*] is appropriate: "Our theories will be superseded by better ones, but the results of conscientious observations in the field will remain as a permanent asset of inestimable value to the profession."

References

[*1*] Terzaghi, K., "Evaluation of the Coefficients of Subgrade Reaction," *Geotechnique*, Vol. 5, No. 4, Dec. 1955, pp. 297-326.

[*2*] McClelland, B. and Focht, J. A., Jr., "Soil Modulus for Laterally Loaded Piles," *Transactions of the American Society of Civil Engineers*, Vol. 123, 1958, pp. 1049-1063.

[*3*] Matlock, H., "Correlations for Design of Laterally Loaded Piles in Soft Clay," *Proceedings of the Offshore Technology Conference*, Vol. 1, Dallas, Tex., 1970.

[*4*] Reese, L. C. Cox, W. R., and Koop, F. D., "Analysis of Laterally Loaded Piles in Sand," *Proceedings of the Offshore Technology Conference*, Paper No. 2080, Dallas, Tex., 1974, pp. 473-483.

[*5*] Reese, L. C., Cox, W. R., and Koop, F. D., "Field Testing and Analysis of Laterally Loaded Piles in Stiff Clay," *Proceedings of the Offshore Technology Conference*, Paper No. 2312, Dallas, Tex., 1975, pp. 671-690.

[*6*] Welch, R. C. and Reese, L. C., "Lateral Loading of Deep Foundations in Stiff Clay," *Journal of the Geotechnical Engineering Division, Proceedings of the American Society of Civil Engineers*, Vol. 101, No. GT7, Feb. 1975, pp. 633-649.

[*7*] Sullivan, W. R., Reese, L. C., and Fenske, C. W., "Unified Method for Analysis of Laterally Loaded Piles in Clay," *Numerical Methods in Offshore Piling*, Institution of Civil Engineers, London, 1979, pp. 107-118.

[*8*] Bhushan, K., Haley, S. C., and Fong, P., "Lateral Load Tests on Drilled Piers in Stiff Clay," *Journal of the Geotechnical Engineering Division, American Society of Civil Engineers*, Vol. 105, No. GT8, Aug. 1979, pp. 969-985.

[*9*] Stevens, J. B. and Audibert, J. M. E., "Re-examination of *p-y* Curve Formulations," *Proceedings of the Offshore Technology Conference*, Paper No. 3402, 1979, pp. 397-403.

[*10*] Focht, J. A., Jr. and Koch, K. J., "Rational Analysis of the Lateral Performance of Offshore Pile Groups," *Proceedings of the Offshore Technology Conference*, Paper No. 1896, Dallas, Tex., 1973, pp. 701-708.

[*11*] Poulos, H. G., "Behavior of Laterally Loaded Piles: I—Single Piles," *Journal of the Soil*

Mechanics and Foundation Engineering, Proceedings of the American Society of Civil Engineers, Vol. 97, No. SM5, May 1971, pp. 711-731.

[*12*] Poulos, H. G., "Behavior of Laterally Loaded Piles: II—Pile Groups," *Journal of the Soil Mechanics and Foundations Division, Proceedings of the American Society of Civil Engineers*, Vol. 97, No. SM5, May 1971, pp. 733-751.

[*13*] Jamiolkowski, M. "Behavior of Laterally Loaded Pile Groups," *Proceedings of the Sixth European Conference on Soil Mechanics and Foundation Engineering*, Vol. 2, International Society for Soil Mechanics and Foundry Engineering, London, March 1976, pp. 165-169.

[*14*] Matlock, H., Ingram, W. B., and Kelley, A. E., "Field Tests of the Lateral-Load Behavior of Pile Groups in Soft Clay," *Proceedings of the Offshore Technology Conference*, Paper 3871, Dallas, Tex., 1980, pp. 163-174.

[*15*] Skempton, A. W., "The Bearing Capacity of Clays," *Proceedings of the Building Research Congress*, Vol. 1, Building Research Congress, London, 1951, pp. 180-189.

[*16*] Reese, Lymon C., "Laterally Loaded Piles: Program Documentation," *Journal of the Geotechnical Engineering Division, Proceedings of the American Society of Civil Engineers*, Vol. 103, No. GT4, April 1977, pp. 287-305.

[*17*] Terzaghi, K., *From Theory to Practice in Soil Mechanics*, Wiley, New York, 1960, p. 65.

Sol M. Gleser[1]

Generalized Behavior of Laterally Loaded Vertical Piles

REFERENCE: Gleser, S. M., **"Generalized Behavior of Laterally Loaded Vertical Piles,"** *Laterally Loaded Deep Foundations: Analysis and Performance, ASTM STP 835*, J. A. Langer, E. T. Mosley, and C. D. Thompson, Eds., American Society for Testing and Materials, 1984, pp. 72-96.

ABSTRACT: A method previously presented by the author (in ASTM STP 154) is generalized to encompass soils having nonlinear *p-y* characteristics. This results in a method that can handle, but is not restricted to, pile-soil systems having (1) piles greater than 9 m (30 ft) in length having free, fixed, or partially fixed heads, and any cross-sectional shape and length relationship, for example, constant, tapered, or stepped, and of any materials or combination of materials; (2) soils of any variation with depth, whether homogeneous, stratified, or combinations thereof, and having *p-y* characteristics of any nature; (3) ability to qualitatively and quantitatively predict behavior and stresses under static, fluctuating, and repetitive lateral loadings, or where larger emergency loads can be interspersed between normal loads. Ways are suggested for dealing with each of these factors. In addition, a method is proposed for obtaining the effective soil constant at a given site for a range of lateral loads, using empirical test data from free-head piles of the same characteristics subjected to lateral loads. The method is validated by use on previously published data of a comprehensive series of tests on free-head piles by Assadeh and Davison (*Journal of the Soil Mechanics and Foundation Division, Proceedings of the American Society of Civil Engineers*, Vol. 96, No. SM5, Sept. 1970, pp. 1583-1603). Using the soil constants resulted in computed load-deflection curves closely approximating actual data. These constants are used in turn to compute the expected deflections and pile stress of those same piles under fixed-head conditions.

A serendipitous finding of the analysis was that there is a significant shape factor affecting the ability of piles to mobilize soil resistance to lateral loads, for example, under any given lateral load applied to free-head piles having approximately equal moments of inertia, those having circular cross sections were substantially more resistant to lateral movement than square or H-beam cross sections. This in turn significantly altered the effective soil modulus.

To determine the usefulness of the method in economic as well as structural design, an analysis was made of a built-up pile consisting of a 360-mm (14-in.) H-beam cut diagonally along its length and rewelded to form a tapered I beam 500 mm (20 in.) at the butt and 200 mm (8 in.) at the tip, with constant flanges. Although having the same weight as the basic H beam, the tapered pile was computed to have a lateral deflection under a load of 13 000 kg (30 000 lb), which is half of that of the basic beam under free-head conditions and 0.6 of that under fixed-head conditions.

[1]Retired, 3604 Lansdowne Ave., Cincinnati, OH 45236.

KEY WORDS: foundations, piling, lateral loads, soil mechanics, design, deflection, footings, loads (fluctuating), subsurface structures

There have been a number of suggested methods to provide solutions for the behavior of laterally loaded vertical piles in soils having behavior characteristics other than elastic [*1–15*]. Several such methods have involved the use of the method developed in my paper, "Lateral Load Tests on Vertical Fixed-Head and Free-Head Piles," [*16*] as a means for computing soil modulii [*6–9*]. The method, referred to as "the Gleser method," is used in an indirect manner to compute the modulii by iterative means. However, the Gleser method, as published, is only applicable to soils exhibiting elastic behavior; that is, to soils whose *p-y* curve is a straight line through the origin. There is an existing need for a simple means for dealing with soil resistance configurations that are nonlinear at any one point along the length of the pile, but also upon depth below ground surface (surcharge or confining load), and on the lateral stresses at that location.

The equations developed for the original "Gleser method" [*16*] were generalized expressions to cover any configuration of soil resistances and pile stiffness throughout the length of a vertical pile subjected to lateral loads. They have the virtue that they can be programmed for a once-through solution on a digital computer rather than the iterative procedures required for solution of the matrix of the difference equation method proposed by Palmer and Thompson [*17*]. However, as indicated above, the solution was limited to soils exhibiting elastic behavior. Furthermore, implicit as a condition for use of the method was availability of the soils modulus at each point along the length of the pile, or a reasonable method of approximating it. On further study, it has become apparent that the equations set forth therein can be further generalized. Accordingly, this paper has been prepared to provide a generalized solution applicable to laterally loaded vertical piles of any configuration of stiffness throughout their length, embedded in foundations comprising any arrangement of layers of any types of soil, and where the soil behavior at any point m along the length of the pile can vary from elastic through semielastic to plastic as a known function of the applied stress at that point. Another way of expressing the latter condition is that the *p-y* curve at each point m is known.

It should be noted that the developed equations are predicated on use of soil modulii pertaining to the various depths of the area in question. Accordingly, it was deemed necessary that ready means be developed for determination of such soil modulii (or effective equivalents) without the necessity of extensive (and expensive) soils investigations in the affected area throughout the estimated depths of the proposed pile foundations. This paper proposes one such method and validates it by means of previously published data of actual tests on free-head piles subjected to lateral loads [*18*].

The derivation of the equations is set forth in the Appendix. Practical methods for using the equations are discussed below. Since all computations in this paper were made in inch-pound units, appropriate factors for conversion to SI units are provided in the footnote below for ready reference.[2]

Generalized Procedure and Rationale for the Iterative Solution

Before proceeding, set up the constants to be used in the computations for each point as follows.

Pile Constants

Length, pile head fixity, number of pile divisions t, loads, and the modulus of elasticity of the pile material and the moment of inertia of the pile cross section at each point along the pile are the pile constants.

Soil Constants

At each point, the soil constants are the soil modulus α, the deflection at yield point YE_m, the deflection at plastic point YP_m, the slope of the semiplastic line ϕ_m. (A suggested method of obtaining these is proposed below.)

After the pertinent constants have been obtained, continue as follows.

1. For the first run, assume that the soil condition at each point along the embedded length of the pile is "elastic"; that is, for each point m, $U_m = 0$ and $W_m = \lambda^4 b_m \alpha_m / E_m I_m$.
2. Using the selected constants, compute each γ and δ by means of Eqs 5.4(o) through 5.4(p) and 5.5(o) through 5.5(p), respectively, and A, B, and C for each point along the pile to and including p by means of Eqs 6.0(o) through 6.0(p), respectively.[3]
3. Using the load, compute F and G for each point at and above p (ground level), by means of Eqs 7.1 through 7.5, respectively.
4. Compute Y_{t+2}, using the applicable Eq 8 or 9.
5. Compute Y_{t+1} through Y_p, in turn, using the applicable Eqs 7.5 through 7.1.
6. Compute each Y_p through Y_o, in turn, using applicable Eq 6.0(p) through 6.0(o), respectively. As each such Y is computed, compare it with its associated transition deflections for that point, that is, with YE_m and YP_m.

[2] 1 in. = 25.4 mm, 1 in.^{2} = 645.16 mm^2, 1 Pa = 1 N/m^2, 1 lb/ft^2 = 16.0185 kg/m^2, 1 lbf/in.^{2} = 6.89476 kPa, and 1000 lb = 454 kg.

[3] The numbering system used with the equations is a mnemonic to identify the source of the equation and the point along the length of the pile (measured in λ units from the bottom of the pile) at which it is to be applied. For example, Eq 2.2(o) denotes Eq 2.2 applied at point o (bottom of pile). Similarly, Eq 4.2(m) denotes Eq 4.2 applied at point m. In like manner (with the exception of constants F, G, and D), the subscripts to the various elements of the equations denote the point along the pile at which they are measured. For example, Y_m denotes the deflection at point m, Y_{t+2-r} denotes deflection at point $t + 2 - r$, and α_m denotes alpha at point m.

(a) If $Y_m < YE_m$, compute the deflection for the next lower point.

(b) If $YE_m < Y_m < YP_m$ change the U for that point to $\lambda^4 b_m \gamma_m / E_m I_m$ and the W to $\lambda^4 b_m \phi_m / E_m I_m$ and go on to compute the deflection for the next lower point.

(c) If $YP_m < Y_m$, change the U for that point to $\lambda^4 b_m \delta_m / E_m I_m$ and the W to 0 and compute the deflection for the next lower point.

7. Repeat Steps 2 through 6, using the revised Us and Ws obtained from the next preceding run until there is no change required in the U and W for any point from those of the next preceding run. At this point, no further iterations are necessary. It should be noted that where the computed deflection at a point m is not significantly different from a transition deflection at that point it is not necessary to make the indicated change in U and W; for example, suppose that for the next previous run Y_m was less than YE_m but is now but a few thousandths of an inch greater than YE_m, it is unnecessary to change U_m and W_m. However, if Y_m for the next previous run was less than YP_m but is now but a few thousandths of an inch greater than YP_m, the change should be made in the U_m and W_m as indicated in Step 6c.

8. Having the deflections at each point, the moments and shears can be computed for such points as may be desired, using Eqs 2.2(m) and 3.2(m), respectively.

9. Go on to the computation for next selected set of loads. For the first trial run, the number of necessary iterations may be reduced by using the Us and Ws employed in the final run of the preceding set of loads, providing that there has been no change in the conditions of head fixity, and that the loads are larger than in the preceding set.

Piles Subjected to Fluctuating Loads

Cases often arise where a structure to be supported by piling will be subjected to fluctuating, and in many cases reversing, lateral loads, for example, buildings subjected to wind loads, dams or bridges subjected to varying water loads, and so forth. In such cases, the structures and their foundations are designed to resist the maximum loads to which they may be subjected. The problem then arises as to what subsequent deflections may be expected in the piles under loads less than the maximum after the structure had been previously subjected to a maximum load.

The derived equations and the suggested procedures previously set forth herein can be further generalized to permit computations of deflections under the above-contemplated circumstances after consideration of the following.

1. Under maximum load, it can be noted whether certain regions of the foundation soils have been subjected to strains that have exceeded the yield point or plastic point or both and hence are partially or entirely irreversible, that is, whether

$$_{\max} Y_m > YE_m \text{ or } YP_m \text{ or both}$$

2. Where YP_m has been exceeded, that is

$$_{\max}Y_m > YP_m$$

the deflection is entirely irreversible. Hence any subsequent pile deflection at point m will meet zero resistance until it equals $_{\max}Y_m$. Thereafter resistance is equal to δ_m.

3. Where $YE_m < {}_{\max}Y_m < YP_m$ the deflection is partially irreversible, that is, the portion less than YP_m. Hence any subsequent deflection will meet zero resistance until it equals YE_m. Thereafter resistance will follow Eq 5.2(m).

It is evident from the above analysis that under such conditions deflection under a load P will be greater if the pile had previously been subjected to a load $P + \Delta$ than if such a greater load had not been previously applied. This is borne out by much experimental data; for example, Conclusion 2 of my discussion on Feagin's paper [*19*], and by Fig. 3 of Alizadeh and Davisson [*18*].

Under such circumstances, the desired deflections can be obtained by altering the "generalized" procedure, hereafter called "general" procedure.

1. Use the general procedure to compute the deflections for the higher loading (usually the maximum loading).
2. Determine for each point whether a partially irreversible or entirely irreversible deflection has occurred.
3. Where an irreversible deflection has occurred, that is, $_{\max}Y_m > YP_m$, set U_m and $W_m = 0$.
4. Where a partially irreversible deflection has occurred, that is, $YE_m < {}_{\max}Y_m < YP_m$ set $U_m = \lambda^4 b_m \gamma_m / E_m I_m$ and $W_m = \lambda^4 b_m \phi_m / E_m I_m$.
5. Where the yield point has not been exceeded, that is, $_{\max}Y_m < YE_m$, set $U_m = 0$ and $W_m = \lambda^4 b_m \phi_m / E_m I_m$.
6. Proceed with Phases 2, 3, 4, and 5 of the general procedure.
7. Proceed with Phase 6, subject to the following. If under load being computed $Y_m < YE_m$, but under maximum load $YE_m < {}_{\max}Y_m < YP_m$, set $U = 0$ and $W = 0$ for Phase 6b.

Similarly, if under a load being computed $Y_m < {}_{\max}Y_m$, but under maximum load $_{\max}Y_m > YP_m > YE_m$, $U = 0$ and $W = 0$ for Phase 6c.

However, if $Y_m > {}_{\max}Y_m$, set $U = \lambda^4 b_m \delta_m / E_m I_m$ and $W = 0$.

8. Continue with Phases 7, 8, and 9 of the general procedure, subject to the above-listed criteria.

Proposed Method for Determination of Effective Soil Modulus

In order to use the general method of analysis, it is proposed that the following procedure be used to evaluate the pertinent soil constants.

1. Drive piles of the type proposed for use into the foundation and subject the free-head piles to lateral loads applied at the ground line. Apply the loads in equal increments of size to provide at least six load points to reach an estimated maximum deflection of about 19 mm (3/4 in.). As each increment is applied, measure deflection at the ground line to an accuracy of ± 0.01 mm (± 0.0005 in.) every 10 min while maintaining each load constant until movement stabilizes (that is, difference in 10 min is less than 0.05 mm [0.002 in.]) before applying the next load increment. A relatively inexpensive means is to drive a pair of piles a distance of five diameters apart and jack between them while measuring the deflection of each pile thus providing check measurements at each load.

2. Using methods of Matlock and Reese [*8*], compute the estimated k (modulus of soil reaction) for load and deflection at first (lowest) load. In the case of a granular or semi-granular foundation, a good first assumption is $E_s = kx$.

Using Eqs 17 and 55 of Matlock and Reese [*8*]

$$A_y = Y_A EI^3/PT^3$$

and

$$T^{n+4} = EI/k$$

and noting that under the assumption $E_s = kx$, Eq 55 [*8*] becomes Eq 55′ [*8*]

$$T^5 = EI/k$$

If, for example, the first load was 1134 kg (2500 lb) and produced a deflection at ground line ($x = 0$) of y_o, and noting that $A_y = 2.43546$ when $x = 0$, the equation for k becomes Eq 55″ [*8*]

$$k = 203\ 0182/(EI)^{2/3} y_o^{5/3}$$

To avoid confusing this k with that in Eq 4.1, we shall hereafter designate the Matlock and Reese k as K.

3. In order to use the general procedure developed above for the case $r = 0$, that is, load applied at ground line, it is first necessary to develop U_m and W_m as expressed by Eq 5.1(m), 5.2(m), and 5.3(m). As may be noted from Fig. 1, these in turn are functions of p_m.

For the elastic range, we note from Eq 5.1(m) that $U_m = 0$ and $W_m = Kx_m = -\lambda^4 b_m \alpha_m / E_m I_m$, where x_m is distance of point m below ground level.

To arrive at a first approximation for the constants α_m, γ_m, ϕ_m, and δ_m, we note first that α_m is the slope of Eq 5.1(m), ϕ_m is the slope of Eq 5.2(m), and

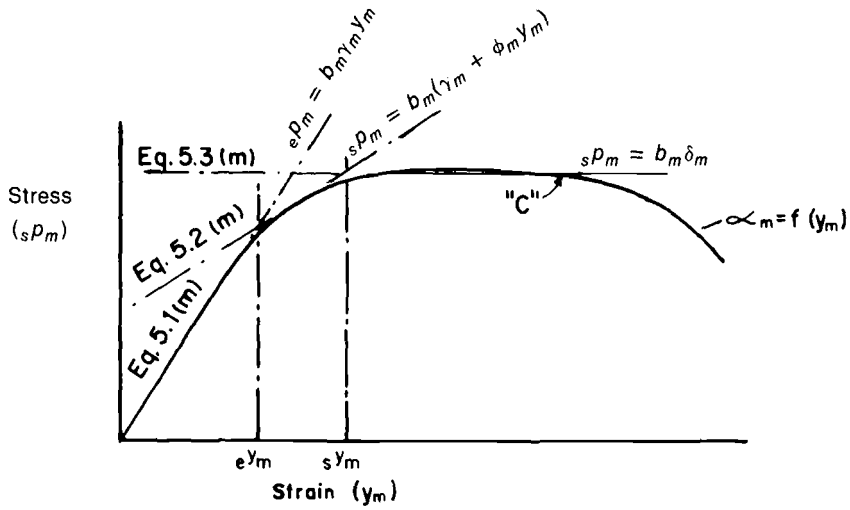

FIG. 1—*Linear approximation of stress-strain curve.*

δ_m is a constant for the plastic state. If we assume that the "shape" of the p-y curve $p_m = f(y_m)$ is the same for all points and only varies in the value of its ordinate with x, then we can assume that deflection at soil elastic limit YE_m, and deflection at initiation of fully plastic behavior YP_m, do not change with depth, and we can assign a trial value to each. We can then compute the point of intersection of Eq 5.1(m) with $y = YE_m$, that is, $P_m = b_m\alpha_m\gamma F$. If we now assume that $\phi_m = \alpha_m$, and note from Fig. 1 that by definition Eqs 5.1(m) and 5.2(m) both pass through the point ($_ep_m$, YE_m), we can compute $b_m\gamma_m$, that value of p_m where Eq 5.2(m) intersects the line $y_m = 0$. This is the constant U_m for Eq 5.2(m). Finally, we can compute the point of intersection, $_sP_m$, of Eq 5.2(m), and $y_m = YP_m$, that is, $_sP_m = b_m(\gamma_m + \phi_m YP_m)$. Since this is equal to $b_m\delta_m$, it is seen that $\delta_m = \gamma_m + \phi_m YP_m$, and U_m for the plastic range is $k_m b_m(\gamma_m + \phi_m YP_m)$.

4. Using these relationships, compute the deflections of the tested piles at the ground line for each of the loadings imposed and compare with the actual deflections. Modify the constants as appears desirable and rerun the computations until an acceptable fit is obtained between the computed and actual load-deflection curve. At this point the effective soil constants for use in computing the expected pile behavior under design conditions have been obtained.

Validation of Proposed Schema

In order to validate the proposed schema, it was necessary, as indicated above, to have empirical test data to use as a criterion for comparison. Fortu-

nately, such was already available, that is, the results of an extensive series of tests on piles in the Arkansas River, published by Alizadeh and Davisson [*18*]. For ease in reference, these data are hereafter referred to by the designation A&D, for example, in their Fig. 2a.

A&D Fig. 2a, shows the initial load-deflection curves of the piles tested at Lock and Dam 4 in the Arkansas River. It should be noted that the scale of deflections along the abscissa of that figure is in error in that points 0.6 and 0.7 should read 0.5 and 0.6, respectively. Their [*18*] Table 1 lists the physical properties of the tested piles.

As may be noted from A&D Fig. 2a, deflections at any one load are approximately consistent with the inverse ratio of *EI* for a particular type of pile. For example, in the case of the square concrete piles, the deflections at a lateral load of 9 100 kg (20 000 lb) are 2 and 4 mm (0.075 and 0.180 in.) for Piles 11A and 5, respectively, and their respective *EI*s are in the ratio of 8.4 and 3.45. If we multiply 0.075, the deflection of Pile 11A, by 8.4/3.45, we obtain 0.182, approximately the deflection of Pile 5 as listed above. However, this is not the case as between the square concrete piles and either the pipe piles or the H piles. As a case in point, deflections at a load of 9 071.8 kg (20 000 lb) of Pile 2 (a 406.4-mm [16-in.] pipe), Pile 6 (a 355.6-mm [14-in.] H-pile), and Pile 13A (a 355.6-mm [14-in.] H-pile) were 4.06, 6.35, and 610-mm (0.163, 0.255, and 0.245 in.), respectively, and their respective *EI*s were in the ratio of 2.435, 2.15, and 2.482. If we now multiply 0.075 (deflection of square concrete Pile 11A) by 8.4/2.435, 8.4/2.15, and 8.4/2.482, we obtain 0.259, 0.293, and 0.254, which bear little resemblance to the actual deflection of Pile 2, listed above, but are in the approximate range of those listed for Piles 6 and 13A. In fact, it may be noted that even though the *EI* of Pile 2 is approximately equal to that of Pile 13A, the deflection of Pile 13A was almost 50% greater than that of Pile 2. A similar situation exists with respect to Piles 2 and 5, where even though the *EI* of Pile 5 is about 40% greater than that of Pile 2, its deflection is only about 10% greater. Since the soil conditions for all of the above-listed piles can be assumed to have been approximately identical, a reasonable explanation for the noted discrepancies is that a shape function is involved. In other words, cylindrical piles appear to be more efficient in mobilizing soil resistance to lateral loads than either square or H piles. This conclusion appears consistent with the Boisonesque theory and with results implied by Baguelin and Frank [*20*].

From the above, it is clear that in order to determine the effective soil constants for the soil-shape-materials combination of a selected pile, tests must be made on that soil-shape-materials combination, since using an effective soil constant derived from tests on a different soil-shape-material pile would be subject to error.

For purposes of rapid computation, a computer program was developed, using FORTRAN H, extended, and arranged to use the following:

alpha α = kxb, since foundation was of a granular or semi-granular material.
phi ϕ = the constant in the equation $\phi = \alpha$ times a constant.
YE = soil deflection at elastic limit.
YP = soil deflection at beginning of fully plastic behavior.
t = 100, number of divisions along pile length.

Using deflections at load of 1134 kg (2500 lb) taken from A&D of Fig. 2, the apparent soil constants K were computed for each of the tested piles in order to obtain a first trial figure for α. The first trial figure for each of the other constants were arbitrarily assumed to be

phi ϕ = 8 mm (1/3 in.).
YE = 0.2 mm (0.006 in.).
YP = 3 mm (0.120 in.).

Computer runs were made for each of the piles, using loads of 5, 10, 15, 20, 30, 40, 50, and 60 kips, and the physical constants in A&D Table 1, and the computed deflections compared with those shown on A&D of Fig. 2. It quickly became evident that while the computed deflections were within an acceptable range for lower loads, they were radically undervalued at the higher loads unless ϕ was reduced to 6 mm (0.225 in.) and YE increased to 0.3 mm (0.01 in.). Furthermore, although a YP of 3 mm (0.1 in.) was found suitable for piles having a flat face in the direction of load, that is, for square or H piles; a value of 8 mm (0.3 in.) was more appropriate for piles of circular cross section. Once these values were determined, only minor adjustments in alpha were found appropriate.

Computer runs were made for each of the tested piles to calculate the deflections, moments, shears, and stresses in both the free-head and fixed-head mode. Results of these runs are listed in Tables 1 through 6, together with the actual free-head deflections taken from A&D Fig. 2a, for comparison. It will be noted that the actual and computed deflections in free-head mode for each of the tested piles are so close that it would be difficult to see any differences on a load/deflection curve drawn to any reasonable scale. The greater efficiency of the pipe pile in comparison with either that of either the H pile of equal EI or that of the square pile of greater EI is readily apparent.

In order to provide an example of the usefulness of the developed method, computer runs were made to develop the behavior of a tapered H pile in both the free-head and fixed-head mode. The assumed pile was that of a 14 BP 73, of the same length as Pile 13A, split longitudinally and rewelded so that its butt end was 510 mm (20 in.) in depth and tip end 180 mm (7 1/4 in.). Results of the computations are also listed in Tables 1 and 2. It is readily apparent that to produce any given deflection requires about 40% greater load for the tapered pile than for Pile 13A even though they each weigh the same.

TABLE 1—*Parameters for actual and computed deflections under lateral loads (round piles).*

Parameters	Pile Number					
	2 and 10		16		0.8	
Size and shape	16-in. pipe		16-in. pipe		14-in. round	
Material	steel		steel		tapered wood	
Soil constants	first	final	first	final	first	final
Alpha	437	465	240	280	252	240
Phi	0.333	0.225	0.333	0.225	0.333	0.225
YE (in.)	0.006	0.01	0.006	0.01	0.006	0.01
YP (in.)	0.10	0.30	0.10	0.30	0.10	0.12

A glance at the effective alphas computed for Piles 2 and 16, and for Piles 5 and 14, quickly confirms the A&D conclusions that jetting piles into place seriously affects the lateral resistance of the soil foundation.

It is believed that the foregoing has provided adequate validation of the general theory and proposed procedures presented above for computing the soil constants pertaining to free-head piles in noncohesive soils having *p-y* curves similar to Fig. 1, subjected to lateral loads, particularly their behavior at higher loads. In the case of *p-y* curves similar to Fig. 2, the method can be modified by use of an additional Eq 5.3a to approximate the downward portion depicting the strain-softening behavior. It is further believed that computation of effective soil constants, as proposed above, will provide a more useful, meaningful, and accurate basis for obtaining design constants than the use of an arbitrarily selected n_h as indicated on A&D Fig. 2b.

Conclusions

The analysis provided herein is believed to provide a method for computing the behavior of free-head and fixed-head pile foundations, covering vertical

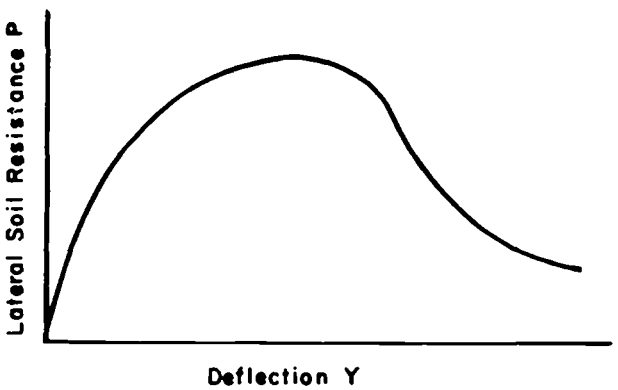

FIG. 2—*Characteristic* p-y *curve for short-term static load for strain softening soil* [12].

TABLE 2—*Actual and computed deflections under lateral loads (round piles).*

	Head Fixation											
	Free-Head Deflections, in.			Fixed-Head Stress, lb/in.^{2},	Free-Head Deflections, in.			Fixed-Head Stress, lb/in.^{2},	Free-Head Deflections, in.			Fixed-Head Stress, lb/in.^{2},
Lead, lb	Actual	Actual	Computed	Computed	Actual	Computed	Computed	Computed	Actual	Computed	Computed	Computed
5 000	0.029	0.0242	0.0082	1 550	0.040	0.037	0.0112	1 736	0.095	0.1087	0.030	435
10 000	0.068	0.0645	0.0181	3 266	0.095	0.098	0.0279	3 854	0.250	0.2564	0.081	957
15 000	0.115	0.1119	0.0321	5 269	0.153	0.1658	0.0500	6 171	0.430	0.4129	0.1367	1 483
20 000	0.163	0.1617	0.0487	7 354	0.225	0.235	0.0746	8 530	...	...	0.1933	2 007
30 000	0.262	0.2638	0.0851	11 579	0.395	0.377	0.1265	13 249	...	...	0.3083	3 053
40 000	0.368	0.3683	0.1231	15 805[a]	0.595[a]	0.5828	0.1798	17 946	...	...	...	...
50 000	0.480[a]	0.4892	0.1624	20 018	...	...	0.233	22 627	...	...	...	...
60 000	0.605	0.6751	0.2013	24 223	...	...	0.2877	27 323	...	...	...	...
70 000	...	...	0.2415	28 427	...	...	...	...	...	...	...	...
80 000	...	...	0.2812	32 622	...	...	...	...	...	...	...	...

[a]Extrapolated.

TABLE 3—*Parameters for actual and computed deflections under lateral loads (square concrete piles).*

Parameters	Pile Number					
	11A		5		14	
Size and shape	20		16		16	
Material	concrete		concrete		concrete	
Soil constants	first	final	first	final	first	final
Alpha	534	450	266	315	188	285
Phi	0.333	0.225	0.333	0.225	0.333	0.225
YE (in.)	0.006	0.01	0.006	0.01	0.006	0.01
YP (in.)	0.10	0.12	0.10	0.12	0.10	0.12

piles of known configurations and materials or combinations of materials of known physical properties, set in any soil of known type and physical characteristic, and subjected to any combination, order of application, and location of lateral load applied at or above ground level, which imposes stresses on the soil ranging from elastic to plastic behavior. It is to be noted that the soils need not be homogeneous, but can be stratified, or even have hard lenses. Similarly, pile cross sections need not be constant, but can vary in any arbitrarily selected manner. Similarly, the modulus of elasticity of the pile material can be arbitrarily varied anywhere along the pile length.

While computations can be made manually, it is usually highly uneconomical and cumbersome when electronic computers are conveniently available.

It is further believed that the procedures presented provide a rapid, simple ready means for predicting the behavior of piles subjected to fluctuating or cyclical lateral loads or piles subjected to lesser lateral loads after having been subjected to maximum design lateral loads.

It should be noted that the procedures take full cognizance of the behavior of soils having nonlinear *p-y* response curves in predicting the behavior of piles in such soils when subjected to lateral loads.

The serendipitous finding of the presence of shape factors as a result of the herein described validation process using the A&D data is believed to warrant further study to more precisely define the parameters of such shape factors. It is believed that knowledge of such parameters would greatly facilitate selection of the most economical piles for use in a given foundation without the necessity for actual testing in the foundation of several types of piles.

In view of the demonstrated ability of the suggested procedure to closely track the behavior of the eight different types of piles as set forth in Tables 1 through 6, it is further believed that the proposed method of computing soil constants by use of data from tests on piles in a proposed foundation subjected to lateral loads at ground level is a valid economical measure for ob-

TABLE 4—*Actual and computed deflections under lateral loads (square concrete piles).*

	Head Fixation											
	Free-Head Deflections, in.			Fixed-Head Stress, lb/in.^{2},	Free-Head Deflections, in.			Fixed-Head Stress, lb/in.^{2},	Free-Head Deflections, in.			Fixed-Head Stress, lb/in.^{2},
Load, lb	Actual	Computed	Computed	Computed	Actual	Computed	Computed	Computed	Actual	Computed	Computed	Computed
5 000	0.012	0.0135	0.0051	157	0.030	0.0276	0.0090	276	0.035	0.0300	0.0096	281
10 000	0.028	0.0327	0.0102	314	0.070	0.0735	0.0205	591	0.082	0.0800	0.0223	609
15 000	0.048	0.0583	0.0164	491	0.120	0.1265	0.0368	952	0.145	0.1367	0.0402	981
20 000	0.075	0.0869	0.0244	688	0.180	0.1864	0.0555	1 325	0.218	0.2032	0.0605	1 363
30 000	0.140	0.1484	0.0439	1 107[a]	0.342	0.362	0.0964	2 078	0.385	0.4040	0.1041	2 130
40 000	0.221	0.2241	0.0659	1 535	0.650[a]	0.6296	0.1399	2 843[a]	0.770[a]	0.7681	0.1521	2 928
50 000	0.325[a]	0.3247	0.0890	1 963	...	...	0.1956	3 722	...	...	0.2158	3 856
60 000	0.463[a]	0.4564	0.1130	2 394	...	...	0.2684	4 717	...	...	0.3004	4 912
70 000	0.650[a]	0.6145	0.1375	2 830	...	...	0.3603	5 813	...	...	0.4062	6 065
80 000	...	...	0.1667	3 312	...	...	...	...	...	...	...	...
90 000	...	...	0.2009	3 836	...	...	...	...	...	...	...	...

[a]Extrapolated.

TABLE 5—*Parameters for actual and computed deflections under lateral loads (steel H-beams).*

Parameters	Pile Number				
	6		0.13A		TH
Size and shape	14-in. H-beam		14-in. H-beam		20-in. Butt by 8-in. tip H-beam
Material	steel		steel		tapered steel
Soil constants	first	final	first	final	
Alpha	323	300	332	300	300
Phi	0.333	0.225	0.333	0.225	0.225
YE, in.	0.006	0.01	0.006	0.01	0.01
YP, in.	0.10	0.12	0.10	0.12	0.12

taining such constants when the soils throughout the length of the piles are relatively homogeneous.

APPENDIX

Derivation of Equations[3]

The fundamental differential equations expressing behavior at any point m of a vertical pile subjected to lateral load P in terms of deflection Y_m, depth below ground surface X, moment of inertia of the pile at that point I_m, and Young's modulus of the pile material at that point E_m are

$$\text{Eq (1.0): slope at } m; \qquad S_m = (dY/dX)_m$$

$$\text{Eq (2.0): moment at } m; \qquad M_m = E_m I_m (d^2Y/dX^2)_m$$

$$\text{Eq (3.0): shear at } m; \qquad V_m = E_m I_m (d^3Y/dX^3)_m$$

$$\text{Eq (4.0): pressure at } m; \qquad P_m = E_m I_m (d^4Y/dX^4)_m$$

These differential equations can be rewritten as algebraic equations by the method of finite-difference equations, wherein the various orders of differentials are expressed in terms of the pile deflections and increments of pile length, namely

[3]The numbering system used with the equations is a mnemonic to identify the source of the equation and the point along the length of the pile (measured in λ units from the bottom of the pile) at which it is to be applied. For example, Eq 2.2(o) denotes Eq 2.2 applied at point o (bottom of pile). Similarly, Eq 4.2(m) denotes Eq 4.2 applied at point m. In like manner (with the exception of constants F, G, and D), the subscripts to the various elements of the equations denote the point along the pile at which they are measured. For example, Y_m denotes the deflection at point m, Y_{t+2-r} denotes deflection at point $t + 2 - r$, and α_m denotes alpha at point m.

$$\text{Eq (1.1): } (dY/dX)_m = \Delta(y_m) = (Y_{m-1} - Y_{m-1})/2\lambda$$

$$\text{Eq (2.1): } (d^2Y/dX^2)_m = \Delta^2(y_m) = (Y_{m+1} - 2Y_m + Y_{m-1})/\lambda^2$$

$$\text{Eq (3.1): } (d^3Y/dX^3)_m = \Delta^3(y_m)$$

$$= (Y_{m+2} - 2Y_{m+1} + 2Y_{m-1} - Y_{m-2})/2\lambda^3$$

$$\text{Eq (4.1): } (d^4Y/dX^4)_m = \Delta^4(y_m)$$

$$= (Y_{m+2} - 4Y_{m-1} + 6Y_m - 4Y_{m-1} + Y_{m-2}/\lambda^4$$

where λ is the selected increment of pile length, that is, $\lambda = L/t$; L is the length of the pile in inches and t is the selected number of pile divisions. It should be noted that the accuracy of the indicated approximations increases as the absolute value of λ decreases.

Using the above, Eqs 1.0 through 4.0 can be rewritten as follows

$$\text{Eq (1.2): } Y_{m+1} - Y_{m-1} = 2\lambda S_m$$

$$\text{Eq (2.2): } Y_{m+1} - 2Y_m + Y_{m-1} = -\lambda^2 M_m/E_m I_m = g_m M_m$$

where $g_m = -\lambda^2/E_m I_m$

$$\text{Eq (3.2): } Y_{m+2} - 2Y_{m+1} + 2Y_{m-1} - Y_{m-2} = -2\lambda^3 V_m/E_m I_m = j_m V_m$$

where $j_m = -2\lambda^3/E_m I_m$

$$\text{Eq (4.2): } Y_{m+2} - 4Y_{m+1} + 6Y_m - 4Y_{m-1} + Y_{m-2}$$

$$= -\lambda^4 p_m/E_m I_m = k_m p_m$$

where $k_m = -\lambda^4/E_m I_m$

Consider now a pile embedded in earth for a depth L_e and subjected to lateral loads $P_1, \ldots, P_m$ at points a distance of $L_1, L_2, \ldots, L_m$, respectively, above ground surface. In the equations presented in the Gleser method [*16*], length L was measured from ground surface to pile tip, that is, that which is designated L_e; point zero was considered to be the tip of the pile and point t was considered to be at ground surface. On further consideration it became apparent that such designations created problems in the solution of cases where the distances of points of load application or of head fixation above ground were significant multiples of λ, for example, pile dolphins and piles supporting structures above ground such as pile bents. Accordingly, such difficulties have been avoided in this paper by designating pile length L as the distance from the pile tip to the uppermost point of application of pile load or pile restraint, whichever is higher, and designating the uppermost point as point t. Diagrammatically, this can be represented as in Fig. 4. It will be noted that points -1, -2, $t + 1$, and $t + 2$ have no "physical" significance.

Starting from the bottom of the pile ($m = 0$) we can write the following equations (see Table 7) for both free-head and restrained-head piles.

TABLE 6—*Actual and computed deflections under lateral loads (steel H-beams).*

	Head Fixation										
	Free-Head Deflections, in.			Fixed-Head Stress, lb/in.^{2},	Free-Head Deflections, in.			Fixed-Head Stress, lb/in.^{2},	Free-Head Deflections, in.		Fixed-Head Stress, lb/in.^{2},
Load, lb	Actual	Computed	Computed	Computed	Actual	Computed	Computed	Computed	Computed	Computed	Computed
5 000	0.035	0.0374	0.0113	1 573	0.042	0.0346	0.0106	1 417	0.0218	0.0075	1 195
10 000	0.095	0.0986	0.0279	3 537	0.093	0.0915	0.0257	3 124	0.0571	0.0160	2 475
15 000	0.168	0.1681	0.0503	5 670	0.150	0.1555	0.0464	5 020	0.1000	0.0279	3 974
20 000	0.255	0.2604	0.0750	7 835	0.245	0.2385	0.0693	6 946	0.1448	0.0421	5 555
30 000	0.500	0.5495	0.1270	12 165	0.485	0.4909	0.1184	10 824	0.2558	0.0739	8 788
40 000	...	...	0.1934	17 120	...	...	0.1769	15 072	0.4227	0.1078	12 027
50 000[a]	...	...	0.2849	22 859	...	...	0.2576	20 052	...	0.1437	15 351
60 000[a]	...	...	...	...	...	...	...	...	...	...	...
70 000[a]	...	...	...	...	...	...	...	...	...	...	...
80 000	...	...	...	...	...	...	...	...	...	...	...
90 000	...	...	...	...	...	...	...	...	...	...	...

[a]Extrapolated.

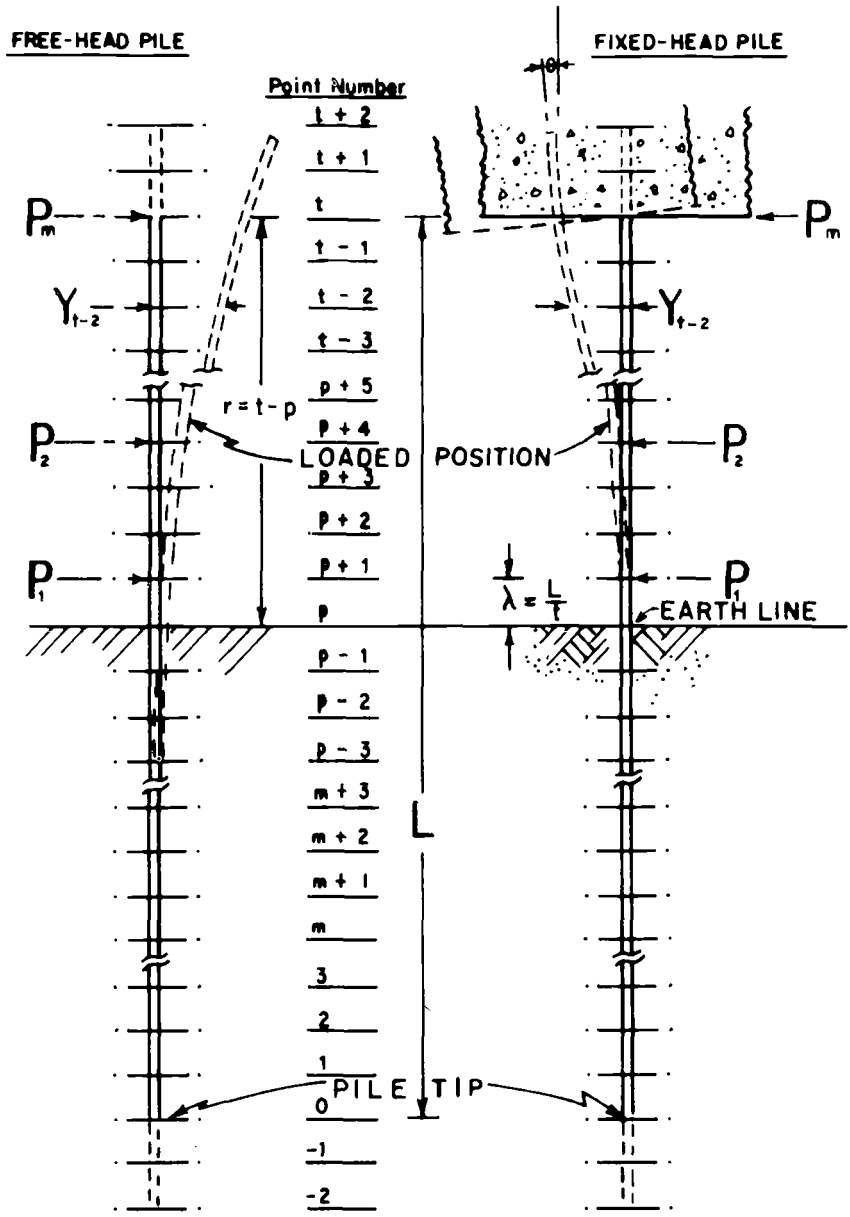

FIG. 3—*Diagrammatic description of nomenclature.*

Table 7 comprises $t + 4$ equations in the $t + 5$ unknown deflections. The $(t + 5)$th equation must express the condition of fixity of the pile head.

For the free-head pile, moment at the topmost point of load application ($m = t$) is zero. Hence we can write the $(t + 5)$th equation for that case as

$$\text{Eq } 2.2'(t): \quad Y_{t+1} - 2Y_t + 2Y_{t-1} - Y_{t-1} = 0 \quad \text{(for free head pile)}$$

For the fixed-head pile, the slope of the pile head S_t is maintained constant. Hence we can write the $(t + 5)$th equation for that case as

$$\text{Eq } 1.2'(t): \quad Y_{t+1} - Y_{t-1} = 2\lambda S_t = s_t \quad \text{(for fixed-head pile)}$$

In order that the listed system of equations be capable of solution, it is necessary that the $F(Y_m)$s be linear expressions in the unknown Ys. Let us now consider the relationships between unit pressure ρ and deflection y of a soil, that is, $\rho_m = f(y_m)$.

Soil Characteristics

There have been a sizeable number of papers dealing with p-y curves, among which are Stevens and Audibert [*21*] and Sullivan et al [*11*]. Figure 4 shows a p-y curve proposed by Matlock [*15*] for short-term static load for a strain-hardening clay. Figure 3 shows a similar curve proposed by Reese et al [*12*] for short-term static load for a strain-softening clay. It seems reasonable to propose that a generalized curve would

TABLE 7—*Generalized equations applicable to laterally loaded vertical piles.*

Equation	Comment[a]
Eq 2.2(0): $Y_1 - 2Y_0 + Y_{-1} = 0$	(1)
Eq 3.2(0): $Y_2 - 2Y_1 + 2Y_{-1} - Y_{-2} = 0$	(2)
Eq 4.2(0): $Y_2 - 4Y_1 + 6Y_0 - 4Y_{-1} + Y_{-2} = k_0F(Y_0)$	(3)
Eq 4.2(1): $Y_3 - 4Y_2 + 6Y_1 - 4Y_0 + Y_{-1} = k_1F(Y_1)$	(4)
Eq 4.2(m): $Y_{m+2} - 4Y_{m+1} + 6Y_m - 4Y_{m-1} + Y_{m-2} = k_mF(Y_m)$	(5)
Eq 4.2(p): $Y_{p+2} - 4Y_{p+1} + 6Y_p - 4Y_{p-1} + Y_{p-2} = k_pF(Y_p)$	(6)
Eq 3.2(p): $Y_{p+2} - 2Y_{p+1} + 2Y_{p-1} - Y_{p-2} = j_p\Sigma_p$ where Σ_p = sum of all loads at and above p	(7)
Eq 3.2(p): $Y_{t+2-r} - 2Y_{t+1-r} + 2Y_{t-1-r} - Y_{t-2-r} = j_p\Sigma_p$	(8)
Eq 3.2($p + a$): $Y_{t+2-r+a} - 2Y_{t+1-r+a} + 2Y_{t-1-r+a} - Y_{t-2-r+a} = j_{p+a}\Sigma_{p+a}$	(9)
Eq 3.2(t): $Y_{t+2} - 2Y_{t+1} + 2Y_{t-1} - Y_{t-2} = j_t\Sigma_t$	(10)

[a]The comments are as follows:

(1) Moment at pile tip is zero.

(2) Shear at pile tip is zero.

(3) Expression for pressure at pile tip multiplied by k_0.

(4) through (6) Similar expressions at Points 1, m, and p, respectively. (It should be noted that the $F(Y_m)$s are obtained from the p-y curves at each point m).

(7) Expression for shear at ground line, multiplied by j_p.

(8) Equation recast in terms of Points t and p; that is, $p = t - r$.

(9) Equation for Point $p + a$ expressed in terms of t, r, and a.

(10) Expression for shear at top of pile, multiplied by $j_t (m = t)$.

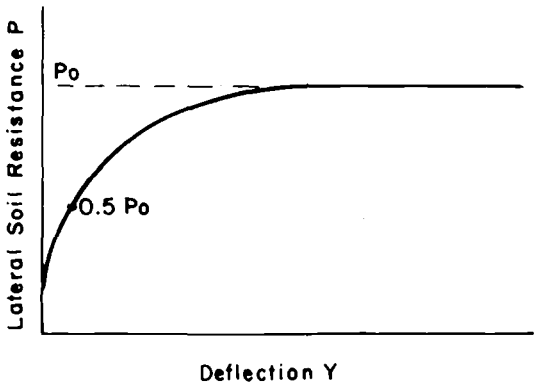

FIG. 4—*Characteristic* p-y *curve for short-term static load for strain hardening soil* [15].

look somewhat like the curve shown in Fig. 5. In each case the curve can be expressed as

$$\text{Eq (5.0): } p_m = b_m \rho_m$$

where $\rho_m = f(y_m)$ and b_m is the projected width of the pile in the direction of load, for example, for a cylindrical pile, b_m is the diameter at point m.

In Fig. 5, the portion from the origin to point a can be described as the "elastic" range, from points a to b as the "semi-elastic" or "semi-plastic" range, and the remainder as the plastic range. However, the relationship can be recast into linear configurations to a fairly high order of approximation by representation as a series of straight lines as schematically indicated in Fig. 1. The portion of the curve $f(y_m)$ to the right of the point designated as c is usually outside of the range of engineering usefulness and can be disregarded. For all practical purposes the stress-strain relationship can normally be expressed to a fair degree of approximation within the range of engineering usefulness by three lines having the following equations

$$\text{Eq 5.1: } p_m = b_m \alpha_m y_m \quad \text{(range of elastic behavior)}$$

$$\text{Eq 5.2: } p_m = b_m(\gamma_m + \phi_m y_m) \quad \text{(range of semi-plastic behavior)}$$

$$\text{Eq 5.3: } p_m = b_m \delta_m \quad \text{(range of plastic behavior)}$$

In such an arrangement, ${}_e y_m$ (point of intersection of Eqs 5.1(m) and 5.2(m) and ${}_s y_m$ (point of intersection of Eqs 5.2(m) and 5.3(m) would mark the transition points between the elastic and semi-elastic ranges and between the semi-elastic and plastic ranges, respectively, as may be noted on Fig. 1. For ease in notation, ${}_e y_m$ and ${}_s y_m$ are hereafter designated as YE_m and YP_m, respectively.

From Eqs 5.1(m), 5.2(m), and 5.3(m) we obtain

$$\text{Eq 5.4: } YP_m = \gamma_m/(\alpha_m - \phi_m)$$

$$\text{Eq 5.5: } YP_m = (\delta_m - \gamma_m)/\phi_m$$

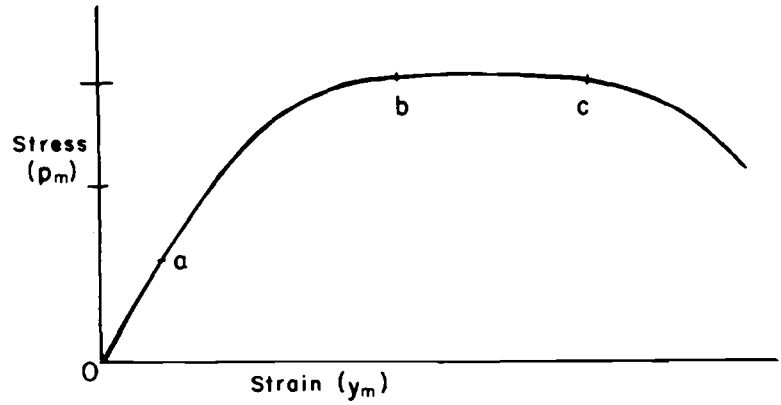

FIG. 5—*Generalized stress-strain curve.*

Returning to Eq 4.2(m), we can write the right-hand side as

$$\text{Eq 5.6}(m): -k_m F(Y_m) = (\lambda^4/E_m I_m)p_m = (\lambda^4/E_m I_m)b_m \rho_m$$
$$= (\lambda^4/E_m I_m)f(y_m) = U_m + W_m Y_m$$

where $U_m + W_m Y_m$ is the generalized expression for $k_m p_m$, as expressed in Eqs 5.1(m), 5.2(m), and 5.3(m), and k_m is defined in 4.2(m).

These equations can be rewritten as follows for the three ranges of soil condition

$$\text{Eq 5.1}'(m): k_m p_m = U_m + W_m Y_m = 0 + k_m b_m \alpha_m Y_m \quad \text{(elastic range)}$$

$$\text{Eq 5.2}'(m): k_m p_m = U_m + W_m Y_m = k_m b_m (\gamma_m + \phi_m Y_m) \quad \text{(semi-elastic range)}$$

$$\text{Eq 5.3}'(m): k_m p_m = U_m + W_m Y_m = k_m b_m \delta_m + 0 \quad \text{(plastic range)}$$

General Solution

Using the procedure of the original Gleser paper [*16*] and starting with Eqs 2.2(0), 3.2(0), and 4.2(0), we can eliminate Y_{-1} and Y_{-2} and express Y_o in terms of Y_1 and Y_2; namely

$$\text{Eq 6.0(0)}: Y_0 = -A_0 - B_0 Y_2 + C_0 Y_1$$

where

$B_0 = 2/(2 + W_0)$,
$A_0 = B_0 U_0/2$, and
$C_0 = 2B_0$.

Similarly, using Eqs 2.2(0), 4.2(1), and 6.0(0), we obtain

$$\text{Eq 6.0(1)}: Y_1 = -A_1 - B_1 Y_3 + C_1 Y_2$$

where

$$B_1 = 1/(5 + W_1 - 2C_0),$$
$$A_1 = B_1(U_1 + 2A_0), \text{ and}$$
$$C_1 = 2B_1(2 - B_0) = B_1(4 - C_0).$$

Again, using Eqs 4.2(2), 6.0(0), and 6.0(1), we obtain

$$\text{Eq 6.0(2): } Y_2 = -A_2 - B_2 Y_4 + C_2 Y_3$$

where

$$B_2 = 1/[6 + W_2 - B_0 - C_1(4 - C_0)],$$
$$A_2 = B_2[U_2 - A_0 + A_1(4 - C_0)], \text{ and}$$
$$C_2 = B_2[4 - B_1(4 - C_0)] = B_2(4 - C_1).$$

In like manner, using Eqs 4.2(3), 6.0(1), and 6.0(2) we obtain

$$\text{Eq 6.0(3): } Y_3 = -A_3 - B_3 Y_5 + C_3 Y_4$$

where

$$B_3 = 1/[6 + W_3 - B_1 - C_2(4 - C_0)],$$
$$A_3 = B_3[U_3 - A_1 + A_2(4 - C_1)], \text{ and}$$
$$C_3 = B_3[4 - B_2(4 - C_1)] = B_3(4 - C_2).$$

Thereafter, $p \geq m \geq 3$, we can write the general equation as

$$\text{Eq 6.0}(m)\text{: } Y_m = -A_m - B_m Y_{m+2} + C_m Y_{m+1}$$

where

$$B_m = 1/[6 + W_m - B_{m-2} - C_{m-1}(4 - C_{m-2})],$$
$$A_m = B_m[U_m - A_{m-2} + A_{m-1}(4 - C_{m-2})], \text{ and}$$
$$C_m = B_m[4 - B_{m-1}(4 - C_{m-2})] = B_m(4 - C_{m-1}).$$

until we come to point p, where in addition to Eq 6.0(p), we can write Eq 3.2(p) as follows

$$\text{Eq 3.2}(p)\text{: } Y_{p+2} - 2Y_{p+1} + 2Y_{p-1} - Y_{p-2} = j_p \Sigma_p$$

Substituting Eqs 6.0(p), 6.0($p - 1$), and 6.0($p - 2$) in Eq 3.2(p) and eliminating all terms in Y except Y_{p+1} and Y_{p+2}, and then expressing Y_{p+1} in terms of Y_{p+2}, we obtain

$$\text{Eq 7.1: } Y_{p+1} = F_1 - G_1 Y_{p+2}$$

where

$$F_1 = [-j_p \Sigma_p - (2 - C_{p-2})(A_{p-1} + A_p C_{p-1}) + A_{p-2} - A_p B_{p-2}]/D_1,$$
$$G_1 = \{B_p[C_{p-1}(2 - C_{p-2}) + B_{p-2}] - 1\}/D_1, \text{ and}$$
$$D_1 = (2 - C_{p-2})(B_{p-1} - C_{p-1} C_p) + 2 - B_{p-2} C_p.$$

Similarly, substituting Eqs 6.0(p), 6.0($p - 1$), and 7.1 in Eq 3.2($p + 1$) and eliminating all terms but those in Y_{p+2} and Y_{p+3}, we obtain

$$\text{Eq 7.2: } Y_{p+2} = F_2 - G_2 Y_{p+3}$$

where

$$F_2 = -G_2[-j_{p+1}\Sigma_{p+1} + B_{p-1}F_1 + A_{p-1} - (2 - C_{p-1})(C_pF_1 - A_p)],$$
$$G_2 = -1/D_2, \text{ and}$$
$$D_2 = 2 + B_{p-1}G_1 + (2 - C_{p-1})(B_p + C_pG_1).$$

In like manner, using Eqs 3.2($p + 1$), 6.0(p), 7.1, and 7.2, we obtain

$$\text{Eq 7.3: } Y_{p+3} = F_3 - G_3 Y_{p+4}$$

where

$$F_3 = -G_3[A_p + B_pF_2 - j_{p+2}\Sigma_{p+2} - (2 - C_p)(G_1F_2 - F_1)],$$
$$G_3 = -1/D_3, \text{ and}$$
$$D_3 = 2 - G_2[G_1(2 - C_p) - B_p].$$

Again, using Eqs 3.2($p + 3$), 7.1, 7.2, and 7.3 we obtain

$$\text{Eq 7.4: } Y_{p+4} = F_4 - G_4 Y_{p+3}$$

where

$$F_4 = -G_4[-j_{p+3}\Sigma_{p+3} - F_1 + (2 + G_1)(F_2 - G_2F_3)],$$
$$G_4 = 1/D_4, \text{ and}$$
$$D_4 = 2 - G_2G_3(2 + G_1).$$

Thereafter, for points $p + 4$ up to and including t, we can write the general equation ($a \leq r$) as follows

$$\text{Eq 7.5: } Y_{p+a+1} = F_{a+1} - G_{a+1} Y_{p+a+2}$$

where

$$F_{a+1} = -G_{a+1}[-j_{p+a}\Sigma_{p+a} - F_{a-2} + (2 + G_{a-2})(F_{a-1} - G_{a-1}F_a)],$$
$$G_{a+1} = -1/D_{a+1},$$
$$D_{a+1} = 2 - G_{a+1}G_a(2 + G_{a-2}).$$

It will be noted that all equations derived to this point are identical for both the free-head and fixed-head condition. This follows as a result of the previously noted observation that the only difference between the two conditions is in the ($t + 5$)th equation, that is, Eq 2.2(t) for the free-head pile and Eq 1.2(t) for the fixed-head pile, each of which are functions of Y_{t+1}, Y_t, and Y_{t-1}. These equations can be rewritten in terms of Y_{p+r+1}, Y_{p+r}, and Y_{p+r-1} by noting that $t = p + r$.

Let us now examine three special cases for r, namely, $r = 0$, 1, and 2, and then derive the general case.

For $r = 0$

Free-Head Condition

Using Eqs 6.0(p), 6.0($p - 1$), 7.1, and 2.2(p) and noting that $t = p$ when $r = 0$, we eliminate all terms in Y except those in Y_{p+2} and obtain

$$\text{Eq 8.1: } Y_{p+2} = Y_{t+2} = [F_1(1 - B_{p-1}) + (2 - C_{p-1})(A_p - C_pF_1) - A_{p-1}] \div [G_1(1 - B_{p-1}) - (2 - C_{p-1})(B_p + C_pG_1)]$$

Fixed-Head Condition

Similarly, using Eqs 6.0(p), 6.0($p - 1$), 7.1, and 1.2(p) we obtain

$$\text{Eq 9.1: } Y_{p+2} = Y_{t+2} = [F_1(1 - B_{p-1}) + C_{p-1}(A_p - C_pF_1) - s_p + A_{p-1}] \div [G_1(1 + B_{p-1}) - C_{p-1}(C_pG_1 + B_p)]$$

For $r = 1$

Free-Head Condition

Using Eqs 6.0(p), 7.1, 7.2, and 2.2($p + 1$), and noting that $t = p + 1$ when $r = 1$, we eliminate all terms in Y except those in Y_{p+3} and obtain

$$\text{Eq 8.2: } Y_{p+3} = Y_{t+2} = [F_2(1 - B_p) - A_p + (2 - C_p)(F_2G_1 - F_1)] \div [G_2(1 - B_p) + G_1(2 - C_p)]$$

Fixed-Head Condition

Using the same first three equations and Eq 1.2($p + 1$), we obtain

$$\text{Eq 9.2: } Y_{p+3} = Y_{t+2} = [-s_{p+1} + F_2(1 + B_p + C_pG_1) - C_pF_1 + A_p] \div [G_2(1 + B_p + C_pG_1)]$$

For $r = 2$

Free-Head Condition

Using Eqs 7.1, 7.2, 7.3, and 2.2($p + 2$) and noting that $t = p + 2$ when $r = 2$, we obtain

$$\text{Eq 8.3: } Y_{p+4} = Y_{t+2} = \{F_3[1 + G_2(2 + G_1)] - F_2(2 + G_1) + F_1] \div [G_3[1 + G_2(2 + G_1)]\}$$

Fixed-Head Condition

Using the same first three equations and Eq 1.2($p + 2$), we obtain

$$\text{Eq 9.3: } Y_{p+4} = Y_{t+2} = [F_3(1 - G_1G_2) + G_1F_2 - F_1 - s_{p+2}] \div [G_3(1 - G_1G_2)]$$

Thereafter, ($2 \leqq r$), we can write the generalized equation as follows.

For $r = r$

Free-Head Condition

$$\text{Eq } 8.r\text{: } Y_{p+r+2=Yt+2} = \{F_{r+1}[1 + G_r(2 + G_{r-1})] - F_r(2 + G_{r-1}) + F_{r-1}\} \div \{G_{r+1}[1 + G_r(2 + G_{r-1})]\}$$

Fixed-Head Condition

$$\text{Eq } 9.r\text{: } Y_{p+r+2} = Y_{t+2} = [F_{r+1}(1 - G_rG_{r-1}) + G_{r-1}F_r - F_{r-1} - s_{p+r}] \div [G_{r+1}(1 - G_rG_{r-1})]$$

Final Computations

Having evaluated Y_{t+2} in terms of the applied load and of the soil and pile constants by means of the appropriate Eq 8 or 9, we can compute the above-ground deflections ($0 \leq a \leq r$) by means of Eq 7.5, that is,

$$\text{Eq (7.5): } Y_{p+a+1} = F_{a+1} - G_{a+1}Y_{p+a+2}$$

Thereafter, the deflections at and below point p (ground level) up to and including point 3 can be evaluated by use of Eq 6.0(m), that is,

$$\text{Eq } 6.0(m)\text{: } Y_m = -A_m - B_mY_{m+2} + C_mY_{m+1}$$

Finally, we can evaluate the deflections for points 2, 1, and 0 by means of Eqs 6.0(2), 6.0(1), and 6.0(0), respectively, that is

$$\text{Eq } 6.0(2)\text{: } Y_2 = -A_2 - B_2Y_4 + C_2Y_3$$

$$\text{Eq } 6.0(1)\text{: } Y_1 = -A_1 - B_1Y_3 + C_1Y_2$$

$$\text{Eq } 6.0(0)\text{: } Y_0 = -A_0 - B_0Y_2 + C_0Y_1$$

Having computed the deflections, the shear, moment and slope at each point of the pile can be computed by use of Eqs 3.2(m), 2.2(m), and 1.2(m), respectively.

References

[1] Spillers, W. R. and Stoll, R. D., "Lateral Response of Piles," *Journal of the Soil Mechanics and Foundations Division, Proceedings of the American Society of Civil Engineers*, Vol. 90, No. SM6, Nov. 1964, pp. 1-9.

[2] Terzaghi, K., "Evaluation of Coefficients of Subgrade Reaction," *Geotechnique*, Vol. 5, Dec. 1955, p. 300.

[3] Broms, B. B., "Lateral Resistance of Piles in Cohesionless Soils," *Journal of the Soil Mechanics and Foundations Division, Proceedings of the American Society of Civil Engineers*, Vol. 90, No. SM3, May 1964, pp. 123-156.

[4] Broms, B. B., "Lateral Resistance of Piles in Cohesive Soils," *Journal of the Soil Mechanics and Foundations Division, Proceedings of the American Society of Civil Engineers*, Vol. 90, No. SM2, March 1964, pp. 27-63.

[5] McClelland, B. and Focht, J. A., Jr., "Soil Modulus for Laterally Loaded Piles," *Transactions of the American Society of Civil Engineers*, Vol. 123, 1958, pp. 1049-1063.

[6] Reese, L. and Matlock, H., "Non-dimensional Solutions for Laterally Loaded Piles With Soil Modulus Assumed Proportional to Depth," *Proceedings of the Eighth Texas Conference on Soil Mechanics and Foundation Engineering*, Special Publication No. 29, Bureau of Engineering Research, The University of Texas, Austin, TX, Sept. 1956.

[7] Reese, L. and Matlock, H., "Numerical Analysis of Laterally Loaded Piles," *Conference Papers, ASCE 2nd Conference on Electronic Computation*, American Society of Civil Engineers, New York, Sept. 1960, pp. 657-668.

[8] Matlock, H. and Reese, L., "Generalized Solutions for Laterally Loaded Piles," *Transactions of the American Society of Civil Engineers*, Vol. 127, Part I, 1962, pp. 1220-1246.

[9] Reese, L. C. and Ginzbarg, A. S., "Difference Equation Method for Laterally Loaded Piles with Abrupt Changes in Flexural Rigidity," Publication No. 221, Shell Development Company, Exploration and Production Research Division, Houston, TX, 1960.

[10] Desai, C. S. and Kuppusamy, T., "Application of a Numerical Procedure for Laterally Loaded Structures," *Numerical Methods in Offshore Piling*, Institution of Civil Engineers, London, England, 1980, pp. 93-99.

[11] Sullivan, W. R., Reese, L. C., and Fenske, C. W., "Unified Method for Analysis of Laterally Loaded Piles in Clay," *Numerical Methods in Offshore Piling*, Institute of Civil Engineers, London, England, 1980, pp. 135-146.

[12] Reese, L. C. et al, "Analysis of Laterally Loaded Piles in Sand," *Proceedings of the Annual Offshore Technology Conference*, Paper OTC 2080, Houston, TX, 1974.

[13] Gill, H. and Demara, K., "Displacement of Laterally Loaded Structures in Nonlinearly Responsive Soil," Technical Report R670, Naval Civil Engineering Laboratory, Port Hueneme, CA, 1970.

[14] Reese, L. C. et al, "Field Testing and Analysis of Laterally Loaded Piles in Stiff Clay," *Proceedings of the 7th Annual Offshore Technology Conference*, Paper No. 2312, Houston, TX, 1975.

[15] Matlock, R., "Correlations for Design of Laterally Loaded Piles in Soft Clay," *Proceedings of the 2nd Annual Offshore Technology Conference*, Paper No. 1204, Houston, TX, 1970.

[16] Gleser, S. M., "Lateral Load Tests on Vertical Fixed-Head and Free-Head Piles," *Symposium on Lateral Load Tests on Piles, STP 154*, American Society for Testing and Materials, Philadelphia, 1953, pp. 75-93.

[17] Palmer, L. A. and Thompson, J. B., "Horizontal Pressure on Pile Foundations," *Proceedings of the Third International Conference on Soil Mechanics and Foundation Engineering*, Vol. 5, Rotterdam, Netherlands, 1948, pp. 156-161.

[18] Alizadeh, M. and Davisson, M. T., "Lateral Load Tests on Piles—Arkansas River Project," *Journal of the Soil Mechanics and Foundations Division, Proceedings of the American Society of Civil Engineering*, Vol. 96, No. SM5, Sept. 1970, pp. 1583-1603.

[19] Feagin, L. B., *Lateral Load Tests on Groups of Battered and Vertical Piles, STP 154*, American Society for Testing and Materials, Philadelphia, 1953, pp. 20-27.

[20] Baguelin, F. and Frank, R., "Theoretical Studies of Piles Using the Finite Element Method," *Numerical Methods in Offshore Piling*, Institution of Civil Engineers, London, England, 1980, pp. 83-91.

[21] Stevens, J. B. and Audibert, J. M. E., "Re-examination of *P-Y* Curve Formulations," *Proceedings of the 11th Annual Offshore Technology Conference*, Paper 3402, Houston, TX, 1975.

Jean-Louis Briaud,[1] *Trevor Smith,*[1] *and Barry Meyer*[2]

Laterally Loaded Piles and the Pressuremeter: Comparison of Existing Methods

REFERENCE: Briaud, J.-L.. Smith, T., and Meyer, B., **"Laterally Loaded Piles and the Pressuremeter: Comparison of Existing Methods,"** *Laterally Loaded Deep Foundations: Analysis and Performance. ASTM STP 835*, J. A. Langer, E. T. Mosley, and C. D. Thompson, Eds., American Society for Testing and Materials, 1984, pp. 97-111.

ABSTRACT: The first part of this article deals with the determination of the critical depth D_c, below which the ground surface has little influence on the soil-structure interaction problem, and with the variation of soil resistance within that critical depth. A new approach is proposed to determine D_c using the relative rigidity of the pile with respect to the soil strength as measured by the pressuremeter limit pressure.

The second part of the article summarizes seven pressuremeter methods to predict the lateral behavior of piles. Predictions by four of the methods are compared with the results of a full-scale load test. All methods predict the measured behavior with reasonable accuracy suggesting that the pressuremeter provides a sound testing base for the behavior prediction of laterally loaded piles.

KEY WORDS: soils, pressuremeter, lateral load, piles, load test

One of the most technically sound applications of the pressuremeter test is its use to obtain data for predicting movements of piles subjected to lateral loads (Fig. 1). There are at least seven methods of analysis based on pressuremeter test results. These methods are discussed in this article.

The first part of this article involves the determination of the critical depth D_c, that is, the depth below which the stress-free ground surface has little influence on the soil-structure interaction problem, and the variation of lateral soil resistance within this critical depth.

The second part of this article is a discussion and summary of the seven

[1] Associate professor and graduate student, respectively, Civil Engineering Department, Texas A&M University, College Station, Tex. 77843.

[2] Supervising engineer, McClelland Engineers, Inc., 6100 Hillcroft Ave., Houston, Tex. 77081.

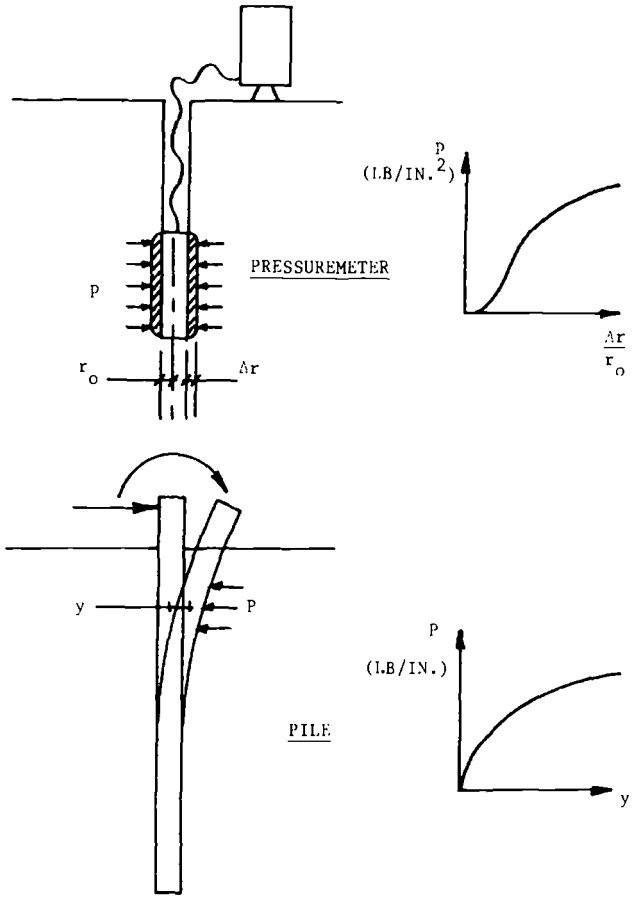

FIG. 1—*Pressuremeter pile analogy.*

pressuremeter methods. The predictions obtained by using four of the seven methods are compared with the results of a field load test of a pile in stiff clay.

Critical Depth: Existing Values

When a pile is loaded laterally to failure, there is a zone just below the ground surface where the lateral soil resistance is reduced. This zone of reduced lateral resistance extends to the ultimate critical depth D_c. Below D_c, the absence of constraint caused by the stress-free ground surface has negligible influence on the lateral soil resistance, and the lateral soil resistance will be called the deep soil resistance. Above D_c, it will be called the shallow soil resistance. Within D_c, the shallow soil resistance is obtained by multiplying the deep resistance by a reduction factor $S(R)$.

Many researchers have made recommendations on the values of D_c and $S(R)$. For clays and for methods based on the use of the undrained shear strength (S_U approach) recommendations have been made by Broms [*1*], Matlock [*2*], Reese and Welch [*3*], Reese et al [*4*], Hansen [*5*], and Stevens and Audibert [*6*]. Also, Skempton [*7*] proposed values of D_c and $S(R)$ for strip footings in clay. The increase of the bearing capacity factor N_c with depth, proposed by Skempton, is related to the D_c-$S(R)$ relationship of laterally loaded piles. For clays and for methods based on the use of the pressuremeter test results (PMT approach), recommendations have been made by Menard et al [*8*] and Baguelin et al [*9*].

For laterally loaded piles in sands, Broms [*1*] and Hansen [*5*] do not consider a zone of reduced resistance. However, Reese et al [*10*] suggest to determine D_c and $S(R)$ by a method based on the use of the friction angle (ϕ approach). Menard [*8*] and Baguelin et al [*9*], for a method based on the use of pressuremeter tests, also make recommendations on the values of D_c and $S(R)$. In linear elasticity the influence of the stress-free ground surface can be evaluated by using Mindlin's equations [*11*]. The various approaches are summarized on Fig. 2.

Critical Depth: Soil-Structure Interaction Approach

The variation of soil resistance along a laterally loaded pile can be approximated by the solid curve *CBA* on Fig. 3. The horizontal pile displacement y increases from Point E to the ground surface. If there are no weakening influences caused by the close proximity of the stress-free ground surface, the variation of resistance in a soil of constant strength with depth is described by the dotted line *CD*. Instead, the soil resistance (in force per unit length of pile) follows *CBA* with a maximum resistance $p_{(max)}$ at a depth z_c. Within z_c the soil resistance p is less than $p_{(max)}$. For a horizontal load H the depth z_c is the instantaneous critical depth, and the ratio $p/p_{(max)}$ is the instantaneous reduction factor $S(R)$.

As the horizontal load increases, Point B of Fig. 3 moves downward as shown on Fig. 4, and z_c reaches the ultimate critical depth D_c when the pile deflection at the ground surface reaches 20% of the pile radius. Examples of the progression of z_c obtained from field tests are shown on Fig. 5. The average value of z_c during the load test is D_c (av) as shown on Fig. 4. Although the experimental evidence is limited, pressuremeter tests performed at sites of well documented load tests indicate that at large deflections the soil resistance against the pile, $p_{(max)}$ in force per unit length of pile, approaches the ultimate soil pressure obtained from pressuremeter tests times the width of the pile. This observation permits the conclusion that there is no need for a reduction factor to be applied to the pressuremeter model below D_c and validates the above definition of D_c.

The shape of the portion *AB* of the soil resistance distribution (Fig. 3) re-

$$S(R) = \frac{\text{Pressure at depth } z}{\text{Pressure at critical depth}}$$

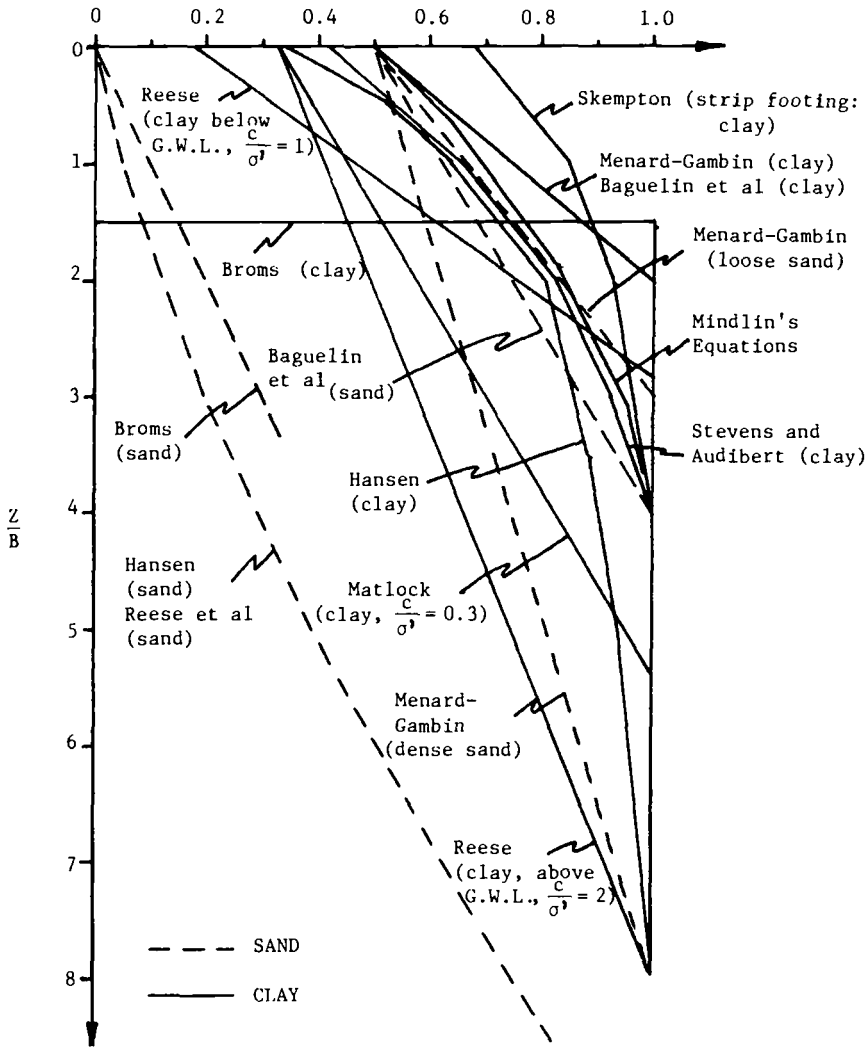

FIG. 2—*Critical depth—existing recommendations.*

mains approximately the same as the horizontal load H increases (Fig. 4). Therefore within z_c the reduction factor $S(R) = p/p_{(max)}$ is independent of H and varies only with z. Examples of $S(R)$ versus z/D_c curves are shown on Fig. 6, and an average curve is presented.

The critical depth D_c, as described above, is a soil-structure interaction

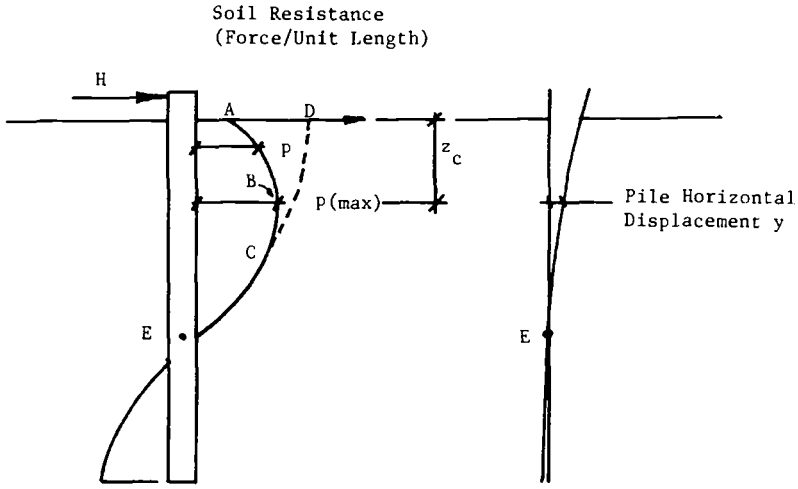

FIG. 3—*Definition of the instantaneous critical depth.*

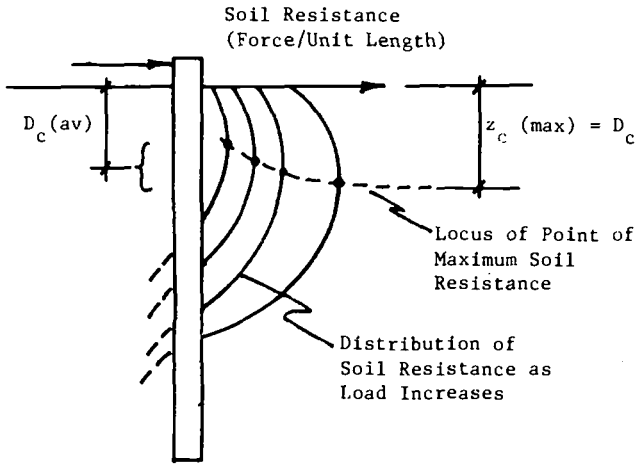

FIG. 4—*Definition of the ultimate critical depth.*

phenomenon. The close form solution of the interaction problem in linear elasticity makes use of the key interaction parameter l_0

$$l_0 = \sqrt[4]{4EI/E_{sh}}$$

where E is the modulus of the pile material, I is the moment of inertia of the pile cross section, and E_{sh} is the modulus of subgrade reaction of the soil. The

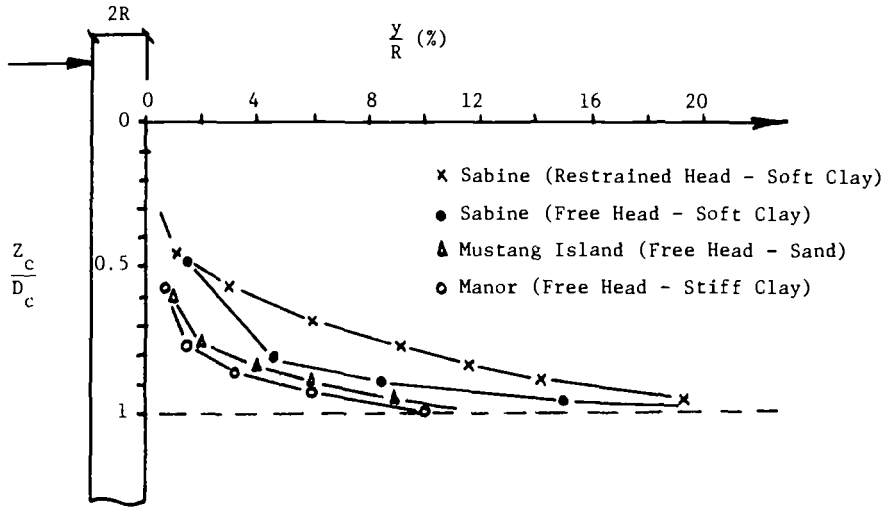

FIG. 5—*Examples of the locus of the point of maximum soil resistance.*

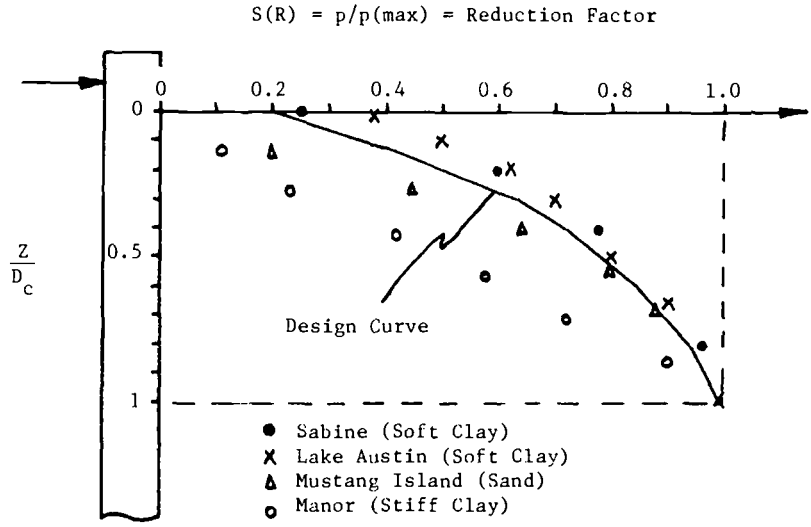

FIG. 6—*Reduction factor within the critical depth.*

following interaction parameter, called relative rigidity, was defined for this study as

$$RR = (1/B)\sqrt[4]{4EI/p_L^*}$$

where B is the pile width, or diameter, and p_L^* is the pressuremeter net limit pressure within the critical depth.

The correlation of Fig. 7 is a plot of the relative critical depth $D_c(av)/B$ versus RR. These data show that in the same soil, piles of different rigidity generate different relative critical depths (caisson and H pile in the silt of Plancoet, France) and that the same pile generates different relative critical depths in different soils (pipe pile at Sabine and at Lake Austin, Tex.).

At shallow depths the stress-free ground surface influences the results of pressuremeter tests [*12*]. There is a critical depth for pressuremeter tests that is different from the critical depth for laterally loaded piles. This difference is taken into account in Fig. 7 since the correlation involves the average p_L^* measured within the critical depth of the pile.

Existing Pressuremeter Methods

When a pile is loaded laterally, there are several components to the soil resistance (Fig. 8), namely, the front resistance resulting from normal stresses σ_r, the friction resistance resulting from shear stresses $\tau_{r\theta}$, the friction resistance resulting from shear stresses τ_{rz}, the base friction resistance resulting

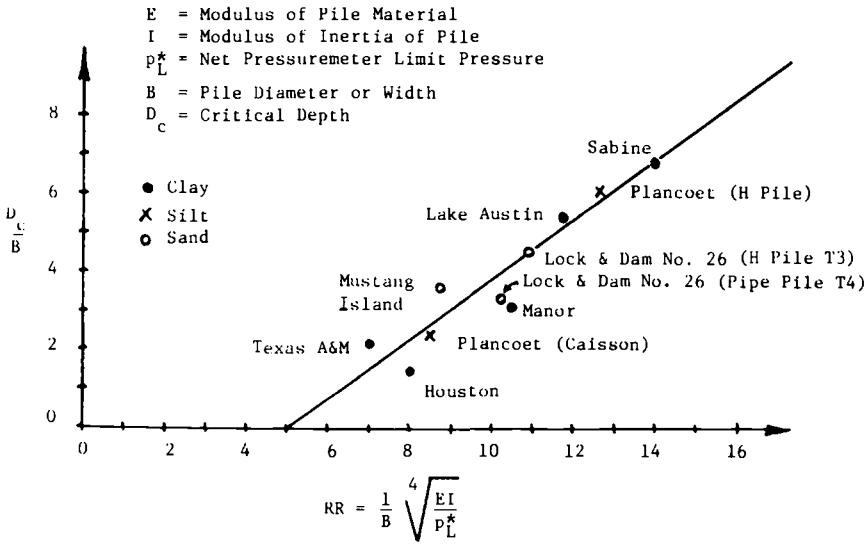

FIG. 7—*Critical depth as a function of relative rigidity.*

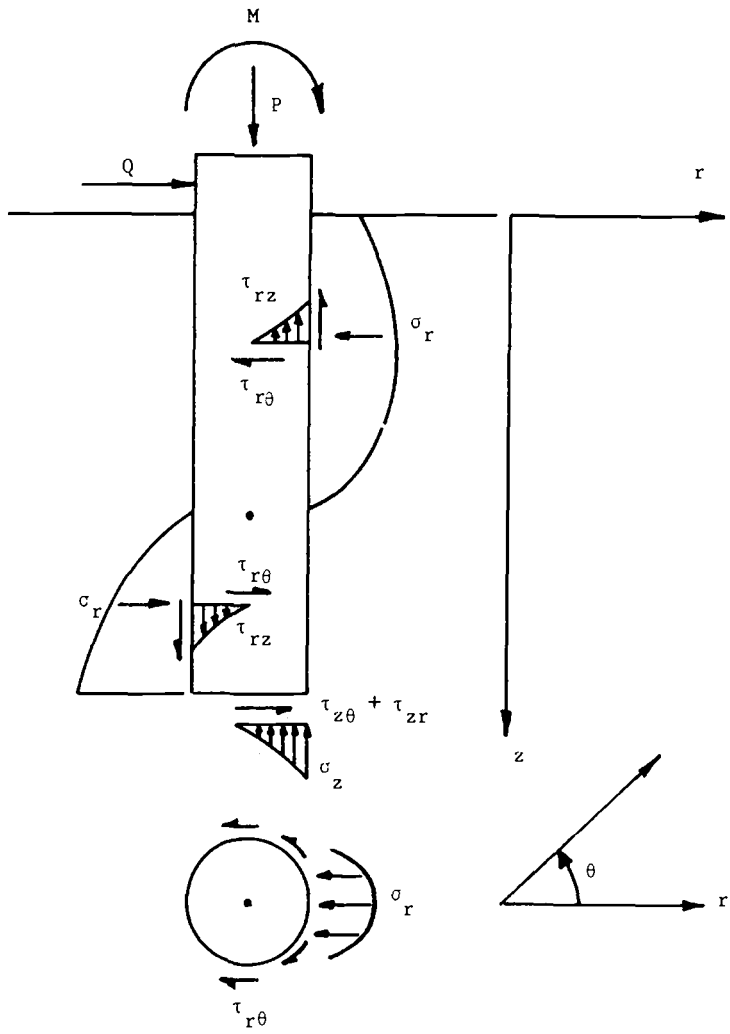

FIG. 8—*Components of soil resistance* [15].

from shear stresses $\tau_{z\theta}$ and τ_{zr}, and the base moment resistance resulting from normal stress σ_z. Except for very short stubby piles ($D/B \leq 3$) the major components of soil resistance are caused by σ_r and $\tau_{r\theta}$. At working loads the contribution resulting from the $\tau_{r\theta}$ effect may be as much as 50% of the total resistance [*13*].

At any depth z the resultant of the above soil resistances is the pile p-y curve where p is the resultant soil resistance in force per unit length, and y is the horizontal displacement.

At least seven methods have been proposed for predicting the horizontal

movement of a laterally loaded pile on the basis of pressuremeter test results. These methods are summarized below. Methods 1 through 5 make use of pressuremeter test results obtained from a prebored test cavity; whereas, Methods 6 and 7 make use of self-boring pressuremeter test results.

Method 1 [*8,9,14*] considers the p-y curve to be bilinear elastic-plastic. The slope of the first linear portion of the curve is obtained from Menard's equation for the settlement of a strip footing [*9*]. The second slope is half of the first slope and the soil ultimate resistance p_{ult} is given by the pressuremeter limit pressure. The critical depth is considered as shown on Fig. 2.

Method 2 [*15,16*] was developed for rigid drilled shafts and has the advantage of including all the components shown on Fig. 8. The σ_r and $\tau_{r\theta}$ resistances are combined into one lateral resistance model. This load-deformation model is a parabola with a limit on p_{ult} according to Hansen's theory [*5*]. The three other resistance models are elastic-plastic. The initial part of all models is correlated to the first load pressuremeter modulus. The limiting values are calculated by using the cohesion and friction angle of the soil. The critical depth effect is incorporated through Hansen's theory.

Method 3 [*17*] considers that the soil is homogeneous and has an average pressuremeter modulus. An equation is presented that describes the top horizontal load versus the top horizontal movement for the pile. This equation is based on the theory of linear elasticity [*9*] and is empirically modified for nonlinear material behavior. The parameters involved are the relative pile-soil stiffness, the pressuremeter modulus, the pile diameter, and the restraint conditions at the pile top. The critical depth is not considered directly.

Method 4 [*13,18*] uses the entire pressuremeter curve to obtain the Q (front)—y (pile) model (the σ_r effect) and the F (side)—y (pile) model (the $\tau_{r\theta}$ effect). Equations 1 through 3 and Fig. 9 are used to obtain these models.

$$Q\,(\text{front}) = p\,(\text{pmt}) \times B\,(\text{pile}) \times S(Q) \tag{1}$$

where

Q (front) = the portion of the soil resistance to pile movement resulting from the front reaction, force/unit length of pile,
p (pmt) = the net pressuremeter pressure,
B (pile) = the pile width or diameter, and
$S(Q)$ = a shape factor = 1.0 for square piles and 0.75 for round piles.

$$y\,(\text{pile}) = y(\text{pmt}) \times [R\,(\text{pile})/R\,(\text{pmt})] \tag{2}$$

where

y (pile) = the lateral deflection of the pile,
R (pile) = pile radius,

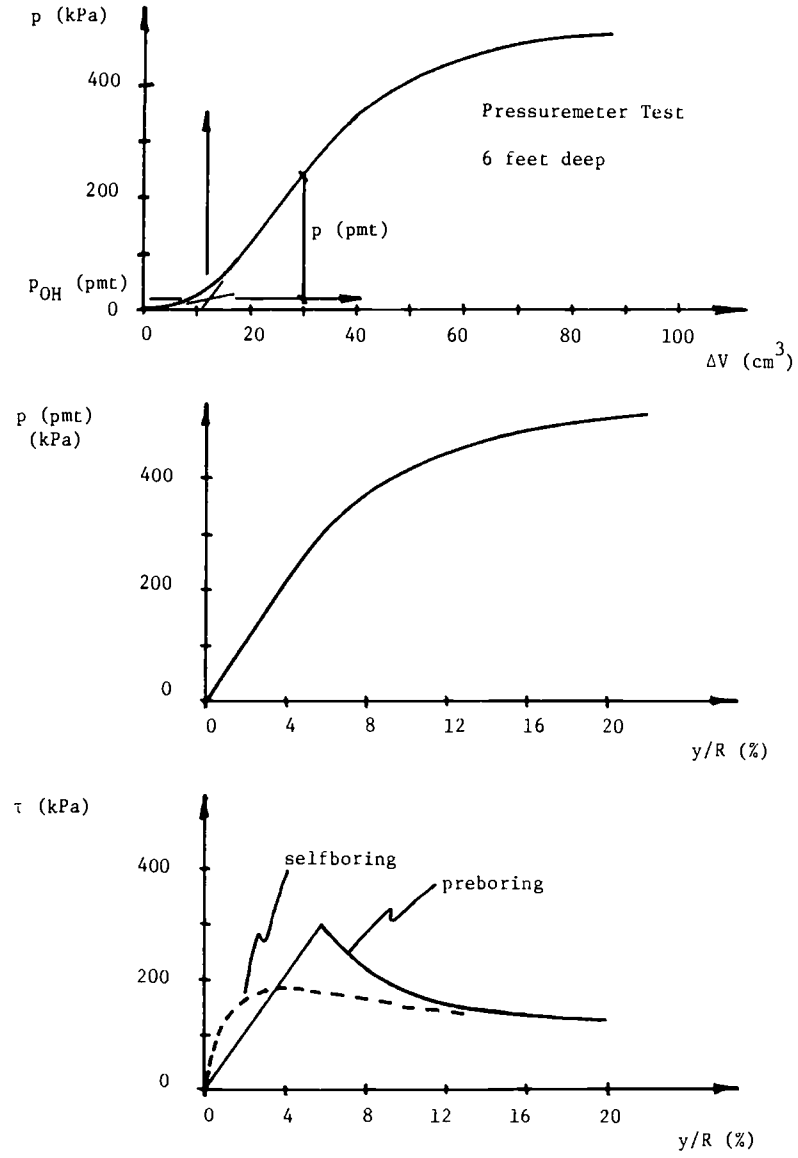

FIG. 9—*Pressuremeter* p-y *curve model.*

y (pmt) = increase in radius of the soil cavity in the pressuremeter test, and

R (pmt) = initial radius of the soil cavity in the pressuremeter test.

$$F\,(\text{side}) = \tau\,(\text{soil}) \times B\,(\text{pile}) \times S(F) \tag{3}$$

where

F (side) = the soil resistance resulting from friction, force/unit length of pile,
$S(F)$ = the shape factor = 2 for square piles and 1 for round piles, and
τ (soil) = soil shear stress obtained from the pressuremeter curve by the subtangent method.

The critical depth is determined from the correlation presented on Fig. 7, and the reduction factor given by the design curve of Fig. 6 is applied within the critical depth to the Q-y curves only. The p-y curve at a depth z is then obtained by the addition of the Q-y curve and the F-y curve at the same depth.

Method 5 [*19*] uses an elastic-plastic model for the frontal reaction. The slope of the elastic curve is obtained from the pressuremeter modulus and elasticity theory, while the ultimate value is considered to be the limit pressure from the pressuremeter. A friction model is also proposed, and the critical depth approach is the same as in Method 1.

Method 6 [*20*] uses the entire expansion curve from the self-boring pressuremeter as the p-y curve for the pile. Critical depth is considered as in Method 1.

Method 7 [*21*] uses the entire expansion curve from the self-boring pressuremeter but multiplies all pressure ordinates by two before considering it as the pile p-y curve. This method does not consider critical depth.

Comparison of the Methods on One Case History

The predictions of Methods 1 through 4 are compared below to the results of a pile load test performed on the campus of Texas A&M University [*22*]. The pile is a 0.92-m-diameter cast-in-place reinforced concrete drilled shaft (a nondisplacement pile) embedded 6.10 m in a stiff clay (Fig. 10). A horizontal load was applied at 0.76 m above the ground surface and was increased at the rate of approximately 5000 kg/day (5 tons/day). The load test results are shown on Fig. 11.

The soil at the test site is a stiff clay with the following average characteristics: liquid limit 50, plastic limit 20, natural water content 25, and total unit weight 20.1 kN/m^3. Unconfined compression test values and miniature vane test values were averaged to obtain the shear strength design profile shown on Fig. 10. Pressuremeter tests were performed with a pavement pressuremeter [*23*] in a hand-augered hole advanced without using drilling mud. The net limit pressure p_L^* and the pressuremeter modulus E_M [*9*] are shown on Fig. 10.

Figure 11 shows the prediction according to Methods 1 through 4. The computations according to Methods 1, 3, and 4 were performed by the authors. The computations according to Method 2 were performed by Davidson [*15,16*]. Davidson made his predictions without knowledge of the load test

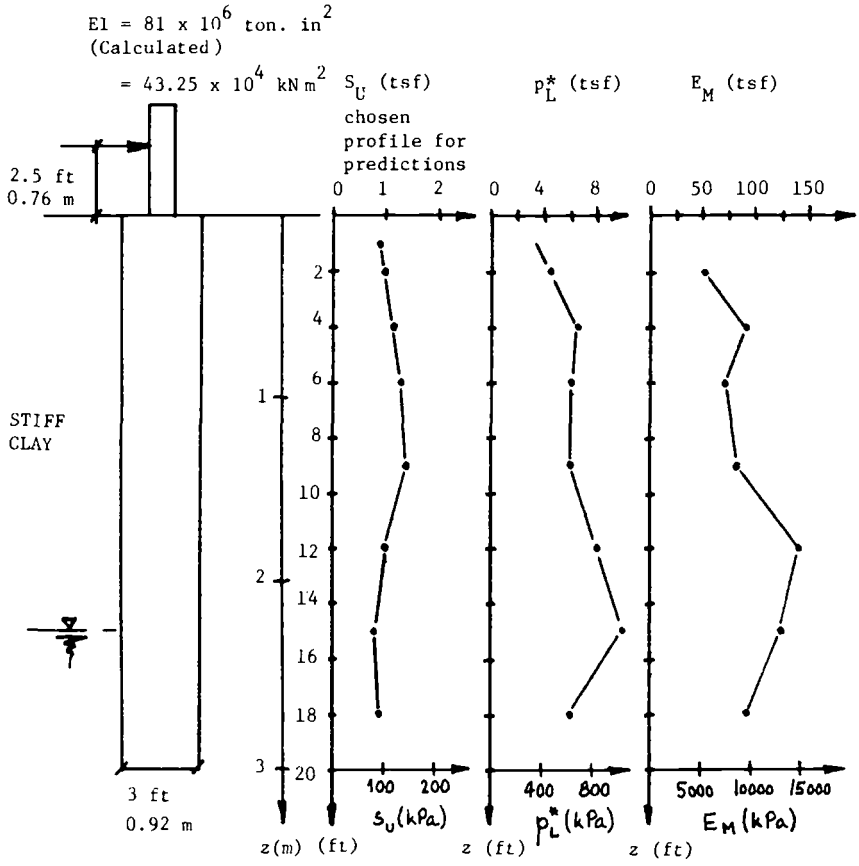

FIG. 10—*Soil properties.*

results. When comparing the four predictions to the load test results, the first general impression is that all of the predictions are relatively accurate with respect to the measured values. This case indicates that the pressuremeter provides a sound testing base for the behavior prediction of laterally loaded nondisplacement piles in stiff clays.

It is believed that none of the prediction curves show as much curvature as the load test because

1. The pile broke at 84 500 kg (84.5 tons) of lateral load, and it is probable that as the load increased, the stiffness *EI* of the pile decreased to become zero at rupture; yet in all methods the stiffness *EI* is kept constant through the modeling process.

2. The friction resistance ($\tau_{r\theta}$ effect on Fig. 8) is fully mobilized at very small displacements before full mobilization and predominance of the frontal resistance.

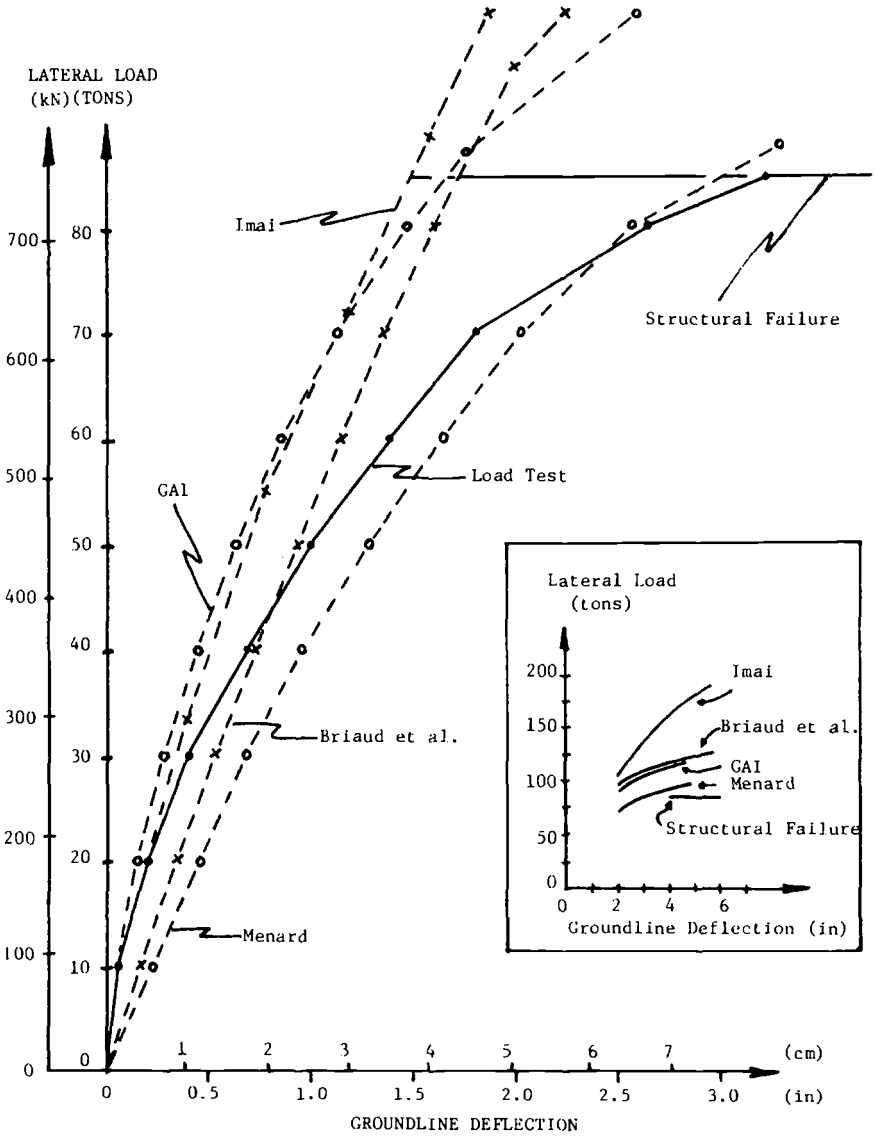

FIG. 11—*Comparison of predictions and measurement.*

The result of this friction-front resistance phenomenon is a change of curvature in the load deflection curve (at about 25 000 kg [25 tons] on Fig. 11). This change of curvature is often observed during vertical loading of piles.

Conclusions

A method is proposed for obtaining the depth D_c of the zone of reduced resistance in front of a laterally loaded pile. The proposed method of obtaining D_c is unique in that it includes the relative rigidity of the pile with respect to the strength of the soil. A reduction factor by which the soil resistance is multiplied in order to obtain the appropriate model for the pile within the depth of reduced resistance is also proposed.

Seven existing pressuremeter methods have been reviewed. It is shown with a comparison of four of these methods to a field load test in stiff clay that these four methods all give reasonable predictions. This tends to indicate that the pressuremeter provides a sound testing base for predicting the behavior of laterally loaded piles.

Acknowledgments

This study was totally funded by the National Science Foundation under a joint University-Industry Cooperation Grant No. CME 8006727. The authors wish to thank the following companies who contributed in various ways: Shell Development Company and the Texas State Department of Highways and Public Transportation. Dr. H. L. Davidson of GAI Consultants performed his computations on very short notice; his most cooperative effort is very much appreciated.

References

[1] Broms, B. B., "Design of Laterally Loaded Piles," *Journal of the Soil Mechanics and Foundations Division, Proceedings of the American Society of Civil Engineers*, Vol. 91, No. SM3, 1965.

[2] Matlock, H., "Correlations for Design of Laterally Loaded Piles in Soft Clay," *Offshore Technology Conference*, Vol. 1, Houston, 1970, pp. 577-588.

[3] Reese, L. C. and Welch, R. C., "Lateral Loading of Deep Foundations in Stiff Clay," *Journal of the Geotechnical Engineering Division, Proceedings of the American Society of Civil Engineers*, Vol. 101, No. GT7, 1975.

[4] Reese, L. C., Cox, W. R., and Koop, F. D., "Field Testing and Analysis of Laterally Loaded Piles in Stiff Clay," *Offshore Technology Conference*, Vol. 2, Houston, 1975, pp. 671-690.

[5] Hansen, B. J., "The Ultimate Resistance of Rigid Piles Against Transversal Forces," *The Danish Geotechnical Institute Bulletin No. 12*, Copenhagen, Denmark, 1961.

[6] Stevens, J. B. and Audibert, J. M. E., "Re-examination of *P-Y* Curve Formulations," *Offshore Technology Conference*, OTC Paper 3402, Houston, 1979.

[7] Skempton, A. W., "The Bearing Capacity of Clays," *Proceedings of the Building Research Congress*, Vol. 1, London, 1951.

[8] Menard, L., Bourdon, G., and Gambin, M., "Methode Generale de Calcul d'un Rideau ou d'un Pieu Sollicite Horiaontalement en Fonction des Resultats Pressiometriques," *Sols, Soils*, No. 22-23, 1969.

[9] Baguelin, F., Jezequel, J. F., and Shields, D. H., *The Pressuremeter and Foundation Engineering*, Trans Tech Publications, Rockport, Mass., 1978.

[10] Reese, L. C., Cox, W. R., and Koop, F. D., "Analysis of Laterally Loaded Piles in Sand," *Offshore Technology Conference*, OTC Paper 2080, Houston, 1974.

[11] Mindlin, R. D., "Forces at a Point in the Interior of a Semi-Infinite Solid," *Physics*, Vol. 7, May 1936, p. 195.

[12] Briaud, J.-L. and Shields, D. H., "Pressuremeter Tests at Very Shallow Depth," *Journal of the Geotechnical Engineering Division, Proceedings of the American Society of Civil Engineers*, Vol. 107, No. GT8, 1981.

[13] Briaud, J.-L., Smith, T. D., and Meyer, B. J., "Pressuremeter Gives Elementary Model for Laterally Loaded Piles," *International Symposium on In Situ Testing of Soil and Rock*, International Association of Engineering Geology, Paris, May 1983.

[14] Gambin, M., "Calculation of Foundations Subjected to Horizontal Forces Using Pressuremeter Data," *Sols, Soils*, No. 30/31, 1979.

[15] DiGioia, A., Davidson, H. L., and Donovan, T. D., "Laterally Loaded Drilled Piers: A Design Model," *Proceedings of a Session Entitled Drilled Piers and Caissons*, American Society of Civil Engineers, St. Louis, Oct. 1981.

[16] GAI Consultants, Inc., "Laterally Loaded Drilled Pier Research, Volume 1: Design Methodology, Volume 2: Research Documentation," Research Reports EPRI EL-2197, Monroeville, Pa., Jan. 1982.

[17] Imai, T., "The Estimation Method of Pile Behavior," OYO Corporation Intermal Memorandum, Technical Center, 2-6 Kudan Kita 4-Chome, Chiyeda-Ku, Tokyo, 102, Japan, 1969.

[18] Briaud, J.-L., Smith, T. D., and Meyer, B. J., "Design of Laterally Loaded Piles Using Pressuremeter Test Results," *Symposium on the Pressuremeter and Its Marine Applications*, Editions Technip, Paris, April 1982.

[19] Dunand, M., "Etude Experimentale du Comportement des Fondations Soumises au Renversement," These de Docteur Ingenieur, Institut de Mecanique de Grenoble, France, 1981.

[20] Baguelin, F., "Rules for the Structural Design of Foundations Based on the Self-boring Pressuremeter Test," *Symposium on the Pressuremeter and Its Marine Applications*, Editions Technip, Paris, April 1982.

[21] Hughes, J. M. O., Goldsmith, P. R., and Fendall, H. D. W., "Predicted and Measured Behavior of Laterally Loaded Piles for the Westgate Freeways Melbourne," Victoria Geomechanics Society, Australia, Aug. 1979.

[22] Kasch, V. R., Coyle, H. M., Bartoskewitz, R. E., and Sarver, W. G., "Lateral Load Test of a Drilled Shaft in Clay," Research Report 211-1, Texas Transportation Institute, Texas A&M University, College Station, Tex., 1977.

[23] Briaud, J.-L. and Shields, D. H., "A Special Pressuremeter and Pressuremeter Test for Pavement Evaluation and Design," *Geotechnical Testing Journal*, Vol. 2, No. 3, Sept. 1979, pp. 143-151.

John S. Horvath[1]

Simplified Elastic Continuum Applied to the Laterally Loaded Pile Problem—Part 1: Theory

REFERENCE: Horvath, J. S., **"Simplified Elastic Continuum Applied to the Laterally Loaded Pile Problem—Part 1: Theory,"** *Laterally Loaded Deep Foundations: Analysis and Performance, STP 835*, J. A. Langer, E. T. Mosley, and C. D. Thompson, Eds., American Society for Testing and Materials, 1984, pp. 112-121.

ABSTRACT: In 1958, Reissner showed that solving the problem of an elastic continuum subjected to a surface pressure was simplified if certain stress components were assumed to be equal to zero. The particular case he solved was for an isotropic, homogeneous layer of finite thickness. The writer named this the Reissner simplified continuum subgrade model and solved two other cases of Young's modulus varying with depth for a layer of finite thickness. The writer also demonstrated that Winkler's modulus of subgrade reaction model can also be derived using the general approach of applying simplified assumptions to an elastic continuum and studied the behavior of mat foundations on simplified continua. This paper presents the theoretical development of the application of the simplified continuum approach to the laterally loaded pile problem. A subsequent paper will compare results obtained using the simplified continuum approach with other, established methods.

KEY WORDS: elastic deformation, elastic media, elastic theory, lateral forces, pile lateral loads, piles, subgrade reaction

The general subject of this paper is analytical methods for estimating the deformation of laterally loaded piles. A brief review and critique of existing methods is presented. A new method, based on the simplified elastic continuum approach, is then developed. The purpose of proposing a new method is to offer a better compromise between theoretical exactness and computational ease than is currently available.

[1] Project engineer, Woodward-Clyde Consultants, Inc., 1250 Broadway, Suite 1500, New York, N.Y. 10001 and adjunct associate professor, Columbia University, School of Engineering and Applied Science, Department of Civil Engineering and Engineering Mechanics, New York, N.Y. 10027. Dr. Horvath is a member of ASTM.

Existing Methods of Analysis

Reference *1* contains a fairly recent and complete summary of the principal existing methods for estimating the load versus deflection behavior of laterally loaded piles. These methods fall into two broad groups: one using Winkler's modulus of subgrade reaction concept as the soil model, and the other using an elastic continuum as the soil model.

The traditional approach has been to use the modulus of subgrade reaction model that is normally attributed to Winkler [*2*, *4*]. This model assumes that the relationship between an applied pressure p from a pile and the horizontal deflection of the pile y at a point can be expressed as

$$p = k_h y \tag{1}$$

where k_h is a constant that is normally referred to as the horizontal modulus of subgrade reaction. The usual physical model used to depict this relationship is a series of linear springs (Fig. 1).

Solutions of Eq 1, assuming either that k_h is constant or varies linearly with depth, are available in chart form as is a solution for two layers, each with a different, but constant, value for k_h. The simplicity of this model, availability of chart solutions, and ease of hand calculation favor its use to this day.

However, it has long been recognized that the behavior of laterally loaded piles is frequently nonlinear because failure of near-surface soil develops in many situations, even under relatively small load levels. Probably the best known approach to overcoming this shortcoming has been the development of p-y curves by Reese and his co-workers. A p-y curve is simply a nonlinear pressure versus deflection curve that is calculated a priori for a finite number of points along a pile. These curves substitute for the linear springs of the Wink-

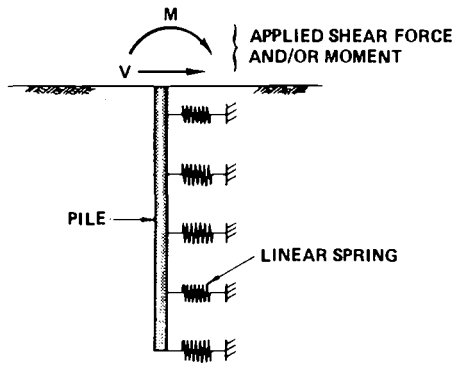

FIG. 1—*Winkler's modulus of subgrade reaction model applied to laterally loaded piles.*

ler model. Therefore, the *p-y* approach is essentially an evolutionary refinement of the basic Winkler model. Although the *p-y* approach requires a computer program for solution of a problem, it is readily solved using finite differences and presents no significant obstacle for routine use in analysis and design.

The writer [*2,3*] has shown that the Winkler modulus of subgrade reaction model is actually a very crude approximation of an elastic continuum, which many researchers believe is often a reasonable model for soil. Because of the approximate nature of the Winkler model, it has always been difficult to equate k_h, or *p-y* curves, to fundamental soil parameters such as Young's modulus or Poisson's ratio. Rather, the general practice has been to use back-calculated values from full-scale load tests. This may be an acceptable approach, particularly if a large number of observations are made to validate the correlations. However, there is a basic uncertainty in any empirical or semi-empirical approach, particularly if an extrapolation to untested conditions is required. This is a reflection on the approximate nature of the basic Winkler soil model.

Researchers have long recognized this inability of the simple Winkler model to simulate soil. Perhaps the most glaring shortcoming is that shear coupling between the soil "springs," to simulate the shear behavior of actual soil, is not modelled explicitly, but only in some uncontrolled way if k_h is back-calculated from full-scale tests. References *2* and *4* discuss some of the numerous attempts applied mechanics researchers have made to introduce shear coupling into the Winkler model. One of the very few applications of these improved models to a civil engineering problem was made recently by Georgiadis and Butterfield [*5*] who applied Pasternak's model to laterally loaded piles. The Pasternak model as applied to this problem is shown in Fig. 2. Note that Pasternak's improvement to the Winkler model was the introduction of an interspring shear layer to approximate soil shear. However, the difficulty still exists in relating the Pasternak model coefficients to soil parameters. Georgiadis and Butterfield used values back-calculated from model-test results; however, there are drawbacks to this as discussed by the writer [*6*].

The other extreme has been to model the soil as an elastic continuum. Theoretically, this should eliminate the problem with evaluating the model coefficients. Although this approach has been published for nearly 20 years, extensive work has only been published for about the past 10 years, primarily by Poulos. Reference *1* contains the most complete summary on this subject that is currently available. While an elastic continuum may be a more elegant approach to the laterally loaded pile problem, there are difficulties in adapting it to handle nonlinear behavior, a Young's modulus that varies linearly with depth, and other practical considerations. In the writer's opinion, the elastic continuum model appears to be too cumbersome in its present form to be embraced by practicing engineers as a replacement for methods based on Winkler's model.

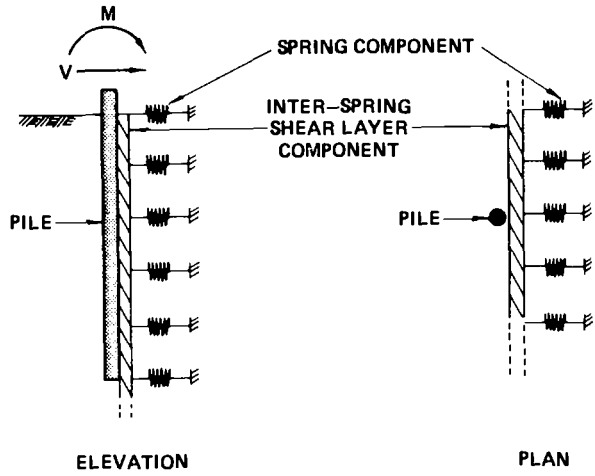

FIG. 2—*Pasternak's model applied to laterally loaded piles.*

Background of a Proposed New Method of Analysis

In 1958, Reissner [7] solved the problem of an isotropic, homogeneous elastic continuum of infinite lateral extent but finite thickness. This layer was underlain by a rigid base and subjected to a surface pressure p (Fig. 3). To facilitate solution, Reissner assumed that certain stresses (σ_x, σ_y, τ_{xy}) within the elastic layer that resulted from the applied pressure were equal to zero. In addition, he neglected body forces. Values of the remaining stress components and all strain components were not assumed a priori. These simplifying assumptions were then applied to the usual equations of stress-strain, strain-displacement, and equilibrium that govern the behavior of an elastic continuum. The resulting partial differential equation relating the surface pressure p and surface displacement W is

$$C_1 W - C_2 \nabla^2 W = p - C_3 \nabla^2 p \tag{2}$$

where C_1, C_2, and C_3 are constants and $\nabla^2 = \partial^2/\partial x^2 + \partial^2/\partial y^2$. The constants are only functions of the elastic parameters E and G of the layer and the layer thickness H.

The writer [2,8] used Reissner's stress assumptions to solve the problem shown in Fig. 3 but assuming that Young's modulus E varied linearly or with the square root of depth. This was done to more closely simulate the actual behavior of soil. The resulting differential equation relating surface pressure and displacement is still of the form given by Eq 2. The coefficients C_1, C_2, and C_3 are likewise still constant and functions of E, G, and H.

The writer has named this subgrade model the Reissner simplified con-

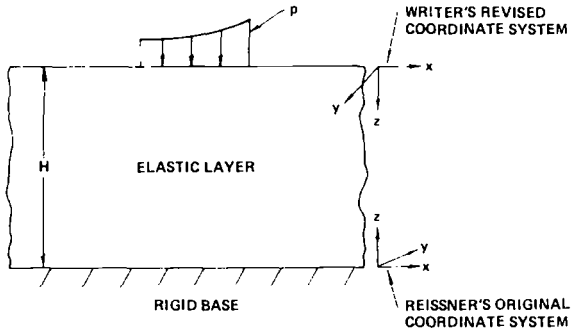

FIG. 3—*Reissner's simplified elastic continuum.*

tinuum (RSC) and investigated its use for the mat foundation problem [*2,8*]. Studies [*2,8*] indicated that the RSC agrees quite favorably with closed-form theory of elasticity solutions, and offers a substantial improvement over the Winkler subgrade model. At the same time, the differential equation that governs the RSC is relatively simple and can be solved readily using finite differences.

Proposed New Method

As discussed previously, the problem of analyzing the response of piles to lateral loads was first attempted using the simple Winkler subgrade model. The history of analyzing mat foundations is quite similar in its evolution. This suggests that the simplified continuum approach could be extended logically to the laterally loaded pile problem.

Figure 4 illustrates the problem formulation for a simplified continuum as applied to laterally loaded piles. After some consideration, it appeared that a set of simplifying assumptions similar to those used by Reissner for mat foundations facilitated solution of the laterally loaded pile problem. Specifically, σ_y, σ_z, and τ_{yz} were assumed to be equal to zero. In addition, all displacements were assumed to be equal to zero at some horizontal distance T from the pile. At any given depth, Young's modulus was assumed to be constant in a horizontal direction. This appears to be quite reasonable. Variations of Young's modulus with depth can be handled readily in a computer-solved finite-difference formulation of the problem by simply assigning different values for E at each node point.

A complete derivation of the Reissner-type simplified continuum (RTSC) for a laterally loaded pile is presented in the Appendix. The resulting partial differential equation relating the pressure p, which the pile exerts on the elastic continuum and displacement of the pile parallel to the axis U, is

$$K_1U - K_2\nabla^2U = p - K_3\nabla^2p \tag{3}$$

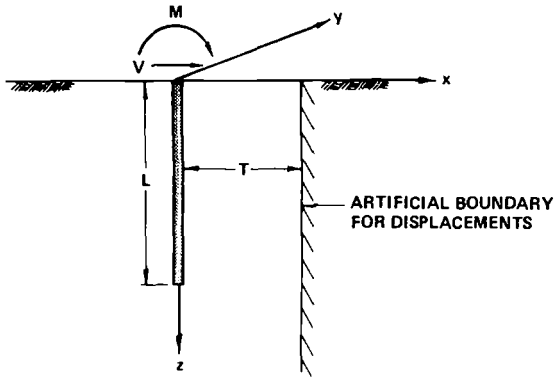

FIG. 4—*Reissner-type simplified elastic continuum applied to laterally loaded piles.*

where K_1, K_2, and K_3 are constants that are functions only of the elastic parameters E and G of the body and the distance to the artificial boundary T. Rearranging terms, we can express Eq 3 as

$$p = K_1 U - K_2 \nabla^2 U + K_3 \nabla^2 p \tag{4}$$

Future Work

Reference *1* contains a number of case histories that were analyzed using the exact theory of elasticity method that was previously discussed. Work is currently underway to evaluate these case histories using the simplified continuum approach discussed in this paper. The results will be presented at a later date.

Acknowledgments

The writer is grateful to Woodward-Clyde Consultants, Inc., for providing the typing and drafting services associated with preparation of this paper.

APPENDIX

Derivation of the RTSC for Laterally Loaded Piles

The equations relating stress-strain, strain-displacement, and equilibrium for an elastic continuum can be found in any number of texts, for example, Ref *9*.

The pile is assumed to be a thin strip of width or diameter d. The boundary conditions for this problem are

° at $x = T$: $u = v = w = 0$

° at $x = 0$ (that is, the face of the pile) $\sigma_x(0, 0, z) = -p(y, z)$

$U = u(0, 0, z)$

$v(0, 0, z) = w(0, 0, z) = 0$

Here, $p(y, z)$ is the contact pressure between the pile and elastic continuum. Because it is a compressive stress and this derivation is using mechanics of materials convention (tension positive), $\sigma_x(0, 0, z)$ is a negative (that is, compressive) stress.

The simplifying assumptions made with regard to stresses within the elastic continuum are that $\sigma_y = \sigma_z = \tau_{yz} = 0$. In addition, body forces are neglected. The remaining stress components can be redefined as follows

$$\sigma = \sigma_x$$
$$\tau_y = \tau_{xy}$$
$$\tau_z = \tau_{xz}$$

By combining the stress-strain and strain-displacement equations and inserting the above values of the various stress components, we get

$$\partial u/\partial x = \sigma/E \tag{5}$$

$$(\partial u/\partial y) + (\partial v/\partial x) = \tau_y/G \tag{6}$$

$$(\partial u/\partial z) + (\partial w/\partial x) = \tau_z/\mathrm{G} \tag{7}$$

These three equations are used to derive the RTSC model. The following remaining stress-displacement equations are not used

$$\partial v/\partial y = \partial w/\partial z = -\nu\sigma/E$$
$$\partial v/\partial z + \partial w/\partial y = 0$$

The following are the simplified equilibrium equations

$$\partial\sigma/\partial x + \partial\tau_y/\partial y + \partial\tau_z/\partial z = 0 \tag{8}$$

$$\partial\tau_y/\partial x = 0 \tag{9}$$

$$\partial\tau_z/\partial x = 0 \tag{10}$$

Note that Eqs 8 and 10 imply that τ_{xy} and τ_{xz} are constant in the horizontal direction parallel for the x axis.

For simplicity in subsequent derivations, we define the term

$$S = \partial\tau_y/\partial y + \partial\tau_z/\partial z$$

Derivation

From Eq 8

$$\partial\sigma = -S\partial x \tag{11}$$

$$\sigma = \int -S\partial x \tag{12}$$

$$\sigma = -Sx + c + f(y,z) \tag{13}$$

where c is an integration constant and $f(y, z)$ is an integration function of y or z or both. At $x = 0$, $\sigma = -p$, so

$$c + f = -p \tag{14}$$

$$\sigma = -p - Sx \tag{15}$$

Note that this implies that σ_x varies linearly between the pile and the artificial boundary.

From Eq 5

$$\partial u = (\sigma/E)\,\partial x \tag{16}$$

$$u = 1/E \int_c^x \sigma \partial x \tag{17}$$

$$u = 1/E \int_c^x (-p - Sx)\,\partial x \tag{18}$$

$$= 1/E\,[-px - S(x^2/z)] + c + f(y,z) \tag{19}$$

Because $u = 0$ at $x = T$

$$0 = 1/E\,[pT + S(T^2/2)] + c + f \tag{20}$$

$$c + f = 1/E\,[pT + S(T^2/2)]$$

$$u = p\,[(T/E) - (x/E)] + S\,[(T^2/2E) - (x^2/2E)] \tag{21}$$

Because $u(0, 0, z) = U$

$$U = p(T/E) + S(T^2/2E) \tag{22}$$

$$S = (2E/T)U - 2p/T \tag{23}$$

From Eq 6

$$\partial v/\partial x = \tau_y/G - (\partial u/\partial y) \tag{24}$$

$$v = \tau_y/G \int_c^x \partial x - \int (\partial u/\partial y)\,\partial x \tag{25}$$

$$v = (\tau_y/G)x - (\partial p/\partial y)(T/E)x + (\partial p/\partial y)(x^2/2E)$$
$$- (\partial S/\partial y)(T^2/2E) + (\partial S/\partial y)(x^3/6E) + c + f(y,z) \tag{26}$$

Because $v = 0$ at $x = T$

$$c + f = (\tau_y/G)T + (\partial p/\partial y)(T^2/2E) + (\partial S/\partial y)(T^3/2E) \tag{27}$$

$$v = (\tau_y/G)(x - T) + (\partial p/\partial y)[(T^2/2E) - (T/E)x + (x^2/2E)]$$
$$+ (\partial S/\partial y)|(x^3/6E) - (T^2/2E)x + (T^3/3E)| \tag{28}$$

Similarly, from Eq 7 we get

$$w = (\tau_z/G)(x - T) + (\partial p/\partial z)[(T^2/2E) - (T/E)x + (x^2/2E)] + (\partial S/\partial z)[(x^3/6E) - (T^2/2E)x + (T^3/3E)] \quad (29)$$

From Eqs 28 and 29, evaluated at $x = 0$, we get

$$\tau_y = (2G/3)(\partial U/\partial y) - (GT/6E)(\partial p/\partial y) \quad (30)$$

$$\tau_z = (2G/3)(\partial U/\partial z) - (GT/6E)(\partial p/\partial z) \quad (31)$$

From Eq 8, we get

$$(2G/3)(\partial^2 U/\partial y^2) - (GT/6E)(\partial^2 p/\partial y^2) + (2G/3)(\partial^2 U/\partial z^2) - (GT/6E)(\partial^2 p/\partial z^2) - (2E/T^2)U + (2p/T) = 0 \quad (32)$$

Defining $\partial^2/\partial y^2 + \partial^2/\partial z^2 = \nabla^2$, after rearranging terms we get

$$(E/T)U - (GT/3)\nabla^2 U = p - (GT^2/12E)\nabla^2 p \quad (33)$$

This can be expressed as

$$K_1 U - K_2 \nabla^2 U = p - K_3 \nabla^2 p \quad (34)$$

where

$K_1 = E/T$,

$K_2 = GT/3$, and

$K_3 = GT^2/12E$.

Equation 34 is the same as Eq 3 in the main text of this paper.

References

[1] Poulos, H. G. and Davis, E. H., *Pile Foundation Analysis and Design*, Wiley, New York, 1980, Chapter 8.

[2] Horvath, J. S., "A Study of Analytical Methods for Determining the Response of Mat Foundations to Static Loads," Ph.D. thesis, Polytechnic Institute of New York at Brooklyn, 1979.

[3] Horvath, J. S., "Modulus of Subgrade Reaction: A New Perspective," *Journal of Geotechnical Engineering, Proceedings of the American Society of Civil Engineers*, Vol. 109, No. 12, Dec. 1983.

[4] Horvath, J. S., "Historical Review of Subgrade Model," *Geotechnique*, in press.

[5] Georgiadis, M. and Butterfield, R., "Laterally Loaded Pile Behavior," *Journal of the Geotechnical Engineering Division, Proceedings of the American Society of Civil Engineers*, Vol. 108, No. GT. 1, Jan. 1982, pp. 155-165.

[6] Horvath, J. S., "Discussion of 'Laterally Loaded Pile Behavior' by Georgiadis and R. Butterfield," *Journal of the Geotechnical Engineering Division, Proceedings of the American Society of Civil Engineers*, Vol. 109, No. 5, May 1983, pp. 773-775.

[7] Reissner, E., "A Note on Deflection of Plates on a Viscoelastic Foundation," *Journal of Ap-*

plied Mechanics, Vol. 25; *Transactions of the American Society of Mechanical Engineers*, Vol. 80, 1958, pp. 144-145.

[8] Horvath, J. S., "New Subgrade Model Applied to Mat Foundations," *Journal of Geotechnical Engineering. Proceedings of the American Society of Civil Engineers*, Vol. 109, No. 12, Dec. 1983, pp. 1567-1587.

[9] Timoshenko, S. P. and Goodier, J. N., *Theory of Elasticity*, McGraw-Hill, New York, 1970.

William R. Cox,[1] *David A. Dixon,*[2] *and Benton S. Murphy*[3]

Lateral-Load Tests on 25.4-mm (1-in.) Diameter Piles in Very Soft Clay in Side-by-Side and In-Line Groups

REFERENCE: Cox, W. R., Dixon, D. A., and Murphy, B. S., **"Lateral-Load Tests on 25.4-mm (1-in.) Diameter Piles in Very Soft Clay in Side-by-Side and In-Line Groups,"** *Laterally Loaded Deep Foundations: Analysis and Performance, ASTM STP 835*, J. A. Langer, E. T. Mosley, and C. D. Thompson, Eds., American Society for Testing and Materials, 1984, pp. 122-139.

ABSTRACT: Studies were made to investigate efficiencies of pile groups under lateral loading. The loading was in one direction at slow displacement rates approaching static conditions. The test piles were 25.4-mm (1-in.) diameter tubes open-ended, with penetrations of two, four, six, or eight diameters. Tests were made on single piles and on three- and five-pile groups with clear spacings of 0.5, 1, 2, 3, and 5 diameters in side-by-side or in-line arrangements. The tests were run in a very soft clay with a moisture content of 59% and a shear strength of 2 kPa (42 psf).

Summaries are given of efficiencies of 20 combinations of pile numbers, penetrations, arrangements, and clear spacings. Efficiencies are given for individual piles in a pile group as well as for the entire group. Distances from the soil surface to the load resultant on individual piles and to the load resultant on the total group are also given.

KEY WORDS: piles, foundations, lateral loads, group action, efficiency, clay, instrumentation

The purpose of the studies presented herein was to investigate efficiencies of side-by-side and in-line groupings of piling under lateral loading. The term in-line designates a series of piles, one behind the other, with the line of piles parallel to the direction of lateral loading. The term side-by-side designates a series of piles positioned on a line perpendicular to the direction of lateral loading.

[1] Senior consultant, McClelland Engineers, Inc., Houston, Tex. 77274.
[2] Chief engineer, Amco Exploration Co., London, England.
[3] Staff research engineer, Amco Production Co., Tulsa, Okla.

Scope of Study

The lateral loading was applied in one direction at a slow rate of movement of the piles through the soil that approached static loading conditions. The piles were short stubs inserted into the soil two to eight diameters below the soil surface. The pilings were machined from 25.4-mm (1-in.) diameter stainless-steel tubing with a wall thickness of 0.71 mm (0.028 in.). The near-surface behavior of groups of piles under lateral loading is believed obtained by studies on the efficiencies of these stubs since it is only in the upper few diameters of a pile's penetration where significant lateral movements are experienced. Furthermore, it is easier to set up tests in which pile stubs are used as opposed to long piles. The ease of setup permits a larger number of tests to be run in a given period for investigation.

Tests were made on single piles and on three- and five-pile groups. Clear spacings of 0.5, 1, 2, 3, and 5 diameters were used in the group tests. The soil was a very soft clay with a moisture content of 59% and a shear strength of 2 kPa (42 psf).

The system of instrumentation and the scheme of analysis yielded load-deflection relationships for individual piles in the group tests. From these load-deflection relationships it was possible to arrive at efficiencies of the pile group and of individual piles in the group.

Soil

Selection of Soil

The soil used for the tests was a Wilcox clay, which is blackish in color and contains predominately kaolinite. A number of tests performed by Desai [*1*] revealed low thixotropic properties for the Wilcox clay that can be attributed to the high kaolinite content. The mineralogical composition of the clay is shown in Table 1.

The Atterberg limits of the Wilcox clay are 61% for the liquid limit and 21% for the plastic limit. On the plasticity chart developed by Casagrande [*2*] the clay is identified with inorganic clays of high plasticity. The grain sizes expressed as percentage of total weight of the soil specimen are shown in Table 2.

TABLE 1—*Mineralogical composition of clay.*

Mineral	Composition, %
Quartz	0 to 5
Montmorillonite and illite	10 to 20
Kaolinite	85 to 90

TABLE 2—*Grain sizes expressed as percentage of total weight of the soil specimen.*

Specimen	Grain Size, mm	Percent of Total Weight
Fine sand	0.25 to 0.05	7
Silt	0.05 to 0.005	23
Clay	<0.005	70

Preparation of Wilcox Clay

The clay was dried in a large oven and then sieved over a 850-μm (No. 20) sieve, which has a nominal opening size of 0.833 mm. The sieved soil was blended with water using a large batch mixer. Three mixings were required to yield a soil with a uniform moisture content of approximately 59%. At this percent of moisture the Wilcox clay has a shear strength of 2 kPa (42 psf) as determined by a miniature vane.

The test box had a stainless-steel liner. The plan dimensions of the liner were 64 by 64 cm (25 by 25 in.), and the clay was filled in the liner to a depth of 41 cm (16 in.). The soil surface was screeded to a level plane, and then approximately 13 mm (0.5 in.) of water was placed on top of the soil to prevent drying. After a series of tests had been run, the soil was discarded, and new soil was placed in the box for the next series. A total of 14 boxes of soil were used in the investigation.

Since Wilcox clay is relatively nonthixotropic, no waiting was necessary between placing soil in the box and initiating testing; however, testing was never initiated sooner than 12 to 16 h after soil placement.

Vane Tests for Determining Shear Strength

A miniature vane with a width of 21 mm (0.83 in.) and a height of 42 mm (1.66 in.) was used for determining the shear strength of the Wilcox clay in the test box. Two shear tests were made in a single hole. For example, for pile penetrations of eight diameters the first test was taken with the bottom of the vane located three diameters beneath the soil surface. The vane was removed, cleaned, and reinserted in the same hole and advanced to a depth of eight diameters where a second shear test was made.

Test Equipment and Procedures

Strain Bars

Strain bars were used as the transducers for measuring load in individual piles. The four strain bars, shown in Fig. 1, had reduced thicknesses in a sec-

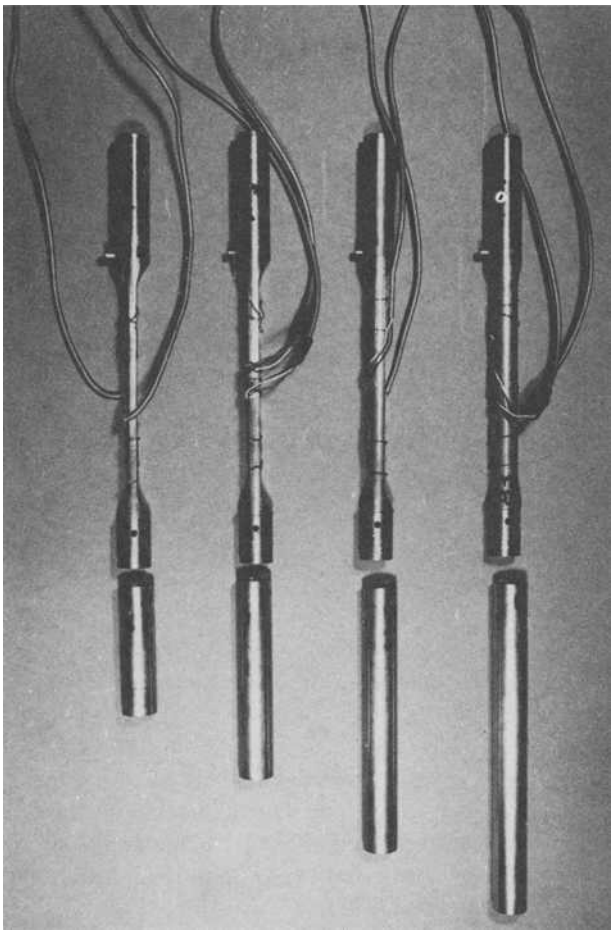

FIG. 1—*Strain bars and test piling for soil penetrations of two, four, six, and eight diameters.*

tion on which strain gages were installed. From left to right the strain bars are for pile penetrations of two, four, six, and eight diameters. The corresponding thicknesses in the reduced section for these strain bars are 5, 8, 10, and 15 mm (0.2, 0.3, 0.4, and 0.6 in.). Shown below each of the strain bars are pilings, which were used for the tests at penetrations of two, four, six, and eight diameters.

Interpretation of Loads on Test Piles

Two methods were used to interpret the load history of the soil on a pile during testing, as indicated in Fig. 2. In one method (Fig. 2*a*) it was assumed that the total load on a pile could be represented by a pressure diagram of

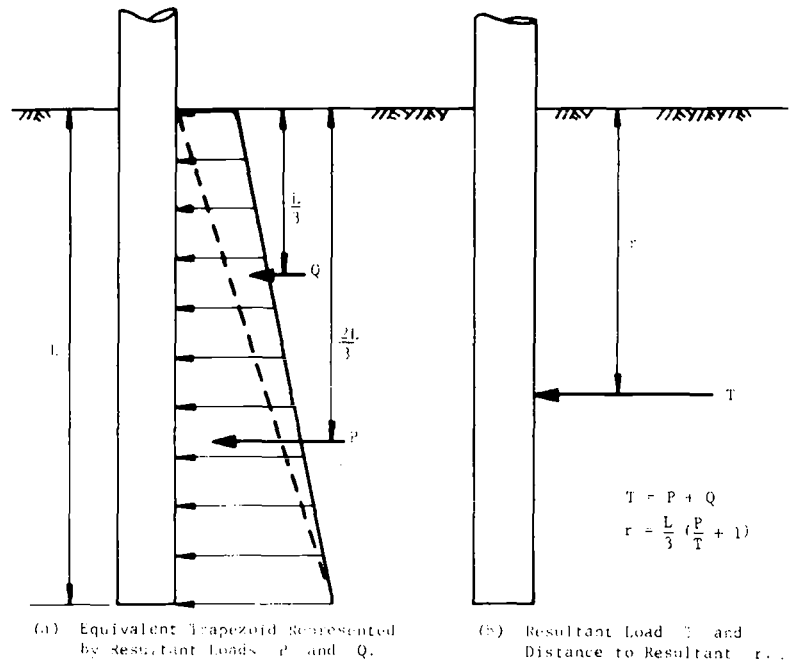

FIG. 2—*Two methods for representing the resultant of the lateral load of soil on pile.*

trapezoidal shape. In turn, the trapezoidal shape can be represented by two triangles. The loads that were used during calibration of the strain bars correspond to the resultant load of each of these triangular shapes. The resultant load in the lower triangle was referred to as P, and the resultant load in the upper triangle was referred to as Q.

In the second method (Fig. 2*b*), the total load on the pile was represented as a resultant load T, and the distance from the soil surface to the point of action of T was represented as r. If the distance r from the soil surface to the resultant of the total load on the pile is less than one-third of the penetration of the pile L then the sign of P in Fig. 2*a* will be negative. If r is greater than two-thirds of L then the sign of Q in Fig. 2*a* will be negative.

Wagon Assembly

The wagon assembly used for the lateral loading tests is shown in Fig. 3. This assembly was made up of four square plates with 38 cm (15 in.) side dimensions. The two center plates were connected by bushings to form a box section with an overall height of 9 cm (3.5 in.). In the top plate of the box section there were holes that were machined to receive a reduced diameter at the top of the strain bar. In the bottom plate of the box section holes were ma-

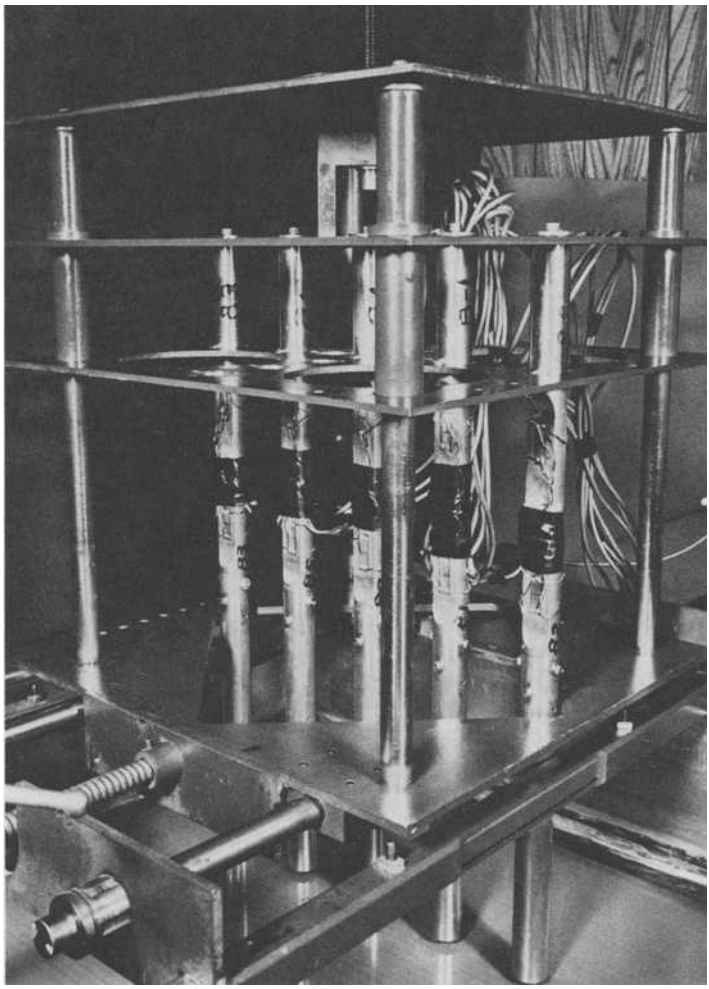

FIG. 3—*Wagon assembly with strain bars and test piles in position before vertical penetration into the soil.*

chined to receive the full 25.4 mm (1 in.) diameter of the strain bars, and, in addition, slots were machined to receive a pin in the strain bar that restricted the strain bar from rotation. Holes in the upper and lower plates of the box were positioned to provide for the various pile groups and clear spacings that were investigated.

The wagon assembly was supported on horizontal solid bars. The bars extend approximately 18 cm (7 in.) beyond the edge of the bottom wagon plate. The horizontal bars extend through linear bearings, one of which is shown in the bottom left-hand corner of Fig. 3. There are five strain bars positioned

side by side with two-diameter clear spacing in Fig. 3. The pilings shown are for eight-diameter penetration, and they are in position just before being pushed into the soil in readiness for tests.

The linear bearings that received the horizontal shafts of the wagon assembly were supported in a vertical plate connected to two rails. The rails spanned the test box and were of sufficient length to provide for a variety of positions of the piling within the test box.

Horizontal movement of the wagon assembly was provided by means of a 0.015-kW (0.02-hp) electric motor that provided thrust to a shaft with Acme threads, which is shown just above the linear bearing in the lower left-hand part of Fig. 3. Horizontal movement of the wagon was monitored with a linear motion potentiometer.

Soil Box

The soil box is shown in Fig. 4. This box was fabricated from 19-mm (¾-in.) plywood, which was inserted inside a frame made from steel angle iron. A metal liner, made from 0.45-mm (26-gage) stainless-steel plates, was

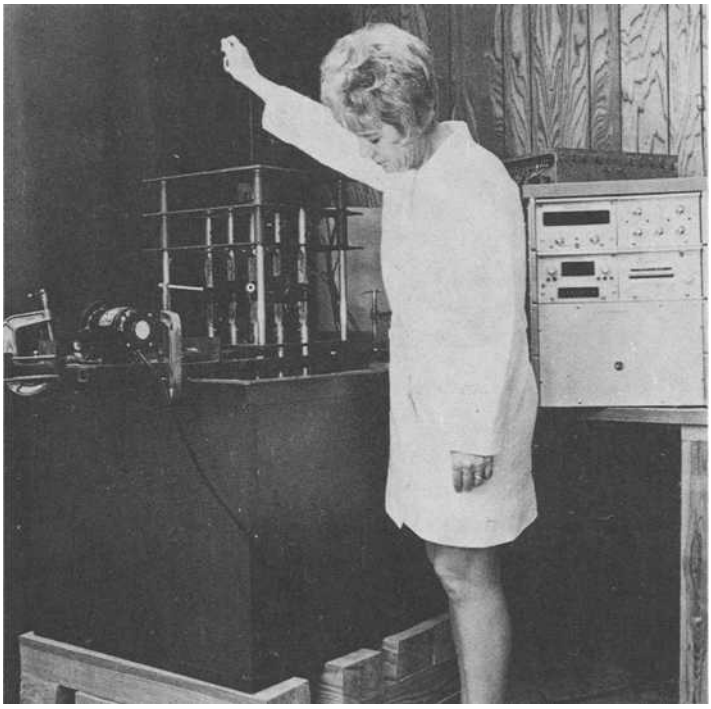

FIG. 4—*Lowering the wagon assembly to push the piling into the soil.*

inserted inside the box. The box had inside plan dimensions of 64 by 64 cm (25 by 25 in.) and a height of 58 cm (23 in.). The space between the stainless-steel liner and the plywood box was filled with grout, and the stainless-steel liner was forced in contact with the grout by means of bolts that extended through the ply wood box.

Instrumentation

Lead wires from the strain bars were connected into a balance unit. The balance unit was in turn connected to a digital data-acquisition system shown in Fig. 4. The data-acquisition system included a digital-volt meter, a millivolt preamplifier, and a 200-channel crossbar scanner and printer.

Test Procedures

The elevating box-section that is shown in Fig. 3 can be removed from the four vertical shafts of the wagon assembly and turned 90° to select a particular spacing and number of piling for a given test. The strain bars were next assembled into the wagon plates as shown in Fig. 3, and the piling sections of proper length were then connected to the bottom of the strain bars by means of a ferrule joint and two bolts through each of the piles.

The elevation screw was activated as shown in Fig. 4 to bring the bottoms of the piles in contact with the surface of the soil. At this point a measurement was made on the wagon assembly to use as a reference for positioning the bottom of the piles at the correct depth in the soil. Before forcing the piles into the soil, a reading was made of the strain-gage bridges on the strain bars in order to establish a zero reference. A reading was also made of the linear potentiometer.

After the piling had been pushed into the soil the prescribed distance, a second series of readings was made to determine the preload that was placed on the soil as a result of the penetration of the piles. Any slight variation in soil homogeneity or in the alignment of the pile resulted in some preloading of the pile before the horizontal movement of the wagon was started.

The group tests were run at a motor control setting for a rate of horizontal movement of 0.97 mm/min (0.038 in./min). The rate of scanning of the digital data-acquisition system was approximately 46 channels/min. Since there were two full-bridges on each strain bar and since the wiring was provided for reading of the linear potentiometer between the readings on successive strain bars, this meant that for groups of five pilings there were 10 full-bridges to be scanned and 5 readings of the potentiometer for a total of 15 readings/cycle or a rate of reading of approximately 3 cycles/min. The slow rate of horizontal movement through the soil was compatible with the rate of scanning of the digital data-acquisition system, and analyses indicate that a

sufficient number of readings were made to accurately reflect the load-time history of the pile-soil interaction.

Most group tests were run for a total of 7.5 min. This resulted in a total horizontal travel of approximately 7.4 mm (0.29 in.). This amount of travel was sufficient to develop the ultimate resistance of pile groups.

The strain bars were recalibrated after tests in each soil box to assure that there had been no damage to the strain gages or any damage to wiring that would cause a change in the calibration. The successive calibrations of the strain bars indicated that there were three significant figures in the calibration constant, and the fourth figure seldom varied more than 0.2 to 0.3. A check calibration was also made on the linear potentiometer, and the change in this number was also in the fourth figure.

Test Results

Series of Tests

The results of 58 tests on single piles and 41 tests on groups of piles were considered in this study. The scheme for identifying group-pile tests is 43-S-0.5-1-3 where

- 43 In the first position the number 4 signifies penetration of the piles and the 3 signifies the number of piles in the group tests; hence this was a 3-pile group test at 4 diameter penetration.
- S or I The letter in the second position signifies the arrangement of the piles in either a side-by-side (S) or an in-line (I) arrangement.
- 0.5 The third position signifies the clear spacing in pile diameters between piles in the group.
- 1 The fourth position signifies the sequence number of the test in the 43-S-0.5 series.
- 3 The fifth position signifies the sequence number of the soil box.

Location of Tests

Information developed during the tests indicated that clearances as low as 3.5 diameters from the side of the box did not influence the results of the test as long as the direction of movement of the single pile or group of piles was not directly towards the nearest side of the box. For most tests the minimum clearance between the side of the box and a pile was maintained at approximately four pile-diameters, or 10 cm (4 in.). Multiple tests were run in each box of soil.

Crack Patterns and Soil Movements

When single piles or group piles were pushed into the soil, there developed a pattern of cracks around the piling. These cracks were the result of the piles displacing soil and the lateral loading caused by the slight out-of-plumb of the piles as they were pushed into the soil. This cracking should be expected since it has been observed during installation of full-size piles in soft clays. The cracks occur in the field for the same two primary reasons that they occurred in these tests.

During the lateral loading, the crack pattern expanded and intensified. Attempts were made to determine the depths of cracks after lateral loading but, because of the very soft nature of the soil, it was difficult to determine the depth without destroying the crack. The width of the crack is indicative of the depth that might exist. The various widths of cracks are indicated in Fig. 5, which is a photograph taken of the crack pattern that existed after an 85-S-2.0

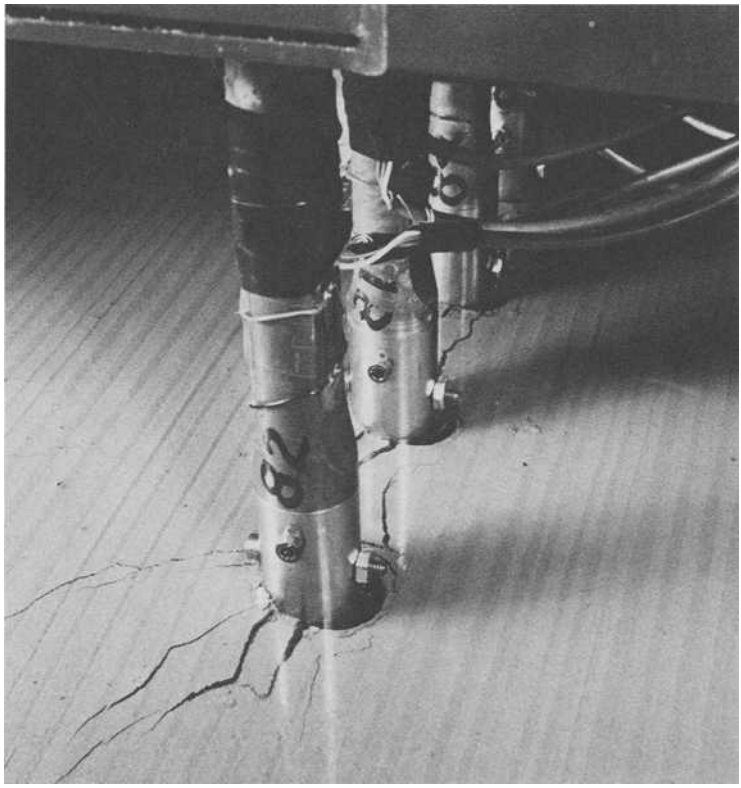

FIG. 5—*Crack pattern in the soil at the conclusion of an 85-2-2.0 series test.*

series test. The horizontal stripes on the soil surface indicated in Fig. 5 were the result of the screeding that was used to level the soil surface.

It can be seen in Fig. 5 that the gap between the soil surface and the back of the pile was well defined. This gap was shown to exist to the total depth of the pile and indicated that there was no flow around of soil even at depths of eight diameters. There was a slight buildup of soil in front of the piles caused by a wedging action and a breaking of the tip of the wedge adjacent to the piles.

Normalizing Data from Group-Pile Tests

In each soil box several tests were run on single piles in order to determine a load-deflection curve that was representative for a single pile in that particular box. The raw data from single-pile tests were reduced first, and the load-deflection curves were reviewed to select that particular single-pile test that would be used as representative of load-deflection relationships for that particular soil box. The single pile that was selected was referred to as the "normalizing" pile.

Summary of Tests

A key is given in Fig. 6 that explains the organization of data that are presented in Figs. 7 through 13.

The summary of data was made for loads corresponding to a horizontal displacement of 0.2 diameter, 5.1 mm (0.2 in.). A study of load-displacement plots for all group tests indicated that load had reached a reasonably constant value at or before 0.2-diameter movement. Representative plots of load-displacement relationships for three-pile groups at eight diameter penetration are presented in Figs. 14 and 15 for side-by-side and in-line tests, respectively.

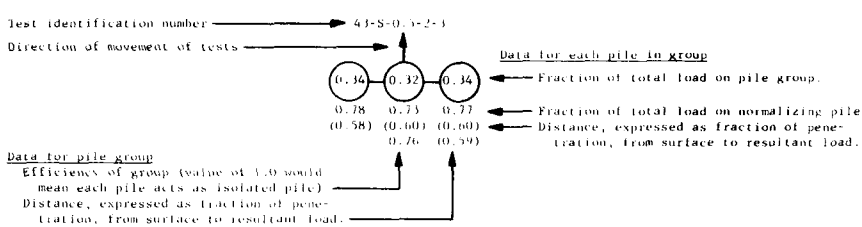

FIG. 6—*Key to data given on Figs. 7 through 13 summarizing results of the tests.*

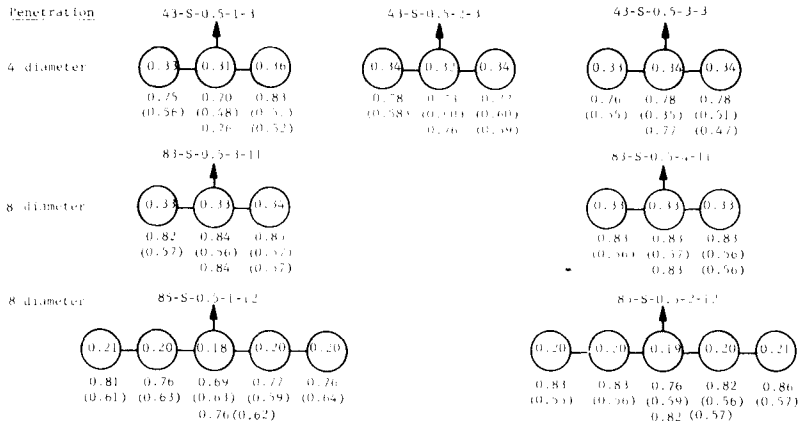

FIG. 7—*Summary of side-by-side tests with 0.5-diameter clear spacing.*

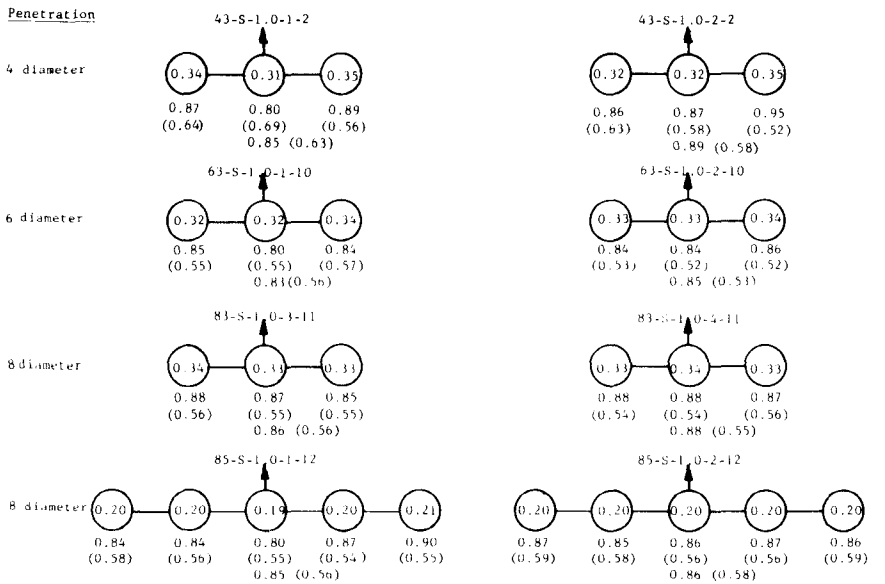

FIG. 8—*Summary of side-by-side tests with 1.0-diameter clear spacing.*

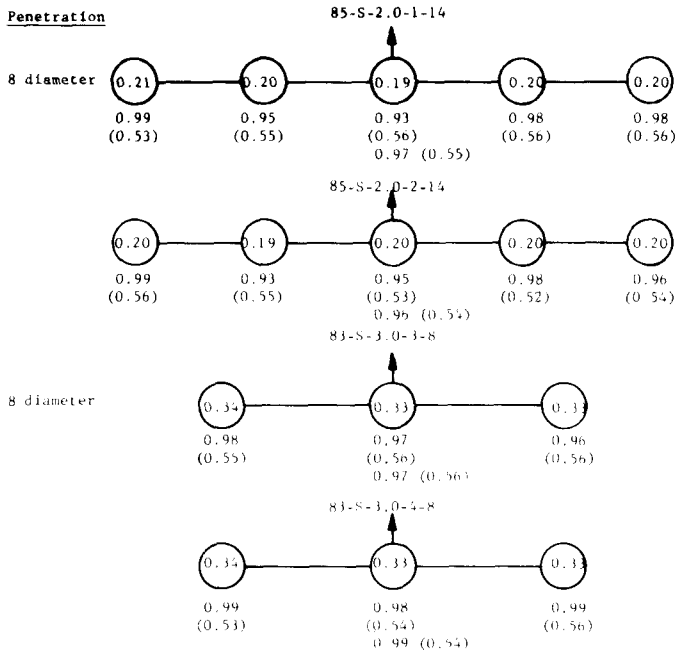

FIG. 9—*Summary of side-by-side tests with 2.0- and 3.0-diameter clear spacing.*

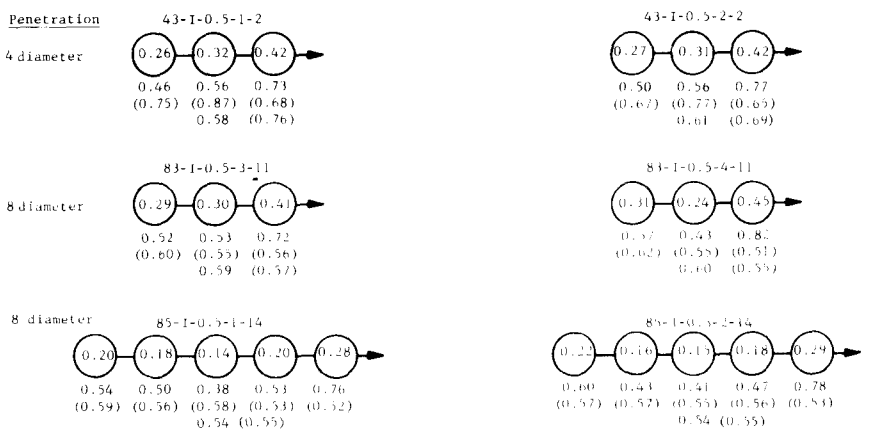

FIG. 10—*Summary of in-line tests with 0.5-diameter clear spacing.*

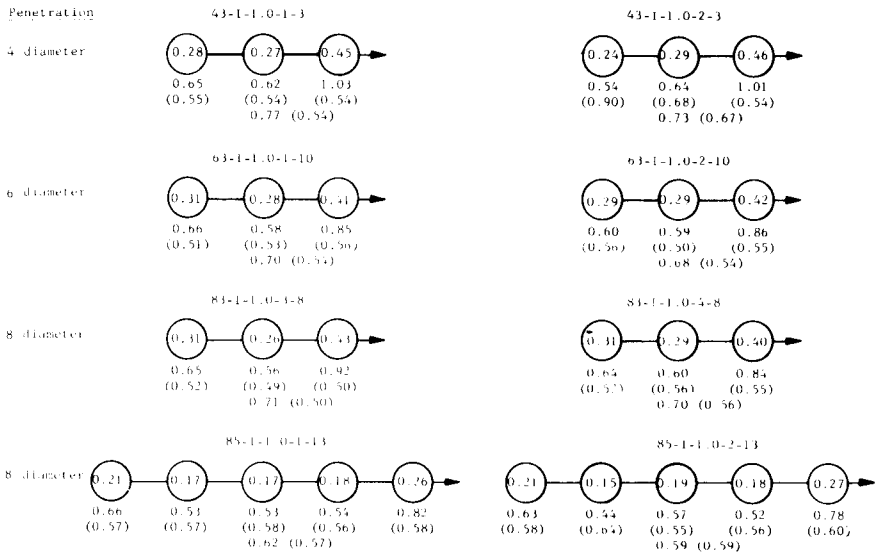

FIG. 11—*Summary of in-line tests with 1.0-diameter clear spacing.*

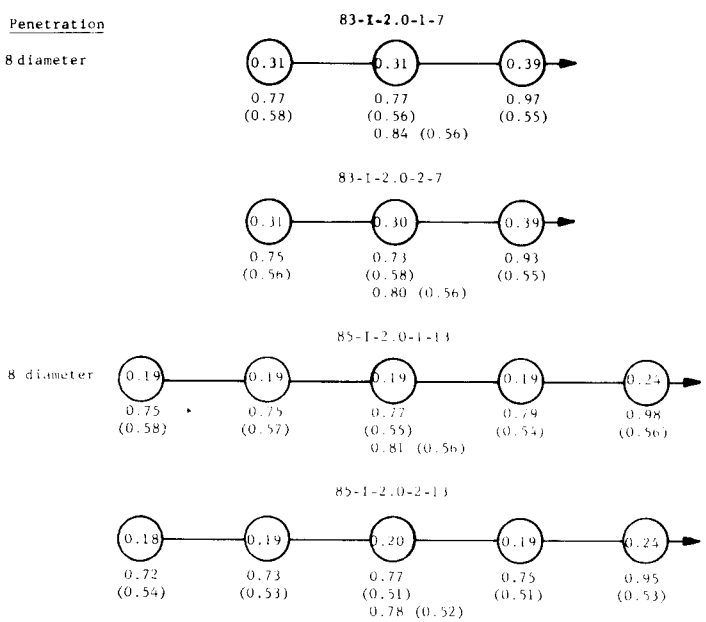

FIG. 12—*Summary of in-line tests with 2.0-diameter clear spacing.*

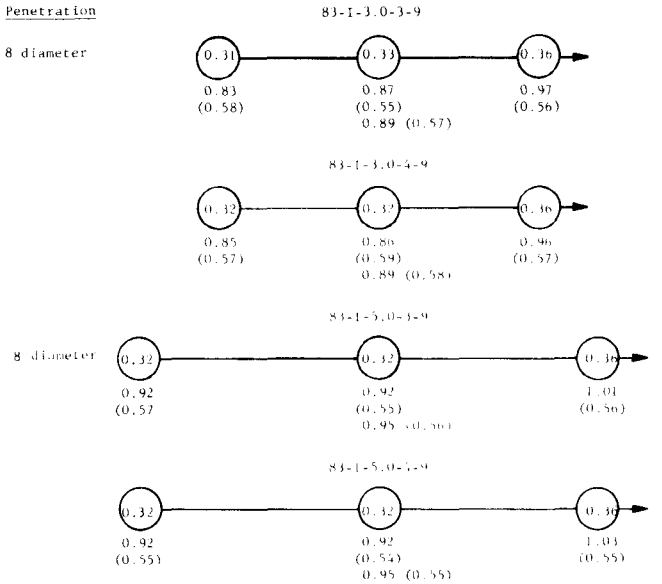

FIG. 13—*Summary of in-line tests with 3.0- and 5.0-diameter clear spacing.*

Conclusions

Composite of Group Efficiencies

Data on group efficiencies from Figs. 7 through 13 have been used to develop trend lines for efficiencies of three- and five-pile groups at varying clear spacings between the piles. These trend lines are given in Fig. 16 for side-by-side and in-line arrangements.

Side-by-Side Tests

In all of the side-by-side tests there was a remarkably uniform distribution of the total load on the pile group to each of the individual piles in the groups. The lowest efficiency of the groups was 0.76 for three piles at four-diameter penetration and 0.5-diameter clear spacing. The highest efficiency was 0.99 for three piles at eight-diameter penetration with a clear spacing of three diameters.

Trend lines in Fig. 16 indicate that side-by-side arrangements of pilings with clear spacings of two or three diameters are sufficient for developing strengths that approach those of isolated piles.

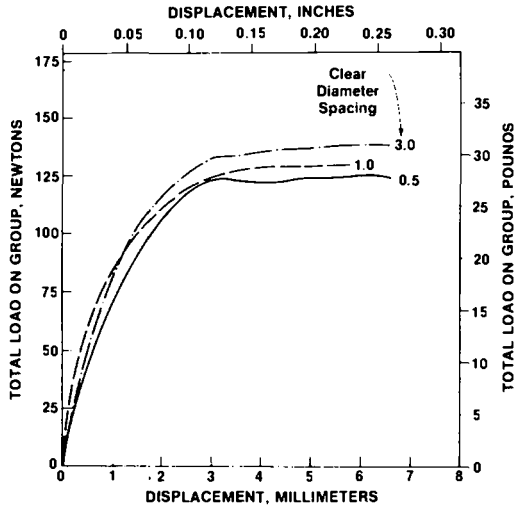

FIG. 14—*Load displacements for side-by-side three-pile groups with eight-diameter penetration.*

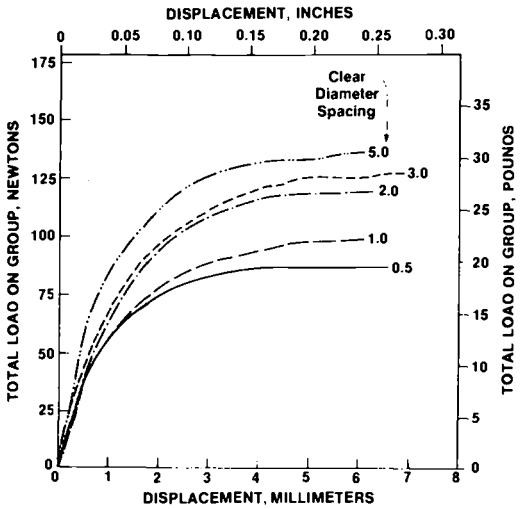

FIG. 15—*Load displacements for in-line, three-pile groups with eight-diameter penetration.*

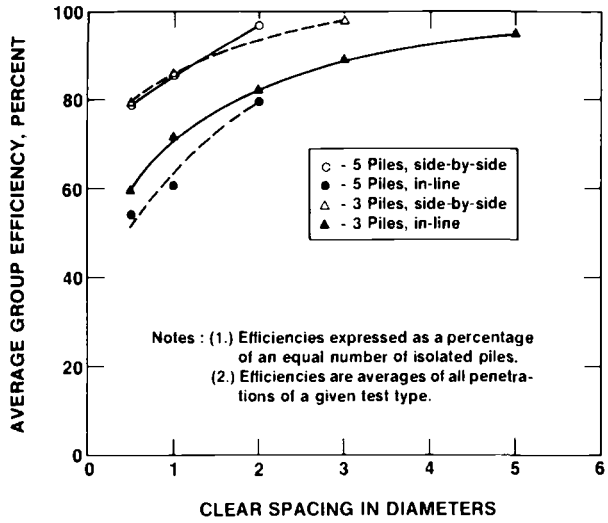

FIG. 16—*Efficiency of pile groups.*

In-Line Tests

For piling groups in-line, clear spacings of 0.5 and 1 diameter showed a decrease in efficiency as the pile numbers were increased from three to five. Three piles at 8 diameter penetration and 0.5 diameter clear spacing had an efficiency of 0.59 as compared to 0.54 when the number of piles were increased to five. Three piles at eight-diameter penetration and one-diameter clear spacing had an efficiency of 0.70 as compared to as low as 0.59 when the pile numbers were increased to five.

The distribution of load to individual piles in in-line groups was highly dependent upon the magnitude of horizontal displacements of the pile group. The summaries in this report were made for a horizontal displacement of 0.2 diameter. Load-displacement characteristics of individual piles at horizontal displacments less than 0.2 of the diameter of the pile were recorded but are not reported in this paper.

An extrapolation of the test data shown in Fig. 16 for in-line groups indicates that an efficiency of 100% would be obtained with clear diameter spacings of approximately eight or nine.

Acknowledgment

The study was sponsored by Amoco Production Company and was conducted in the Austin, Texas offices of TERA, Inc., a subsidiary of McClelland Engineers, Inc. of Houston. Dr. Arthur Lubinski was administrator

of the project for Amoco and Dr. Kenneth A. Blenkarn and Mr. William D. Greenfield represented Amoco in planning and organization. The authors extend appreciation to Amoco for permission to publish the results of the study.

References

[1] Desai, C. S., "Solution of Stress Deformation Problems in Soil and Rock Mechanics Using Finite Element Methods," Ph.D. dissertation, The University of Texas at Austin, Tex., 1968.

[2] Casagrande, A., "Research on the Atterberg Limits of Soils," *Public Roads*, Vol. 13, 1932, pp. 121-136.

Kul Bhushan[1] *and Shahen Askari*[2]

Lateral-Load Tests on Drilled Pier Foundations for Solar Plant Heliostats

REFERENCE: Bhushan, K. and Askari, S., **"Lateral-Load Tests on Drilled Pier Foundations for Solar Plant Heliostats,"** *Laterally Loaded Deep Foundations: Analysis and Performance. ASTM STP 835*, J. A. Langer, E. T. Mosley, and C. D. Thompson, Eds., American Society for Testing and Materials, 1984, pp. 140-156.

ABSTRACT: The first commercial-sized solar generating station in the United States, the 10-MW Solar Pilot Plant near Daggett, Calif., required 1818 sun-tracking mirrors (heliostats). To ensure accurate focusing of the mirrors on the central receiving tower, stringent wind load rotation criteria were specified for the top of the heliostat foundation. Soils at the site are medium dense to very dense sands and gravelly sands. Because little data were available to predict lateral deflections of drilled piers under low-level cyclic loads, a full-scale load test program was undertaken to obtain the necessary soil-resistance pier-deflection parameters. Piers with a diameter of 0.91 m (3 ft) and length of 5.5 m (18 ft) were tested under cyclic loads of up to 23.0 kN (5.16 kips) applied at a height of 5.43 m (17.8 ft). Test results indicated lateral movements of less than 0.61 mm (0.024 in.) under maximum loading. A design based on site-specific soil-pier parameters resulted in about a 40% reduction in pier length and significant cost savings when compared to the original design based on existing methods.

KEY WORDS: drilled piers, piles, lateral loads, *p-y* analysis, load tests, solar plant, field tests, lateral pressure, sands, heliostat

Central-receiver type solar-thermal power plants require large numbers of heliostats (sun-tracking mirrors) for focusing the sunlight onto the central receiver boiler. The design for the collector field of the 10-MW Solar Thermal-Central Receiver Pilot Plant, Solar One, near Daggett, Calif., included 1818 heliostats with a reflective area of 40 m^2 (430 ft^2). The overall size of each heliostat is nearly 7 m (23 ft) wide by 7 m (23 ft) high. The field of heliostats surrounds the tower. To focus the sunlight, the heliostats adjust

[1]Senior technical specialist, Flour Engineers, Inc., Irvine, Calif.; formerly, project manager, Woodward-Clyde Consultants, Santa Ana, Calif.
[2]Senior engineer, Southern California Edison Company, Rosemead, Calif.

continuously as the sun moves. Each heliostat is supported on a drilled pier foundation and is capable of being stowed in a facedown horizontal position during storms exceeding 22-m/s (50-mph) wind velocity.

The primary loading for the design of the heliostat foundation comes from lateral loads of up to 18.4 kN (4.13 kips) applied at a height of 4.9 m (16 ft) corresponding to maximum wind speed of 22 m/s (50 mph). Allowable rotation at a plane 50 mm (2 in.) above the top of the foundation was specified not to exceed ± 1.5 mrad total angular deflection under a 12-m/s (27-mph) operational wind. The allowable permanent rotation under a 22-m/s (50-mph) wind load should not exceed 0.45 mrad. These rotational criteria are equivalent to lateral deflections of 0.6 to 2.0 mm (0.02 to 0.08 in.) at the ground surface.

While a number of methods [*1–4*] are available for prediction of the lateral load-deflection behavior of piers, few full-scale load tests have been performed to define the behavior of piers under low-level cyclic lateral loading. Because of the potential significant cost savings in the construction of a large number of piers, a full-scale load testing program was undertaken to develop site-specific design parameters.

This paper presents the results of full-scale lateral-load tests performed on drilled and cast-in-place piers in medium dense to very dense sands and compares the observed and predicted behavior of the piers. The tests were conducted on piers with diameters of 0.61 to 0.91 m (2 to 3 ft) and lengths of 5.2 to 5.5 m (17 to 18 ft). These piers were constructed at three sites within the solar plant heliostat field. Lateral loads up to 23.0 kN (5.16 kips) were applied at a height of 5.43 m (17.8 ft) by using a loading frame. Measurements of tilt, torsional rotation, and lateral deflection were made at the base plate of the loading frame. Lateral deflection was also measured directly on the piers. Comparisons between the observed and predicted behavior using existing published procedures show that predicted deflections are generally two to six times greater than the observed deflections. Therefore, a new procedure is proposed for predicting lateral deflections of drilled piers in sand.

Pier and Soil Conditions

Five piers were constructed at three different locations within the solar plant site. The pier characteristics are shown in Table 1. The piers were constructed by excavating the holes by a track-mounted auger rig, placing the reinforcing steel and the rod bolt-template assembly, and depositing the concrete. Small quantities of water were added to the hole to minimize caving. However, some caving did occur during construction of Piers 1 and 5. The average 7 and 30-day strengths of the concrete were 30 325 and 39 903 kN/m^2 (4395 and 5783 psi), respectively.

Soil conditions at Sites A, B, and C were investigated by drilling a soil boring, performing standard penetration and static cone penetration tests, and

TABLE 1—*Pier characteristics.*[a]

Pier Number	Nominal Diameter, m	Length, m		Reinforcement	Test Site	Remarks
		Total	Embedded			
1	0.91	5.91	5.42	14 #6-bars	A	...
2	0.61	5.67	5.18	0 to 1.52 m, 20 #6-bars 1.52 to 5.18 m, 12 #6-bars	A	pier diameter was 0.91 m to a depth of 1.52 m
3	1.07	5.52	5.03	20 #6-bars	A	not tested
4	0.91	5.70	5.49	14 #11-bars	B	...
5	0.91	5.70	5.49	14 #11-bars	C	...

[a]Conversion factors: 1 m = 3.28 ft; 1 cm = 0.394 in.; #6 bar = 0.75 in. diameter; and #11 bar = 1.41 in. diameter.

performing laboratory strength and classification tests on intact specimens. Pressuremeter tests were also performed at Site B. Standard penetration blow counts are shown in Fig. 1, and static cone penetration resistance is given in Fig. 2. The soils at all three sites are predominantly fine to coarse-grained sands and silty sands with variable amounts of gravel below 1.22 m (4 ft).

The natural moisture content varied between 2 and 10% with an average value of 4%, and the dry density varied between 1335 and 1809 kg/m^3 (83 and 113 pcf) with an average value of 1585 kg/m^3 (99 pcf). The effective angle of internal friction for the near-surface silty sands was found to be 36° from triaxial compression tests with confining pressures in the range of 47.9 to 479 kN/m^2 (1 to 10 ksf).

The results of pressuremeter tests at Site B are summarized in Table 2. No groundwater was encountered to the maximum depth explored.

Test Program and Measurements

At Site A, Piers 1 and 2 were tested by applying both one- and two-directional loading by use of a deadman. At Sites B and C, only one directional loading was applied. The loading arrangement at Site A is shown in Figs. 3 and 4. For space limitations and clarity, only tests at Site A are discussed. The reader is referred to Woodward-Clyde's report [5] for details of the program.

Lateral loading was applied by bolting a 4.88-m (16-ft) high frame to the pier with eight 3.18-cm (1.25-in.) diameter and 0.84-m (33-in.) long bolts set in the concrete during pier construction. All of the load was transferred from

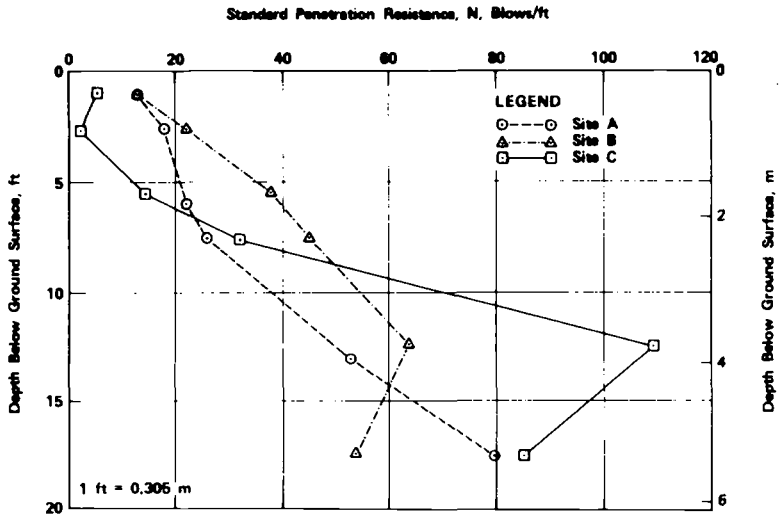

FIG. 1—*Penetration resistance.*

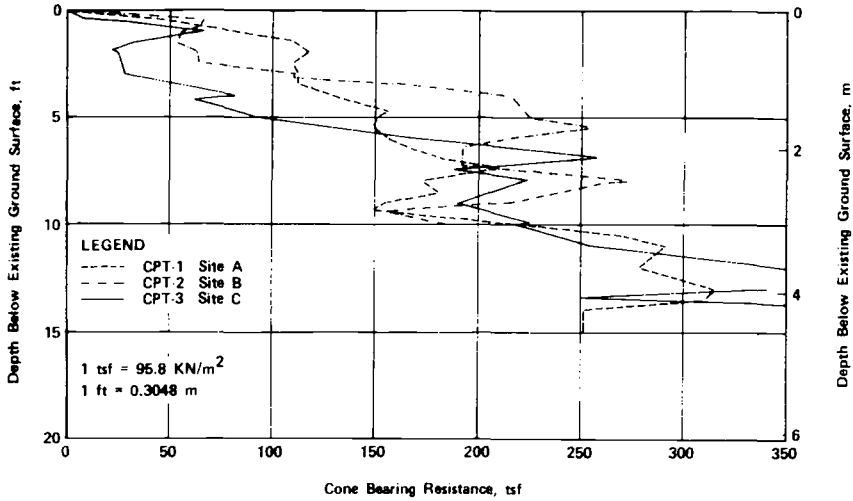

FIG. 2—*Cone penetrometer tests.*

TABLE 2—*Summary of pressuremeter tests.*[a]

Depth, m	Pressuremeter Modulus, kN/m^2	Limit Pressure, kN/m^2
0.6	5940	766
1.5	19160	1916
2.5	20700	2060
4.0	47900	4790

[a]Conversion factors: 1 ft = 0.3048 m and 1 ksf = 47.9 kN/m^2.

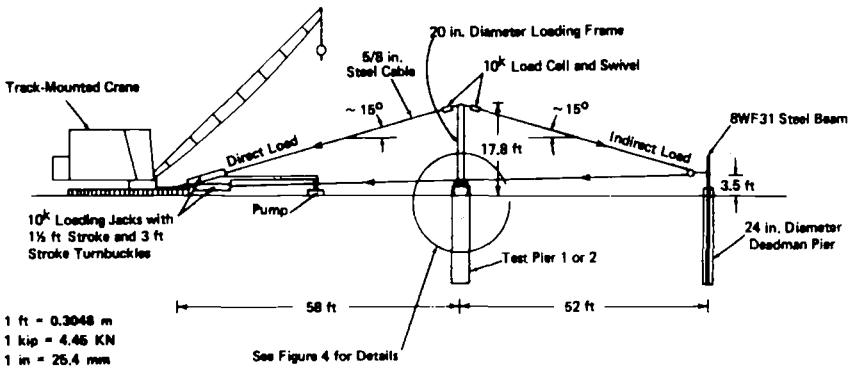

FIG. 3—*Schematic test setup of test Piers 1 and 2.*

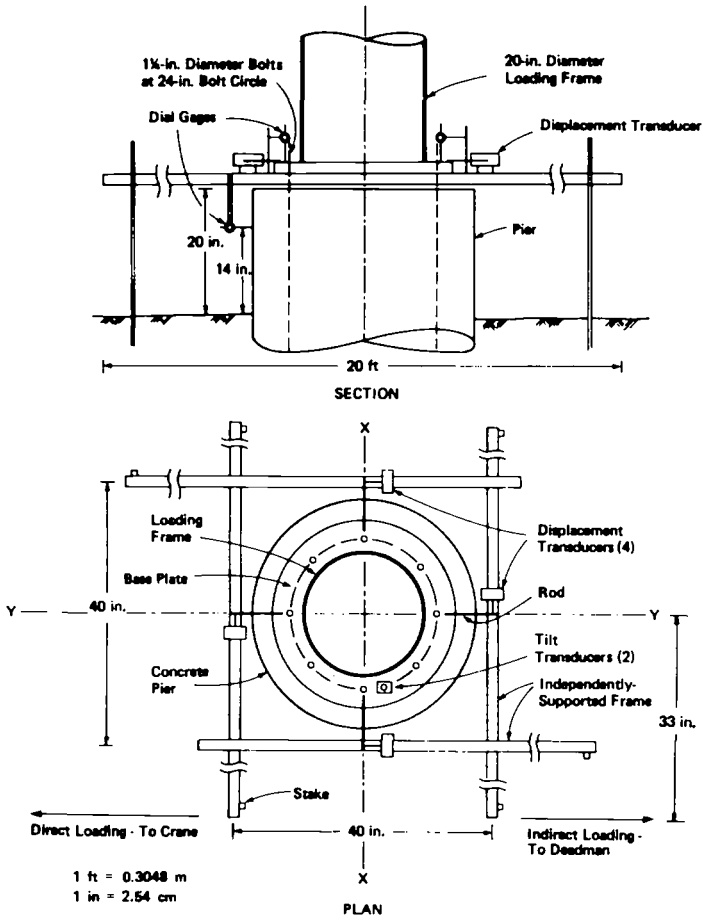

FIG. 4—*Details of test setup.*

the frame to the pier through the bond between concrete and the bolts and through the bearing on a plate washer at the bottom of each bolt.

The loading was accomplished by pulling on a steel cable attached to an arm 4.88 m (16 ft) above the base plate. The arm extended 0.84 m (33 in.) horizontally from the vertical centerline of the pier. The loading system shown in Fig. 3 was used to apply loading and unloading in two opposite directions. The load was applied by opening the valve on the electric pump controlling the hydraulic cylinder. The load readout on the digital display of the data recorder was monitored, and the valve was closed as the desired load was approached. The tension in the unloaded cable was subtracted from the load cell reading to obtain the net load. It was possible to achieve net loads generally within 5 to 10% of the desired load. The load was released by opening the

valve. Additional cycles of the loading in the same or opposite direction or alternately in each direction were applied by operating the appropriate valves.

The loads were measured by two calibrated load cells. The properly scaled load signal was monitored on the digital display of the data recorder and recorded along with readings from displacement and tilt transducers.

Tilt measurements were made by using two tilt gages stacked together and mounted on the loading frame base plate. The tilt measurements were made in two perpendicular directions, one parallel (*yy* direction) and one perpendicular (*xx* direction) to the direction of the applied load. In addition to the tilt gages, two dial gages with a resolution of 0.03 mm (0.0012 in.) were mounted on an independently supported frame to measure the vertical movement of the base plate at two points along a diameter in the *yy* direction. These measurements were used to compute the tilt of the base plate in the direction of loading by dividing the total vertical movement by the distance between the two gages. This reading provided a check on the tilt measured by the tilt gage.

Horizontal displacements of the base plate were measured by four displacement transducers with a resolution of 0.06 mm (0.0024 in.). The frame on which the transducers were mounted was supported independent of the pier. Horizontal displacements were measured at quarter points along the base plate circumference. The two transducers located on a diameter perpendicular to the loading direction measured the displacements parallel (*yy* direction) to the loading. The two transducers located on a diameter parallel to the loading direction measured the displacement perpendicular to the loading. With this arrangement, the translation of the base plate in both the *xx* and *yy* directions and the rotations of the plate about a vertical axis were obtained.

In addition to the measurements at the base plate, a dial gage was suspended from the frame to measure horizontal displacement in the *yy* direction at a point about 7.6 cm (3 in.) below the top of the pier. This measurement provided data to evaluate the pier-soil response and to assess the relative movements between the pier and the base plate.

Loading Sequence and Test Results

The planned loading sequence consisted of applying horizontal cyclic loads of 1.66, 5.36, 9.00, and 18.37 kN (372, 1204, 2023, and 4129 lb) corresponding to wind velocities of 6.7, 12.1, 15.6, and 22.3 m/s (15, 27, 35, and 50 mph). The maximum test load was 23.0 kN (5161 lb) representing a 25% overload above the 22.3-m/s (50-mph) wind velocity load. To account for cable inclination, the applied cable loads were about 3.5% greater than the horizontal loads.

During initial testing, it became apparent that no measurable data could be obtained for loads corresponding to 6.7-m/s (15-mph) wind loads; therefore, the minimum loads applied corresponded to the 12.1-m/s (27-mph) wind ve-

locity. The actual loading sequence and test results are shown in Table 3 for Piers 1 and 2.

The test on Pier 1 consisted of applying the indicated number of cycles of direct loading, indirect loading (shown by negative load in Table 3), and alternating direct-indirect (wobble-cycle) loading. Each cycle of direct or indirect loading consisted of load-unload while the wobble cycle consisted of direct load, unload, indirect load, and unload.

After the dry test, to simulate the effects of ponding of rainwater, a 6-m (20-ft) diameter dike around the pier was filled with water to a depth of about 0.3 m (1 ft). After 5 h about 5 cm (2 in.) of water had soaked into the soils, and it was decided to drain the area and conduct the soaked test. Five cycles of wobble-cycle loading at 5.36 and 18.37 kN (1204 and 4129 lb) were applied, and data were recorded. After testing, soil around the pier was excavated, and it was seen that the depth to which water had penetrated varied from about 13 cm (5 in.) at distances of more than 0.3 m (1 ft) from the pier to about 0.4 m (16 in.) immediately next to the pier.

Pier 2 consisted of a 0.61-m (24-in.) diameter pier with a 0.91-m (36-in.) diameter cap to a depth of 1.52 m (5 ft) below grade. The test on Pier 2 was performed in the dry.

Loads in the first column in Table 3 represent the net horizontal load in the direction of loading. Positive load represents direct load while negative load represents indirect load. The tilt in milliradians in the *yy* (parallel to the load) and *xx* (perpendicular to the load) directions was obtained by the two tilt gage readings. Permanent set in the tilt in the *yy* direction is yy_{perm}. The lateral movements in both the *xx* and *yy* direction are the movements in millimetres in a horizontal direction at the top of the base plate. The top of the base plate was at a height of 0.56 m (22 in.) above the surrounding grade. The lateral movement at the pier in millimetres in the *yy* direction was measured at a point about 0.36 m (14 in.) above the surrounding grade. The torsional rotation in milliradians was computed from the four displacement transducer readings and the horizontal distance (about 1.02 m [40 in.]) between the two opposite points.

The last column shows the number of cycles for which the readings were averaged. Data on wobble cycles are shown as averages of all positive and negative loads, although both positive and negative loads were applied in each complete cycle. Loads and other measurements in each column represent averages for the number of cycles shown and have been normalized to the design loads. Actual applied loads were within 10% of the design loads.

Measured Tilt and Lateral Deflection at the Base Plate

The measured values of tilt in the direction of the loading, *yy* direction, under the load corresponding to 12.1-m/s (27-mph) wind velocity (5.36 kN [1204 lb]) was about 0.2 mrad for the one-directional loading. For wobble-

TABLE 3—*Summary of test results.*[a]

Load, kN	Tilt at Plate, mrad			Lateral Movement, mm				
				At Plate				
	yy	*xx*	yy_{perm}	*yy*	*xx*	At Pier *yy*	Torsional Rotation, mrad	Number of Cycles
				PIER 1				
Dry								
5.36	0.20	0.013	0.052	0.048	0.005	0.074	0.066	4
9.00	0.30	0.048	0.106	0.19	0.034	0.163	0.126	5
18.37	0.75	0.183	0.224	0.485	0.039	0.351	0.387	5
−9.00	−0.34	−0.028	−0.047	0.198	0.029	0.093	−0.151	5
−18.37	−0.77	−0.097	−0.165	0.544	0.074	0.32	−0.427	5
9.00[b]	0.54	0.085	...	0.32	0.058	0.229	0.303	5
−9.00[b]	−0.53	−0.095	−0.161	0.333	0.034	0.216	−0.313	5
18.37[b]	1.07	0.191	...	0.653	0.002	0.434	0.564	5
−18.37	−1.11	−0.102	−0.174	0.767	0.063	0.442	−0.611	5
23.0[b]	1.32	0.190	...	0.861	0.022	0.559	0.752	2
−23.0[b]	−1.38	−0.162	−0.172	0.996	0.061	0.615	−0.869	2
23.0	1.09	0.228	0.109	0.663	0.003	0.401	0.525	8
Soaked								
5.36[b]	0.36	0.040	...	0.246	0.022	0.137	0.249	5
−5.36[b]	−0.38	−0.038	0.105	0.236	0.007	0.091	−0.239	5
18.37[b]	1.24	0.204	...	0.851	0.012	0.498	0.649	5
−18.37[b]	−1.19	−0.106	−0.053	0.785	0.10	0.469	−0.750	5

PIER 2

Dry								
5.36	0.18	0	0	0.132	0.004	0.104	0.04	4
9.00	0.30	0.06	0	0.264	0.008	0.185	0.055	5
18.37	0.84	0.07	0.16	0.742	0.018	0.533	0.247	5
−9.00	−0.41	−0.09	−0.05	0.302	0.002	0.229	−0.024	4
−18.37	−0.86	−0.17	−0.26	0.782	0.004	0.630	−0.158	5
9.00[b]	0.62	0.01	...	0.549	0.025	0.361	0.172	5
−9.00	−0.63	−0.07	−0.16	0.528	0.009	0.406	−0.128	5
18.37[b]	1.30	0	...	1.062	0.061	0.818	0.466	5
−18.37	−1.27	−0.24	−0.26	1.12	0.024	0.828	−0.33	5
23.00[b]	1.69	0.06	...	1.48	0.069	1.08	0.70	5
−23.00	−1.87	−0.34	−0.22	1.60	0.045	1.23	−0.54	5

[a] Conversion factors: 1 in. = 25.4 mm and 1 kip = 4.45 kN.
[b] Represents a wobble cycle defined as load, unload, indirect load, unload.

cycle loading of Pier 1 after soaking and applying the maximum loads, the maximum tilt under this loading was 0.38 mrad. This represents an increase of about 90% over the one-directional cyclic loading of Pier 1. These values are within the elastic deflection criteria of 1.5-mrad maximum rotation.

The permanent set under the loading corresponding to the 22.3-m/s (50-mph) wind velocity (18.27 kN [4129 lb]) was about 0.16 to 0.26 mrad.

The horizontal movement at the plate for the one-directional 12.2-m/s (27-mph) wind load (5.36 kN [1204 lb]) was less than 0.05 mm (0.002 in.) for Pier 1 (straight shaft) and was about 0.13 mm (0.005 in.) for Pier 2 (with cap).

Lateral Movement and Tilt at the Top of the Pier

Measurements of lateral movement were made near the top of the pier. The measured values of lateral movement on the pier were adjusted for the height difference between the point of measurement and the base plate on the basis of the computed bending. A comparison of these values for Pier 1 at a loading of 18.73 kN (4129 lb) for a soaked condition indicates a relative movement between the pier and the plate of about 0.28 mm (0.011 in). Assuming the maximum movement at the top of the pier is about 0.56 mm (0.022 in.), the computed tilt at the top of the pier is about 0.4 mrad. This compares with the measured tilt on the plate of about 1.24 mrad. The shortening and stretching of bolts and the slip between the concrete and the steel bolts appear to contribute significantly to the measured tilt. This points out the importance of the design of the connection between the loading frame and the pier since movements and rotations at the top of the pier can be significantly magnified at the base plate as shown by the measured data.

Comparison of Predicted and Observed Behavior

Comparisons of predicted and observed behavior were made for Pier 1 by computing the predicted deflection using the procedures suggested by Broms [*2*] and Reese and Sullivan [*4*]. Pier data used in these calculations are: pier diameter $b = 0.914$ m (3 ft), pier length $L = 5.42$ m (213 in.), and pier rigidity $EI = 8.9 \times 10^8$ N · M^2 (3.1×10^{11} lb · in.^{2}). The average blow count to a depth of about 3.7 m (12 ft) or four times the pier diameter is about 26 blows/ft, and the cone penetration resistance is 16 286 kN/m^2 (340 ksf). These data indicate that the sand may be considered medium dense to dense. The maximum values of coefficient of subgrade reaction n_h suggested by Terzaghi [*6*] (adopted by Broms [*2*]) and Reese and Sullivan [*4*] for dense sand are 17 647 and 61 088 kN/m^3 (65 and 225 lb/in.^{3}), respectively.

Computed values of ground-line deflection using suggested values of n_h for dense sand are compared in Fig. 5, with the range of observed deflection for Pier 1. The lower values of observed deflection correspond to the measured values for the first load, and the higher values correspond to the maximum observed deflection under wobble cycling.

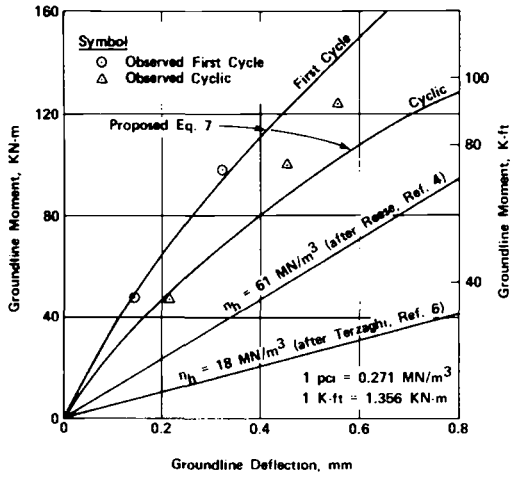

FIG. 5—*Comparison of predicted and observed deflections.*

A review of these data indicates that for applied moments of 26.2 and 90.2 kN · m (19.3 and 66.4 ft · kips), corresponding to wind velocities of 12.1 and 22.3 m/s (27 and 50 mph), the ratio of predicted and observed deflections ranges between 1.8 and 6. This ratio depends on the selected value of n_h, after Terzaghi [*6*] or Reese and Sullivan [*4*], and on the observed deflection (first load or wobble cycling).

Theoretical Considerations

Consider a single vertical pier of diameter b, length L, and structural stiffness EI placed in a soil mass of known characteristics. The statical influences along the pier can be determined by considering the pier as a beam and using the differential equation of bending

$$EI(d^4y/dz^4) = -p(z) \tag{1}$$

where

E = modulus of elasticity of pier,
I = moment of inertia of pier,
y = deflection, and
$p(z)$ = lateral soil pressure at depth z in force per unit length units.

The ratio of lateral soil pressure to the deflection is the subgrade reaction modulus so that

$$p/y = K_h \tag{2}$$

where K_h is the subgrade reaction modulus.

Closed form solutions of Eq 1 are available for a constant K_h. However, observations [*1*] on laterally loaded piles in granular soils indicate that a more realistic assumption is a modulus K_h linearly increasing with depth according to

$$p/y = K_h = n_h z \tag{3}$$

where n_h is the empirical quantity called the coefficient of subgrade reaction.

The solutions of the differential equation, Eq 1, for K_h linearly increasing with depth have been obtained using the method of finite differences and have been presented as nondimensional coefficients [*4,7,8*]. These solutions give deflection as

$$y = (A_y P T^3)/(EI) + [B_y (Pa) T^2]/EI \tag{4}$$

and slope as

$$S = (A_s P T^2)/(EI) + (B_s M T)/(EI) \tag{5}$$

where

y = deflection,
P = lateral load,
a = height of application of the applied load P above the ground surface,
S = slope,
M = applied moment = $P(a)$,
A_y, B_y, A_s, B_s = nondimensional deflection and slope coefficients, and

$$T = (EI/n_h)^{0.2} = \text{the characteristic pier length} \tag{6}$$

For values of L/T greater than 2.0, the values of A_y and B_y for deflection at the ground surface are shown in Fig. 6. The values of A_s and B_s for slope are shown in Fig. 7. Similar coefficients are available for moment and shear [*4,7,8*].

Proposed Procedure

On the basis of the analyses of a number of full-scale load tests, Bhushan et al [*1*] proposed curves for n_h versus y/b for values of y/b between 0.5 and 10% as a function of relative density of sand. These curves can be approximated by a series of straight lines on a log-log plot and can be extended to y/b range of 0.01 to 0.5% by using the relationship

$$\log(n_h) = 0.82 + \log(N) - 0.62 \log(y/b) \tag{7}$$

where

n_h = coefficient of subgrade reaction for first cycle loading, lb/in.^{3} (1 lb/in.^{3} = 271.5 kN/m^3),

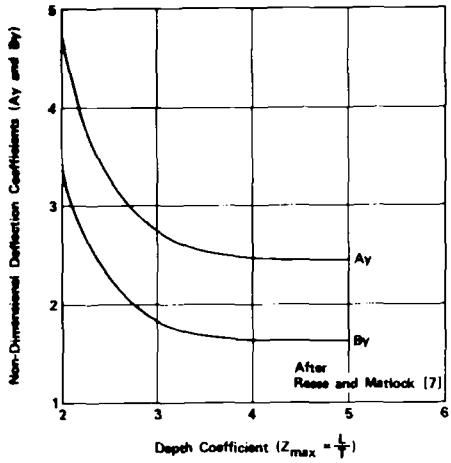

FIG. 6—*Deflection coefficients,* A_y *and* B_y *at ground surface.*

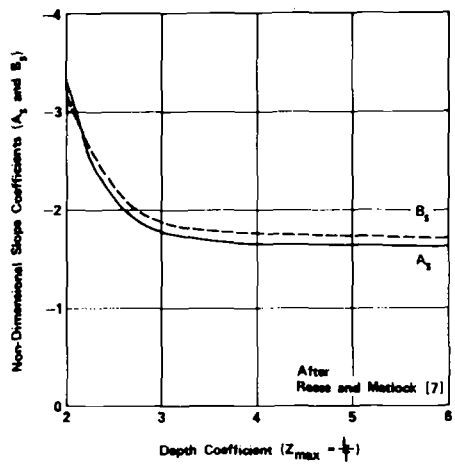

FIG. 7—*Slope coefficients,* A_s *and* B_s *at ground surface.*

N = standard penetration resistance, blows/ft (1 ft = 0.3048 m), and
y/b = normalized deflection, %.

Equation 7 is applicable for values of y/b between 0.01 and 15%. Limited data on cyclic loading including load reversal suggest that values of n_h for cyclic loading should be about 50% of the values obtained by Eq 7. Using an average N-value of 26 for the soils and a y/b of 0.05%, the estimated value of n_h for the first cycle using Eq 7 is 298.6 MN/m^3 (1100 lb/in.^{3}). The corresponding value applicable to cyclic loading is 149.3 MN/m^3 (550 lb/in.^{3}).

Predicted values of lateral ground-line deflection for Pier 1 using the n_h obtained by Eq 7 are presented in Fig. 5, along with the observed values of ground-line deflection. For plotting in Fig. 5, the measured values shown in Table 3 were adjusted to obtain the values at the ground surface on the basis of tilt measurements. Details of a step-by-step procedure to compute the load-deflection curve are given in Bhushan et al [*1*].

To check the applicability of Eq 7 for estimating n_h values in the range of y/b of 0.01 to 0.1, computations were made to predict the rotation at the top of five heliostat foundations for load tests reported by Davidson [*9*]. In obtaining values of n_h using Eq 7, the average blow count N-value in the upper four times the pier diameter was used. The rotation at the top of the foundation was calculated by using Eq 5 and the appropriate value of n_h. The results of this computation are compared with the average measured rotation in Fig. 8. These results indicate that the values of n_h obtained by Eq 7 provide reasonable prediction of rotation or deflection at the top of the pier foundation.

Conclusions

On the basis of the results of the load tests and the analyses, the following general conclusions can be made concerning lateral-load response of piers under low-level cyclic lateral loads in sands.

1. In the range of deflection/diameter y/b of 0 to 0.05% the observed lateral deflection versus load response is essentially linear.

2. Low-level cyclic loading with load reversal increases the first cycle deflection by 20 to 50%. The deflection stabilizes after the first few cycles, and an increased number of cycles after that does not appear to cause further increase in the deflection.

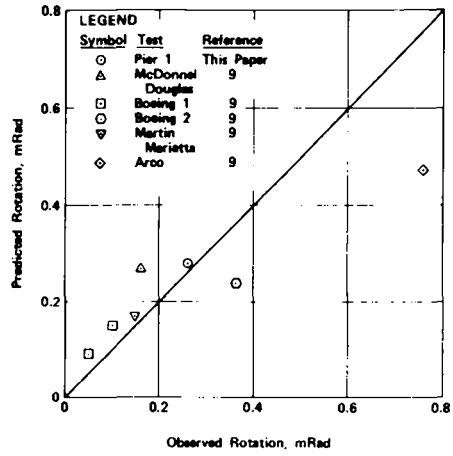

FIG. 8—*Comparison of predicted and observed rotations.*

3. The permanent set after cycling appears to be on the order of 25% of the deflection under the same load.

4. About 50 to 75% of the measured tilt and lateral deflection at the base plate appears to be caused by the slip between concrete and bolts attaching the loading frame to the pier. Therefore, the connection between the heliostat frame and the foundation should be designed to minimize relative movement between the frame and the foundation.

5. The values of lateral deflection predicted by using published values of n_h are two to six times greater than the observed values.

6. A simple empirical relationship is proposed to obtain values of n_h from the standard penetration blow count for a range of y/b values and appears to provide reasonable results.

7. The effects of soaking to simulate the ponding from rain did not appear to be significant (less than 10%) in increasing the deflections.

8. Comparisons of data for Piers 1 and 2 indicate that at loads corresponding to 12.1-m/s (27-mph) wind velocity, the effects of a smaller pier diameter (0.61 versus 0.91 m) below a depth of 1.52 m (5 ft) are small. At maximum loads, the deflections for the smaller diameter pier with cap are 1.5 to 2.0 times the deflections for the straight 0.91-m (3-ft) diameter pier.

9. The analyses based on load test data resulted in a design pier length of about 3.05 m (10 ft) instead of the original design length of 5.49 m (18 ft) calculated by previous methods.

Acknowledgments

The test program for the Solar One Pilot Plant was conducted for Rockwell International Corporation and was jointly sponsored by the Department of Energy and the Southern California Edison Company (SCE). Their permission to use the data is gratefully acknowledged. The writers thank their colleagues at Rockwell, Sandia, Stearns Roger, McDonnell Douglas, SCE, and Woodward-Clyde Consultants for their help in the test program. Special thanks are due to Dr. I. M. Idriss for review and helpful suggestions.

References

[1] Bhushan, K., Lee, L. J., and Grime, D. B., in *Proceedings of a Session on Drilled Piers and Caissons*, Geotechnical Engineering Division at the American Society of Civil Engineers National Convention, St. Louis, Mo., Oct. 1981.

[2] Broms, B. B., *Journal of the Soil Mechanics and Foundations Division, Proceedings, American Society of Civil Engineers*, Vol. 90, No. SM3, Proceedings Paper 3909, May 1964, pp. 123–156.

[3] Poulos, H. G. and Davis, E. H., *Pile Foundation Analysis and Design*, Wiley, New York, 1980.

[4] Reese, L. C. and Sullivan, W. R., "Documentation of Computer Program COM624, Parts I and II, Analysis of Stresses and Deflections for Laterally-Loaded Piles Including Generation of p-y Curves," Geotechnical Engineering Center, Bureau of Engineering Research, The University of Texas at Austin, 1980.

[5] Woodward-Clyde Consultants, "Lateral Load Test Program, Heliostat Drilled Pier Foundations, 10 MW Solar Pilot Plant, Daggett, California," Report to Rockwell International Corporation, Canoga Park, Calif., Oct. 1979.
[6] Terzaghi, K., *Geotechnique*, Vol. 5, No. 4, Dec. 1955, pp. 297–326.
[7] Reese, L. C. and Matlock, H., "Non-Dimensional Solutions for Laterally Loaded Piles with Soil Modulus Assumed Proportional to Depth," *Eighth Texas Conference on Soil Mechanics and Foundation Engineering*, Austin, Tex., 1956, pp. 1–41.
[8] Matlock, H. and Reese, L. C., *Journal of the Soil Mechanics and Foundations Division, Proceedings, American Society of Civil Engineers*, Vol. 86, No. SM5, Proceedings Paper 2626, Oct. 1960, pp. 63–91.
[9] Davidson, H. L., "Laterally Loaded Drilled Pier Research, Vol. 2: Research Documentation," EL-2197, prepared by GAI Consultants, Inc., for Electric Power Research Institute, Palo Alto, Calif., Jan. 1982.

Dennis R. Gle[1] *and Richard D. Woods*[2]

Suggested Procedure for Conducting Dynamic Lateral-Load Tests on Piles

REFERENCE: Gle, D. R. and Woods, R. D., **"Suggested Procedure for Conducting Dynamic Lateral-Load Tests on Piles,"** *Laterally Loaded Deep Foundations: Analysis and Performance, ASTM STP 835*, J. A. Langer, E. T. Mosley, and C. D. Thompson, Eds., American Society for Testing and Materials, 1984, pp. 157-171.

ABSTRACT: There are several analytical procedures available to predict the soil-pile interaction parameters required for the analysis of a pile-supported foundation subjected to vibratory forces. A procedure for performing a dynamic lateral field test on a single pile is presented. Results of this test are used to verify the adequacy of the assumptions made for the analytic solution and to judge the appropriateness of the soil-pile interaction parameters.

Dynamic lateral-load tests were conducted on eleven steel-pipe piles at three sites in southeastern Michigan. The piles were 324 and 356 mm (12.75 and 14 in.) in diameter, had lengths from 15 to 49 m (50 to 160 ft) long, and were embedded in both cohesive and cohesionless soils. The procedure consisted of attaching a steel-plate mass, vibratory oscillator, and vibration monitoring instrumentation to the head of each pile. The oscillator was then used to drive the soil-pile-mass system at selected force levels through frequencies from 5 to 55 Hz. The dynamic response was recorded on a strip-chart recorder for later evaluation. The data are presented in figures showing frequency versus response amplitude for each oscillator force level.

The soil-pile-mass system was also set into free vibration using the plucking technique. Results of the steady-state vibration testing are compared with the plucking test results on the same pile.

Conventional soil boring and testing methods were used to determine the subsurface soil profile and static soil properties. Dynamic soil properties adjacent to the tested piles were determined using the seismic cross hole and SH refraction (horizontal polarization of the shear wave) techniques.

Because of the way piles are inserted into the soil, the assumed boundary conditions between the soil and pile used in the analytical solutions seldom match the field conditions. This dynamic testing procedure enables the geotechnical engineer to make a judgment as to the adequacy of the assumptions in the analytical model and to make suitable corrections to match the field-observed results.

KEY WORDS: lateral loads, piles, vibrations, foundations, horizontal oscillation, machine foundations, deep foundations, soil dynamics, soil-structure interaction, load testing, pile foundations

[1] Engineering applications analyst, Bechtel Power Corp., Ann Arbor, Mich. 48106.
[2] Professor of civil engineering, The University of Michigan, Ann Arbor, Mich. 48109.

Design of deep foundations supporting vibratory equipment requires evaluation of the dynamic stiffness and damping parameters for each foundation degree of freedom. Although these parameters can be evaluated by various analytical techniques, the soil-pile boundary conditions assumed by the analytical methods are seldom achieved in practice. Pile installation methods used in conventional pile-driving operations can have a significant effect on the soil-pile boundary conditions and the dynamic behavior at the pile-foundation interface.

To evaluate the magnitude of this effect, a field-testing procedure was developed [*1*] to record the dynamic lateral response of a full-scale isolated soil-pile-mass system subjected to a steady-state vibratory force. The dynamic soil-pile interaction parameters and their variation can be evaluated from the recorded dynamic-response data obtained during field testing. After evaluation of the dynamic stiffness and damping parameters, the geotechnical engineer is able to make a judgment regarding the dynamic response of a soil-pile-mass system at various frequencies and dynamic force levels.

Both steady-state vibration and plucking tests were conducted on eleven steel-pipe piles at three sites in southeastern Michigan. The piles were 324 and 356 mm (12.75 and 14 in.) in diameter, had lengths from 15 to 49 m (50 to 160 ft) long, and were embedded in both cohesive and cohesionless soils. Dynamic soil properties of the soils adjacent to the tested piles were determined using seismic cross hole and SH refraction (horizontal polarization of the shear wave) techniques [*2*]. Static soil properties and the subsurface profile were obtained by conventional soil boring and testing methods.

Summary of Testing Procedure

A steel-plate mass, Lazan eccentric-mass oscillator, and vibration monitoring equipment were attached to the head of each pile to be tested. The Lazan oscillator was used to drive the soil-pile-mass system through a range of frequencies, recording the dynamic response amplitude at each selected frequency. The weight on top of the pile was selected such that the lateral-translation resonance was bounded with sufficient response data to each side of resonance to obtain a well-defined dynamic response curve. This procedure was repeated for several Lazan oscillator force levels to generate a family of dynamic response curves for each soil-pile-mass system tested. The observed resonant frequency of the soil-pile-mass system and the corresponding displacement amplitude are used to evaluate the dynamic stiffness and damping parameters for the system.

Because the eccentric-mass oscillator produces only horizontal force, the motion of the mass attached to the head of the pile is a two degree of freedom coupled horizontal translation and rocking response. In addition, the recording instrumentation is not located at the center of mass of the system. Thus, the recorded motion is a combination of both the horizontal translation and

rocking rotation response of the system. Evaluation of the recorded dynamic response data must consider both aspects.

The soil-pile-mass system will behave as a free-headed pile with coupled lateral translation and rocking degrees of freedom. Each degree of freedom has a resonance. The horizontal resonance can usually be defined reasonably well. However, depending on the power of the oscillator and the stiffness of the soil-pile-mass system, the rocking resonance may or may not be observed completely.

Initially, a simplified single degree-of-freedom model with viscous damping is used to evaluate the lateral-translation damping ratio using the recorded frequency at maximum response and the measured amplitude. From this, the natural frequency and the spring constant for the system in the horizontal translation direction can also be calculated. If the rocking resonance is well defined, a similar procedure can be used to calculate the damping ratio and spring constant associated with the rocking resonance. If not, the values for damping and spring stiffness in the rocking mode may either be assumed or calculated with one of the available analytical techniques [*3–5*]. The effect of assumed values can be evaluated analytically with a two degree-of-freedom solution. Plotting the response curve predicted analytically on the same figure as the field-response data enables an evaluation of how well the calculated stiffness and damping parameters match the recorded data.

Apparatus

To reduce the natural frequency of the soil-pile-mass system to the range in which the Lazan oscillator could operate, it was necessary to add mass (weight) at the top of the pile. This was accomplished by welding and bolting steel plates, 610 by 610 mm square and 19 mm thick, and weighing approximately 560 N each to the head of the pile. A hole slightly larger than the diameter of the pile to be tested is machined or burned in the center of one of the steel plates. This plate is slipped over the head of the pile and welded to the pile as shown in Fig. 1. A selected number of additional steel plates are then stacked on top of the base plate along with a housing, which is used to mount the Lazan oscillator. The entire stack of steel plates is fastened together through

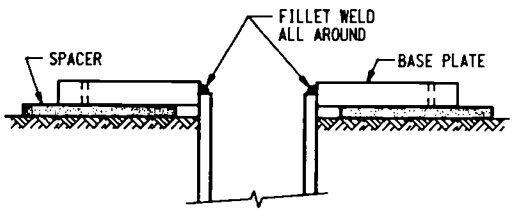

FIG. 1—*Cross section showing attachment of base plate to pipe pile.*

each corner and at the center of each side with eight threaded steel rods. The steel rods are tightened enough to force the steel-plate mass to act as a rigid body.

A steady-state sinusoidal force was provided by a Lazan mechanical oscillator, Model LA-1. The Lazan oscillator uses the centrifugal force of unbalanced masses mounted on two counterrotating shafts to generate a variable alternating force in a horizontal plane. The magnitude of this force can be controlled by adjusting the phase angle between the masses. Speed of the oscillator is controlled by a variable speed electric motor that is connected to the oscillator with a flexible shaft. This enabled a variable force within a frequency range of about 5 to 55 Hz to be applied to the piles.

To measure the dynamic response of the pile, it is necessary to determine the displacement amplitude of the mass at each frequency accurately. This was done with two velocity transducers mounted on each side of the mass as shown in Fig. 2. Output signals from the velocity transducers were recorded on a dual-channel strip-chart recorder for later evaluation. Calibration of the velocity transducers enabled relatively accurate conversion of the recorded velocity to displacement amplitude. Mounting both transducers in a horizontal plane on each side of the mass as shown provides an independent check on the calculated displacement amplitude.

Procedure

The procedure described below is specifically for conducting a dynamic lateral-loading test on a steel-pipe pile. However, the procedure is sufficiently general to be applicable to H piles and drilled piers with appropriate modifi-

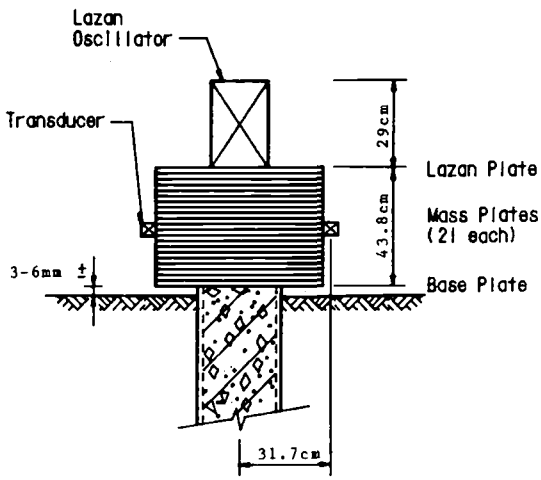

FIG. 2—*Typical cross section of a dynamic lateral-pile test.*

cation to the connection detail between the mass and the head of the pile or drilled pier.

To determine the dynamic lateral response of the mass caused by the soil-pile interaction alone, it is desirable to locate the mass as close to the ground surface as possible without touching the soil. As the distance between the soil surface and the bottom of the mass is increased, the dynamic response becomes essentially the structural response of a mass on a cantilever, and minimal information is obtained on the soil-pile interaction.

Use of a thin removable spacer facilitates positioning the base plate perpendicular to the centerline of the pile. When the base plate is level in both directions, it can be tack welded in place until a fillet weld can be completed around the circumference of the pile. When the base plate is securely attached to the head of the pile, a selected number of mass plates and the Lazan oscillator housing plate are added and tightened in place. Threaded connections for the velocity transducers are welded to a few of the mass plates before the field testing. These steel plates are positioned as desired within the stack of mass plates. Usually, it is desirable to locate them as close to the elevation of the center of mass as possible to minimize the contribution of the rocking mode to the recorded response unless the rocking response is of particular interest. The Lazan oscillator is connected to the drive motor to complete the mechanical connections necessary to conduct the test. Approximately 9.70 to 12.83 kN of steel plates were added to the head of each pile for all dynamic lateral-load tests to bring the resonant frequency within the range in which the Lazan oscillator was capable of operating.

Initially, a relatively low-force level (mass eccentricity) is set on the Lazan oscillator. The Lazan oscillator is then used to drive the soil-pile-mass system through a frequency spectrum from about 5 to 55 Hz, stopping long enough at each desired frequency to record the steady-state response. When the maximum output of the Lazan oscillator is reached, additional response data are obtained as the frequency is reduced, particularly around resonance. When one set of data is complete, the mass eccentricity of the Lazan oscillator is increased and the test repeated. Five to seven tests (using different Lazan force levels) are usually conducted on the same pile. Typical double-amplitude force levels range from about 20 to 4450 N. This will usually provide a broad spectrum of response curves sufficient to bracket the amplitude of vibration for most full-scale foundations unless stiff soils or high displacement amplitudes are expected.

In addition to the steady-state vibration testing, supplemental vibration information can also be obtained by conducting a plucking test on the soil-pile-mass system. The steel-plate mass is "plucked" by applying an impulse force to the mass and recording the free-vibration response of the soil-pile-mass system. The impulse force is applied by striking the mass horizontally with a wooden plank. From the measured free-vibration response, it is possible to determine the percent of critical damping and the damped natural frequency

of the soil-pile-mass system. This information supplements the values obtained by the steady-state testing technique presented above. Because the amplitude of vibration cannot be controlled and is usually much higher than the steady-state testing, this test is normally conducted at the conclusion of the steady-state dynamic testing. It is also desirable to conduct the test in a direction perpendicular to the steady-state testing direction to minimize the effect of any soil disturbance around the pile.

Evaluation of Experimental Data

At the frequency at maximum response for a rotating mass excitation, the ordinate of the response curve is given by the equation

$$A/(m_e\bar{e}/M) = 1/[2D_x(1 - D_x^2)^{1/2}] \quad (1)$$

where

A = measured amplitude, m,
$m_e\bar{e}$ = $\sin(\theta/2)/(2\pi^2)$ (for double-amplitude Lazan force output),
M = mass on the pile head, kg, and
D_x = damping ratio in the horizontal translation direction.

Solving Eq 1 for the translation damping ratio D_x and using the single degree of freedom differential equation (with viscous damping) enable an evaluation of the natural frequency of the system from the observed resonant frequency. An approximate value for the translation spring constant k_x can also be back-calculated knowing the mass on the head of the pile. A similar procedure can be used for the rocking resonance if the peak response is well defined.

Because of the rigid attachment of the steel-plate mass near the ground surface and the relative stiffness of the soil-pile-mass system in the rocking mode, the rocking stiffness and damping values do not significantly affect the shape of the predicted dynamic response around the lateral-translation resonance. Usually, the rotation stiffness and damping values predicted using the analytical solutions are adequate to define the dynamic response curve in the region of the horizontal-translation resonance. Variation of the translation and rotation stiffness parameters control the location of the resonant frequency while variation of the damping value controls the dynamic response amplitude. The rotation damping ratio D_ψ is usually so low that its variation has essentially no effect on the predicted dynamic response curve.

The dynamic response of the soil-pile-mass system can be adequately represented with a coupled sliding and rocking two degree-of-freedom solution. Equations of motion can be written for each of the translation and rotation degrees of freedom and solved simultaneously for the dynamic response. Summing forces and moments about the center of mass in Fig. 3 gives

$$\begin{bmatrix} A & B & C & -D \\ -B & A & D & C \\ C & -D & E & F \\ D & C & -F & E \end{bmatrix} \begin{bmatrix} A_{x1} \\ A_{x2} \\ A_{\psi 1} \\ A_{\psi 2} \end{bmatrix} = \begin{bmatrix} -Q_0 \\ 0 \\ -Q_0 h_2 \\ 0 \end{bmatrix} \tag{2}$$

Where Q_0 is the steady-state double-amplitude force generated by the Lazan oscillator, and the variables A through F are as defined as

$$\begin{aligned} A &= M\omega^2 - k_x & D &= C_x h_1 \omega \\ B &= C_x \omega & E &= I_0 \omega^2 - k_\psi - h_1^2 k_x \\ C &= h_1 k_x & F &= C_\psi \omega + h_1 C_x \omega \end{aligned}$$

where the variables are defined as

M = mass on the head of the pile, kg,
I_0 = mass polar moment of inertia, N-m-s^2,
ω = circular frequency, rad/s,
k_x = lateral-translation spring stiffness, N/m,
C_x = lateral-translation damping value, N-s/m,
k_ψ = rotational spring stiffness, N-m/rad, and
C_ψ = rotational damping value N-s/rad.

The horizontal translation of the mass is defined by

$$X = A_x \sin(\omega t - \theta_x) \tag{3}$$

and the rocking rotation of the mass by

$$\Psi = A_\psi \sin(\omega t - \theta_\psi) \tag{4}$$

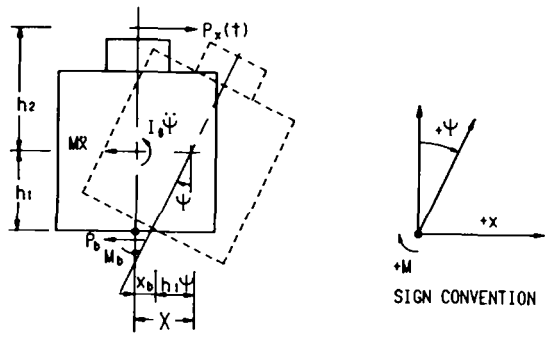

FIG. 3—*Free-body diagram of forces and moments acting on the steel-plate mass.*

where

$$A_x = (A_{x1}^2 + A_{x2}^2)^{1/2},$$
$$A_\psi = (A_{\psi 1}^2 + A_{\psi 2}^2)^{1/2},$$
$$\Theta_x = \tan^{-1}(A_{x2}/A_{x1}), \text{ and}$$
$$\Theta_\psi = \tan^{-1}(A_{\psi 2}/A_{\psi 1}).$$

In general, the phase angle for horizontal translation Θ_x will be different from the phase angle for rotation Θ_ψ, and the maximum translation and rotation will not occur at the same time. Because the transducers are offset from the center of mass and the translation and rotational phase angles are different, the maximum transducer response is a function of X and Ψ and must be evaluated by maximizing the combination of the horizontal contribution from translation and rotation and the vertical contribution from rotation of the mass. The horizontal dx and vertical dy contribution of the rotation can be evaluated using trigonometry. Because the transducers record the arc length, the total horizontal translation and rocking components ($X + dx$) and the vertical rocking component dy are added vectorially to determine the distance traveled by the transducer.

Figure 4 shows a comparison of the dynamic response data from a field test to that predicted analytically using the two degree-of-freedom solution. The translation stiffness and damping parameters were back-calculated from the

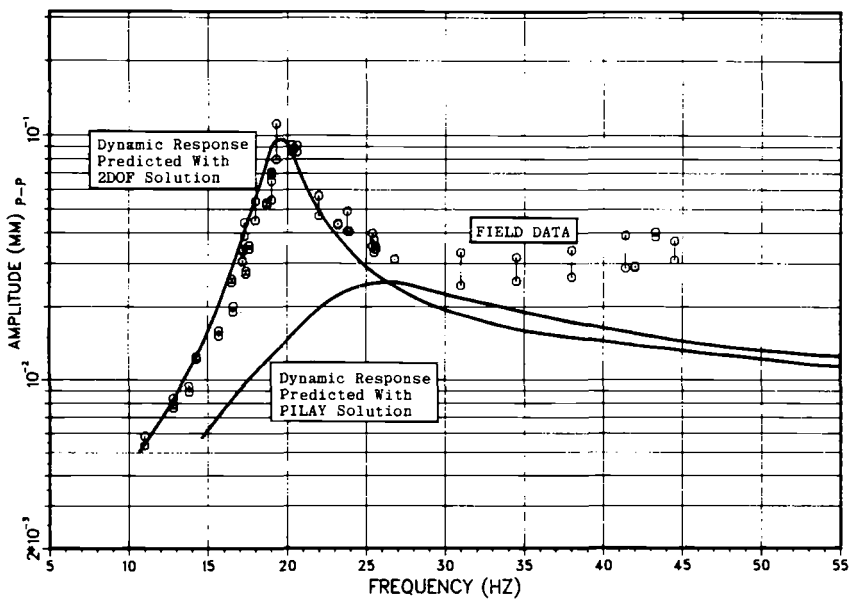

FIG. 4—*Typical response curve predicted analytically and superimposed on field response data.*

single degree-of-freedom equations (with viscous damping), and the rotational stiffness and damping parameters were as predicted by the PILAY [*3*] program using soil modulus values measured in situ by the cross-hole method. The dynamic response curve predicted using the PILAY stiffness and damping values for both the translation and rotation parameters is also shown for comparison. Linear modification of the stiffness value is used to match the frequency of the observed dynamic response curve, and appropriate modification of the translation damping ratio is used to match the lateral-translation amplitude at resonance.

The damping ratio of the soil-pile-mass system can also be evaluated from the plucking tests. Applying an impulse force to the soil-pile-mass system sets the system into damped free vibration. The amplitude decay with time is an indication of the geometric (radiation) and hysteretic (material) damping present within the system. The relative decrease in amplitude for each successive cycle of decay determines the logarithmic decrement, which is related mathematically to the damping ratio for a single degree-of-freedom system with viscous damping. This procedure is described by Richart et al [*6*]. Plucking the pile several times and plotting the relative vibration amplitude for each cycle of decay as shown in Fig. 5 provides a rapid graphical means of evaluating the logarithmic decrement and its variation with each cycle of oscillation. Normalizing these data to a convenient value as shown facilitates determination of the variability of the logarithmic decrement and the calculation of the damping ratio. A straight line on the semi-log plot indicates the measured soil-pile damping produces the same effect as that predicted by the theory for viscously damped free vibration. Obviously, the damping observed for the soil-pile-mass system is not the result of viscous behavior, however, the damping in the system can be treated mathematically as though it is a viscous behavior.

Results

A total of 56 steady-state pile-vibration tests were conducted on the eleven piles selected for testing. The frequency-amplitude data for each steady-state test are plotted as previously shown on Fig. 4. Corresponding amplitudes at each frequency for both velocity transducers mounted at the same elevation are connected with a vertical line.

Because of the presence of nearby equipment, one dynamic pile test was conducted with the steel-plate mass mounted approximately 1.5 m above the ground surface. The effect of attaching the mass at this level was to significantly decrease the observed damping and sharply increase the response amplitude at frequencies near the lateral-translation resonance. This behavior is expected because of the absence of soil resistance within the upper few pile diameters that controls the dynamic lateral response of the pile. The sharp increase in amplitude occurred at all force levels, and there was no difference between the sharpness recorded at a height of 1.5 m versus that recorded just

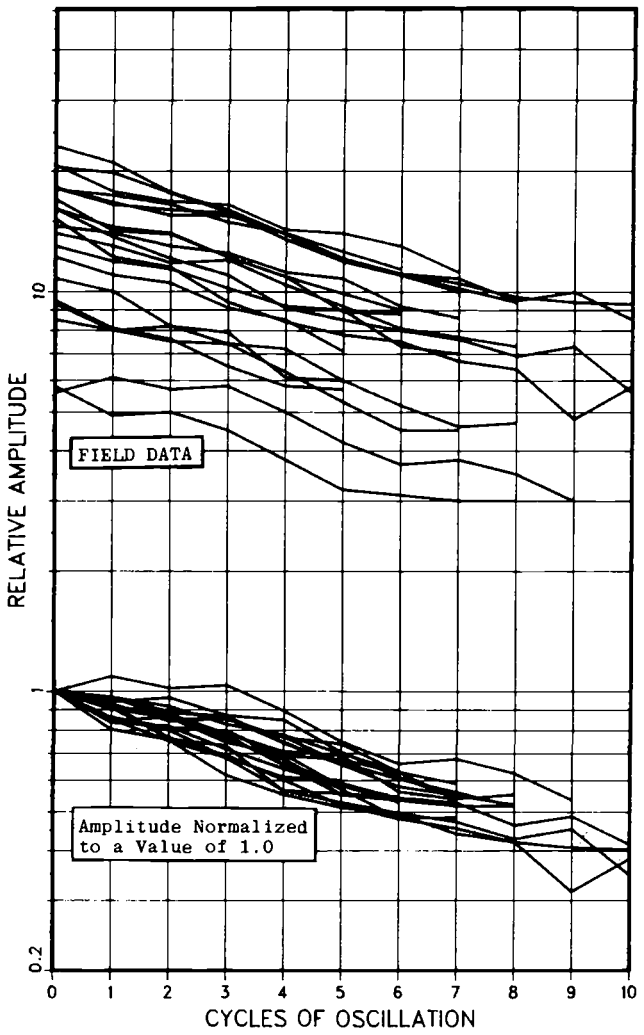

FIG. 5—*Relative amplitude versus cycles of oscillation from plucking test.*

above the ground surface. The amount of soil-pile interaction increased significantly as the height of the mass was lowered to just above the ground surface for the remaining dynamic lateral-load tests.

For those tests that experienced the higher Lazan oscillator force levels and tests with relatively loose granular soils at the ground surface, a nonlinear soil-pile response was observed from the results of some of the dynamic pile testing. The nonlinear response is indicated by a decreasing resonant frequency as the Lazan oscillator force level was increased. This is shown in Fig. 6 for one set of five steady state vibration tests conducted on the same pile. As

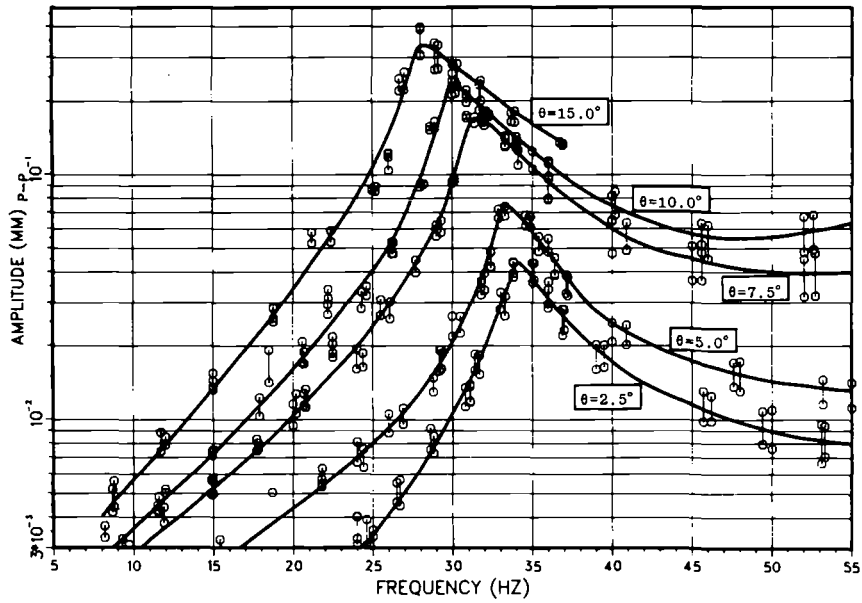

FIG. 6—*Dynamic response curves showing a decrease in resonant frequency with increasing amplitude.*

the Lazan oscillator force level (mass eccentricity θ) was increased from 2.5 to 15°, the resonant frequency decreased from 34 to 28 Hz. This test exhibited the most noticeable and well-defined nonlinear behavior. Although masked to varying degrees by the spread of data around resonance, some nonlinear response was apparent for all of the dynamic pile testing, irrespective of soil type and force levels.

If the dynamic response were linear, resonance for all of the dynamic response curves would occur at the same frequency, indicating no change in the soil-pile stiffness with increasing force level. Similarly, when the measured amplitudes for each test are divided by the quantity $m_e\bar{e}/M$, the response curves for all steady state vibration tests on the same pile should collapse onto a single curve if there is no change in the damping. This dimensionless form is shown in Fig. 7 for four steady-state vibration tests conducted on a pile that had been backfilled with a dense well-graded compacted granular backfill around the upper 1.25 m of the pile. For a rotating mass excitation, the quantity $A/(m_e\bar{e}/M)$ will asymptotically approach the value 1.0 for a single degree-of-freedom system.

At least one reasonably well-defined lateral resonance was obtained for each steady-state dynamic pile test conducted. In addition, a definite increase in amplitude was noted at frequencies above the lateral-translation resonance. In general, the observed dynamic response amplitudes above the lateral-

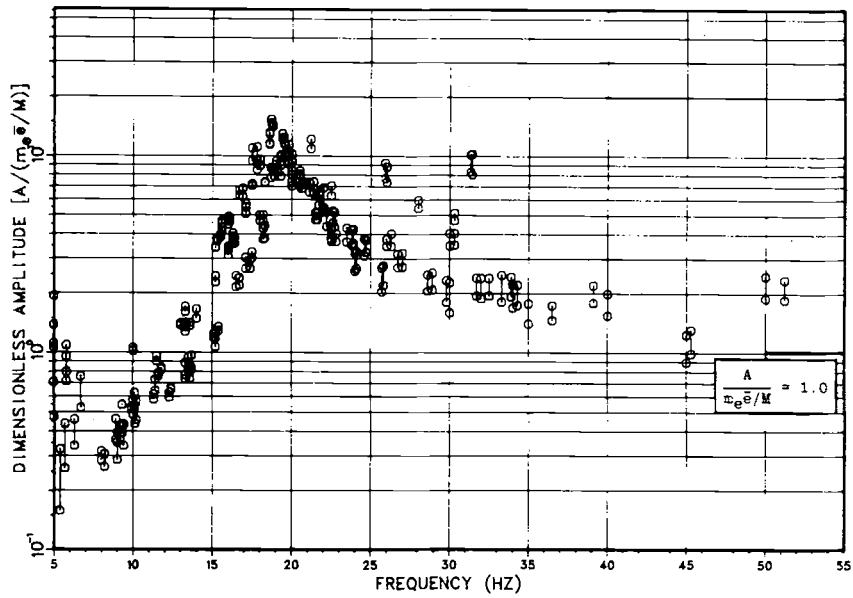

FIG. 7—*Dimensionless amplitude versus frequency for four steady state vibration tests on a pile.*

translation resonance were 1.5 to 2 times the amplitude predicted by the two degree-of-freedom solution, even when the damping ratios for the rocking mode were decreased to very low values. A well-defined rocking resonance was never obtained during any of the dynamic testing, thus the effect of various rocking stiffness and damping values on the dynamic response of the soil-pile-mass system was evaluated analytically. Figure 8 shows a comparison of the field-obtained data with the dynamic response curve predicted using a range of values for the rocking stiffness k_ψ. The initial value of k_ψ was that predicted by the PILAY program using the in situ dynamic soil properties. This shows that even with the wide variation in rocking stiffness, the field-observed dynamic response amplitude is still higher for frequencies above the lateral-translation resonance. Again, the dynamic response curve as predicted using the PILAY stiffness and damping values is shown for comparison.

The dynamic response of the soil-pile-mass system is uniquely defined by the stiffness and damping parameters present at the head of each pile. Thus, comparison of the plucking test results and the steady-state vibration test results can be based entirely on the damping ratio since this value is used to back-calculate the stiffness parameter for both procedures. Considering all steady-state vibration force levels, the resonant frequencies are generally lower and the damping ratios higher for the plucking tests compared to the steady-state vibration tests.

For the steady-state vibration tests, the general trend was for the damping

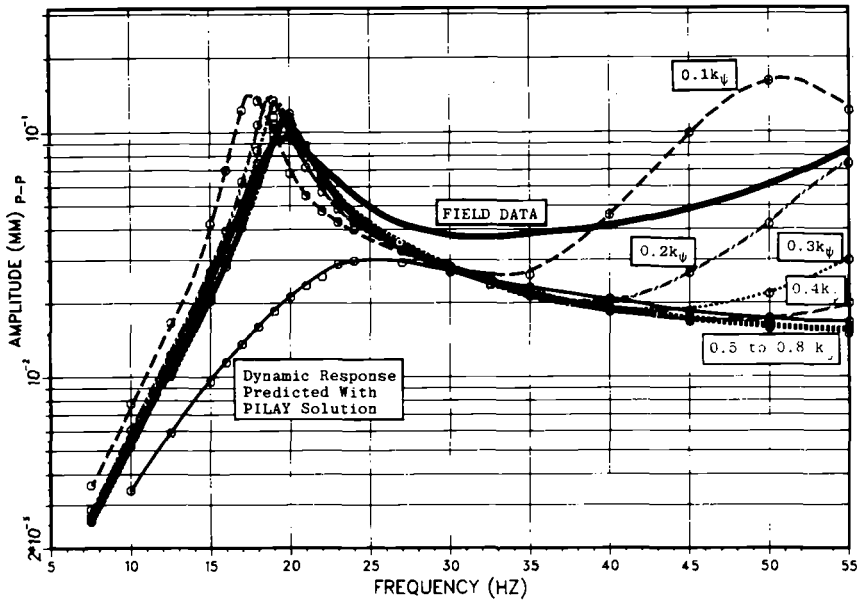

FIG. 8—*Effect of reducing the rocking stiffness on the predicted dynamic response curve.*

ratio to decrease with increasing Lazan oscillator force levels. Exceptions occurred during the second of the series of steady-state vibration tests for six of the piles. After the initial low-amplitude steady-state vibration test, the damping ratio increased substantially (factor of 2+) before resuming the downward trend with increasing force levels (higher displacement amplitudes). This effect occurred for piles that had a relatively loose granular soil around the head of the pile. The increase did not occur where a densely compacted granular backfill was placed around the pile. This effect for the second steady-state vibration test of the series is likely caused by vibration settlement of the adjacent granular soil increasing the soil-pile contact condition, thus increasing the geometric damping.

A reduction in the damping ratio with increasing displacement amplitude has to be associated with a reduction in the geometric damping. Thus, the pile may not have been fully in contact with the soil during each complete cycle of oscillation. Horizontal shifting of the steady-state vibration response curves indicated relatively small but definite amounts of nonlinear soil behavior, which may have been sufficient to cause some permanent soil deformation.

Although the resonant frequencies for the plucking tests correlate well with the higher amplitude steady-state vibration tests, there is a discrepancy between the damping ratio obtained by the two procedures. The calculated values for the steady-state vibration damping ratio appear to be inversely related to the displacement amplitude experienced by the soil-pile-mass

system. Generally, the higher amplitude plucking tests have damping ratios of almost twice those obtained by the steady-state vibration procedure. Apparently, this discrepancy is a result of the way in which the two tests are performed. The steady-state vibration test causes the soil to experience a large number of cyclic repetitions during the test that do not occur during the plucking test. The continued cyclic deformation during the steady-state testing may be responsible for weakening the soil, thus causing the soil to separate from the pile during part of the oscillation cycle.

Summary

A successful dynamic design depends primarily on knowledge of the dynamic forcing function and the ability to predict the interaction between the foundation and its supporting medium correctly. Agreement between the predicted and observed dynamic response has not been acceptable when the field-measured dynamic soil properties were used in analytical solutions [*7*]. This is primarily because of the effect of the soil-pile boundary condition. The advantages of dynamic testing of full-scale piles are obvious. Because the full-scale pile develops the full depth of lateral soil-pile interaction at the site where it will be used, the geotechnical engineer is able to make a judgment as to the adequacy of the assumptions for the dynamic soil-pile interaction parameters that are to be used in design.

The overall shape of the observed dynamic lateral-response curve can be matched quite well up to and slightly above the lateral-translation resonance if stiffness and damping values obtained from dynamic field testing of a pile are used. At frequencies where the predicted dynamic response curve do not match the observed response data, appropriate modification of the design parameters can be made. Adjustment of the foundation stiffness and damping values can also be made for the type of loading and amplitude range that the foundation will be subjected to during its design life.

References

[*1*] Gle, D. R., *The Dynamic Lateral Response of Deep Foundations*, Ph.D. dissertation, The University of Michigan, Ann Arbor, Mich., 1981, 278 pp.

[*2*] Woods, R. D., "Measurement of Dynamic Soil Properties," *Proceedings of the Conference on Earthquake Engineering and Soil Dynamics*, Geotechnical Engineering Division, American Society of Civil Engineers, Pasadena, Calif., 19-20 June 1978, pp. 91-178.

[*3*] Novak, M. and Aboul-Ella, F., "Stiffness and Damping of Piles in Layered Media," *Proceedings of the Conference on Earthquake Engineering and Soil Dynamics*, Geotechnical Engineering Division, American Society of Civil Engineers, Pasadena, Calif., 19-20 June 1978, pp. 704-719.

[*4*] Kuhlemeyer, R. L., "Static and Dynamic Laterally Loaded Floating Piles," *Journal of the Geotechnical Engineering Division, Proceedings of the American Society of Civil Engineers*, Vol. 105, No. GT2, Feb. 1979, pp. 289-304.

[5] Blaney, G. W., Kausel, E., and Roesset, J. M., "Dynamic Stiffness of Piles," *Proceedings of the Second International Conference on Numerical Method in Geomechanics*, American Society of Civil Engineers, New York, 1976, pp. 1001–1012.

[6] Richart, F. E., Jr., Hall, J., Jr., and Woods, R. D., *Vibrations of Soils and Foundations*, Prentice-Hall, Inc., Englewood Cliffs, N.J., 1970, 414 pp.

[7] Novak, M. and Grigg, R. F., "Dynamic Experiments with Small Pile Foundations," *Canadian Geotechnical Journal*, Vol. XIII, No. 4, Nov.–Dec. 1976, pp. 372–385.

Lawrence D. Johnson,[1] *Jean-Louis Briaud*,[2] *and W. R. Stroman*[3]

Lateral-Load Test of an Aged Drilled Shaft

REFERENCE: Johnson, L. D., Briaud, J.-L., and Stroman, W. R., **"Lateral-Load Test of an Aged Drilled Shaft,"** *Laterally Loaded Deep Foundations: Analysis and Performance, ASTM STP 835*, J. A. Langer, E. T. Mosley, and C. D. Thompson, Eds., American Society for Testing and Materials, 1984, pp. 172-181.

ABSTRACT: A lateral-load test was conducted on a 0.46-m-diameter concrete drilled shaft constructed July 1966 in stiff expensive-clay soil. This 10.5-m-long test shaft had been subject to considerable uplift thrust from swelling of adjacent soil. The lateral-load behavior was reasonably simulated by solutions of the elastic beam-column differential equation. Solutions assuming a linearly increasing soil modulus with depth evaluated from triaxial strength tests were found in good agreement with the field load test results up to at least ½ of the yield load. Solutions using *p-y* curves developed from laboratory undrained strengths, and field pressuremeter tests provided good overall agreement with the field load test results.

KEY WORDS: lateral loads, drilled shafts, bored piles, caissons, pressuremeter, undrained strength, elastic modulus

The resistance of drilled shafts to lateral loads is of much interest because drilled shafts are often selected as the foundation for bridges, towers, and many other structures and can be designed to economically resist relatively large lateral loads and moments imposed on the structure. There is little information on the long-term performance of the resistance of deep foundations to lateral loads. Cyclic loading and long-term wetting of the foundation soil can reduce the original soil strength and modulus, thereby reducing the long-term resistance of shaft foundations to lateral loads. This paper presents results of a lateral load test performed in 1982 on an aged drilled shaft constructed in 1966 and left unloaded until the current load test. This shaft had

[1]Research civil engineer, U.S. Army Engineer Waterways Experiment Station, Vicksburg, Miss. 39180.
[2]Associate professor, Department of Civil Engineering, Texas A&M University, College Station, Tex.
[3]Project engineer, U.S. Army Engineer District, Fort Worth, Tex.

been constructed in swelling soil that had caused the shaft to heave 5 to 6 cm while the adjacent ground surface had heaved approximately 10 cm. The shaft heave exceeded the soil heave of 2 cm, observed adjacent to the shaft base such that stretching or fracture of the shaft was possible. Strain gage data from a vertical load test conducted before this lateral test indicated that the shaft had fractured at the neck of the underream [*1*]. The load test data were compared with estimates of load behavior using elastic and nonlinear *p-y* curves based on triaxial strength and field pressuremeter tests.

Site

The shaft selected for testing is part of a test site located in Lackland Air Force Base near San Antonio, Tex. The overburden material consists of about 2.4 m of expansive black to gray CH clay underlain with 1.2 to 1.5 m of GC clayey gravel with caliche. The primary material encountered below the gravel is a fissured and expansive tan CH clayey shale of the Upper Midway formation. The soils are uniform within the test area with a perched ground water level 2.4 m below ground surface.

Load Test

The drilled shaft selected for load testing is 0.46 m in diameter by 10.5 m long, including a 0.9-m-diameter underream. The original elastic modulus E_c of the concrete evaluated by compression tests on small cylinders was 35×10^6 kPa [*2*]. A compression test performed on core material taken from the shaft after the load test indicated a current modulus of 20.7×10^6 kPa. The shaft flexural rigidity E_cI based on the current modulus is 44 MN · m^2, and the compressive strength f_c' of the core concrete is 37.3 MPa. The amount of reinforcing steel is 2%. Figure 1 shows a small sketch of the shaft.

The lateral-load test was performed with a 600-kN hydraulic jack placed on the ground surface between the shaft and a reinforced concrete block cast against an anchor shaft originally constructed to conduct vertical load tests. Displacements were measured by a single extensometer gage mounted on a wood frame. The shaft was laterally loaded at the ground surface up to 125 kN, rebounded to zero, and reloaded to yield near 169 kN (Fig. 1). Additionally, load-displacement curves from theoretical solutions discussed later are shown in this figure.

The test shaft had originally been equipped with 21 strain gages mounted on the reinforcing bars at multiple depths. Fourteen of these gages were operable in 1982; however, the locations of the gages and data were insufficient to accurately characterize the bending moment distribution with depth. The strain gage data did indicate an unusually large bending moment and yielding of the shaft about 2 m below ground surface.

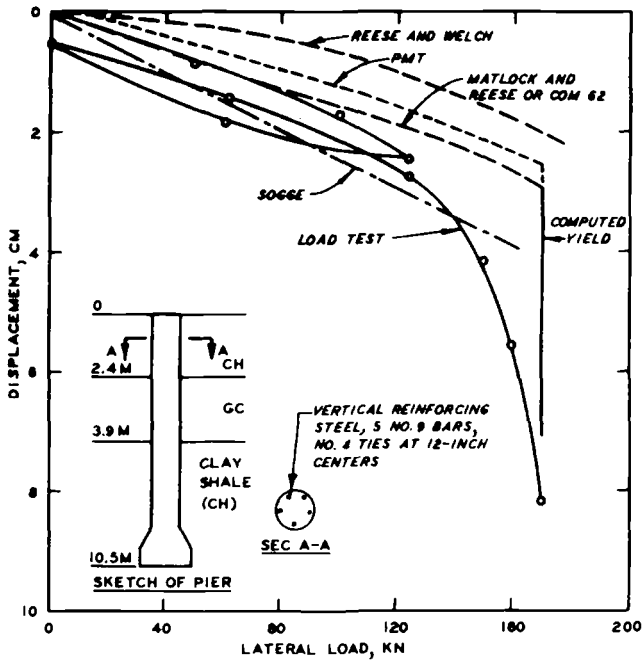

FIG. 1—*Lateral-load test Shaft 1.*

Methodology

Methods for evaluating the lateral-load displacement behavior of shaft foundations are based on solutions of the elastic beam-column differential equation [*3*]

$$E_c I(d^4y/dz^4) + Q(d^2y/dz^2) = p \tag{1}$$

where

E_c = elastic modulus of the concrete shaft, kPa,
I = moment of inertia of the shaft cross section, m^4,
Q = axial load, kN,
y = lateral displacement, m,
z = depth along shaft, m, and
p = lateral soil reaction per unit length, kN/m.

The lateral soil reaction p is expressed as a linear function of the lateral displacement y by

$$p = -E_s y \tag{2}$$

where E_s is the lateral soil modulus in kiloPascals. The lateral soil modulus is assumed herein similar to the soil modulus determined from pressuremeter tests, and the vertical soil modulus is assumed identical with the lateral soil modulus as in an isotropic linear material.

Many solutions had been determined from Eq. 1 for an elastic soil [*1*]. Elastic solutions by Matlock and Reese [*4*] and Sogge [*5*] were selected for analysis based on a comparative study [*1*]. These methods are among those that may provide less stiff estimates of loading behavior. Equation 1 may also be solved using nonlinear *p-y* curves and finite different methodology described by Reese and Allen [*6*]. A computer program COM62 [*7*] was used to calculate solutions from *p-y* curves. The *p-y* curves were developed from results of pressuremeter tests, undrained strength data, and results of the field load tests. Methodology of evaluating *p-y* curves from pressuremeter data is described by Briaud et al [*8*].

Elastic Analysis

Solution of the beam-column Eq 1 for zero moment at the ground surface is given by Matlock and Reese [*4*]

$$y_0 = A_y (P_0 T^3 / E_c I) \tag{3}$$

where

y_0 = displacement at the ground surface, m,
A_y = constant coefficient,
P_0 = lateral load at the ground surface, kN,
T = relative stiffness factor, m, and
$E_c I$ = flexural rigidity, kPa.

If the soil modulus increases linearly with depth

$$E_s = kz \tag{4}$$

where k = constant, kN/m^3; the relative stiffness factor is given by

$$T = \sqrt[5]{E_c I / k} \tag{5}$$

The coefficient A_y is 2.4 for a soil modulus increasing with depth, Eq 4, from Reese and Allen [*6*].

Sogge [*5*] recently solved Eq 1 for a constant soil modulus and performed parametric analyses from which lateral displacements at the ground surface may be found from

$$y_0 = (P_0 / E_s L) f(\beta L) \tag{6a}$$

and

$$\beta = \sqrt[4]{(E_s/4E_cI)} \tag{6b}$$

where L is the shaft length in metres. Sogge recommended that the soil modulus be evaluated as approximately 67 C_u where C_u is the undrained strength in kiloPascals. The function $f(\beta)$ is given by charts developed from the parametric analysis.

Nonlinear Analysis

Nonlinear p-y curves may be estimated from undrained strength data by [6]

$$p/p_u = 0.5(y/y_{50})^n \leq 1 \tag{7}$$

and

$$P_u = [3 + (\gamma z/C_u) + J(z/D_s)]\, C_u\, D_s \tag{8}$$

where

p_u = ultimate lateral reaction, kN/m,
$y_{50} = C_1\, D_s\, \epsilon_{50}$, m,
ϵ
ϵ_{50} = strain at ½ of the undrained strength C_u,
γ = unit wet weight, kN/m^3, and
D_s = shaft diameter, m.

The constants n, C_1, and J depend on the soil. Reese and Welch [9] suggest for a stiff overconsolidated soil above the water table applicable to this study that $n = 0.25$, $C_1 = 2.5$, and $J = 2$.

Tests

Data required to make estimates of the lateral-load behavior from the above methodology include the flexural rigidity E_cI, the soil modulus E_s, and the undrained soil strength C_u. Laboratory soil-strength tests on undisturbed specimens obtained in May 1982 and field pressuremeter tests were performed to obtain the required information. The shaft flexural rigidity had been determined as above. Details of soil tests and analysis are provided by Johnson [1].

Soil

Unconfined unconsolidated (UU) and consolidated undrained (CU) triaxial tests were performed to evaluate the undrained strength C_u and the soil modulus E_s. Eight UU tests were conducted at confining pressures equivalent with the total overburden pressure at various depths from 0.9 to 12.2 m. *CU*

tests were also performed at confining pressures of 48, 96, and 192 kPa at six different depths from 0.9 to 12.2 m.

The results of the UU tests indicated an undrained strength of 77 ± 10 kPa above the clayey gravel and 144 ± 25 kPa below the clayey gravel within the length of the shaft. The undrained strength C_u of 77 kPa was selected for analysis assuming that the increase in strength below the gravel would not significantly contribute to the mobilized soil resistance. The soil modulus was calculated from results of both *UU* and *CU* tests by the hyperbolic method of Duncan and Chang [*10*] after Kondner [*11*] (Fig. 2). This is an initial modulus given by the reciprocal of the strain/stress ratio at zero strain. The soil modulus above the clayey gravel is about 13 MPa and appears to increase approxi-

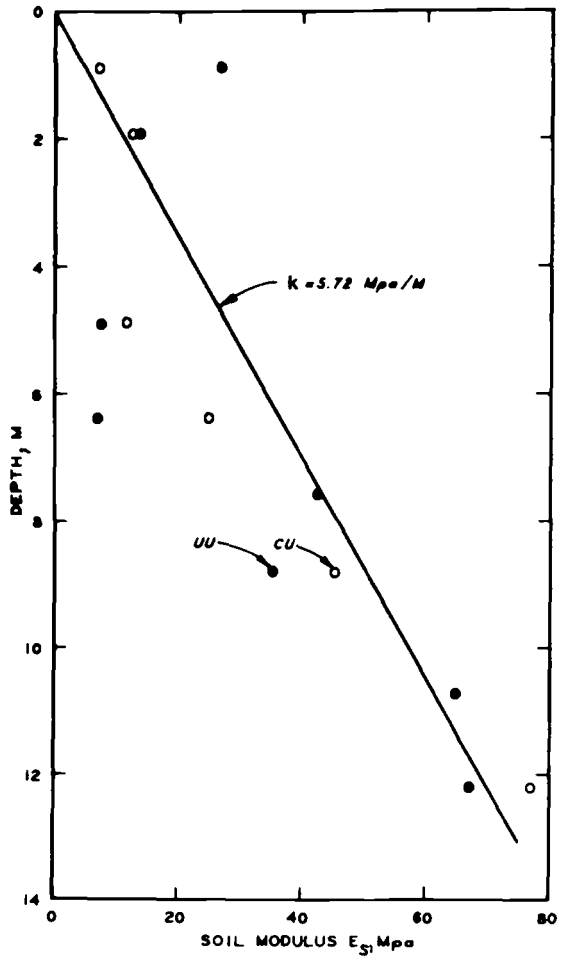

FIG. 2—*Initial soil modulus.*

mately linearly with depth to about 65 MPa near the base of the shaft as given by Eq 4 where k is equal to 5.72 MN/m^3. The strain at ½ of the undrained strength ϵ_{50} is 0.006, and the unit wet weight is 18 kN/m^3. The soil modulus calculated from $67C_u$ used in the Sogge method [5] is only 5.0 MPa.

Pressuremeter

The pressuremeter tests provided nine p-y curves shown in Fig. 3. These curves were evaluated by the methodology of Briaud et al [8]. The tests were conducted within 3 m of the shaft with a TEXAM pressuremeter, which is strain controlled and consists of a monocell probe inflated with water. The probe is 60 mm in diameter with an initial deflated volume of 1000 cm^3. Holes for testing were provided by a slow rotation of a 6-cm-diameter drill bit jetting at low mud pressure and by some hand augered holes bored to the clayey gravel. A drill bit with axial mud injection may have been more suitable for deep holes below the gravel since some side hole erosion was observed. Details of this testing may be found in a contract report by Briaud to the U.S. Army Engineer District, Fort Worth, Tex., sponsored by the Office, Chief of Engineers, through the U.S. Army Engineer Waterways Experiment Station [1].

Results

The selected methodologies provided reasonable correlations with results of the field load test (Fig. 1). The Matlock and Reese elastic method, Eq 3, and using a soil modulus that increases linearly with depth and k of 5.72 MPa/m from Eq 4 agreed extremely well with the initial loading curve for lateral loads less than 100 kN. Significantly, results of this procedure are almost identical to load test results within the range of deflections appropriate for many design problems. The Sogge method is shown for $E_s = 33/C_u$ or $E_s = 2.5$ MPa, which led to excessive initial displacements, but agreed well with observed displacements on reloading for lateral loads less than 100 kN. The Sogge method for $E_s = 67\ C_u$ or $E_s = 5$ MPa as suggested [5] led to results slightly stiffer than Matlock and Reese for E_s increasing linearly with depth and similar to the pressuremeter (PMT). The Reese and Welch p-y curves derived from Eqs 7 and 8 and n, C_1, and J equal to 0.25, 2.5, and 2, respectively, gave a relatively stiff load behavior curve using program COM62 compared to that observed. The PMT curves led to load behavior less stiff than the Reese and Welch p-y curves. The load test curve predicted on the basis of pressuremeter data was prepared before the load test results were available.

The p-y curves predicted from Eq 3 and the load test results for the assumption of a linearly increasing modulus with depth (k = 5.72 MPa/m, Eq 4) indicated that the ultimate reaction p_u in kiloNewtons per centimetre and z in centimetres may be given by

$$p_u = 0.033z\,C_u D_s \leq 10 C_u D_s \tag{9}$$

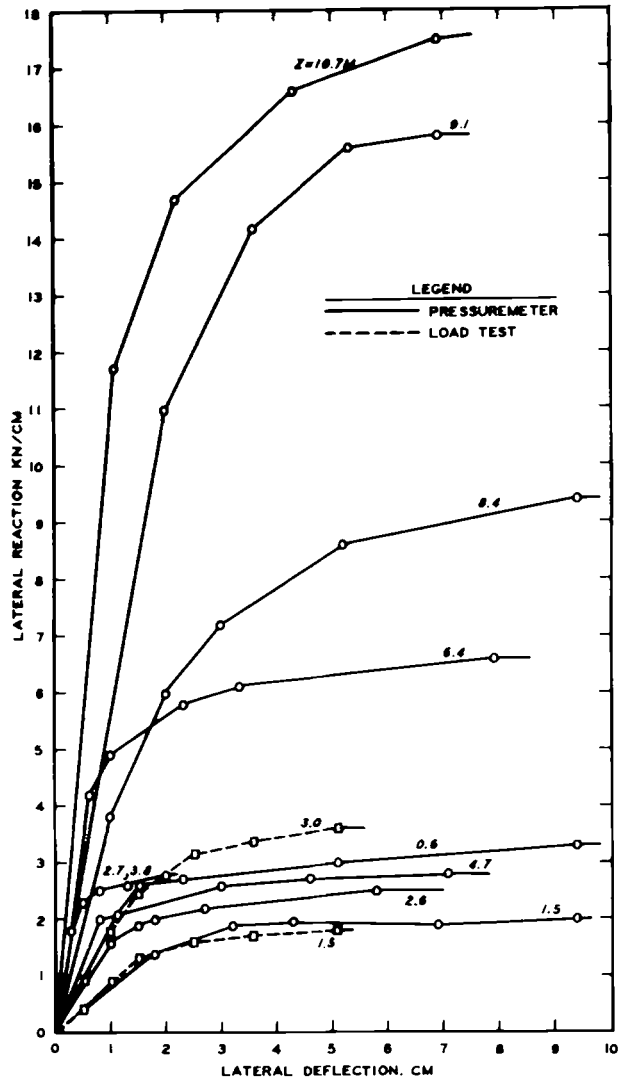

FIG. 3—*Lateral* p-y *curves.*

and that the constants n and C_1 of Eq 7 are best represented by 0.87 and 4, respectively. These curves are reasonably consistent with the pressuremeter curves (Fig. 3). The calculated load behavior of the shaft from program COM62 shown in Fig. 1 for *p-y* curves from the load test is consistent with the Matlock and Reese estimate of the lateral-load behavior.

Detailed analysis of the lateral load test [*1*] indicates that E_cI was less than that assumed in this analysis. This explains the greater displacements observed

compared to those calculated, especially for lateral loads greater than ½ of the yield load.

The yield point p_u was roughly estimated from the maximum bending moment M_{max} and depth of the moment z_{max} by

$$p_u = (2M_{max}/z_{max}) \tag{10}$$

Results of calculations from program COM62 indicated z_{max} was 2.1 m. M_{max} was calculated from

$$M_{max} = (f'_c I/D_s) \tag{11}$$

Conclusions

Both elastic methods and *p-y* curves were suitable for analysis of the lateral-load behavior of an aged drilled shaft by the beam column Eq 1. The most appropriate elastic soil moduli used in analysis compared well with the initial elastic moduli determined by a hyperbolic soil model [*10,11*] from results of triaxial strength tests on undisturbed soil specimens. Criteria for evaluating the lateral-load behavior led to more stiff *p-y* curves than observed from the load test. Long-term field conditions, such as wetting and remolding of the adjacent soil and reduction in the flexural rigidity of the shaft with increasing lateral displacement, may have contributed to the observed performance of the shaft.

Acknowledgment

This research was sponsored by the Office, Chief of Engineers, Washington, D.C., through the U.S. Army Engineer Waterways Experiment Station, Vicksburg, Miss. The field load test was managed by the Fort Worth District, U.S. Army Corps of Engineers.

References

[*1*] Johnson, L. D., "Methodology for Design and Construction of Drilled Shafts in Cohesive Soils," TR GL-83-4, U.S. Army Engineer Waterways Experiment Station, Vicksburg, Miss., 1984.

[*2*] U.S. Army Engineer District, "Investigations for Building Foundations in Expansive Clays," Vol. 1, Fort Worth, Tex., April 1968.

[*3*] Hetenyi, M., *Beams on Elastic Foundations*, University of Michigan Press, Ann Arbor, Mich., 1946.

[*4*] Matlock, H. and Reese, L. C., "Generalized Solutions for Laterally Loaded Piles," *Journal of the Soil Mechanics and Foundations Division, Proceedings of the American Society of Civil Engineers*, Vol. 86, No. SM5, May 1960, pp. 63-91.

[*5*] Sogge, R. L., "Laterally Loaded Pile Design," *Journal of the Geotechnical Engineering*

Division, Proceedings of the American Society of Civil Engineers, Vol. 109, No. GT9, Sept. 1981, pp. 1179-1199.

[6] Reese, L. C. and Allen, J. D., "Drilled Shaft Design and Construction Guidelines Manual: Structural Analysis and Design for Lateral Loading," Vol. 2, Implementation Package 77-21, U.S. Department of Transportation, Federal Highway Administration, Offices of Research and Development, Implementation Division, Washington, D.C., July 1977.

[7] Reese, L. C., "Laterally Loaded Piles: Program Documentation," *Journal of the Geotechnical Engineering Division, Proceedings of the American Society of Civil Engineers*, Vol. 103, No. GT4, April 1977, pp. 287-305.

[8] Briaud, J., Smith, T., and Meyer, B., "Design of Laterally Loaded Piles Using Pressuremeter Test Results," *Symposium on the Pressuremeter and Its Marine Applications*, Institut Francais du Petrole, Paris, April 1982.

[9] Reese, L. C. and Welch, R. C., "Lateral Loading of Deep Foundations in Stiff Clay," *Journal of the Geotechnical Engineering Division, Proceedings of the American Society of Civil Engineers*, Vol. 101, No. GT7, July 1975, pp. 633-649.

[10] Duncan, J. M. and Chang, C. Y., "Nonlinear Analysis of Stress and Strain in Soils," *Journal of Soil Mechanics and Foundations Division, Proceedings of the American Society of Civil Engineers*, Vol. 96, No. SM5, May 1970, pp. 1629-1653.

[11] Kondner, R. L., "Hyperbolic Stress-Strain Response: Cohesive Soils," *Journal of the Soil Mechanics and Foundations Division, Proceedings of the American Society of Civil Engineers*, Vol. 89, No. SM1, Jan. 1963, pp. 115-143.

Michael W. Oakland[1] *and Jean-Lou A. Chameau*[1]

Finite-Element Analysis of Drilled Piers Used for Slope Stabilization

REFERENCE: Oakland, M. W. and Chameau, J.-L, A., **"Finite-Element Analysis of Drilled Piers Used for Slope Stabilization,"** *Laterally Loaded Deep Foundations: Analysis and Performance, ASTM STP 835*, J. A. Langer, E. T. Mosley, and C. D. Thompson, Eds., American Society for Testing and Materials, 1984, pp. 182-193.

ABSTRACT: During the past two decades, the use of bored piles, or drilled piers, has been shown on several occasions to be an effective deterrent to excessive slope movements. The technique is applicable when either the resisting forces of the slope are to be decreased or the driving forces to be increased. These situations arise when cutting a steeper slope or adding a surcharge above a slope, respectively. The movements of landslides can also be controlled by drilled-in piers or piles.

Several investigators have studied the problem of a single pier subject to lateral soil movement, given certain simplifying assumptions with regard to the soil model, soil-pile interface, and repartition of the lateral loads. It is commonly assumed that a plane strain condition prevails, and the piers are analyzed in two dimensions. This does not allow the effects of pier size and spacing to be represented, although finite-difference solutions have shown these to be very significant. Current design practice uses piers spaced closely together in a continuous barrier. Part of the face is usually exposed to form a retaining wall, and in some cases the piers are tied back at the top. The design methods are similar to those used for sheet-pile walls and usually valid for relatively shallow overburden depths. This methodology results in a conservative sizing and spacing of the piers.

In this paper a finite-element based methodology is proposed to model the three-dimensional effects involved in the stabilization of surcharged slopes with drilled piers. The soil is modeled with eight nodes, 24 degrees of freedom isoparametric elements. The piers are represented by three-dimensional spar elements. The program can be used to determine the effects of piers' position, size, spacing, and stiffness on slope movements. This program is the first step towards a more general methodology that will consider soil nonlinearity and creep, and make provisions for slippage around the pile.

KEY WORDS: pile lateral loads, slope stability, drilled-in piles, finite element, drilled piers

[1]Graduate research assistant and associate professor, respectively, Civil Engineering Department, Purdue University, West Lafayette, Ind. 47907.

During the past two decades innovative soil reinforcement techniques, such as reinforced earth, stone column, soil anchors, and cast-in-place piles and piers have been developed to answer many geotechnical problems. In particular these techniques can provide cost-effective solutions to many transportation design and construction problems. Laterally loaded piles and drilled piers have been used on several occasions to stabilize landslides and slopes. In Sweden timber piles are used to increase the slope stability of very soft clays (Fig. 1). Large diameter cast-in-place reinforced concrete piles have been used in the United States to stabilize active landslide areas in stiff clays and shales through dowel action [*1-5*]. The diameter of the piles varied between 1.0 and 1.5 m (Fig. 2). In Japan 300-mm-diameter steel pipes have been used for the same purpose [*6*]. Similar techniques, such as the Fondedile reticulated root pile method (Fig. 3) and stone columns (Fig. 4), although relatively new within the United States, have been proven to be quite effective techniques in Europe for a number of years [*7*].

There are two major problems involved in the design of piers and piles used to correct and stabilize slopes. The first is to determine the load distribution along the axis of the pier in order to assess the shear forces and bending moments the pier has to restrain. The second is to evaluate the overall stability of the corrected slope. In this paper existing design methodologies are reviewed and a finite-element based technique is proposed to analyze slopes stabilized with drilled piers. The finite-element computer program can model three-dimensional effects and evaluate the influence of piers' position, size, spacing, and stiffness on slope movements. Preliminary results are presented, and further developments are discussed.

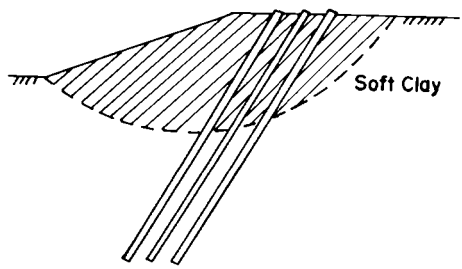

FIG. 1—*Stabilization of slopes with timber piles.*

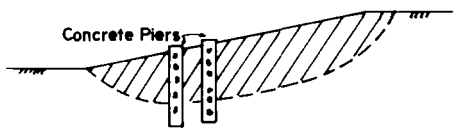

FIG. 2—*Stabilization of slopes with concrete piers.*

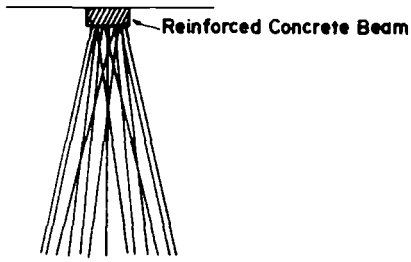

FIG. 3—*Reticulated structure.*

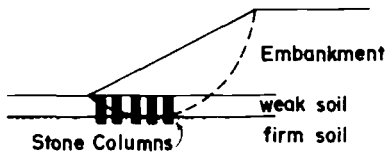

FIG. 4—*Stabilization of slopes with stone columns.*

Design Methodologies

Although the use of these reinforcing techniques is becoming more and more common, very little information is currently available regarding the pier and pile behavior under lateral loading induced by the movement of the surrounding soil. While literature is available for piles subjected to lateral loading [*8–12*], most of it dealt with lateral loading imposed by a supported structure. Computer programs are currently available to assess the stability of drilled piers under such loads [*13*]. The lateral loads developed on a pier by a soil mass undergoing lateral movement are different from externally applied loads from a structure. The major difficulties and differences are related to the location and distribution of the loading (lateral loads induced by the soil are nonuniform and distributed along the axis of the pier) and to the boundary conditions (head and tip restraints).

Thus, the problem of piles and piers subject to a soil induced lateral loading is unique and at present has not received particular attention and treatment. Several investigators have studied the problem of a single pile subjected to lateral soil movement, given certain simplifying assumptions with regard to the soil model, soil-pile interface, and repartition of the lateral loads [*14–19*]. As an example, the model proposed by Poulos [*18*] uses a finite difference technique to compute the displacements, shear forces, and bending moments in a pile, assuming the soil to be elastic plastic, no shear between pile and soil, and the distribution of horizontal movement with depth known from inclinometer data. Ito and Matsui [*15*] derived a theoretical equation to determine the lat-

eral force acting on piles used to stabilize soil movements. This is done by discretizing the soil into layers and assuming a Mohr-Coulomb plastic condition in the soil surrounding the piles. Various end conditions can be considered for the pile tip and top. The computed values of lateral loads compared well with measured values. Later papers by Ito et al [*16,17*] considered specific examples where these piles could be used.

The determination of the shear forces and bending moments along the axis of the pier is only the first aspect of the design of drilled-in piers used to increase slope stability. A second aspect is to make an estimate of the influence of piles or piers on the factor of safety against slope failure. A simplified procedure has been recently proposed to determine the additional resisting moment caused by the pile [*20*]. The added resistance is generated by the lower portion of the pile below the critical failure surface and can be assessed once the pile-soil pressure distribution has been determined. The possibilities of a two-dimensional finite-element analysis of this form of stabilization have been discussed by Rowe and Poulos [*20*], who have used the technique for analyzing soil-structure interaction described by Rowe et al [*21*]. The effect of piers upon slope deformation and stability is also a function of pier arrangement, pier stiffness and restraint condition as well as soil stiffness and strength.

Three-Dimensional Model

A finite-element analysis of the stabilization of a slope should make allowance for soil-pier interaction and three-dimensional effects such as arching between piers. The piers do not form a continuous barrier, and soil movement occurs around the piers in the direction parallel to the slope (Fig. 5). A three-

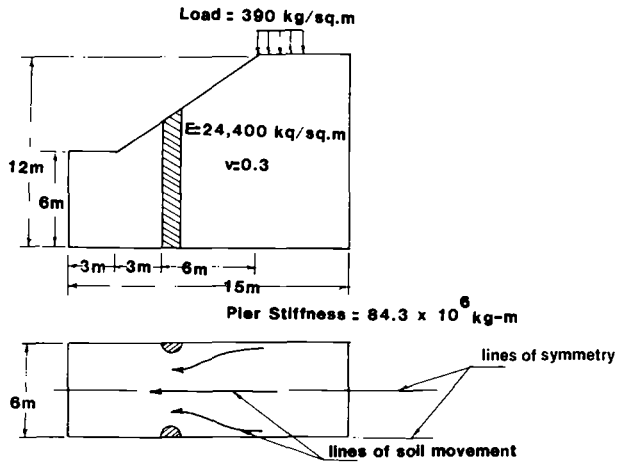

FIG. 5—*General problem.*

dimensional finite-element model can adequately model the geometry of the problem and the effects of piers' position, size, spacing, and stiffness on the amount of soil movement and on the stability of the slope.

Lines of symmetry exist in a slope containing a row of piers (Fig. 5). Through the centerline of each pier and perpendicular to the slope is a line where the soil will not move parallel to the slope. A similar line exists at the midpoint between piers. The size of the model is drastically reduced by considering only the part of the slope between two of these lines. It is then assumed that the rest of the slope is a repetition of this part.

Currently, the program uses eight-node, 24 degrees of freedom, isoparametric parallel-pipeds to model the soil (Fig. 6). These elements are among the simplest three-dimensional elements available, modeling geometry and displacements as linear functions. They are widely used in soil mechanics because the rectangular shape adapts itself well to typical slope and foundation problems [*22*]. Although higher order elements provide a better model, the number of degrees of freedom increases so rapidly that computer space is often a problem. The pier is modeled by eight-node, four degrees of freedom parallel-piped spar or bending elements (Fig. 7). The eight-node spar elements were chosen to be compatible with the eight-node soil element and to reduce the amount of computer space needed. The 24 degrees of freedom in the soil elements represent displacements in three dimensions at each corner. The four degrees of freedom in the pier elements represent displacements and rotations at the ends of the element in the direction perpendicular to the slope. It is assumed that the piers are incompressible and will not bend in any other direction. This assumption is not restrictive because of the high ratio of pier to soil moduli.

The boundaries of the problem are the two lines of symmetry that allow soil movement only in the direction perpendicular to the slope and an underlying rock layer that does not allow slip. The finite-element mesh is assumed long enough in the direction perpendicular to the slope so that the end boundaries can be considered fixed. To simulate the piers being socketted in sedimentary bedrock, the tip of the pier is also fixed against displacement and rotation.

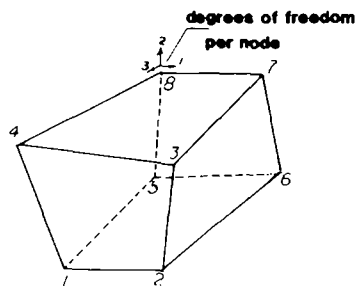

FIG. 6—*Soil element.*

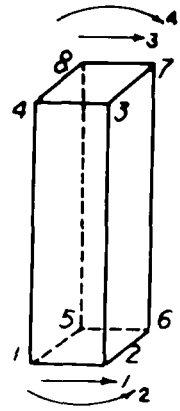

FIG. 7—*Pier element.*

Three options are available in the program for the soil model: (1) linear elastic, (2) hyperbolic Duncan and Chang [*23*] model with nonlinear modulus, and (3) Duncan and Chang model with both nonlinear modulus and Poisson's ratio. The loads are applied in several increments, and an iteration technique is used within each increment to estimate the pier displacement. The basic operations of the program are:

(1) calculate principal soil stresses,
(2) calculate soil parameters (hyperbolic model),
(3) apply a load increment with the piers held perfectly rigid,
(4) generate the soil stiffness matrix and solve for the soil displacements,
(5) determine loads on the rigid pier,
(6) generate the pier stiffness matrix and compute the displacements of the pier,
(7) iterate between pier displacements and soil nodal loads until convergence, and
(8) next cycle of loading (repeat Steps 1 to 7).

The program is a conventional finite-element program except for the interaction between pier and soil elements. There is a compatibility problem between the sides of the soil elements that can only displace linearly and the pier elements that have cubic displacement functions. To circumvent this problem, the soil and pier elements are treated separately. Since all of the transformations between the pier and soil are through the nodes, overlapping or separation of the two meshes will not affect the results. The stresses in the soil caused by a loading increment are transformed into equivalent nodal loads. These nodal loads are then applied to the pier as if it were a cantilever beam in space. The resulting nodal displacements can be related to nodal forces and reapplied to the soil nodes. An iterative technique is necessary to assure compatibility of

stresses between the soil and the pier. The rate of convergence of the iterative process is a function of the initial estimate of the pier displacements. If the difference between this estimate and the sought solution is too large, the forces on each side of the pier may be excessively unbalanced and result in large deflections causing the adjacent soil elements to act in tension. Under these conditions, tension and compression will act on opposite sides of the pier, and the pier displacements will keep increasing. An initial estimate of about one third of the unreinforced slope displacements at the location of the pier has been found to achieve convergence.

Preliminary Results

The three-dimensional computer program described in the previous section is part of an on-going research project on the design of laterally loaded drilled-in piers for landslide corrections. In its present state the program has a lot of deficiencies (to be discussed in a subsequent section) but can nevertheless be used to qualitatively assess the effect of drilled piers on slope movement and help give direction for further developments. As an example, the slope shown in Fig. 5 was analyzed with the three-dimensional program for a uniform surcharge applied at the top of the slope. The horizontal and vertical movements induced by this loading condition in a typical cross section of the nonstabilized slope (without piers) are shown in Fig. 8. (Note the different scales for geometry and displacement in this figure.) The effectiveness of the piers will be based

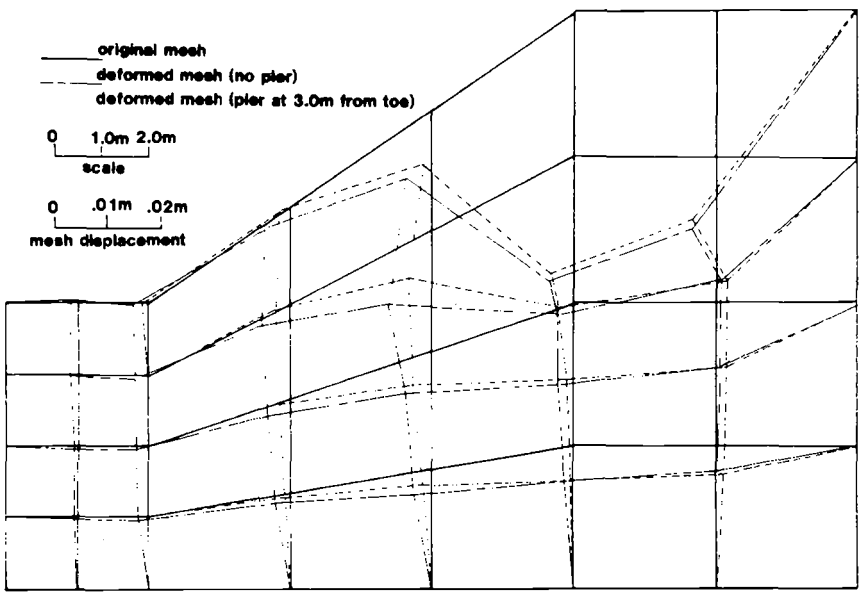

FIG. 8—*Displacement at centerline between piers.*

on reduction of this movement. Rectangular piers (0.90 by 1.80 m) with a center to center spacing of 6.0 m are installed at 3.0 m from the toe of the slope (Fig. 5). The displacements along the cross section at the centerline between the piers are given in Fig. 8. Below the pier (with respect to the slope), the reduction in slope movement is very significant, ranging from 60 to 100% with an average reduction of about 70%. Above the pier, the reduction is less but still significant, especially in the vertical direction. In this region of largest displacements the reduction in movement was less than 40%. As expected the largest movement reduction occurs next to the pier. The horizontal displacements obtained at 12 m from the toe are larger for the stabilized slope. This is because of the proximity of the fixed boundary. Further parametric studies will be necessary to determine how far the finite-element mesh should extend.

The reduction in shear stress was also determined for each element along the cross section between the piers. The reduction in shear stress was of the order of 80% for the elements located below the pier and 30% for elements above the pier. There is a very close correlation between the reduction in displacement and the reduction in shear stress.

In this example, the effect of the piers on the amount of movement is more significant for elements below than above the pier. This tends to indicate that the most effective design would require the piers to be near the top of the slope where the movements are largest for the case of loading at the top of the slope. To examine the influence of the position of the piers, two other cases are considered, one with the piers located at the toe of the slope, and one with the piers located 6 m from the toe. The horizontal surface movements at the centerline between the piers are given in Fig. 9 for these two cases, together with the movements obtained in the previous case (piers at 3 m from the toe) and for the nonstabilized slope. For all three cases of stabilization the horizontal movements are reduced, but the most efficient pier position is near the top of the slope, where the soil movements are the largest. Broms [*8*] found that for distressed slopes, piers placed near the bottom were most effective. In his example, how-

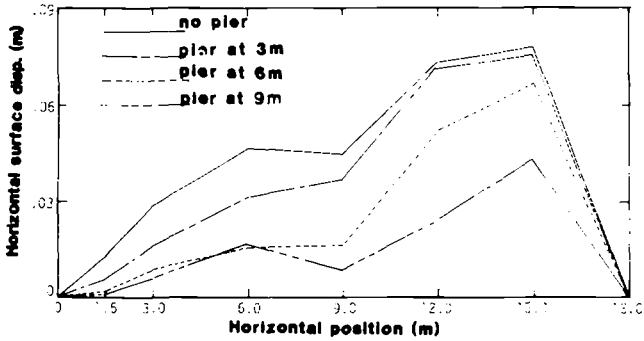

FIG. 9—*Effect of pier position.*

ever, the toe of the slope was the point of maximum soil movement. The results of the present study agree with Broms conclusion that the piers should be placed at the point of maximum soil movement.

As the spacing between piers is decreasing, the piers act more as a continuous barrier, and the effect of soil arching becomes more significant and reduces the soil movements, especially below the pier. In Fig. 10 the slope movements computed for a pier spacing of 3.9 m are compared to the movements obtained in the previous case (6.0 m center to center spacing). The displacements below the pier are reduced by about 50% while the reduction above the piers is not significant. Similar results were found by Ito and Matsui [*15*].

The piers placed near the top of the slope are the most efficient for the present case, despite the piers larger flexibility caused by their increased length. However, previous work by Rowe and Poulos [*20*], showed that the stiffness of the piers has a significant effect on the soil movements. To evaluate the effect of pier stiffness, the previous cases were analyzed with completely rigid piers. Figure 11 shows the horizontal surface movements along the centerline between piers for flexible and rigid piers at 3 m from the toe. The results from the other two cases were similar. In the case of rigid piers, the active pressure condition is not realized on the down-slope face of the pier, and the only soil movements below the pier are due to soil "flowing" around the pier. Consequently, the reduction in soil movement is more important for rigid piers than for flexible piers. However, the forces acting on the rigid piers are significantly increased, which may cause problems for the structural design of the piers. For the case studied, the effect of pier stiffness is not very significant, and more parametric studies will be needed to define under which circumstances the stiffness of the pier or its ratio to the soil stiffness is an important parameter.

Present Limitations and Further Developments

Although the proposed three-dimensional finite-element program is more general than conventional two-dimensional solutions, it is still limited by the

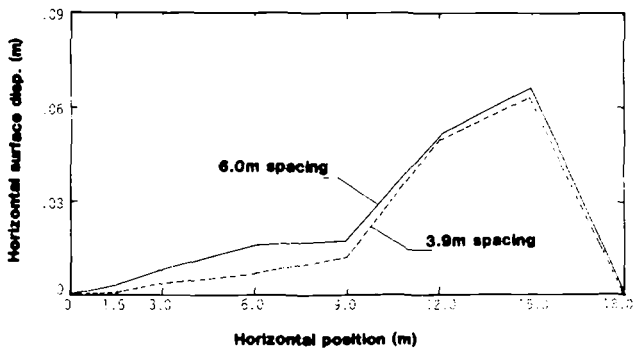

FIG. 10—*Effect of pier spacing.*

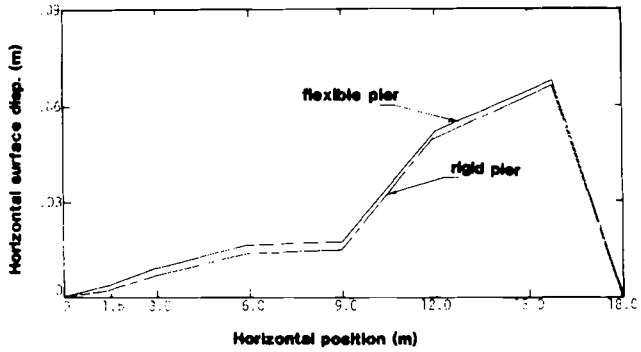

FIG. 11—*Effect of pier stiffness.*

assumptions made regarding the boundary conditions, the geometry of the piers, the soil-pier interface, and the soil model.

In the previous example, the nodes along all boundaries, except the lines of symmetry, were fixed. These boundaries limited the size of the problem and forced the nodes along the slope to displace downward rather than be pulled back towards the top. This was a good assumption for the boundary left of the toe because the amount of deformation was very limited for the elements located in this area. However, the elements at the upper boundary were distorted unrealistically as a result of this assumption. To model actual situations, more elements must be added to this upper portion and the optimum location of the fixed boundary must be determined, or different boundary conditions (frictional boundary) have to be investigated.

In its present form, the eight-node spar element used to model the piers is not sufficient because it limits the analysis to rectangular or square piers. The results can only be applied to the more conventional circular piers in a qualitative manner. Higher order interpolation functions will be introduced in the soil and pier elements to accommodate curved surfaces and model circular piers.

Relative displacements occur at the interface between soil and pier and play an important role in the soil-pier interaction. The interface behavior will be represented using slip elements [*22*]. Three-dimensional slip elements will be necessary to model the interface between the soil and the circular piers. The properties of the slip element depend on the roughness of the pier and the soil characteristics and can be determined from interface direct shear tests. The soil model will also be improved to incorporate the creep effects that occur in unstable slopes.

Conclusion

The effect of piles and piers upon slope deformation and stability is analyzed with a three-dimensional finite-element program. The loads on the slope are applied incrementally and an iteration technique is used within each incre-

ment to model the soil-pier interaction. This technique can evaluate the effects of piers position, size, spacing and stiffness on the amount of slope movement. The piers can significantly reduce the movements, especially below the piers. The maximum pier efficiency is obtained by placing the pier where the largest movements are expected. Further improvements of this program are planned to release some of the assumptions made regarding the boundary conditions, the geometry of the piers, the soil-pier interface, and the soil model.

Acknowledgments

The research is part of an investigation conducted by the Joint Highway Research Project, Engineering Experiment Station, Purdue University, in cooperation with the Indiana Department of Highways and the U.S. Department of Transportation Federal Highway Administration. The opinions, findings, and conclusions expressed in this publication are those of the authors and not necessarily those of the Federal Highway Administration.

References

[1] Merriam, R., "Portuguese Bend Landslides, Palos Verdes Hills, California," *Journal of Geology*, Vol. 68, No. 2, March 1960, pp. 140-153.

[2] Andrews, G. H. and Klasell, J. A., "Cylinder Pile Retaining Wall," Highway Research Record No. 1240, Washington, D.C., 1964, pp. 83-97.

[3] Bulley, W. A., "Cylinder Pile Retaining Wall Construction—Seattle Freeway," Roads and Streets Conference, Seattle, Wash., 1965.

[4] Gould, J. D., "Lateral Pressures on Rigid Permanent Structures," *Specialty Conference on Lateral Stresses in the Ground and Design of Earth Retaining Structures*, Cornell University Press, Ithaca, N.Y., 1970, pp. 219-269.

[5] Offenberger, J. H., "Hillside Stabilized with Concrete Cylinder Pile Retaining Wall," *Public Works*, Vol. 112, No. 9, Sept. 1981, pp. 82-86.

[6] Taniguchi, T., "Landslides in Reservoirs," *Proceedings of the 3rd Asian Regional Conference on Soil Mechanics and Foundary Engineering*, Vol. 1, Southeast Asian Society of Soil Engineering, Bangkok, Thailand, 1967, pp. 258-261.

[7] Goughnour, R. D. and DiMaggio, J. A., "Soil-Reinforcement Methods on Highway Projects," *Symposium on Earth Reinforcement*, American Society of Civil Engineers, New York, 1978, pp. 371-399.

[8] Broms, B. B., "Stability of Flexible Structures (Piles and Piles Groups)," *General Report, Fifth European Conference on Soil Mechanics and Foundary Engineering*, Vol. 2, The Spanish Society for Soil Mechanics and Foundations, Madrid, 1972.

[9] Davisson, M. T., "Lateral Load Capacity of Piles," Highway Research Record No. 333, Washington, D.C., 1970, pp. 104-112.

[10] Davisson, M. T. and Gill, H. L., "Laterally Loaded Piles in a Layered Soil System," *Journal of Soil Mechanics and Foundation Engineering Division, Proceedings of the American Society of Civil Engineers*, Vol. 89, No. SM3, May 1963, pp. 63-94.

[11] Reese, L. C. and Cox, W. R., "Field Testing and Analysis of Laterally Loaded Piles in Stiff Clay," *Proceedings of the 7th Offshore Technology Conference*, Vol. 2, Dallas, Tex., 1975.

[12] Poulos, H. G., "Behavior of Laterally Loaded Piles: II—Pile Groups," *Journal of Soil Mechanics and Foundation Engineering Division, Proceedings of the American Society of Civil Engineers*, Vol. 97, No. SM5, 1971.

[13] Reese, L. C. and Allen, J. D., "Drilled Shaft Design and Construction Guidelines Manual, Volume Two, Structural Analysis and Design for Lateral Loading," Implementation Package 77-21, U.S. Department of Transportation, Federal Highway Administration, Washington, D.C., July 1977.

[14] De Beer, E. E. and Wallays, M., "Forces Induced in Piles by Unsymmetrical Surcharges on the Soil Around the Pile," *Proceedings of the 5th European Conference on Soil Mechanics and Foundation Engineering*, Vol. 1, The Spanish Society for Soil Mechanics and Foundation, Madrid, 1972.

[15] Ito, T. and Matsui, T., "Methods to Estimate Lateral Force Acting on Stabilizing Piles," *Soils and Foundations*, Vol. 15, No. 4, 1975, pp. 43-60.

[16] Ito, T., Matsui, T., and Hong, W. P., "Design Method for the Stability Analysis of the Slope with Landing Pier," *Soils and Foundations*, Vol. 19, No. 4, Dec. 1979, pp. 43-57.

[17] Ito, T., Matsui, T., and Hong, W. P., "Design Method for Stabilizing Piles Against Landslide—One Row of Piles," *Soils and Foundations*, Vol. 21, No. 1, March 1981, pp. 21-38.

[18] Poulos, H. G., "Analysis of Piles in Soil Undergoing Lateral Movement," *Journal of the Soil Mechanics and Foundation Engineering Division, Proceedings of the American Society of Civil Engineers*, Vol. 99, SM5, 1973, pp. 391-408.

[19] Poulos, H. G. and Davis, E. H., *Pile Foundation Analysis and Design*, John Wiley and Sons, New York, 1980.

[20] Rowe, R. K. and Poulos, H. G., "A Method for Predicting the Effect of Piles on Slope Behavior," *Proceedings of the 3rd International Conference on Numerical Methods in Geomechanics*, Vol. 3, American Society of Civil Engineers, New York, April 1979.

[21] Rowe, R. K., Booker, J. R., and Balaam, N. P., "Application of the Initial Stress Method to Soil Structure Interaction, *International Journal of Numerical Methods in Engineering*, Vol. 12, No. 5, 1978, pp. 873-880.

[22] Desai, C. S. and Christian, J. T., *Numerical Methods in Geotechnical Engineering*, McGraw-Hill Book Co., New York, 1977.

[23] Duncan, J. M. and Chang, C. Y., "Nonlinear Analysis of Stress and Strain in Soils," *Journal of the Soil Mechanics and Foundation Engineering Division, Proceedings of the American Society of Civil Engineers*, Vol. 96, No. SM5, Scpt. 1970, pp. 1629-1653.

Vijay K. Puri,[1] *R. W. Stephenson,*[2] *E. Dziedzic,*[3] *and L. Goen*[3]

Helical Anchor Piles Under Lateral Loading

REFERENCE: Puri, V. K., Stephenson, R. W., Dziedzic, E., and Goen, L., **"Helical Anchor Piles Under Lateral Loading,"** *Laterally Loaded Deep Foundations: Analysis and Performance, ASTM STP 835*, J. A. Langer, E. T. Mosley, and C. D. Thompson, Eds., American Society for Testing and Materials, 1984, pp. 194-213.

ABSTRACT: Anchors are used in civil engineering practice to provide resistance against uplift and overturning forces for structures such as transmission line towers, aircraft mooring, pipelines, offshore structures, mobile homes, and so forth. Although there are a wide variety of anchor types available, helical screw anchors, consisting of a steel shaft to which one or more helices are attached by welding, are finding wider usage particularly for the support of transmission line towers. Because these anchors are installed by truck mounted power augurs they can be used immediately after installation.

Although there exists in the geotechnical engineering literature a variety of techniques for evaluating lateral-load capacity of piles, there are no published methods for analyzing helical anchor lateral stability when used as piling. The present study was undertaken to develop suitable mathematical models based upon the current state of the art for determination of lateral-load capacity of helical-type anchor piles. The model selected was patterned after Matlock and Reese's elastic theory model. The model was modified to take into account the influence of the method of installation and other unique characteristics of this type of foundation. Based on the results of this study it was found that helical anchor piles can develop significant resistance to lateral loads, and this resistance is almost exclusively controlled by the extension shaft diameter.

KEY WORDS: anchors, lateral loads, piles, helical piles

Anchors are used in civil engineering practice to provide resistance against uplift and overturning forces for structures such as transmission line towers, aircraft moorings, pipelines, offshore structures, mobile homes, and so forth. Lateral loads (or shear loads) and moments may be transferred to foundation anchors by the supported structures because of a variety of reasons such as wind loading, line breakage, axial load eccentricities and so forth. Anchors

[1]Assistant professor, Department of Civil and Environmental Engineering, Polytechnic Institute of New York, Brooklyn, NY 11201.

[2]Professor, Department of Civil Engineering, University of Missouri at Rolla, Rolla, MO 65401.

[3]A. B. Chance Company, 210 N. Allen St., Centralia, MO 65240.

are manufactured in a variety of configurations such as plate anchors, screw anchors, pile anchors, steel cable grouted anchors, prestressed concrete anchors, and single and multiple helical-type anchors. A helical anchor pile consists of a steel shaft or lead section to which one or more helices are attached by welding. The length of the anchor may be increased by attaching additional steel shafts called extensions. The anchor is installed by screwing it into the ground typically with a truck mounted power auger. A special feature of these anchors is that they can be used immediately after installation for providing resistance against uplift, compressive and lateral loads, or overturning moments.

The present study was undertaken to develop suitable mathematical models based upon the current state of the art for determination of lateral-load capacity of helical type anchor piles manufactured by A. B. Chance Co. [*1*] (Fig. 1).

The main objective of the present study [*2*] was to evaluate the available anchor-soil models and to determine which model provided the most reliable estimate of lateral anchor capacity consistent with sound geotechnical engineering principles and available field test data. A model is suggested herein to estimate the lateral deformation of the anchor-soil system for a given set of applied lateral loads and moments. The analytical model is based on the observed behavior of soil along the embedded depth of the anchor.

In order to evaluate proposed mathematical models it was necessary to acquire high-quality field load tests and corresponding soil property data for comparison to computed capacities. The best data available in this respect are from full-scale lateral-load tests and model tests. Wherever available field information was not adequate, model tests on ¼-scale anchor models were conducted.

The results of this study indicate that the interaction between the anchor extension and the soil is the most significant in resisting the lateral loads. The soil between the helices and the helices themselves generally play a very minor role if the extension length is more than a certain prescribed limiting value. The problem of lateral-load capacity of helical anchors can therefore be analyzed on the same basis as the capacity of piles subjected to lateral loads.

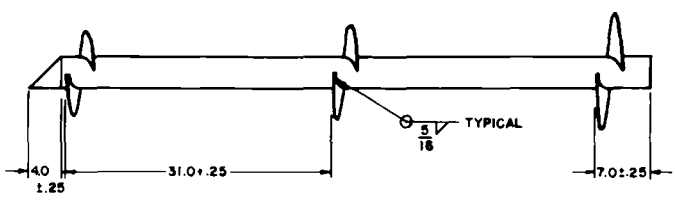

FIG. 1—*Schematic diagram—A. B. Chance helical anchors.*

Analysis of Piles under Static Lateral Loads

The available approaches for the analysis or laterally loaded vertical piles can be broadly grouped under the following categories:

(1) analysis based on limiting equilibrium or plastic theory,
(2) analysis based on elastic theory, and
(3) nonlinear analysis.

Analysis Based upon Limiting Equilibrium or Plastic Theory

The theories of Brinch Hansen [*3*] and Meyerhof and Ranjan [*4*] were developed for rigid piles assuming that the limiting or maximum soil resistance is acting against the pile when it is subjected to the ultimate lateral load. The pile is assumed to deflect sufficiently to develop full soil resistance along the length considered. This is not true for small deflections. Any improvement in this approach will need information on pile deflection and soil resistance characteristics. Because of the small diameter hollow extensions used in the helical anchors, these anchors will behave as flexible piles rather than rigid piles.

Analysis Based on Elastic Theory

Methods based on elastic theory commonly assume that the soil behaves as a series of closely spaced independent elastic springs (Winkler's assumption). Using the beam on elastic foundation approach, basic equations have been developed by various investigators [*5–7*] for different variations of modulus of subgrade reaction k. The governing equation is

$$EI(d^4y/dx^4) = -ky \tag{1}$$

where

d^4y/dx^4 = the fourth differential (displacement) of y with respect to x (position),
E = modulus of pile, and
I = moment of inertia of a pile cross section.

Nondimensional coefficients have been given for the solution of the pile problem to obtain deflection, moment, shear, and so forth along the pile length.

These methods require the proper evaluation of subgrade reaction, which is a function of the pile properties, stress strain relationships of the soil, depth of overburden, deflection of pile, rate and number of cycles of loading, and other time dependent characteristics such as consolidation and creep. In most cases, both for cohesive and noncohesive soils, the soil modulus tends to increase with depth [*8, 9*]. Reese and Matlock [*8*] have further shown that the constant

of proportionality between the soil modulus and depth is not critical as a variation of 32 to 1 in its value is necessary to produce a 2 to 1 variation in moment. The recommended values of modulus of horizontal subgrade reaction n_h for sands and for clays k are given in their paper.

Based upon solution of Eq 1, the following nondimensional solutions have been developed for long piles for cohesionless and cohesive soils.

In cohesionless soils a pile is considered to be a long pile when the embedded length is larger than 4 to 5 T, where T is the relative stiffness factor given by

$$T = (EI/n_h)^{1/5} \tag{2}$$

where

E = modulus of pile,
I = moment of inertia of the pile cross section, and
n_h = modulus of subgrade reaction ranging from 3 to 30 N/cm^3 and proportional to relative density.

The deflection at any depth along the pile caused by a lateral load P applied at the ground level (Fig. 2) and moment M is given by

$$y = A_y (PT^3/EI) + B_y (MT^2/EI) \tag{3}$$

where

A_y = deflection coefficient for lateral load,
B_y = deflection coefficient for moment, and
P = lateral load at ground level (mud line).

The values of A_y and B_y vary with depth. These values are presented by Reese and Matlock [6] as functions of nondimensional depth ($Z = X/T$) where X is

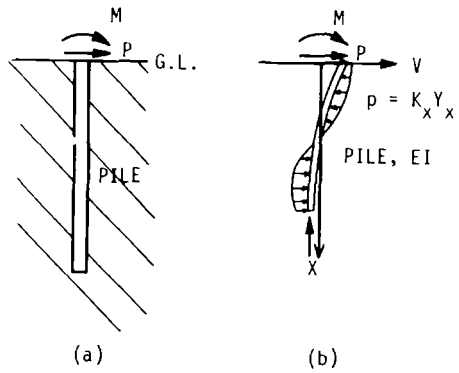

FIG. 2—(a) *Pile loads and* (b) *soil resistance and deflected shape.*

the depth of the point under consideration. The moment M_P acting on the pile at any depth is given by

$$M_P = A_m PT + B_m M \tag{4}$$

The values of A_m and B_m are the moment coefficients and are given by Davisson and Gill [7] versus nondimensional depth Z.

A pile in cohesive soil will be a flexible pile if the embedded length is more than 4 to 5 R where R is given by

$$R = (EI/K)^{1/4} \tag{5}$$

where K = the subgrade modulus, 67 times the undrained shear strength. The deflections and moments at any depth along the pile may be calculated from the following equations

$$y = A_y (PR^3/EI) + B_y (MR^2/EI) \tag{6}$$

$$M_P = A_m PR + B_m M \tag{7}$$

The values of coefficients A_y, B_y, A_m, and B_m in the above equations may be obtained by using either the technique described by Matlock and Reese [6] or Davisson and Gill [7]. In the approach by Davisson and Gill [7], the effect of layering in the case of cohesive soils can also be accounted for.

Nonlinear Analysis

The relationship between pressure (or load) and deflection at any point along a pile is nonlinear. A number of approaches have been developed to account for this nonlinear behavior. Kubo [10] has used the following nonlinear relationship between soil pressure (or soil reaction) P, deflection y, and depth X

$$P = k X^m y^n \tag{8}$$

where k, m, and n are experimentally determined coefficients. Nonlinear behavior has also been accounted for by Madhav et al [11] by using an elastoplastic model.

The most general approach to account for nonlinear soil behavior is the p-y approach developed by Reese and his colleagues. In this approach a finite-difference solution is obtained to the following general equation

$$EI(d^4y/dx^4) + P_z(d^2y/dx^2) + E_s y = 0 \tag{9}$$

where

y = deflection (lateral),
E = Young's modulus of pile material,
P_x = axial load,
I = moment of inertia of pile,
X = depth below top, and
E_s = soil modulus (soil modulus will vary with deflection and depth).

Equation 9 can be written in the finite-difference form. A full description of the resulting equations is available [*12*]. The solution uses as input a series of p-y curves (Figs. 3 and 4) for various points along the depth of the pile. As in the subgrade reaction approach, the p-y curves in Fig. 4 imply that behavior of soil at a particular depth is independent of the behavior at other depths. Design procedures for constructing p-y curves based on the results of field measurements on full-size instrumented piles have been developed by Matlock [*13*] for saturated soft clay, and other cases have subsequently been treated by Reese and his colleagues and are summarized by Reese and Welch [*14*].

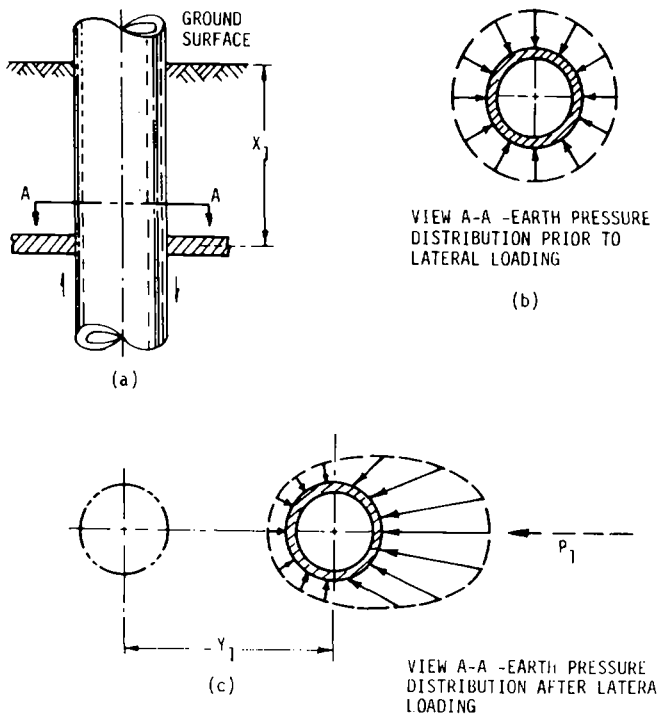

FIG. 3—*Graphical definition of* p *and* y [14].

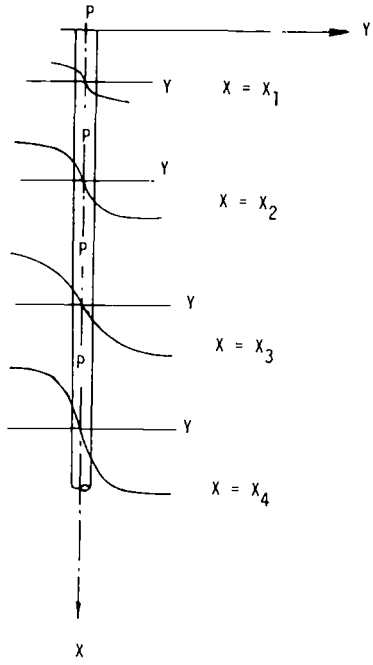

FIG. 4—*Possible family of* p-y *curves.*

Conclusion

A study of the above analysis techniques applied to helical anchor piles proved that their approachs, while each having its own merit, could not provide acceptable lateral-load capacity predictions and still be relatively simple to apply. The use of more sophisticated models (that is, *p-y* curve approach) would require relatively sophisticated soil data not normally developed for tower foundations. Therefore further study was needed to define a lateral-load capacity model.

Proposed Model for Lateral-Load Capacity

The model used to estimate the lateral-load versus deflection behavior of the anchor-soil system must yield information on the following points:

(1) lateral load for a given deflection (usually 2.5 cm),

(2) maximum moment induced in the anchor shaft (for checking structural design of the shaft), and

(3) the computed capacities from the proposed model should be within acceptable limits of geotechnical profession, that is, the computed values should be in reasonable agreement with observed lateral-load test results.

Available Test Data

Field Test

The lateral-load test data on helical anchors are very limited. The only available field data at the time of this study (1981) were

(1) tests conducted by A. B. Chance Co., namely, (a) full-scale test in clay in Houston, TX and (b) Georgia power plant tests that may be considered as predominantly sandy soil and
(2) tests conducted by Ontario Hydro, namely, (a) test at ESSA site in sand [*15*] and (b) test in stiff fissured clay [*16*].

The only available data (as of 1981) are on the head deflection versus lateral load except for the Houston test. Data on variation of soil properties with depth are also not available. There is thus no data on sand giving information on variation of moment with depth or on maximum moment, which might have been resisted by the anchor because of the applied horizontal loads.

The Houston test consisted of installing a fully instrumented helical anchor pile to a depth of 9 m (30 ft) in Houston clay. The pile was then loaded in a variety of lateral load-axial load configurations, and the corresponding deformation and moment profile of the pile were recorded. In addition, a complete subsurface soil investigation was carried out to define the soil properties.

Model Tests

Model tests were conducted on ¼-scale models of single-helix, two-helix, and three-helix anchors to obtain information on the variation of moment versus depth in the pile installed in a sand (Fig. 5). The helix pitch was the same as the prototype anchors.

Tests were conducted in a circular tank 56 cm in internal diameter and 175 cm in height. Tests were conducted using a well-graded dry medium sand (SW), which was deposited in the tank in layers and compacted using a mechanical vibrator. The density of soil in the tank was maintained uniform and was measured at every 23 cm by taking out specimens in metallic cans of known volume placed in position beforehand. The density of sand during the tests was ± 78 N/m^3 (113 pcf), corresponding to a relative density of 85%. The value of the angle of internal friction at this density is 42° (as measured by drained triaxial shear strength tests).

The anchors were instrumented at their third points using strain gages. The calibration of the gages was done before placing the anchor in position. Calibration was checked before and after each test.

Anchors were installed in position by applying torque at the end of an extension rod simulating the process used in installing the prototype anchors in the field. The torque during installation was recorded.

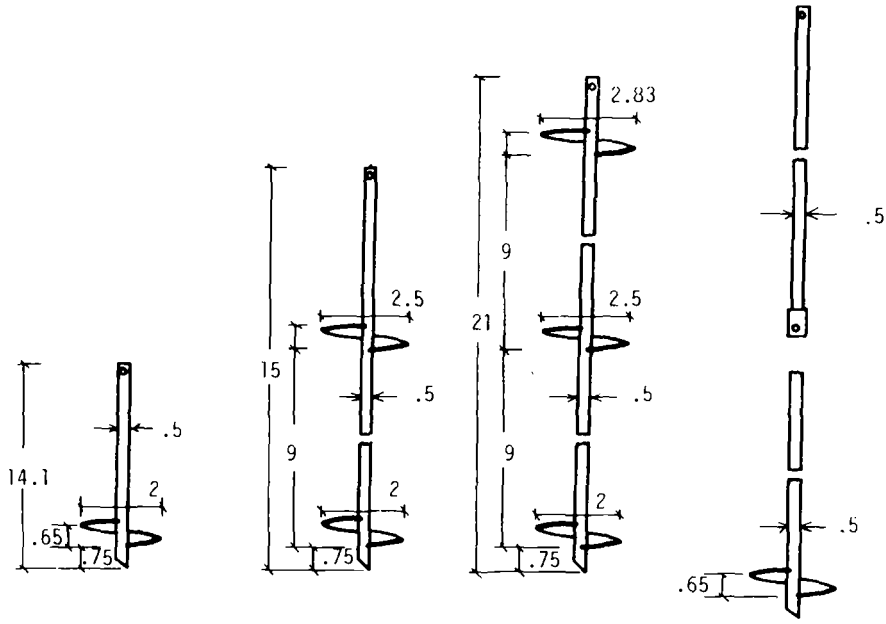

FIG. 5—*1/4-scale model used in tests.*

The tests were conducted by applying static horizontal load at ground level in increments. Observations were recorded on deflection at ground level (using mechanical dial gages) and the output of the strain gages for each load increment. Observations were recorded when there was no further increase in lateral deflection corresponding to the applied load.

From the model, test data plots were made at ground level of deformation versus the applied load. Figure 6 gives typical load-deflection data, and Figure 7 shows the typical variation of moment with depth.

From the lateral deflection- versus lateral-load test data the lateral-deflection behavior of model anchors tested revealed an interesting fact. The ultimate lateral-load capacities of all models were practically the same. Slight variations may be due to variations in placement density and disturbance of soil during installation of anchor. The lateral-load capacity of the anchors is thus governed mainly by the interaction between the soil and the extension rod. The contribution of the helices is not significant. This was also observed from the data obtained during the Houston test. This may be expected to hold for all such cases where the length of extension from ground level to top helix is adequate and meets the criterion for a long pile.

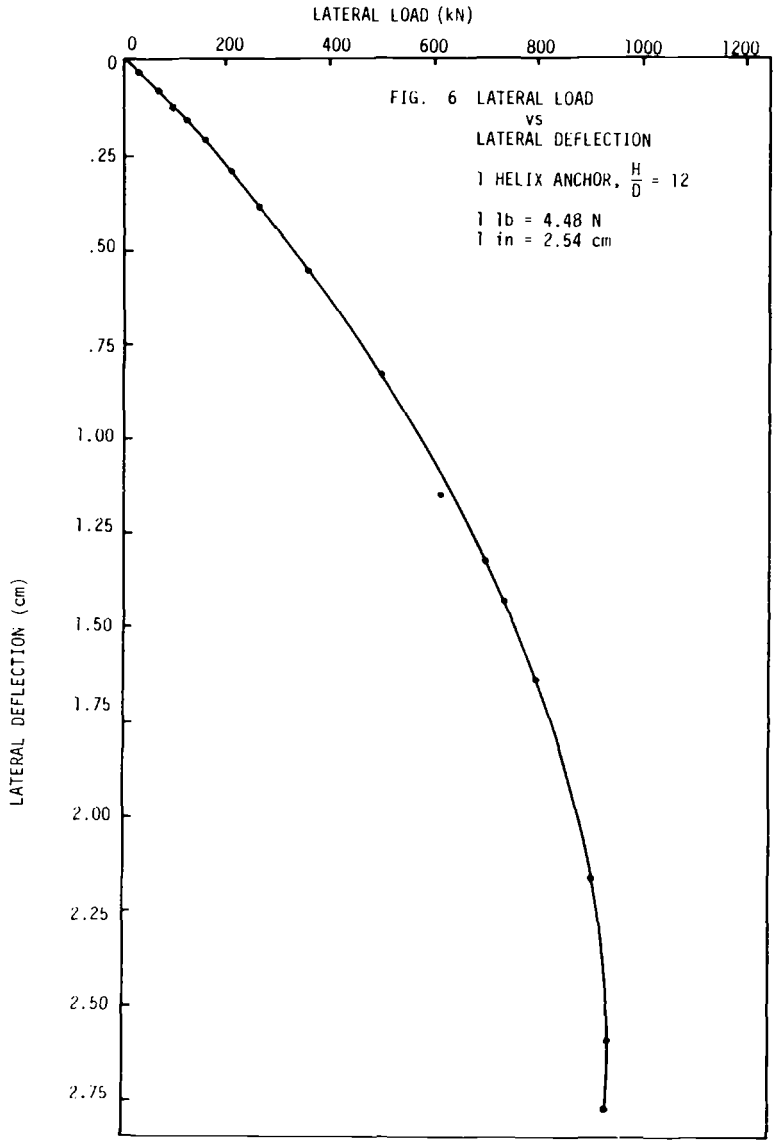

FIG. 6—*Lateral-load versus lateral deflection, one-helix anchor,* H/D = *12.*

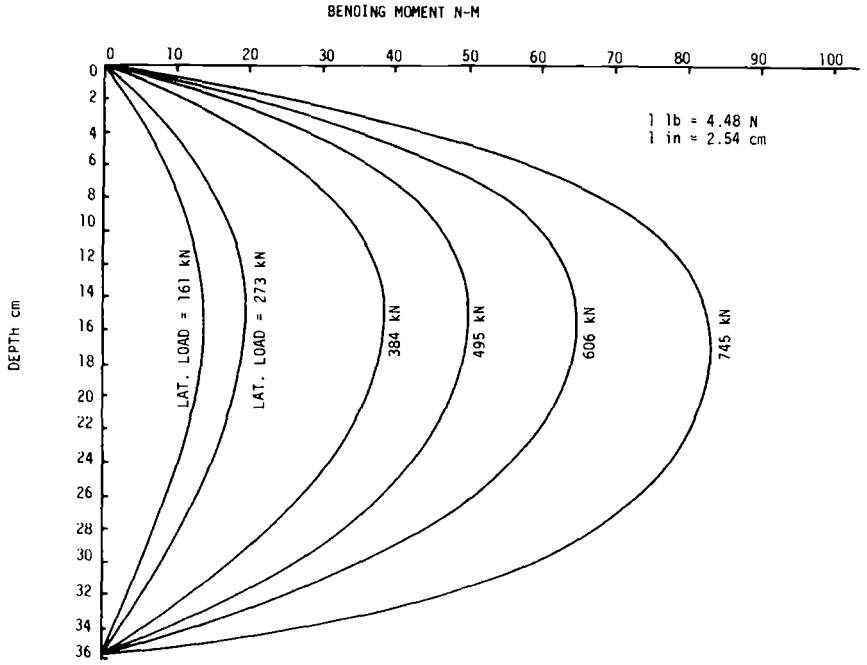

FIG. 7—*Bending moment diagram for single-helix anchor,* H/D = *6.8.*

Recommended Model for Lateral Capacity

In selecting any mathematical relation of a general nature, maximum consideration is given to field test data. Because of the limited nature of available data and lack of information on variation of soil properties with depth for the field tests, (except for the Houston test) the choice in selecting an appropriate mathematical model has been restricted. A working model has been developed for the case of sands and clays based on the following criteria. The model computes deflections at ground level caused by a horizontal force applied at that level. If the force P acts above ground level at a height h, it may be replaced by a force P and a moment $M = Ph$ acting at ground level. Any other moments that may be transmitted by the structure should also be added to M.

Equations 3 and 6 were modified to yield lateral deflections at ultimate loads as determined from the test data in sands and clay. It was observed that Eq 10 gives reasonable values of deflection for loads higher than a threshold value above which behavior becomes nonlinear.

$$y = C_u[A_y(PT^3/EI) + B_y(MT^2/EI) \quad \text{(for sands)} \tag{10a}$$

$$y = C_u[A_y(PR^3/EI) + B_y(MR^2/EI) \quad \text{(for clays)} \tag{10b}$$

The coefficients A_y and B_y in Eqs 10a and b may be obtained from Matlock and Reese [*5, 6*] for cohesionless soils and from Davisson and Gill [*7*] for clays. The coefficient C_u was determined (to be approximately equal to 3.0) by correlation with the observed behavior. This threshold value is a load $P_1/3$ where P_1 is the computed load for 2.54 cm (1 in.) of lateral deflection.

Comparison with Observed Test Data

Deflection at ground level was computed for the case of anchors in sand for the model tests and for the Georgia (A.B. Chance) and ESSA test (Ontario Hydro). Computed and observed values of lateral load for 2.54-cm (1-in.) deflection are compared in Table 1. It should be noted, that 2.54-cm (1 in.) was used as a maximum lateral-deflection criterion to conform with superstructure design limitations. It may be observed from Figs. 8 through 10 that the computed value of lateral load for 2.54-cm (1-in.) deflection using the proposed model is in close agreement with the observed values for the model test ($P_{obs}/P_{comp} < 1.4$). The computed results are somewhat conservative when compared to the Georgia Power field test data (Fig. 10) ($P_{comp}/P_{obs} \simeq 2.0$). This is probably because of inherent variability of the soil conditions at the site compared to that of the laboratory soil. For the model tests, the maximum moment was also computed and compared in Table 2. No field data on maximum moments are available to permit a comparison.

Similarly the deflections at ground level for the case of clays were computed for the Houston test, and the test on HS-11 and PIFA anchors in fissured clay by Ontario Hydro. The comparison of observed and computed values is shown in Figs. 11 and 12. The computed and observed loads for 2.54-cm (1-in.) deflection are compared in Table 3. Maximum moments for the Houston tests are compared in Table 4.

The model for lateral-load capacity of helical anchors as described earlier makes an acceptably close prediction of lateral-load capacity for 2.54-cm (1-in.) deflection as compared to observed values. In addition the errors are generally on the conservative side. The depth of the extension must be sufficient to ensure its behavior as a long pile. The length of extension should be 4 to 5T or 4 to 5R minimum.

Summary and Conclusions

The determination of lateral-load capacity of helical anchors is a difficult problem because of the scarcity of field data with which to compare theoretical calculations. In an effort to improve this condition a limited model test program was conducted. From an analysis of these and available field test results, a mathematical model was developed and used to predict anchor head deflection under a given set of lateral loads and moments.

TABLE 1—*Comparison of observed and computed lateral loads for 2.54-cm (1-in.) deflection at ground level in sands.*[a]

Source	Anchor Details	Embedded Depth, ft	Depth to Top Helix, ft	T	$4T$	P_{obs}, kip	P_{comp}, kip	P_{obs}/P_{comp}
Model test (RGC)	single helix 2 in. diameter extension 1/2 in. square	2.1	2.0	0.366	1.466	0.21	0.255	0.823
Model test (RGC)	two helix 2.5-, 2.0-, 1/2-in. square extension	3.312	2.5	0.366	1.466	0.260	0.255	1.020
Model test (RGC)	two helix 2.5-, 2-,1/2-in.[2] square extension	3.9375	3.125	0.366	1.466	0.21	0.255	0.823
Model test (RGC)	three helix 2.83-, 2.5-, 2.0-, 1/2-in. square extension	4.174	2.611	0.366	1.466	0.22	0.255	0.863
ESSA-TS Ontario Hydro	PIFA[b] 3 helix extension 8 in. diameter	9.5	6.5	2.3	9.2	5.5	5.97	0.921
GA Power A. B. Chance	TC 8-, 10-, 11-, 13-in. with anchor 8-in. diameter extension 7.5 ft long	15	7.5	2.3	9.2	12.5	4.6	2.71

[a]1 ft = 0.3048 m, 1 kip = 4.448 kN, and 1 in. = 2.54 cm. RGC is Rolla Geotechnical Consultants.
[b]The anchor had been tested in uplift previously. PIFA is

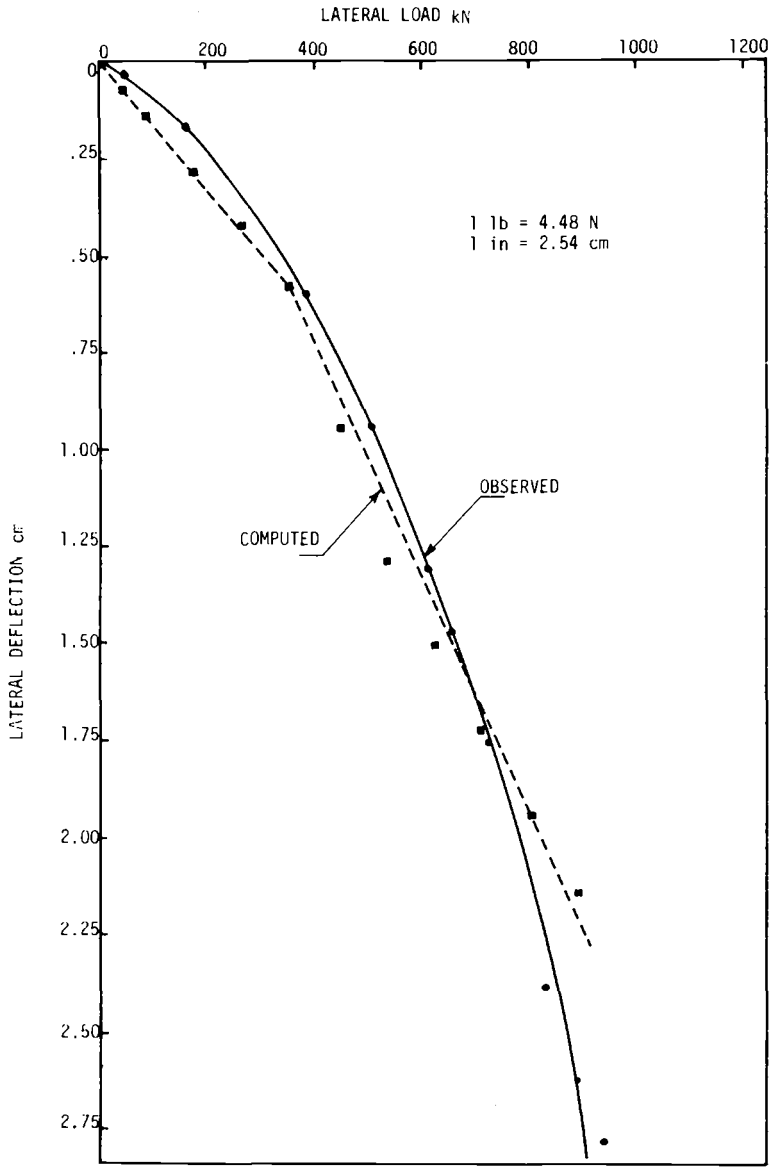

FIG. 8—*Lateral load versus lateral deflection, two-helix anchor,* H/D = *15.*

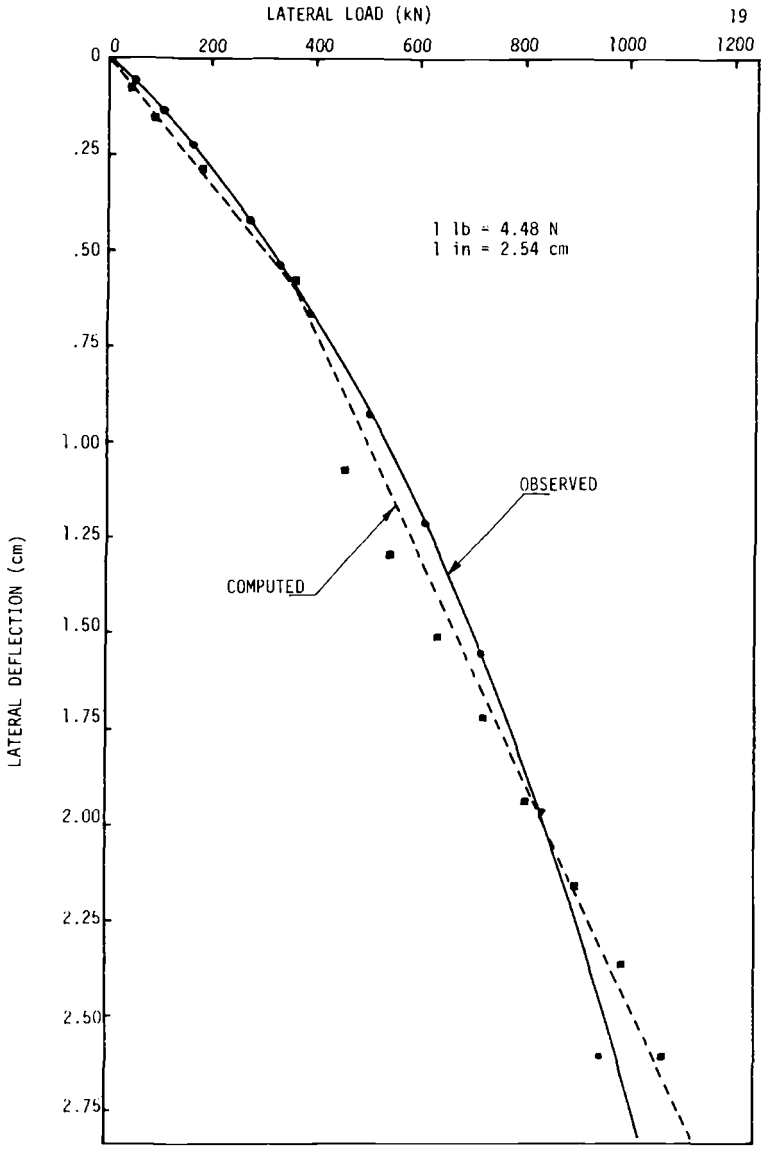

FIG. 9—*Lateral load versus lateral deflection, three-helix anchor,* H/D = *11.07.*

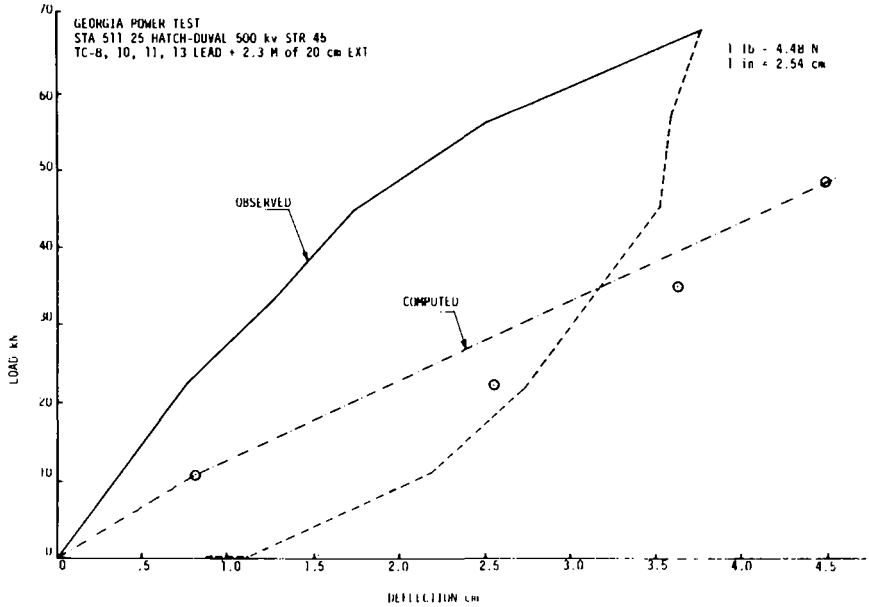

FIG. 10—*Lateral load versus horizontal displacement.*

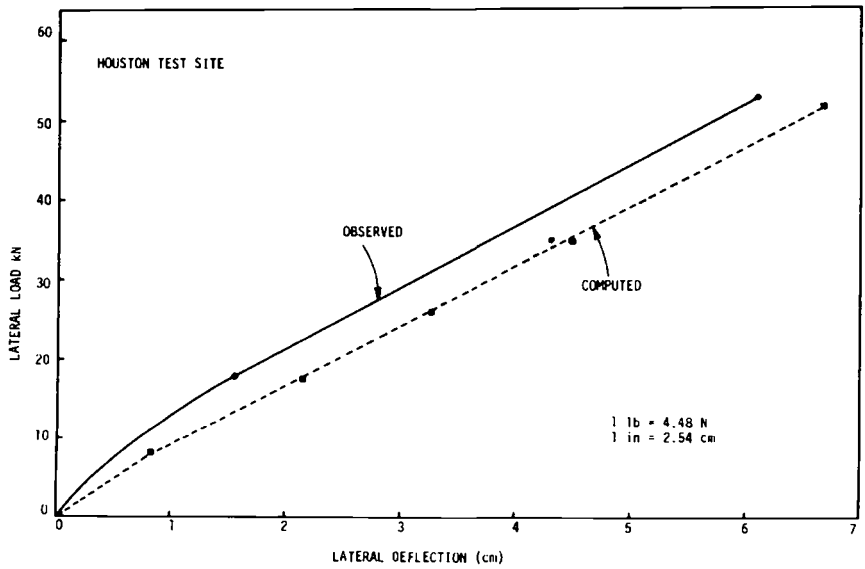

FIG. 11—*Lateral load versus lateral deflection.*

TABLE 2—*Comparison of computed and observed maximum moments on laterally loaded anchors in sand.*[a]

Source	Anchor Details	Embedded Depth, ft	Depth to Top Helix, ft	T	$4T$	Applied Lateral Load, lb	$M_p$obs, in.·lb	$M_p$comp, in.·lb	$M_p$obs/ $M_p$comp
Model test (RGC)	single helix 2 in. diameter 1/2-in. square extension	2.1	2.0	0.366	1.466	47.9	140.0	159.7	0.877
						72.71	235.0	242.4	0.969
						134.7	650.0	449.2	1.447
						221.6	1220.0	738.8	1.651
Model test (RGC)	2 helix 2.5-, 2.0-, 1/2-in. square extension	3.312	2.5	0.366	1.466	111.6	230.0	372.1	0.618
						186.0	530.0	629.2	0.855
						260.4	860.0	868.2	0.991
Model test (RGC)	2-in. helix 2.5-, 2-, 1/2-in. square extension	3.9375	3.125	0.366	1.466	62.0	65.0	206.8	0.314
						111.66	290.0	372.2	0.779
						210.9	640.0	703.2	0.910
Model test (RGC)	3 helix 2.83-, 2.5, 2.0-, 1/2-in. square extension	4.174	2.611	0.366	1.466	61.99	80.0	206.6	0.387
						136.47	275.0	455.0	0.604
						260.46	920.0	868.4	1.059

[a]1 ft = 0.3048 m, 1 in.·lb = 1.66 kg/m, and 1 in. = 2.54 cm.

TABLE 3—*Comparison of observed and computed lateral loads for 1-in. deflection at ground level in clays.*[a]

Source	Anchor Details	Embedded Depth, ft	Depth to Top Helix, ft	R	$4R$	$\frac{P_{obs}}{k}$	$\frac{P_{comp}}{k}$	$\frac{P_{obs}}{P_{comp}}$
Houston A. B. Chance	8 helices, 8 5/8 in. diameter extension	31.5	14.0	3.84	15.3	5.0	4.73	1.057
Stiff fissured clay Ontario Hydro	HS-11 3- to 10-, 11-, 13.5-, 3-in. diameter extension	14.5	7.0	1.38	5.52	4.8	3.89	1.234
Stiff fissured clay Ontario Hydro	PIFA 3- to 11.3-, 11.3-, 11.3-, 8 in. diameter extension	14.5	7.0	2.5	10.0	14.0	8.47	1.652

[a]1 ft = 0.3048 m and 1 in. = 2.54 cm.

TABLE 4—*Comparison of computed and observed maximum moments on laterally loaded anchors in clay.*[a]

Source	Anchor Details	Embedded Depth, ft	Depth to Top Helix, ft	R, ft	$4R$, ft	Applied Lateral Load k	M_p obs, in.-k	M_p comp, in.-k	$\frac{M_p \text{ obs}}{M_p \text{ comp}}$
Houston	8 helices 8 5/8 in. diameter extension	31.5	14.0	3.84	15.3	4	150	157.5	0.952
						8	300	315.1	0.952
						12	425	472.6	0.899

[a]1 ft = 0.3048, 1 in. = 2.54 cm, and 1 in.-k = 23 kg/m.

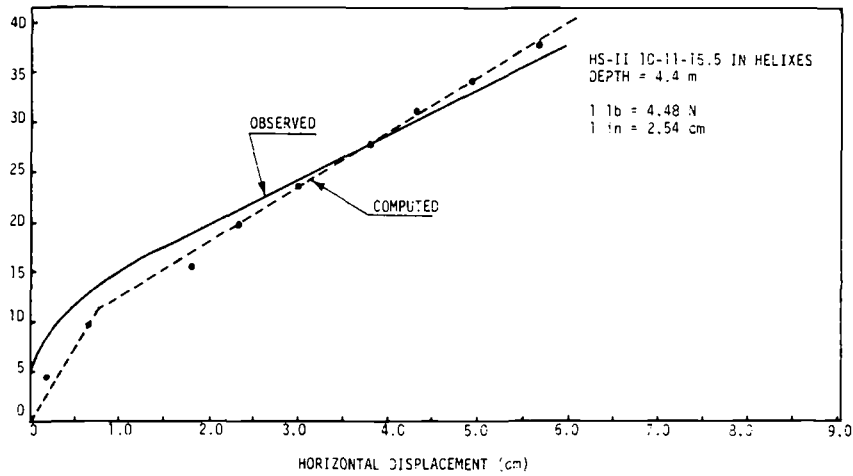

FIG. 12—*Lateral load versus horizontal displacement test on a single helix II type tapered multiple-helix anchor (stiff fissured clay Ontario Hydro).*

Based on the result of this work the following conclusions may be made.

1. Helical anchor pile can develop significant resistance to lateral loads.
2. The lateral-load versus deformation behavior of a helical anchor pile is controlled almost exclusively by the extension shaft for depths greater than three to five times the critical relative stiffness factor R or T.
3. The lateral-load capacity may be estimated using procedures similar to that developed for slender laterally loaded piles but modified to take into account the installation method (augering) used.

Acknowledgment

The investigation reported in this paper was sponsored by A. B. Chance Co., Centralia, MO.

References

[1] *Catalog on Helical Anchors*, A. B. Chance Co., 1975, Centralia, MO.
[2] Stephenson, R. W. and Puri, V. K., "Ultimate Capacity of A. B. Chance Helical Anchor," Report to A. B. Chance Co., Rolla, MO, Oct. 1981.
[3] Brinch Hansen, J., "The Ultimate Resistance of Rigid Foundation Piles Against Transversal Forces," Bulletin-12, Danish Geotechnical Institute, Copenhagen, Denmark, 1951.
[4] Meyerhoff, G. G. and Ranjan, G., "The Bearing Capacity of Rigid Piles Under Inclined Load in Sand, Part I Vertical Piles," *Canadian Geotechnique Journal*, Vol. 9, 1972.
[5] Matlock, H. and Reese, L. C., "Foundation Analysis of Off Shore Pile Supported Structures," *Proceedings of the Fifth International Conference on Soil Mechanics and Foundation Engineering*, Vol. II, Paris, France, 1961.

[6] Matlock, H. and Reese, L. C., "General Solutions for Laterally Loaded Piles," *Transactions of the American Society of Civil Engineers*, Vol. 127, Part I, 1962, pp. 1220-1247.

[7] Davisson, M. T. and Gill, H. L., "Laterally Loaded Piles in Layered Soil System," *Journal of Soil Mechanics and Foundation Division, Proceedings of the American Society of Civil Engineers*, Vol. 89, No. SM3, 1963.

[8] Reese, L. C. and Matlock, H., "Non-dimensional Solution for Laterally Loaded Piles with Soil Modulus Assumed Proportional to Depth," *Proceedings of the Eighth Texas Conference on Soil Mechanics and Foundation Engineering*, 1965.

[9] Davisson, M. T., "Behaviour of Flexible Vertical Piles Subjected to Moment, Shear and Axial Load," Ph.D. thesis, University of Illinois, Urbana, IL, 1960.

[10] Kubo, J., "Experimental Study of the Behaviour of Laterally Loaded Piles," *Proceedings of the 6th International Conference of Soil Mechanics and Foundation Engineering*, Vol. 2, 1965, pp. 275-279.

[11] Madhav, M. R., Rao, N. S. V. K., and Madhavan, K., "Laterally Loaded Pile in Elasto-Plastic Soil," *Soils and Foundations*, Vol. 11, No. 2, 1971, pp. 1-15.

[12] Reese, L. C., "Laterally Loaded Piles: Program Documentation," *Journal of the Geotechnical Engineering Division, Proceedings of the American Society of Civil Engineers*, Vol. 103, No. GT4, April 1977, pp. 287-305.

[13] Matlock, H., "Correlations for Design of Laterally Loaded Piles, in Soft Clay," *Proceedings of the 2nd Offshore Technical Conference*, Houston, TX, Vol. 1, 1970, pp. 577-594.

[14] Reese, L. C. and Welch, R. C., "Lateral Loadings of Deep Foundations in Stiff Clay," *Journal of Geotechnical Engineering Division, Proceedings of the American Society of Civil Engineers*, Vol. 101, No. GT7, July 1975, pp. 633-649.

[15] Radhakrishna, H. S., "Helix Anchor Tests in S nd-ESSATS," Ontario Hydro Research Division Report, Toronto, Canada, 1976.

[16] Radhakrishna, H. S., "Helix Anchor Tests in Stiff Fissured Clay," Ontario Hydro Research Division Report, Toronto, Canada, 1975.

James H. Long[1] *and Lymon C. Reese*[1]

Testing and Analysis of Two Offshore Drilled Shafts Subjected to Lateral Loads

REFERENCE: Long, J. H. and Reese, L. C., **"Testing and Analysis of Two Offshore Drilled Shafts Subjected to Lateral Loads,"** *Laterally Loaded Deep Foundations: Analysis and Performance, ASTM STP 835*, J. A. Langer, E. T. Mosley, and C. D. Thompson, Eds., American Society for Testing and Materials, 1984, pp. 214-228.

ABSTRACT: A lateral-load test was conducted at an offshore site on two 1.22-m-diameter drilled shafts penetrating through 13.1 m of dense sand overlying clay. The lateral-load test was conducted by pulling the two shafts toward each other under a specified lateral load and then relaxing the load to zero. This procedure was repeated for 40 cycles at each load level. With each load increase the application sequence was repeated to a maximum lateral load of 500 kN. Throughout the test, measurements were made of deflection and slope at the top of the shaft, and measurements of slope along the length of the shaft were obtained using a slope inclinometer.

A computer model was used to predict the behavior of a drilled shaft under the test conditions, and computed results were compared with measured results. At a lateral load of 500 kN, values of deflection were computed to be 20 to 30% less than measured.

KEY WORDS: lateral loads, sands, drilled shafts, drilled piers, full-scale test, cyclic loading, offshore

On 12 Nov. 1981, a lateral-load test was performed on two drilled shafts in Tampa Bay, Fla. The two drilled shafts measured 1.22 m (48 in.) in diameter and approximately 22 m (73 ft) in length. The soil profile consisted of about 13 m (43 ft) of fine sand over stiff clay. The water depth was approximately 4.6 m (15 ft).

Instrumentation included a load cell, dial gages to measure horizontal deflection, and an electronic slope indicator to measure the inclination of each test shaft at various points along the length.

The loading sequence consisted of first applying a static load and then 40

[1]Graduate research assistant and The Nasser I. Al Rashid chair, respectively, University of Texas at Austin, Crockrell Hall 6.2, Austin, Tex. 78712.

repetitions of the same load, after which a larger load was applied and the cyclic loads repeated. Readings were taken after 1, 2, 5, 10, 20, and 40 cycles.

Upon completion of the load test, results of the load test were analyzed and compared with predictions obtained by a semi-empirical method [*1*] commonly used for estimating the response of laterally loaded piles.

Site Characteristics

The ground surface at the lateral-load test site, performed in Tampa Bay off the coast of Florida, lies 4.6 m (15 ft) below mean sea level. The soil profile, shown in Fig. 1, consisted of approximately 8.5 m (28 ft) of dense sand with shells overlying 4.6 m (15 ft) of silty and clayey sand underlain by a stiff clay. The strength parameters, also shown in Fig. 1, are based on results of blow counts and other field tests.

Construction of Test Shafts

For each test shaft, a 17.4 m (57 ft) long steel casing was vibrated into the ground to a depth of 11.3 m (37 ft). The top of the drilled shafts were approxi-

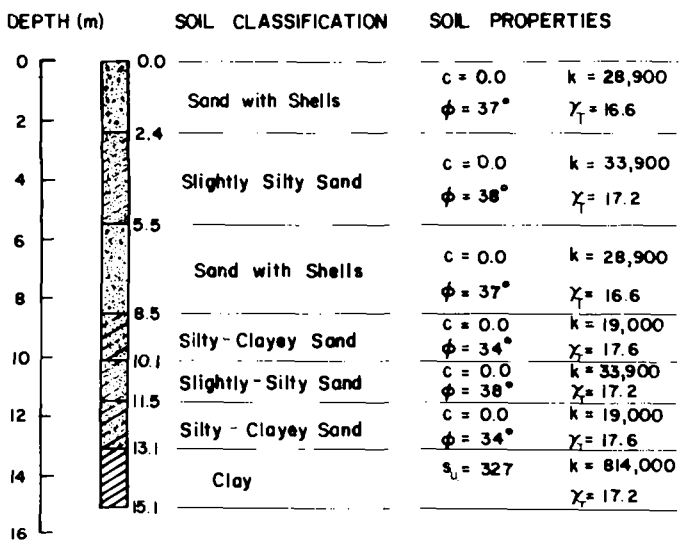

c - cohesion intercept on a Mohr-Coulomb failure diagram (in kN/m²)
ϕ - angle of internal friction on a Mohr-Coulomb failure diagram (in degrees),
S_u - undrained shear strength (kN/m²)
k - subgrade modulus (kN/m³),
γ_T - total unit weight of soil (kN/m³)

FIG. 1—*Soil profile.*

mately 1.5 m (5 ft) above mean sea level. The steel casing had an outside diameter of 122 cm (48 in.) and an average wall thickness of 12.7 m (0.5 in.). After the steel casing was in place, a hole was augered to increase the depth of the shaft to 15.5 m (51 ft) below the ground line, a steel reinforcing cage 91 cm (36 in.) in diameter and consisting of 16 Number 11 bars was inserted into the casing, and concrete was placed in the shaft by use of a tremie. The slump of the concrete was measured to be 203.2 mm (8 in.) with an average eight-day compressive strength of 25.0 MPa (3630 psi).

The distance between the centerlines of the two shafts was 6.1 m (20 ft); the shafts were vertical.

Testing Arrangement

A plan view and a side view of the testing arrangement are shown in Figs. 2 and 3. During testing, loads were measured with an electronic load cell, deflections were measured with dial gages, and the slope along the length of the shaft was measured with a slope indicator. The reliability of each of these measurements was occasionally checked and confirmed using independent measuring devices.

Application and Measurement of Load

Lateral loads were applied to the two shafts by using hydraulic jacks and a long dywidag bar as shown in Fig. 2. Approximately 61 cm (2 ft) below the top of each shaft was a horizontal hole passing through the center of the shafts and aligned longitudinally with the centerline of the other shaft. The dywidag bar was passed through these holes and placed so that a specific length of dywidag bar extended beyond the casing of each shaft. On the east end, the dywidag bar was placed through a loading yoke (to distribute the load to a

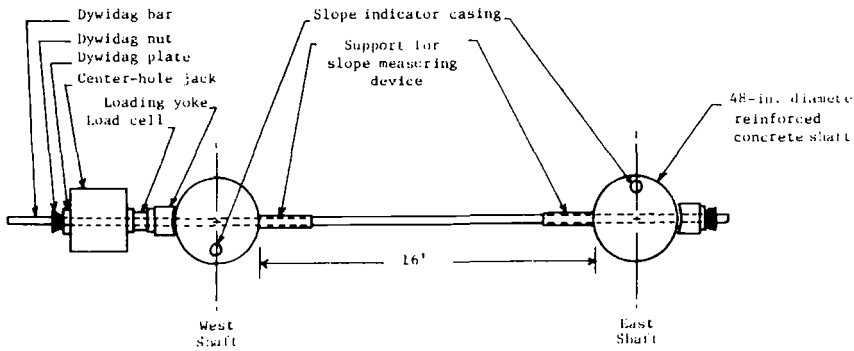

FIG. 2—*Top view of testing arrangement.*

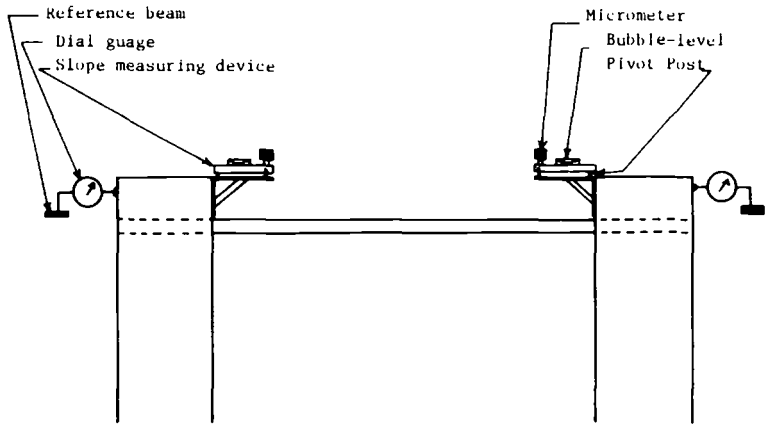

FIG. 3—*Side view of testing arrangement.*

larger area) and a dywidag plate and nut. On the west end, the dywidag bar was placed through the loading yoke, followed by a 996-kN (200-kip) load cell. After the load cell a hydraulic center-hole jack followed, and at the end of the dywidag bar was placed a dywidag plate and nut. With this testing arrangement, as the center-hole jack extended, the two shafts would be pulled together.

In addition to measurements made with the load cell, occasional measurements of hydraulic fluid pressure in the jack were recorded. Because the hydraulic jack was calibrated before the load test was performed, an independent check on the reliability of the load measurement was available.

Measurement of Deflection

Two independent methods were used for determining the lateral deflection of the two shafts. The first method was to measure deflection of the top of the shaft with dial gages. As shown schematically in Fig. 3, the dial gages were fixed to a reference beam that was anchored independently of the two shafts. If the deflections of the two shafts exceeded the range of the dial gage, calibrated spacers were inserted between shaft and the dial gage to allow the displacement to be obtained.

The second method of measuring displacement made use of a surveyor's transit and a tape measure. The surveyor's transit was anchored approximately 12 m (40 ft) from the two test shafts. A mark on the east shaft was etched and the transit cross hairs were sighted on this mark. During the lateral-load test, occasional optical measurements were made by noting how much the east shaft moved. Simultaneously, the distance between the two shafts was measured, thus allowing for an independent measurement of horizontal deflection for both drilled shafts.

Measurements of Slope

Two independent systems were used for measuring the slope of the two drilled shafts during the testing program. The first method involved the use of a slope inclinometer. This device (Digitilt® Inclinometer, Model 50306) is approximately 91 cm (3 ft) in length and designed to travel within guide casing along the length of the drilled shaft.

The second method, limited to measuring the slope at the top of the shaft only, involved the use of a 61-cm (2-ft) long bar, a bubble level, a pivot post, and a micrometer, shown schematically in Fig. 3. As the top of the shaft displaced and rotated, the micrometer was adjusted until the bubble level was centered. By knowing both the original and new position of the micrometer, the slope at the top of the shaft could be computed and checked with the slopes indicated by the slope inclinometer readings.

Loading Sequence

The two test shafts were loaded by first applying a static load long enough to obtain measurements of deflection, then releasing the load to zero, and loading back to the previous load. This "cycling" of the load was repeated 40 times for each load level. Measurements of deflection with dial gages were taken at 1, 2, 5, 10, 20, and 40 cycles. Measurements using the slope inclinometer, bubble level, and surveyor's transit were made on the last cycle of load. The magnitudes of lateral loads were applied in the following sequence: 50, 100, 150, 200, 250, 300, 400, and 500 kN.

The rate of loading of the test shafts was governed by the rate at which an electric pump could force fluid into the jack. At the beginning of the load test, when loads and deflections were small, each cycle of loading required about 30 s; however, at the end of the loading test, when loads and deformations were largest, each cycle of loading required approximately 2 min.

Results of Testing

Load Versus Deflection

Shown in Figs. 4 and 5 are curves showing load versus deflection measured for the two shafts. The deflection was measured at a point near the top of the shaft. Values are shown for cycles 1, 2, 5, 10, 20, and 40. Two values of deflection are given for the 40th cycle. The first value represents the amount of deflection immediately after application of the 40th cycle, and the second value is the deflection after slope indicator readings were completed. The elapsed time between the initial and final measurement of deflection on the 40th cycle was typically between 30 min and 1 h.

Although it has been mentioned that the two test shafts were constructed in

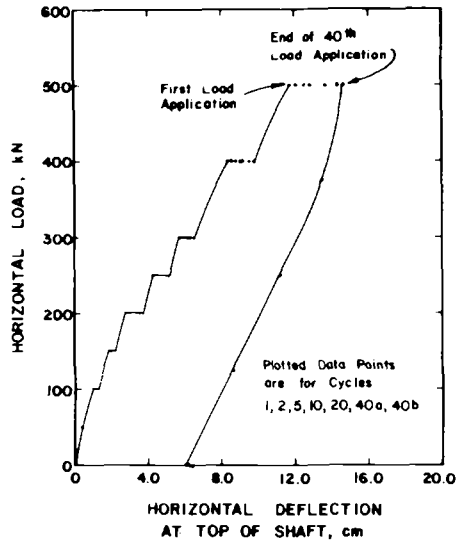

FIG. 4—*Load versus deflection relationship measured for west shaft.*

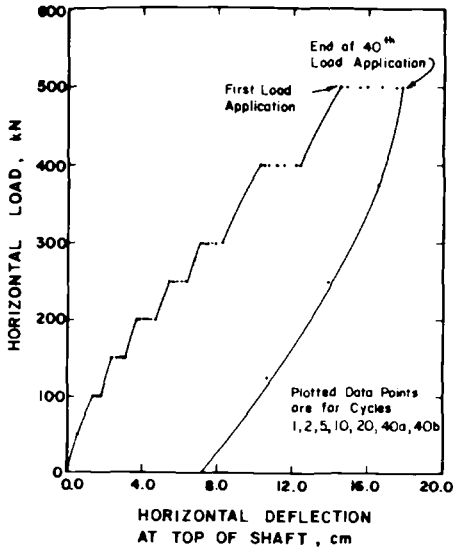

FIG. 5—*Load versus deflection relationship measured for east shaft.*

an identical manner, it is obvious that the two shafts did not behave identically. At a lateral load of 498 kN (50 tons), the maximum lateral deflection at the top of the west shaft was measured to be 146 mm (5.76 in.), whereas the maximum deflection of the east shaft was measured to be 178 mm (7.00 in.). During unloading, permanent lateral displacements of 60.4 and 72.6 mm (2.38 and 2.86 in.) were measured for the west and east shafts, respectively.

Load Versus Slope

Shown in Fig. 6 is the measured relationship between the lateral load and the slope of the top of both test shafts. The data represent values of slope recorded at the end of the 40th cycle of each load. The lines plotting both relationships possess the same general shape; however, the west shaft had a maximum slope of only 0.0140 cm/cm whereas the east test shaft had a maximum slope measuring 0.0169 cm/cm.

Inclinometer Measurements

Shown in Figs. 7 and 8 are the results of inclinometer measurements for the west and east shafts, respectively. These data were recorded while the load for the 40th cycle was held constant. Additionally, these data represent changes in slope with respect to the original configuration of each test shaft.

As shown in Figs. 7 and 8, no significant change in slope was measured near the bottom of each shaft.

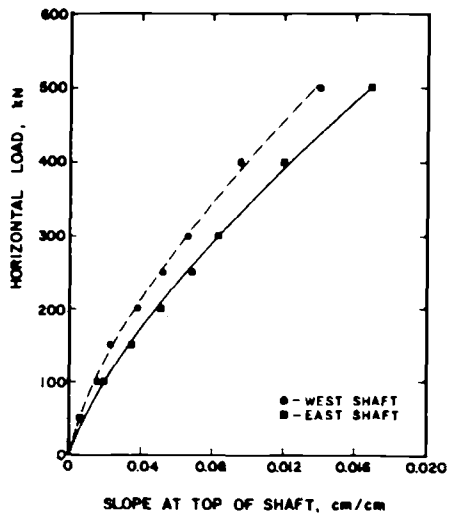

FIG. 6—*Load versus slope relationship measured at top of both shafts.*

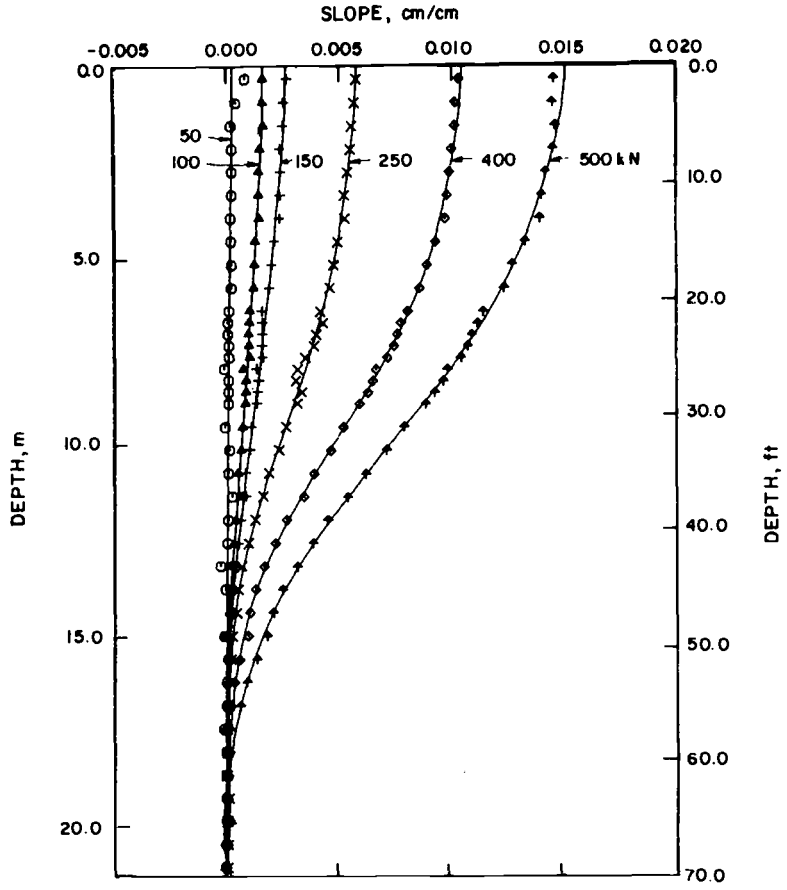

FIG. 7—*Results of slope inclinometer measurements for west shaft.*

Comparison of Measured Results with Analytical Results

One of the purposes of conducting a lateral-load test is to obtain experience in determining how well current numerical models predict behavior measured in a field test. The numerical model investigated in this study uses a beam-on-foundation approach. The resistance provided by the soil along the length of the shaft is modelled with nonlinear mechanisms. The specific relationship between force and deflection for these mechanisms, called p-y curves, is based upon both soil and pile properties. The p-y curves are calculated using semi-empirical equations. A more detailed description of the model has been presented by Reese et al [*1*].

This semi-empirical method of analysis was selected because of the following reasons:

(1) the method is based on results from full-scale lateral-load tests [*2*],

(2) the method suggests well-defined guidelines to account for both static and repetitive loading, and

(3) the method has been used successfully to predict behavior of piles at other sites [*3*].

In order to perform an analysis with the model mentioned above, properties of the soil and structural member must be provided. The soil properties used in the analysis are given in Fig. 1. The strength properties of the sand and clay were determined from field tests; however, the values of subgrade modulus k were selected based on recommendations made by Reese and Sullivan [*4*].

The bending properties of the two test shafts were determined experimen-

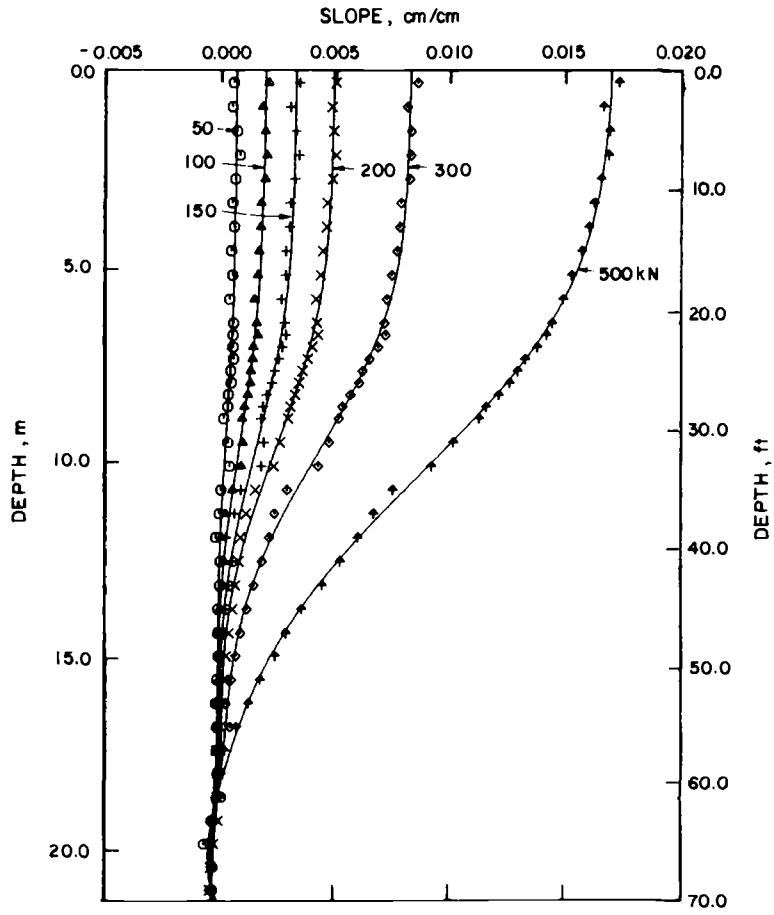

FIG. 8—*Results of slope indicator measurements for east shaft.*

tally using measurements recorded during the load test. The values of bending stiffness EI of each test shaft was determined at a lateral load of 498 kN (50 tons). Assuming the moment to be increasing linearly with depth between the point of load application and the top of the ground surface, the moment at the ground surface was calculated. Then, values of slope versus depth obtained from inclinometer readings were entered into a computer and a seventh-order least-squares polynomial was fitted through the data. Differentiation was used to obtain a relationship for curvature versus depth. Values of moment and curvature at the ground surface were then used to compute values of EI. These values were determined to be 2.87×10^6 and 2.64×10^6 kPa (1.0×10^{12} and 0.92×10^{12} psi) for the west and east shafts, respectively. Additionally, using the results from the slope indicator, values of EI were computed a second way by assuming each test shaft to act as a cantilever beam between the point of load application and the ground surface. A value of EI that corresponds to the change in slope measured along the length of the shaft was calculated to be 4.19×10^6 and 2.72 kPa for the west and east shafts, respectively. However, in deriving the value of EI with the second method, the data were scattered, and consequently, the values of EI are considered to be less reliable than values obtained from the first method described. These values were compared with values of EI obtained from a computer program that models the nonlinear behavior of the reinforced-concrete section. The values of EI were calculated to be 3.03×10^6 kPa when subjected to zero moment, and 2.97×10^6 kPa when subjected to a moment of 4320 kN · m (approximately equal to the maximum moment within the shaft).

The values of EI that seem most appropriate are the values obtained from the seventh-order least-squares polynomial fitted through the slope indicator data. These values were found to be in reasonable agreement with values predicted from the computer program, and very similar values of EI were calculated when a sixth- and eighth-order polynomial was fitted through the data.

Using the parameters described above, numerical analyses of the lateral-load test were conducted. Shown in Figs. 9 and 10 are the predicted and measured values of load versus deflection for the top of the west and east shafts, respectively. Deflections were calculated for the case of static and repetitive loading and are shown in each figure to illustrate the increase in deflection resulting from cyclic loading as predicted by the model. For most load levels, predicted values of the lateral displacement of both test shafts are shown to be less than their measured values. At a lateral load of 498 kN, computed values of deflection were found to be 20 and 30% less than measured for the west and east shafts, respectively. In addition, the increased deflection resulting from cyclic loading is predicted to be less than that measured for the two test shafts.

Shown in Fig. 11 is a plot of computed and measured values of the maximum moment versus lateral load. At a lateral load of 489 kN, values of maximum moment in the shaft were computed to be between 4 and 14% less than measured. Predicted values of maximum moment were obtained using the soil

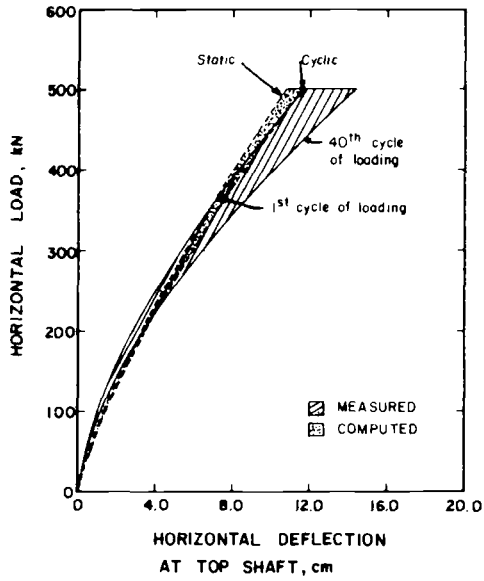

FIG. 9—*Computed and measured relationships of load versus deflection for west shaft.*

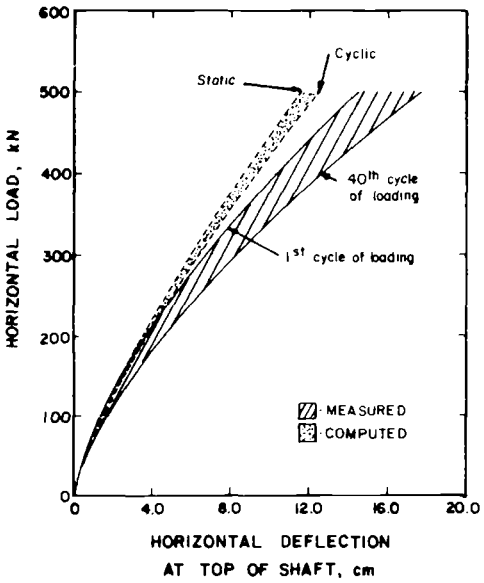

FIG. 10—*Computed and measured relationship of load versus deflection for east shaft.*

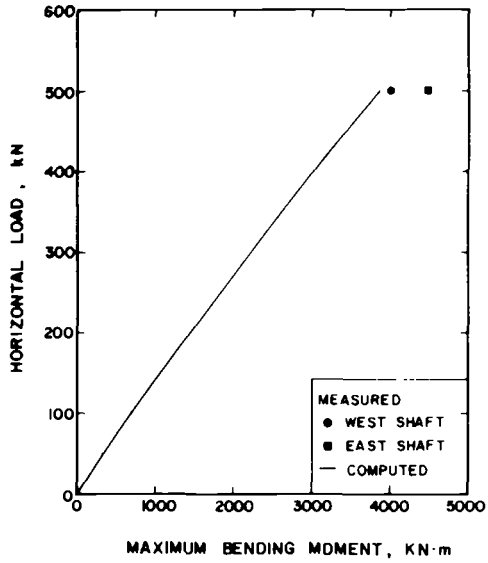

FIG. 11—*Computed and measured relationship between horizontal load and maximum bending moment.*

and pile parameters discussed previously, whereas the measured values of maximum moment were calculated from slope measurements recorded during the lateral-load test. Values of slope versus depth were recorded and a least-squares seventh-order polynomial was fitted through the data. Moments in the test shaft were obtained by differentiating the slope and multiplying by the *EI*. Data on which the measured moments are based were taken on the 40th cycle of loading.

In Figs. 9 through 11, it may be seen that at large values of lateral load (498 kN), values of deflection and moment were computed to be less than measured values. The possible reasons for the lack of close agreement between predicted and measured values are discussed in the following section.

Parametric Effects

The behavior of a laterally loaded shaft is largely dependent on the properties of the shaft and the properties of the upper soil layers. Therefore, a parametric study was conducted by varying the value of the flexural rigidity *EI* of the shaft, and by varying the value of angle of internal friction ϕ of all the sand layers.

In the parametric study where various values of *EI* of the shaft were used, it was found that decreasing the value of *EI* to 1.95×10^6 kPa (0.68×10^{12} psi) allowed the computed deflection to be within $\pm 10\%$ of the measured deflec-

tion of both shafts. Shown in Fig. 12 is the computed relationship between deflection and EI at a horizontal load of 498 kN (50 tons). The calculated deflections are shown to be sensitive to EI, and the discrepancy between measured and computed relationships of load and deflection could be minimized by a 32% reduction in the value EI. All of the three methods used to calculate the value of EI of the test shafts were reviewed, and it seemed unlikely that such a reduction in the value of EI was justified. However, a 10% reduction in the value of EI was allowed for the purpose of this study. Therefore, a value of 2.47×10^6 kPa (0.86 psi) was used for EI in the parametric study.

In order to investigate the sensitivity of the predicted deflections as a function of the soil strength, computations were performed assuming various values of the angle of internal friction ϕ in the sand layers. Shown in Fig. 13 are the computed values of deflection as the values of ϕ in the sand were decreased. Values of ϕ were reduced by approximately 3° in order to obtain agreement between measured and computed values of deflection for the west shaft; however, reductions in ϕ required to match deflections of the east shaft were determined to be too excessive. Therefore, a decrease in the angle of internal friction would allow better agreement between measured and computed values of deflection; however, the difference cannot be explained in terms of ϕ alone.

Other parameters, such as the effective unit weight, subgrade modulus, or properties of the clay underlying the sand, were determined to have little effect on the computed behavior of the shaft.

At this point, differences between the characteristics of the load test performed in this investigation and the characteristics of the load test on which the analytical model is based are considered. Some of these differences can be identified easily. For instance, the cyclic loads were applied in one direction

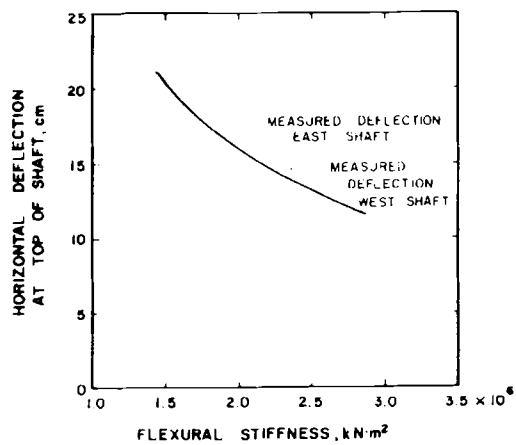

FIG. 12—*Variation in horizontal deflection with flexural stiffness.*

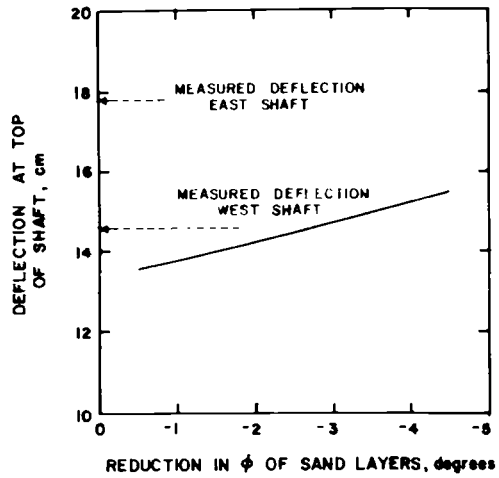

FIG. 13—*Variation of horizontal deflection of shaft with decreasing* ϕ.

only during this lateral-load test; however, in the lateral-load tests in Mustang Island [*1*], the cyclic loads were applied first in one direction, and then in the opposite direction with a smaller magnitude of load. Other differences include the size of the shaft (1.22 m) as opposed to the pile (0.61 m) at Mustang Island, the method of installation (vibrated casing as opposed to pile driving), and specific characteristics of the sand (grain size, angularity, mineral composition, and so forth).

Although these differences in characteristics may be easy to identify, it is difficult to assess the quantitative effect these differences have on the behavior of the test shaft. Therefore, performing lateral-load tests seems to be a necessary element in providing a basis for determining if the current semianalytical model correctly predicts lateral behavior of the shaft.

Summary and Conclusions

An offshore lateral-load test was performed on two drilled shafts 1.22 m in diameter. Values of deflection at the end of the 40th cycle of load application were compared with values of deflection computed using a semi-empirical model. Predicted values of deflection were found to be 21 to 30% less than measured values of deflection; however, values of maximum bending moment calculated with the model were found to be between 4 and 14% less than measured. Although several differences exist between the characteristics of the load test performed in this investigation, and the load test in which the semianalytical model is based, the predicted values of maximum moment and horizontal deflection were in reasonable agreement with measured values.

Acknowledgments

The authors would like to thank the Florida Department of Transportation for permission to publish this paper. In addition, the authors wish to express their appreciation to Dr. David Crapps who was responsible for ensuring proper management of the lateral-load test.

References

[*1*] Reese, L. C. and Cox, W. R., *Proceedings of the Offshore Technology Conference*, OTC 2080, Houston, TX, 1974, pp. 473–483.

[*2*] Cox, W. R., Reese, L. C., and Grubbs, B. R., *Proceedings of the Offshore Technology Conference*, OTC 2079, 1974, pp. 459–487.

[*3*] Meyer, B. J. and Reese, L. C., "Analysis of Single Piles under Lateral Loading," Research Report No. 244-1, Center for Transportation Research, University of Texas, Austin, 1979.

[*4*] Reese, L. C. and Sullivan, W. R., "Documentation of Computer Program COM624," Geotechnical Engineering Software Report No. GS80-1, Bureau of Engineering Research, University of Texas, Austin, 1980.

Peter K. Robertson,[1] *John M. O. Hughes,*[2]
Richard G. Campanella,[1] *and Alex Sy*[3]

Design of Laterally Loaded Displacement Piles Using a Driven Pressuremeter

REFERENCE: Robertson, P. K., Hughes, J. M. O., Campanella, R. G., and Sy, A., **"Design of Laterally Loaded Displacement Piles Using a Driven Pressuremeter,"** *Laterally Loaded Deep Foundations: Analysis and Performance, ASTM STP 835*, J. A. Langer, E. T. Mosley, and C. D. Thompson, Eds., American Society for Testing and Materials, 1984, pp. 229-238.

ABSTRACT: The nonlinear subgrade reaction method is widely used for the design of laterally loaded piles. This method replaces the soil reaction with a series of independent springs. The nonlinear behavior of the soil springs is represented by *P-y* curves, which relate soil reaction and pile deflection at points along the pile length. Most of the existing methods for obtaining *P-y* curves are highly empirical. Often little account is taken of the method of pile installation. The pressuremeter offers an almost ideal in-situ modelling tool for determining directly the *P-y* curves for a pile. As the pressuremeter can either be driven or self-bored into the soil, the results can be used to model either a displacement or a non-displacement pile.

The driven pressuremeter used in the study described in this paper was essentially a standard pressuremeter with a solid 60° cone shoe at the tip. The instrument was pushed into the soil. This paper provides a detailed description of the equipment, testing procedures, and the theory that enables the family of *P-y* curves for laterally loaded displacement piles to be obtained. A case study, using the driven pressuremeter results to predict and compare the performance of two full-scale field lateral pile load tests, is presented.

KEY WORDS: design, piles, in situ, pressuremeter, lateral loading

The nonlinear subgrade reaction method is widely used for the design of laterally loaded piles. This method replaces the soil reaction with a series of independent springs. The nonlinear behavior of the soil springs is represented by

[1] NSERC University research fellow, and professor and head of Civil Engineering Department, respectively, University of British Columbia, 2075 Wesbrook Place, Vancouver, B.C., Canada V6T 1W5.
[2] Consulting engineer, Vancouver, B.C., Canada.
[3] Engineer, Klohn Leonoff Ltd., 10180 Shellbridge Way, Richmond, B.C., Canada.

P-y curves, which relate soil reaction and pile deflection at points along the pile length. Most of the existing methods for obtaining *P-y* curves are highly empirical. Often little account is taken of the method of pile installation and the influence that this may have on soil behavior. The pressuremeter, however, offers the potential to measure the soil reaction in situ under similar loading conditions. The pressuremeter can also be installed to simulate the disturbance to soil during pile installation.

This paper describes a case study where a driven pressuremeter was used to predict the results of two full-scale lateral-load tests on displacement piles driven in soft peat and clay.

Test Site

The test site is located in a low-lying area southwest of Burnaby Mountain in Greater Vancouver, B.C.

A summary of the soil profile based on sampling, laboratory testing, and static cone penetration testing (CPT) is shown in Fig. 1. A 1.2-m-thick loose gravelly sand-fill covers the site. The surface fill is underlain by about 1.8 m of very soft peat with interbedded silt and sand layers. The peat is underlain by about 2.7 m of a soft medium plastic clayey silt. The silt is underlain by a dense glacial till. Groundwater is close to the original ground surface.

Lateral-Load Tests

The test piles were 30-cm^2 (12-in.^{2}) precast concrete piles reinforced with four 2.5-cm (1-in.) diameter longitudinal steel bars and 1-cm (3/8-in.) diameter lateral steel ties. The concrete had a minimum unconfined compressive strength of 41 MPa (6000 psi) before installation. The calculated flexural rigidity or stiffness of the concrete pile (EI) is 8.61 MN · m^2 (3×10^9 lb · in.^{2}).

To avoid tensile cracks during driving, the piles were driven with a 2.7-Mg (6000-lb) drop hammer falling 30 cm (12 in.) when the pile end was penetrating through loose and soft soils, and 90 cm (36 in.) when the pile end was in glacial till. The pile penetration resistance diagrams of the four test piles are shown in Fig. 2.

The lateral-load tests were carried out in general accordance with ASTM Testing Piles Under Lateral Loads (D 3966-81) by jacking apart two free-headed piles installed about 1.52 m (5 ft) apart and measuring their horizontal deflections. A 1200-kN (135-ton) capacity calibrated hydraulic jack was used for applying the test loads. Maximum 5-cm (2 in.) dial gages referenced to 6 m (20 ft) long suspended I-beams were used for measuring lateral-pile deflections.

Load Test 1 was performed on Piles 36 and 37 with the load applied at the existing ground surface with approximately 1 m of loose gravelly sand around the pile heads. Load Test 2 was performed on Piles 41 and 42 with the load ap-

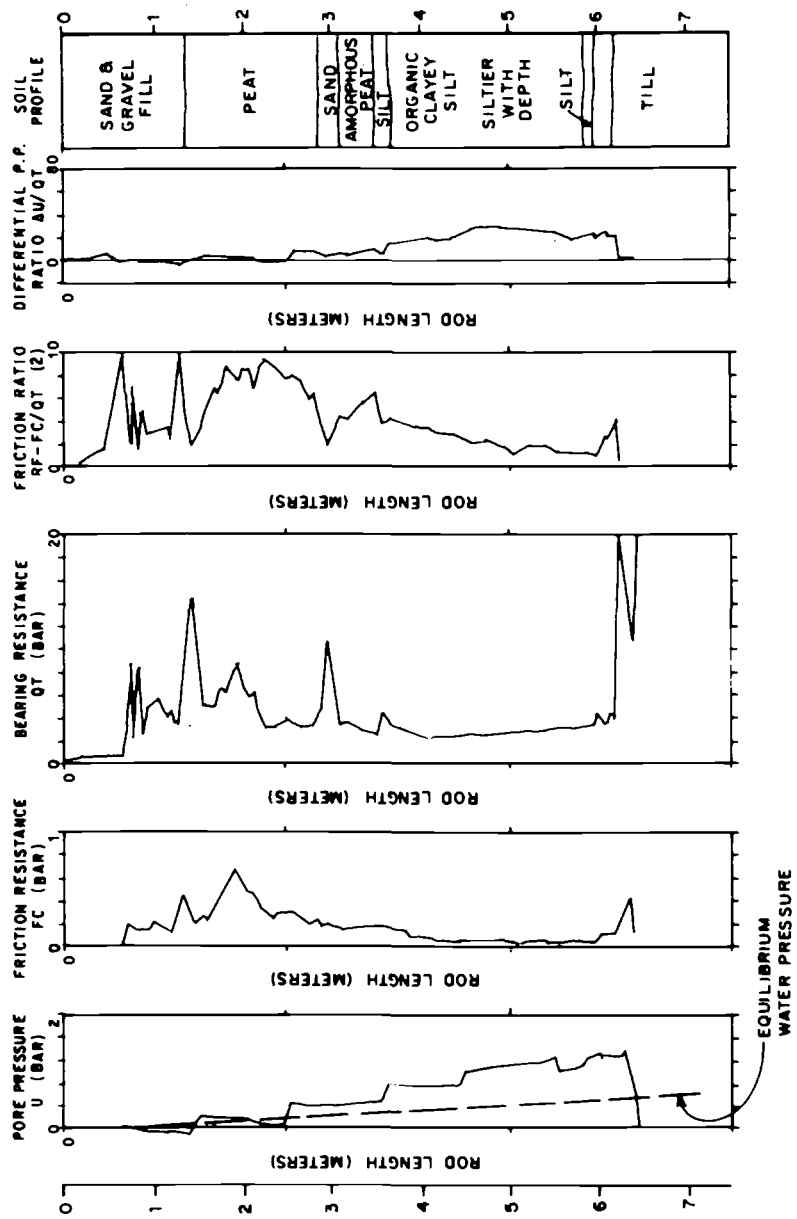

FIG. 1—*Summary of soil profile.*

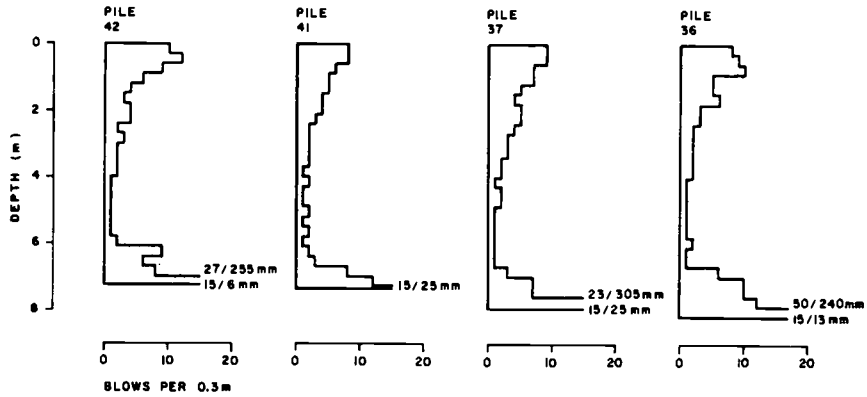

FIG. 2—*Summary of pile penetration diagrams.*

plied at the bottom of a 1-m-deep excavation (that is, at the original ground surface). Load Test 2 was performed to assess the influence of the surface fill on the lateral displacement characteristics of the piles.

For both load tests, the lateral load was applied in increments and was cycled through zero at different stages during the loading sequence. After the maximum test load was reached, the unloading was completed in steps.

After the initial loading cycle to 28 kN (6.29 kips) in Load Test 2, the test piles were subjected to 100 repetitive unloading-loading cycles to 28 kN (6.29 kips) before the test proceeded to the next higher load increment.

Each loading step was maintained for 1 to 2 min until movement was observed to be negligible. The repetitive loads were maintained for 15 to 30 s only.

The schematic lateral-load test setup and the measured load versus deflection plots of the test piles are shown in Fig. 3.

It is interesting to note that in both load tests, the pile adjacent to the jack deflected slightly more than the other pile, which was adjacent to the steel strut or spacer. This observed phenomenon could not be explained by the pile penetration resistances. It could be that friction between the steel plates/steel struts and the ground surface resulted in smaller loads transferred to the pile adjacent to the steel strut.

Determination of the *P-y* Curves

The evaluation of the *P-y* curves was from the results of pressuremeter tests. However, the pressuremeter was not installed in the usual manner, that is, in a predrilled hole; it was pushed into the ground using a vehicle designed for conducting cone soundings. With this technique, the initial disturbance about the pressuremeter may be very similar to the disturbance about a driven pile.

The pressuremeter was a standard self-boring pressuremeter with a solid

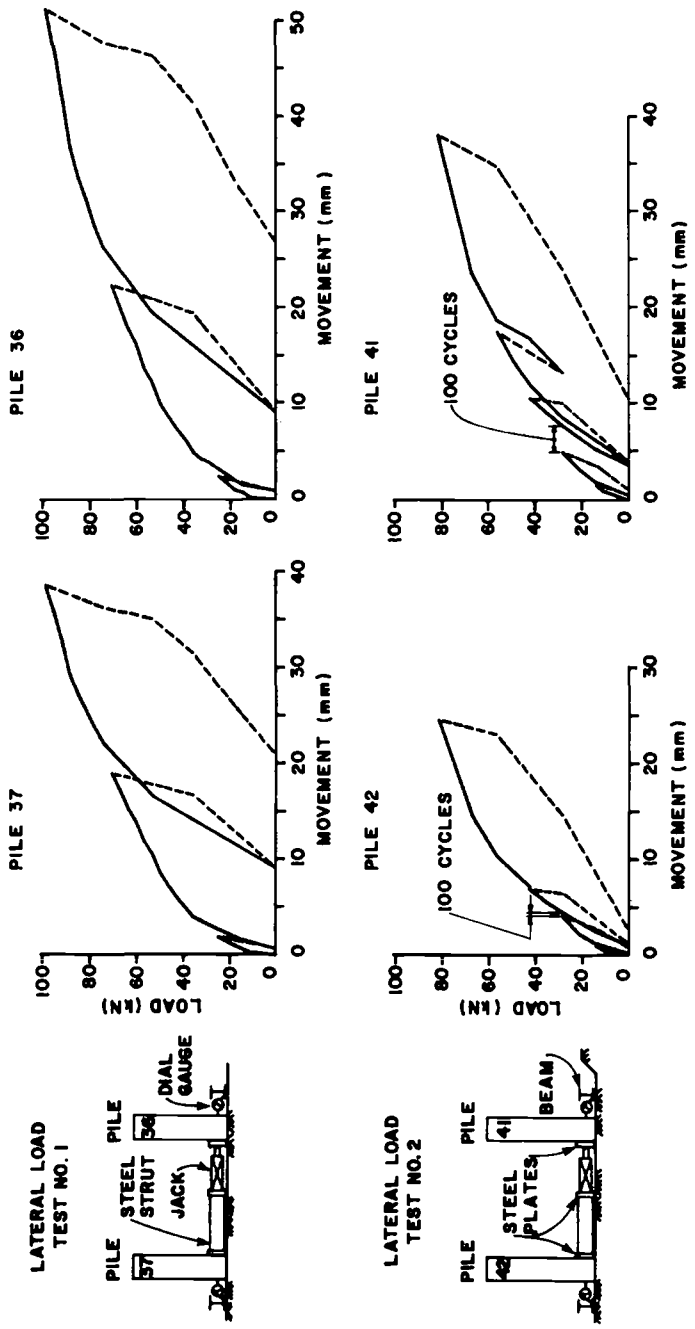

FIG. 3—*Schematic of test setup and load versus deflection plots of test piles.*

60° cone shoe at the tip. A schematic of the pressuremeter used during this study is shown in Fig. 4. The instrument was 76 mm in diameter with a length to diameter ratio for the membrane section of six. The lateral displacements of the central portion of the expanding membrane were measured electrically. A conventional Menard type pressuremeter in which the displacements are measured by volume changes would have been satisfactory.

A total of eleven pressure expansion tests were performed at about 0.5-m intervals. The total time for these tests was approximately 5 h.

Development of the *P-y* Curves

In the previous section, it was hypothesized that the initial displacement induced in the soil surrounding a driven pressuremeter faithfully represents the displacements in the soil surrounding a driven displacement pile.

During the subsequent pressuremeter test, the soil deforms in a simple radial direction, whereas the displacements in the soil surrounding a laterally loaded pile are far more complex as the soil moves away from the front face of the pile and in towards the back face. However, it could be expected that the soil in the center region of the pile (*A-B*) in Fig. 5*a* would deform in a similar manner to that about a pressuremeter. Therefore, it would seem reasonable to suppose that the geometric form of the pressure expansion curve obtained from the pressuremeter would be similar to the load displacement *P-y* curves for the soil acting on the front face of the pile.

If Curve P_0AP_L in Fig. 5*b* represented a typical test from a self-boring pressuremeter in which the probe was inserted into the soil with no disturbance (that is, a model of a nondisplacement caisson pile) where P_0 is the initial stress, and P_L is the limiting stress then the geometric form of the *P-y* curve would be given by P_0AP_L, that is, the origin for the pressure would be moved to P_0 (as shown in Fig. 5*c*).

The limiting pressure at which indefinite expansion occurs for the pressuremeter test $P_L - P_0$ and the limiting pressure required to push a pile sideways through the soil are different.

If the section of the pile considered is at some distance remote from the surface, that is, at a depth greater than about four-pile diameters, then the limiting lateral resistance is approximately 9 c_u, where c_u is the undrained shear strength [*1,2*]. Whereas in the case of the pressuremeter, the limiting pressure $P_L - P_0$ is approximately 5 c_u.

Therefore, for nondisplacement piles in which the initial stress on the pile is the same as the initial stress in the ground, the pressuremeter curves obtained from self-boring pressuremeters have to be increased by about two to give the correct curves from which the *P-y* curves can be constructed. However, for driven displacement piles, the above simple procedure has to be adjusted slightly.

It has been observed that the limiting pressure P_L in a pressuremeter test is

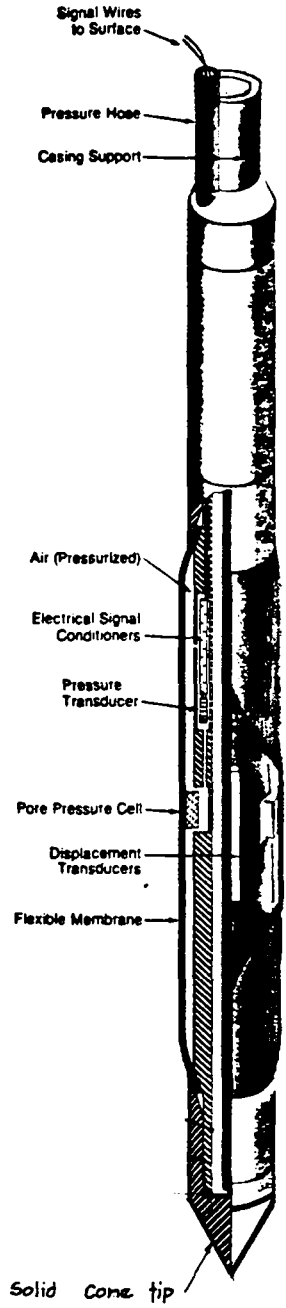

FIG. 4—*Push-in pressuremeter.*

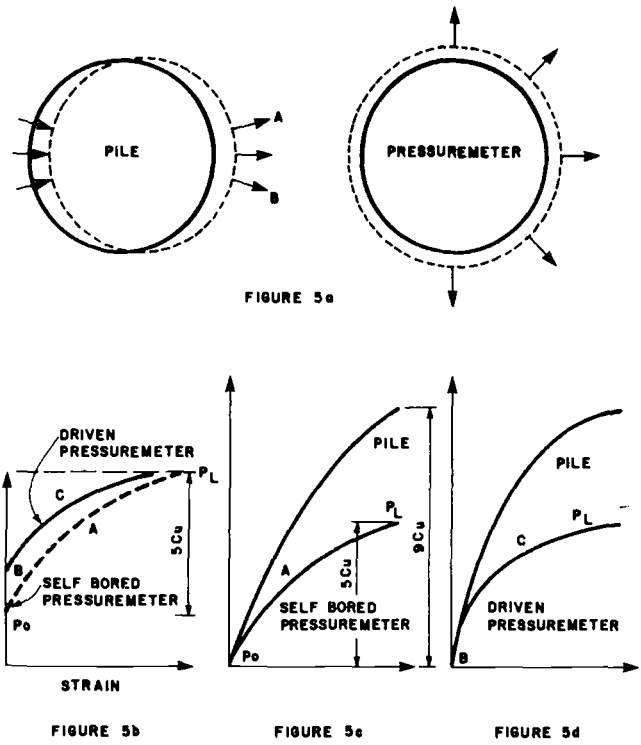

FIG. 5—*Schematic showing development of* P-y *curves from pressuremeter data.*

almost independent of the method of installation of the probe. However, the initial stress before expansion is dependent on the method of insertion. The result of an idealized pushed-in pressuremeter curve is given by BCP_L in Fig. 5*b*. The initial stress on the probe, Point B, is above the in-situ lateral stress P_0. If it is assumed that the shape of the *P-y* curve follows the pressuremeter curves, then they must be magnified further, such that the limiting pressure still equals $9\,c_u$.

In the following field example, the values of c_u used to evaluate the multiplication factors have been determined from the limiting pressures observed in the pressuremeter tests and the calculated in-situ stresses P_0 using the following formula

$$c_u = (P_L - P_0)/5$$

The *P-y* curves required for the analysis are in units of force per unit length P and displacement y whereas the pressuremeter curves are in units of stress σ_r and circumferential strain $(\Delta R)/R$, where R is the initial radius of the probe. Thus, to convert the pressuremeter stress to force per unit length, the stress

data are multiplied by the pile width (that is, 30 cm). The pressuremeter strain data are multiplied by the pile half-width (that is, 15 cm) to obtain the displacement y.

The evaluation of the P-y curves discussed above is for an element of the soil remote from the surface, that is, greater than about four pile diameters below ground surface. For points closer to the surface, the soil reaction is softer [2,3]. In the following analysis, the forces P developed by the above procedure have been halved for the evaluation of the P-y curves in the upper peat and fill.

Figure 6 shows the location of the pressuremeter tests, and the location of the P-y curves used for the pile analysis. The analysis was completed using a computer program developed by Reese [4,5] at the University of Texas.

The first pressuremeter test (PMTI) performed at a depth of 0.5 m in the sand and gravel fill was not used since it showed a very stiff response. The stiff nature of the top 0.5 m of fill was believed to have been caused by compaction resulting from traffic loading along the access road.

The resulting load deflection curves, at the load point, are compared with the measured pile deflection in Fig. 7.

Summary

The pressuremeter data were used to provide data for the analysis of laterally loaded single displacement piles in soft peat and organic clay. The pressure-

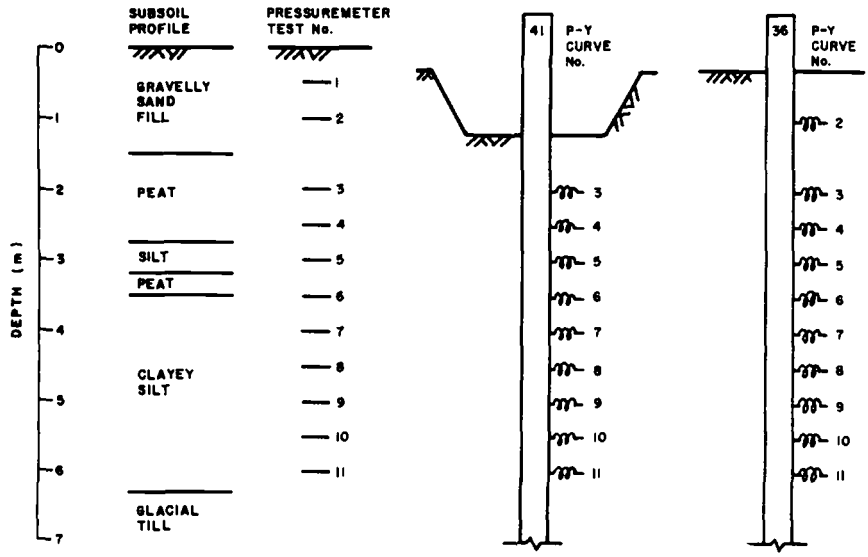

F

FIG. 6—*Location of pressuremeter tests and* P-y *curves for analysis.*

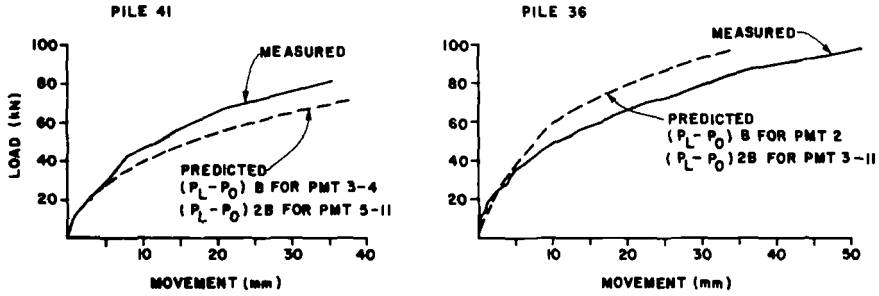

FIG. 7—*Computed and measured load-deflection plots.*

meter was driven into the soil to model, as accurately as possible, the soil disturbance during pile driving. The tests are relatively simple to perform and, if required, can be performed fast. The eleven tests reported in this paper were performed in a 5-h period.

Although the tests discussed in this paper are limited, the agreement between the calculated and measured deflection is encouraging. Therefore the method proposed may have applicability in other situations.

References

[1] Hansen, J. B., "The Ultimate Resistance of Rigid Piles Against Transversal Forces," Danish Geotechnical Institute Bulletin No. 12, Copenhagen, Denmark, 1961.

[2] Matlock, H., "Correlations for Design of Laterally Loaded Piles in Soft Clay," *Proceedings of the Offshore Technology Conference*, Vol. 1, 1970.

[3] Broms, B. B., "Lateral Resistance of Piles in Cohesive Soils," *Journal of the Soil Mechanics and Foundation Division, Proceedings of the American Society of Civil Engineers*, Vol. 90, No. SM3, May 1964.

[4] Reese, L. C., "Laterally Loaded Piles: Program Documentation," *Journal of the Geotechnical Engineering Division, Proceedings of the American Society of Civil Engineers*, Vol. 103, No. GT4, April 1977, pp. 287-306.

[5] Reese, L. C. and Desai, C. S., "Laterally Loaded Piles," *Numerical Methods in Geotechnical Engineering*, Desai and Christian, Eds., McGraw-Hill, New York, 1977.

PANEL DISCUSSION

The panel discussion held on 22 June 1983 at the ASTM symposium on Laterally Loaded Deep Foundations: Analysis and Performance sponsored by Committee D-18 on Soil and Rock was moderated by James A. Langer, Gannett Fleming Geotechnical Engineers, Inc., Harrisburg, Pa. 17105, symposium chairman and coeditor.

The members of the panel were

- R. Pyke, Telegraph Avenue Geotechnical Associates, Berkeley, Calif. 94705
- K. Habibagahi, Gannett Fleming Geotechnical Engineers, Inc., Harrisburg, Pa. 17105
- R. L. Sogge, Desert Earth Engineering, Tucson, Ariz. 85705
- S. Wright, University of Texas, Austin, Tex.
- J.-L. Briaud, Texas A&M University, College Station, Tex.
- M. Bierschwale, McClelland Engineers
- K. Bhushan, Fluor Engineers, Inc., Irvine, Calif.
- D. R. Gle, Bechtel Power Corporation, Ann Arbor, Mich. 48106.
- L. D. Johnson, U.S. Army Engineer, Waterways Experiment Station, Vicksburg, Miss. 39180
- M. Oakland, Purdue University, West Lafayette, Ind. 47907
- S. Gleser, Cincinnati, Ohio

Question to K. Bhushan—It appears that piles shown can be categorized as "stub" piles. What effect did this have on the pile resistance?

Answer—The relative stiffness of the piers and soils was incorporated in the *p-y* curves to calculate the design parameters. The piles were considered to be intermediate in length versus diameter ratio.

Question to M. Oakland—Was the possibility of tension in the elements below the piers checked? Use of elastic elements could give tension whereas soil is poor in tension.

Answer—It was checked to make sure that tension did not occur, and it was assumed that the piles were not moving sufficiently to develop tension. Later finite methods will incorporate the possibility of tension occurring.

Question to Panel—Have any of the panelists used ASTM Testing Piles Under Lateral Loads (D 3966)? If so, what are their comments?

Answer—No one has referred to this procedure for lateral load tests.

Question to S. Wright—Was the analysis of the piles based on the assumption that the tops of the piles were restrained?

Answer—The analysis of the pile group documented in this paper was based on the tops of the piles being restrained.

Question to S. Wright and/or Panel—Laterally loaded pile design is usually controlled by either (1) limiting displacement or (2) structural capacity. The latter is approached by considering the resulting moment in conjunction with other forces. If the p-y curve is nonlinear, the horizontal load-moment curve should also be nonlinear. Hence, when using ultimate strength methods to evaluate the structural adequacy, should the moment calculated, on the basis of service load, be multiplied by a load factor, or should the analysis be performed with a factored load when using nonlinear p-y curves?

Answer (S. Wright)—There was a built-in load factor, in that the forces were conservatively based on a 100-year storm.

Question to S. Gleser and Panel—What displacement (as a percent of pile diameter or width) is required to develop the ultimate p-value?

Answer (S. Gleser)—It is assumed that the question refers to the pile movement at any point necessary to obtain a flat p-y curve at that point; that is, the point at which the soil behaves as a plastic. In the analysis, it was assumed that the movement (referred to in the paper as YP) was independent of the width or depth. For straight face piles (square concrete or steel H-beams) the YP used was 3 mm (0.12 in.) and that used for circular pipe piles was 7.6 mm (0.3 in.). Since the computed behavior closely tracked the tested behavior of all 8 types of piles, the assumption appears to be valid. However, do not confuse the YP at any depth with the actual deflection under test, since p will remain constant upon any deflection in excess of YP.

Answer (K. Bhushan)—The fact that the soil is yielding near the ground surface does not mean that failure has occurred. There will be a progressive distribution of the lateral load deeper into the soil.

Answer (J.-L. Briaud)—Use 20% of radius to determine where p-y curve is flat.

Answer (others)—Maybe at a distortion of 1 to 2% of the pile diameter, depending on the soil.

Answer (R. Pyke)—The limiting lateral movements in offshore piles is often too low. Prefer using 5 to 10% of pile diameter as the limitation.

Question to J.-L. Briaud and Panel—In compression piles, very low friction is transferred directly above the tip, because of arching caused by the tip bearing failure. Shouldn't this same behavior minimize side shear in lateral loading?

Answer (J.-L. Briaud)—At ultimate load, friction represents 20 to 30% of the total, at working loads, it represents more than 50% of the resistance.

Answer (S. Gleser)—There are differences between square and circular section piles. Circular piles develop the pressures more quickly with movement, while square piles must form a cone of resistance in front of the force before

the full lateral resistance is developed. As pointed out in the paper, this is what is shown by the data reported in the paper by Alizadeh and Davisson and is in accordance with Boussinesq theory.

Answer (J.-L. Briaud)—I cannot prove that Gleser is wrong, but experience is that a 101.6 mm (4-in.) H-pile performed almost identically with a 177.8-mm (7-in.) diameter pipe pile.

Question to R. Pyke—The comparison of the 'TAGA' Curve and Matlock Curve showed considerably different ultimate p-values. Did this difference occur because of (1) a difference in the bearing capacity factors used, or (2) because of a difference in strength values?

Answer—The paper only deals with the initial slope of p-y curves, and the full p-y curves that were shown in the presentation are very preliminary but serve as an example of how the work might be extended to nonlinear behavior. It is not certain why there is a difference in the ultimate capacities for clay that were shown.

Question to M. Bierschwale—On the 25.4-mm (1-in.) model pilings, would full-size pilings react the same (because of size ratios to soil used)?

Answer—The question on the magnitude of scale effects cannot be answered, but full-scale piles should exhibit the same type of characteristics as did the small piles in this testing.

Question to M. Oakland—The proposed elastic finite-element analysis should calculate deformations. How are the benefits to the stability (F_s) of the slope calculated?

Answer—The procedure can determine the benefits on stability by (1) determining the reduction of stresses on the potential shear surface by back calculation and (2) by the reduction in strains on the potential slip surface.

Question to Panel—What method should be used to design timber piles with 40-ton vertical load and 5-ton horizontal load (that is, lateral deflection and ultimate lateral load).

Answer (K. Bhushan)—The procedure depends on the soil and which method you want to believe in. n_h must be compatible with the level of pile deflection occurring.

Answer (J.-L. Briaud)—The p-y curve is not linear. It can be measured with the pressuremeter. More sophisticated analyses are warranted if the potential savings justify the cost of the work. The better the tests, the better the data on p-y curves. The pressuremeter is good, but a full-scale load test is best.

Answer (From the Floor)—It should be remembered that Terzaghi in 1953 indicated that the values of n_h will be greater at small deflections. No specific value is gospel; it is only valid at the right level of strain.

Question to J.-L. Briaud—What is the success in using a pressuremeter in sand?

Answer—The pressuremeter tests are only as good as the borehole quality.

There are not many problems with this above the water table. Below the water table, a rotary drill should be used drilling very slowly (60 rpm); the mud flow should be slow enough not to cause disturbance, but fast enough to bring the debris up the hole; there should be axial injection of drilling mud; the rate of penetration should be slow. In effect, you are interested in the quality of the hole left behind. This is different from normal drilling practice, which is more interested in the soil about to be sampled. Drillers need training on this. If driven piles are to be used, it is possible to drive slotted casing and test within it.

Question to J.-L. Briaud—How is the frontal friction issue handled for piles of circular cross section?

Answer—The pressure on the front of a square pile is close to uniform at a specific level. For circular piles, the distribution of the forces on the flat projection of the pile is zero at edge to one in the center. The total shape factor is 0.75. Numbers for shape factors are given in paper.

Question to Panel—What are the effects of soil disturbance on lateral load capacity?

Answer (S. Gleser)—Alizadeh and Davisson show considerable effects of disturbance, especially from jetting. These can result in more than 30% reduction in resistance. This paper also indicates such effects when comparing 406-mm (16-in.) concrete piles installed with and without jetting.

Answer (J.-L. Briaud)—When using pressuremeter results, it is advisable to use the first loading for drilled piers and the reload cycle for driven piles. If piles are to be jetted, the construction procedure should be modeled in the pressuremeter drilling operation. In fact, the procedure of trying to duplicate the result of the construction procedure is a good one.

Answer (K. Bhushan)—In performing load tests on piles driven in predrilled holes in stiff clays and those where the clay was recompacted around the piles, it was found that the former might deflect 3.2- to 6.4-mm (⅛ to ¼-in.) before bearing on competent soil. After that, the p-y curves of the piles had the same shape.

Answer (S. Wright)—There are a number of parameters pertaining to piling for offshore structures that can result in reduced k_h, including pumping. Gaps can be developed around the top of the pile because of the cyclic loading. It is difficult and dangerous to generalize.

Answer (K. Bhushan)—If you are using piles that have been predrilled before being driven, excavation and recompaction to a depth of three-pile diameters can restore the full lateral capacity.

Question to Panel—What computer programs are available to analyze lateral loading?

Answer (R. L. Sogge)—A structural linear-elastic type analysis as described in my paper can be performed. Civil Soft sells a good structural one for $450.00, and Generic Software has a good program. Sogge has one available for $120.00.

Answer (S. Wright)—Com 624 is available from the University of Texas in

Austin. It costs $350.00 and comes in IBM and CDC Cyber version. Mike O'Neill's Pile Group program is available through him at the University of Houston and also possibly through Federal Highway Administration.

Answer (S. Gleser)—As pointed out in the paper a Fortran H computer program was developed to use the proposed equations in computing Tables 1*a*, 1*b*, and 1*c* and is available.

Question to Panel—What are the effects of pile spacing?

Answer—You must be very careful about this. Some of Poulos's work would indicate that there can be group action effects at 20-pile diameter spacings. On the other hand, pile spacing for offshore structures may stop being important at 3- to 5-pile diameters where behavior in the ultimate highly nonlinear range is concerned.

Question to Panel—What are the effects of the timing and sequence of application of loads to lateral resistance?

Answer (S. Gleser)—The load should be applied until the rate of movement reaches some minimal preselected limiting value. Repetitive loading can be a problem, especially where the soil has been strained into the plastic range. It will then leave a gap, which must be closed before resistance is provided by the soil in the next cycle. This is clearly pointed out in the paper. In the paper by Alizadeh and Davisson, the effects of multiple cycles are very graphically demonstrated.

Answer (M. Bierschwale)—Testing of a rigid pile in stiff clay indicated sustained load could double the deflection. In this case, short load durations were for days while long durations were for weeks.

Answer (J.-L. Briaud)—In clays the faster the rate of testing, the more capacity will be measured.

Answer (K. Bhushan)—Capacity or deflections can depend on the number of cycles and how close the load is to the ultimate capacity. At 10% of ultimate resistance, pile deflection will not increase after five cycles. At 50% of ultimate resistance, deflections could easily be doubled by cyclic loading.

Summary

The papers in this book have been divided into two groups: one dealing with analysis and design, and the other dealing with case histories.

Analysis and Design

Eight papers are included in the analysis and design group. A summary for each follows.

The paper by Pyke and Beikae reviews current analytical methods for single piles subjected to lateral loading. Then a new analytical method is described, which takes into account soil fully surrounding the pile but only adhering to it along the part of the circumference where the soil resists pile movement, that is, the front and sides but not the back. A section is included that evaluates methods for determining Young's modulus for soils. A comparison of modulus of subgrade reaction values determined by the new analytical method with those determined by several other methods is presented in tabular form. No attempt is made to compare the various solutions with pile load test results, but the authors believe that the new method for calculating the modulus of subgrade reaction, when used with appropriate Young's modulus values, should provide reasonable results for pile resistance to lateral loading for initial loading and for working loads.

The paper by Habibagahi and Langer presents an extensive review of published methods for determining the coefficient of horizontal subgrade reaction for granular soils and includes a discussion of the factors on which it is dependent. Horizontal subgrade reaction parameters based on eight published methods are presented in tabular form for comparison. They demonstrate the wide range in published values. Another comparison is made in graphical form where the coefficient of subgrade reaction is plotted against relative depth (depth divided by pile diameter) for values given by twelve published methods. The authors suggest that the wide range in values may be due to variations in magnitude of pile deflection, effective overburden pressure, and relative density of the soil. They have proposed an equation for calculating the coefficient of horizontal subgrade reaction, which accounts for these factors. The proposed equation is dependent upon knowing the value of a parameter labeled A, which is a function of pile deflection, the soil's angle of internal friction and the pile width, and must be determined from load test data. Recommended values for A are given for a friction angle of 30° and pile deflection

ranging from 2.54 to 25.4 mm (0.1 to 1.0 in.). Using these values and other parameters given in the previous graph referred to, a similar graph is included that is based on the proposed equation. It demonstrates how sensitive the coefficient of horizontal subgrade reaction is to the pile deflection.

The paper by Sogge describes how a structural analysis computer program may be used for the analysis of a laterally loaded pile. An example is given showing how a pile and the soil in which it is embedded are modeled for the computer solution. The input and output data are given as well. The discussion points out the advantages in making an analysis for the combined super structure and foundation rather than making independent analyses. The discussion also points out a disadvantage in the type of analysis presented in that any vertical arching arising from horizontal pile movement is not accounted for in the solution.

The paper by Selvadurai presents an approximate solution for the torsional stiffness of a rigid cylindrical pier embedded in an isotropic elastic soil mass. The derivation of the approximate solution is outlined, and the results are compared graphically with exact solutions. The graph shows that the relatively simple approximate solution gives results close to those given by complicated exact solutions.

The paper by Reese, Wright, and Aurora compares three methods of analysis for a laterally loaded pile group founded in stiff clay. The three methods are the Poulos-Focht-Koch method, a modification of that method, and the imaginary large-diameter single-pile method. All three methods utilize *P-Y* curves to correlate lateral soil resistance with pile deflection. The selection of an appropriate value for soil modulus and relative stiffness factor is discussed in detail. Graphs are included that show the sensitivity of pile group deflection to these two parameters. The results of parameter studies for lower and upper boundary soil stiffness and for lower and upper boundary relative stiffness factors are presented in tabular form. The imaginary large diameter pile method gave results similar to those where the relative stiffness factors are presented in tabular form. The imaginary large diameter pile method gave results similar to those where the relative stiffness factor was assumed to be unity. The writers conclude that very careful attention must be given to the selection of the soil modulus that is used in the Poulos analysis of a single pile. They recommend that parameter studies be made for a range of possible soil moduli to determine probable pile foundation behavior since currently available methods for determining the relevant properties of natural soil deposits are imprecise.

The paper by Gleser presents a generalized solution for calculating the lateral movement of a vertical pile and resulting stresses due to lateral loading. The solution is based on finite-difference equations, requiring the use of a digital computer. It includes a solution for a nonlinear soil response by characterizing the *P-Y* curve as three straight lines, each applicable for specific ranges of deflection. A procedure is given for making iterative solutions and comparing the calculated lateral deflection with range of deflection applicable for the

P-Y equation used, and making adjustments as necessary. A procedure is also given for using the generalized solution for piles subjected to fluctuating lateral loads. A procedure is given for determining *P-Y* curves for the soil based on data obtained from lateral pile load tests made in a specific manner. Following the procedures for using the generalized solution, the author applies the solution to the test pile results reported by Alizadeh and Davisson for the Arkansas River Project and makes several observations of the results with respect to the influence of pile shape on lateral deflection characteristics.

The paper by Briaud, Smith, and Meyer presents a discussion of the influence of the depth below the ground surface on soil-pile interaction and how the pressuremeter may be used to determine parameters for predicting load-deflection characteristics for piles. Earlier methods for determining the maximum depth where the soil resistance is reduced because of the proximity of the ground surface, termed the critical depth, are reviewed. Then, seven proposed methods for predicting the load-deflection characteristics for laterally loaded piles using pressuremeter test results are outlined. The first four of these methods are applied to a lateral-load test case history, and the results are compared graphically with the load test data. The authors believe that pressuremeter data provides a sound basis for predicting the behavior of laterally loaded piles.

The paper by Horvath reviews the two principal methods for calculating the load-deflection behavior of laterally loaded piles: one using Winkler's modulus of subgrade reaction concept, and the other using the elastic continuum concept. The advantages and disadvantages of each method are discussed. The author then reviews an elastic continuum solution by Reissner using simplifying assumptions for vertical loads applied to the surface of the elastic continuum. He then refers to his previous paper where he used Reissner's simplified continuum approach to solve the problem for vertical loads assuming that Young's modulus varies either linearly or with the square root of depth to more closely simulate the actual behavior of soil. The author then uses this approach to develop a solution for laterally loaded piles, the derivation of which is included in the Appendix to this paper. He notes that this approach can be readily solved by computer using finite-difference equations and that variations in Young's modulus with depth can be used as well. The author is currently evaluating several lateral-load test case histories using the simplified continuum approach and will publish the results after the study is complete.

Case Histories

The papers in this group are, with one exception, case histories. Lateral load testing was carried out on small-scale models (Cox et al and Stephenson et al), drilled piles (Bhushan and Askari, Johnson et al, and Long and Reese), and driven piles (Gle and Woods, and Robertson et al). The soils providing the lat-

eral resistance ranged from very soft clays to very dense sands. Testing was generally at high strains, and deflections and moments correlated reasonably well with existing theories. Bhushan and Askari, however, examined the response at low lateral loads and strains, and found effectively stiffer conditions. Bhushan also examined the effects of cyclic loading and determined that, at the low strains, cyclic loading increased strain only for the first few cycles. This was generally confirmed by Long and Reese at high strains but not by Robertson et al. Gle and Woods dynamically tested the piles and found that the response could be well matched with existing solutions or could be modified to match where necessary. The Oakland and Chameau paper presented a three-dimensional finite-element model for drilled piles as a method to stabilize slopes.

Cox et al investigated the efficiencies of small-scale model pile groups in soft clay under lateral loading conditions. The piles were single-diameter open ended pipe pushed to different depths into the clay in in-line and side-by-side configurations of different numbers and spacings. The authors concluded that there was a remarkably uniform distribution of lateral loads on the side-by-side configuration with group efficiencies in excess of 0.76. For pile groupings in-line, there was considerably more variation both in distribution of loads and the group efficiency with minimum efficiencies of 0.54.

Stephenson et al also carried out lateral load tests on model piles as well as full-scale tests on helical anchor piles to develop a suitable mathematical model of the lateral load versus deflection behavior. The model tests were on ¼-scale helical piles and were carried out in medium sand with an angle of internal friction of 42°. The full-scale load tests, with which they were compared, were in both sands and clays. Stephenson et al concluded that helical anchor piles can develop significant resistance to lateral loads, and that, in most cases, this is controlled by the behavior of the extension shafts. To estimate deflections, they were able to use mathematical models similar to those for slender piles modified to account for the installation procedure used.

Long and Reese presented the results of testing and analysis of two offshore 1.22-m diameter drilled shafts in dense sand subjected to lateral loads of up to 500 kN. The loading was cycled 40 times for each increment. A semi-empirical computer model was used to predict the behavior of the shaft, and the predictions were compared with the measured results. Predicted deflections were found to be 21 to 30% less than measured values but maximum bending moment predictions were within 4 to 14%. It was concluded that, even though there were several differences between the characteristics of the load test and the computer model, there was reasonable agreement of maximum moments and horizontal deflections.

Johnson et al report on a lateral-load test carried out in 1982 on a 0.46-m diameter drilled shaft constructed in 1966 in stiff expansive clay soil. There had been considerable swelling of the soil around the 10.5-m long shaft. Pressure-

meter and laboratory undrained triaxial strength tests were found to be suitable for the analysis of the lateral behavior, although criteria for evaluating the behavior led to less stiff *p-y* curves than frequently used. This may have been due to long term field conditions such as wetting and remolding.

Bhushan and Askari carried out low-level cyclic load tests on 0.91-m diameter by 5.5-m long drilled shafts in dense sands and gravelly sands. The testing resulted in a 40% reduction in lengths for the foundation piers, as it was determined that the *p-y* curves were much stiffer than would be indicated by conventional procedures with high lateral loadings. Other findings include: a linear load-deflection response; the observation of 20 to 50% increase in deflection during the first few cyclic loads with no increase thereafter; a permanent set of approximately 25% of the deflection under the maximum load; and little increase in deflections caused by soaking of the surrounding ground. Bhushan and Askari proposed a semi-empirical relationship to obtain coefficient of subgrade reaction values from the standard penetration resistance, and this appeared to provide reasonable results.

Robertson et al used a driven pressuremeter to measure soil properties and thereby predict the lateral load behavior of four 30-cm^2 precast concrete piles driven to 7 to 8 m depth through loose gravelly sand fill and very soft peat to bearing in glacial till. It was felt that the driven pressuremeter would fairly accurately model the pile driving. The test results were limited, but the agreement between the calculated and measured deflections was good.

Gle and Woods developed a procedure for dynamic lateral-load testing of single piles to investigate the soil-pile interaction parameters for foundations subjected to fairly high frequency cyclic loadings. This consisted of a steel mass plate, Lazan eccentric-mass oscillator, and vibration monitoring equipment attached to the head of the pile as close as possible to the ground surface. The response of the system was then measured on eleven pipe piles at three sites with both cohesive and cohesionless soils. The frequency of the dynamic loading ranged from 8 to 55 Hz. The results were supplemented by plucking tests on the piles. It was found that the observed lateral response could be matched quite well by the PILAY solution up to and slightly above the lateral translation resonance from stiffness and dampness values obtained from the dynamic field testing. At greater frequencies the design parameters could be modified to approximately model the observed response.

Oakland and Chameau report on preliminary development of a three-dimensional finite-element model to analyse the benefits of drilled piers for stabilizing slopes. It was concluded that there is substantial development required of the model, especially as regards to the boundary conditions. However, the model indicates that drilled piers can be used to stabilize slopes and reduce slope movements, mostly below the piers.

In summary, the case histories presented in this session are a valuable addition to data on lateral loading of piles. They are encouraging in that they gen-

erally indicate that existing mathematical and computer models or modifications thereof can be used to predict lateral deflections. The pressuremeter would appear to be a useful instrument for determining the soils properties to employ in these models.

E. T. Mosley

Raamot Associates, New York, NY 10121; symposium cochairman and editor

C. D. Thompson

Trow Ltd., Rexdale, Ontario, Canada M9V 3Y8; symposium cochairman and editor

Index

ISBN 0-8031-0207-0